Many-body correlations and excitonic effects in semiconductor spectroscopy

Article *in* Progress in Quantum Electronics · December 2006

DOI: 10.1016/j.pquantelec.2006.12.002

CITATIONS
390

READS
736

2 authors, including:

Mackillo Kira
University of Michigan
290 PUBLICATIONS **9,196** CITATIONS

SEE PROFILE

ELSEVIER

Progress in Quantum Electronics 30 (2006) 155–296

Progress in Quantum Electronics

www.elsevier.com/locate/pquantelec

Review

Many-body correlations and excitonic effects in semiconductor spectroscopy

M. Kira*, S.W. Koch

Department of Physics and Material Sciences Center, Philipps-University Marburg, Renthof 5, D-35032 Marburg, Germany

Abstract

The optically excited system of electronic excitations in semiconductor nanostructures is analyzed theoretically. A many-body theory based on an equation-of-motion approach for the interacting electron, hole, photon, and phonon system is reviewed. The infinite hierarchy of coupled equations for the relevant correlation functions is systematically truncated using a cluster-expansion scheme. The resulting system of equations describes the optical generation of semiconductor quasi-particle configurations with classical or quantum mechanical light sources, as well as their photon-assisted spontaneous recombination. The theory is evaluated numerically to study semiclassical and quantum excitation under different resonant and non-resonant conditions for a wide range of intensities. The generation of a correlated electron–hole plasma and exciton populations is investigated. It is shown how these states can be identified using direct quasi-particle spectroscopy with sources in the terahertz range of the electromagnetic spectrum. The concept of quantum–optical spectroscopy is introduced and it is predicted that semiconductor excitation with suitable incoherent light directly generates quantum-degenerate exciton states. The phase space for this exciton condensate is identified and its experimental signatures are discussed.

PACS: 42.50.−p; 78.55.−m; 03.75.Kk; 42.25.Kb; 71.35.−y; 78.47.+p

Keywords: Semiconductor quantum optics; Many-body correlations; Excitons; Electron–hole plasma; Exciton condensate

*Corresponding author. Tel.: +49 6421 282422; fax: +49 6421 2827076.
E-mail address: mackillo.kira@physik.uni-marburg.de (M. Kira).

0079-6727/$ - see front matter © 2007 Elsevier Ltd. All rights reserved.
doi:10.1016/j.pquantelec.2006.12.002

Contents

1. Introduction

Semiconductors and their nanostructures efficiently interact with the light field if the optical frequency is in the spectral vicinity of the direct material band gap. This light–matter coupling is mediated by transitions of electrons between the valence and the conduction band. Since the missing valence-band electrons are treated as "holes", we speak of optically assisted electron–hole-pair transitions. The properties of the valence-band holes are those of the missing electrons, i.e. they are Fermions and have a spin, charge, effective mass and so on, which are opposite to those of the valence-band electrons. Since the electron charge is $-|e|$, where e is the elementary charge, the holes are positively charged and there is an attractive Coulomb interaction between the valence-band holes and the conduction-band electrons. (For more details and background information see Refs. [1–4] and work cited therein.)

The quantum mechanical problem of a single electron–hole pair in a homogeneous semiconductor leads to the Wannier equation which, for a parabolic bandstructure, is mathematically identical to the Schrödinger equation for the relative-motion problem of the hydrogen atom [5]. This equation can be solved analytically in three and two dimensions, which is relevant for idealized bulk or quantum-well (QW) structures. Solutions are also available for quasi-one and zero-dimensional systems, however, their treatment requires the regularization of the Coulomb interaction potential [1].

The bound states of the Wannier equation are the excitons [5–9] which are characterized by a binding energy and a Bohr radius that, for systems with not too strong Coulomb attraction, significantly exceeds the characteristic length scale of the atomic unit cell. However, instead of the roughly 13.6 eV binding energy (Rydberg energy) in atomic hydrogen, the excitonic Rydberg energy is typically in the range of a few to 100 meV. This reduction in the pair-state binding energy is a consequence of the effective electron and hole masses which are substantially lighter than the free electron and proton masses. Furthermore, the semiconductor background dielectric constant reduces the Coulomb interaction strength roughly by one order of magnitude compared to that of hydrogen.

Nevertheless, pronounced excitonic resonances can be seen especially in the low-temperature linear optical absorption spectra of most good quality direct-gap semiconductors, see e.g. Refs. [2,10–14]. An interesting topic in this context is the question under which conditions a truly bound exciton population exists and how it can be identified experimentally. Excitonic features in linear absorption spectra clearly cannot be related to any population effect since only an induced optical polarization and no population exists in the linear regime. The presence of some form of an electron–hole-pair population is required to observe photoluminescence (PL) under incoherent conditions. However, the mere appearance of excitonic resonances in PL spectra is not sufficient to draw conclusions about the presence of excitons since also unbound electron–hole pairs can give rise to these features [15].

An unambiguous method to identify exciton populations is to perform terahertz (THz) spectroscopy, i.e. to probe transitions between excitonic eigenstates [16–21]. Under incoherent conditions, the observation of resonances due to these transitions is a clear signature of an exciton population. However, since these resonances correspond to differences between energy eigenvalues related to the relative electron–hole motion, they are independent of the exciton's center-of-mass energy. Therefore, the induced THz absorption is insensitive to the exciton-distribution function.

In the past decade, the consistent microscopic analysis of semiconductor properties on the basis of Coulomb interacting Fermionic electron and hole excitations has lead to a number of new insights [15,18,22–38]. In this review, we give an overview of the microscopic theory for the interacting system of electrons, holes, photons, and phonons. We define our basic system in Section 2 by discussing the different relevant quasi-particle excitations and the basic Hamiltonian governing our many-body system. In Section 3, we present an equation-of-motion approach that allows us to include the different interaction effects in a microscopically consistent way. As a consequence of these interactions, the equations for the correlation functions couple to correlations of ever increasing order. We show how this hierarchy problem can be treated systematically using the cluster-expansion method [39–46]. In Section 4, we discuss the different levels of approximations and show how to obtain consistent solutions.

The optical part of the problem is analyzed in Section 5 where we present the Maxwell-semiconductor Bloch equations (MSBEs) and examples of their solutions. We introduce coherent and incoherent correlation effects and investigate the induced optical polarization, its radiative decay, as well as the concept of excitation induced dephasing.

In Section 6, we analyze in detail the relation between polarization dephasing and the concomitant formation of incoherent populations. Here, we pay particular attention to the build-up and the dynamics of excitonic correlations in the excited semiconductor system. We carefully distinguish between correlated electron–hole plasma configurations and

situations where true exciton populations are formed. For this purpose, we review the microscopic theory of direct optical quasi-particle spectroscopy using light in the THz range of the optical spectrum. We show how the induced THz absorption gives us reliable and unique informations about the transitions between different many-body configurations in the interacting semiconductor system.

Numerical solutions of the full set of coupled equations are presented in Sections 7 and 8 where we study a wide variety of optical and excitonic effects. In Section 7, we analyze uniquely different optical excitation configurations, starting from resonant pumping at the 1*s*-exciton frequency, pumping at the 2*s*-resonance, all the way to non-resonant interband continuum excitation. For all these cases, we present the conversion dynamics from coherent optical polarization into incoherent populations. We discuss the nature of the generated quasi-particle states and their dynamic evolution.

The entire Section 8 is devoted to the analysis of exciton formation under incoherent conditions. Quasi-stationary exciton populations are determined for different density and temperature conditions. These results are compared to estimates obtained by postulating a pure quasi-thermodynamic configuration.

The developed theory can directly be generalized to include quantum-optical effects. In Section 9, we derive the semiconductor luminescence equations (SLEs) [15,23,26] which are the basis for our consistent description of the spontaneous light emission from semiconductors and the accompanying recombination of different quasi-particle excitations. We first discuss specific properties of the excitonic luminescence and the recombination rates of different quasi-particle states. This analysis leads us to the new concept of *quantum-optical spectroscopy* [36,37] where the quantum statistics of the light field controls important aspects of the generated quasi-particle states. In particular, we show that one can directly excite a quantum-degenerate exciton population with a macroscopic occupation of one single state, i.e. an exciton condensate.

Finally, we discuss in the Appendices some technical aspects and explicit equations that appear in our derivations. In Appendix A, we present the detailed Hamiltonian of the system. In Appendix B, we introduce a highly compact implicit notation that allows us to perform the systematic derivations of the many contributions arising at advanced levels of the cluster-expansion scheme. The explicit forms of the coupled equations arising at the singlet–doublet approximation level are summarized in Appendices C and D. In Appendix E, we present a useful classification of the different correlation contributions. Appendix F then summarizes the explicit form of the exciton correlation dynamics and Appendix G focuses on the contributions due to excitation induced dephasing effects.

2. Quantum-electrodynamic theory

The quantum properties of the interacting carrier–photon–phonon system in semiconductors are governed by the many-body Hamiltonian $H_{\rm sys}$. Since most aspects of this Hamiltonian are thoroughly discussed in the literature [1,26,47,48], we present here only a brief overview with the goal to define our notation and the concepts relevant for the theoretical developments in this review. We present the equations in a form which is directly applicable to planar nanostructures of direct-gap semiconductors, such as QW systems or planar arrangements of identical quantum wires (QWIs). These QWIs are assumed to be electronically uncoupled and spatially arranged with a mutual distance much less than the relevant optical wavelength such that no diffraction pattern is

generated. Consequently, the QWI arrangement is as close as possible to an effectively one-dimensional simplification of the effectively two-dimensional QW, see e.g. Ref. [46].

2.1. Quantization of carriers, photons, and phonons

The semiconductor electrons can be described quantum mechanically using field operators,

$$\Psi(\mathbf{r}) = \sum_{\mathbf{k}} a_{\mathbf{k}} \phi_{\mathbf{k}}(\mathbf{r}), \quad \Psi^{\dagger}(\mathbf{r}) = \sum_{\mathbf{k}} a_{\mathbf{k}}^{\dagger} \phi_{\mathbf{k}}^{\star}(\mathbf{r}), \tag{1}$$

that annihilate (Ψ) or create ($\Psi^{\dagger}$) an electron at position $\mathbf{r}$. It is often useful to express these field operators in the basis of single-particle wavefunctions $\phi_{\mathbf{k}}(\mathbf{r})$ which form a complete set of orthogonal states. Each of these states is uniquely identified by the generic quantum number $\mathbf{k}_{\parallel}$, which will be specified in more detail later.

Since electrons are Fermions, the operators $a_{\mathbf{k}}$ and $a_{\mathbf{k}}^{\dagger}$ obey anticommutation relations:

$$[a_{\mathbf{k}}, a_{\mathbf{k}'}^{\dagger}]_{+} = a_{\mathbf{k}} a_{\mathbf{k}'}^{\dagger} + a_{\mathbf{k}'}^{\dagger} a_{\mathbf{k}} = \delta_{\mathbf{k},\mathbf{k}'},$$

$$[a_{\mathbf{k}}, a_{\mathbf{k}'}]_{+} = [a_{\mathbf{k}}^{\dagger}, a_{\mathbf{k}'}^{\dagger}]_{+} = 0. \tag{2}$$

In most cases, it is convenient to choose an orthogonal basis which diagonalizes the Schrödinger equation for the electron moving in the effective lattice periodic potential $U_{\mathrm{L}}(\mathbf{r})$

$$\left[\frac{\hat{\mathbf{p}}^2}{2m_0} + U_{\mathrm{L}}(\mathbf{r})\right] \phi_{\mathbf{k}}(\mathbf{r}) = \varepsilon_{\mathbf{k}} \phi_{\mathbf{k}}(\mathbf{r}), \tag{3}$$

where m_0 is the free-electron mass. The eigenstates to this equation define the bandstructure $\varepsilon_{\mathbf{k}}$ of the system.

For many experimentally relevant situations, it is sufficient to consider carrier transitions between one conduction and one valence band. We therefore restrict most of the explicit calculations in this review to such a two-band model which is well suited to investigate many interesting semiconductor optical effects. Unless noted otherwise, we will always use in our explicit examples and numerical evaluations typical GaAs parameters providing 4.18 meV exciton binding energy and a Bohr radius of $a_0 = 12.5$ nm for a three-dimensional system.

Since we deal with planar structures and use QWs (QWIs) as explicit examples, it is useful to separate the three-dimensional space coordinate $\mathbf{r} = (\mathbf{r}_{\parallel}, r_{\perp})$ into the two-(one-) dimensional component $\mathbf{r}_{\parallel}$ in the QW plane and the one-(two-)dimensional component $r_{\perp}$ perpendicular to it. For the QW system, the corresponding electron wavefunction within the envelope-function approximation [1] is given as

$$\phi_{\lambda,l,\sigma,\mathbf{k}_{\parallel}}(\mathbf{r}) = \xi_{\lambda,l}(r_{\perp}) \frac{1}{\sqrt{\mathsf{S}}} \mathrm{e}^{\mathrm{i}\mathbf{k}_{\parallel}\cdot\mathbf{r}_{\parallel}} w_{\lambda,l,\sigma,\mathbf{k}_{\parallel}}(\mathbf{r}), \tag{4}$$

where λ refers to a specific band, l defines the subband index, σ denotes the spin index, and $\mathbf{k}_{\parallel}$ is the carrier momentum in the QW plane. In total, ϕ contains the confinement wavefunction $\xi_{\lambda,l}(r_{\perp})$, a plane wave contribution with quantization area S, and the lattice-periodic Bloch function $w_{\lambda,l,\sigma,\mathbf{k}_{\parallel}}(\mathbf{r})$.

In practice, $\xi_{\lambda,l}(r_\perp)$ can be solved from the one-dimensional Schrödinger equation for a particle confined to a potential structure. Since such a problem typically has many bound-state solutions, they introduce several confinement levels, i.e. subbands, labeled by the quantum number l. To retain our two-band approximation, we assume a sufficiently strong confinement potential and consider only the transitions between the states corresponding to the lowest level $l = 1$. In order to simplify the notation, we use from now on the index λ as a general label which implicitly includes also the subband index l as well as the spin index σ. Hence, we define

$$a_{\lambda,\mathbf{k}_\parallel} \equiv a_{\lambda,l,\sigma,\mathbf{k}_\parallel}. \tag{5}$$

For the case of two bands, we only need to consider the cases where $\lambda = c$ refers to conduction-band electrons and $\lambda = v$ denotes valence-band electrons.

For a quantum mechanical description of the transverse electro-magnetic field, we start from the vector potential $\mathbf{A}$ within the canonical quantization scheme (for textbook discussions, see e.g. Refs. [48,49]). The general vector potential is expanded in terms of the steady-state eigenmodes $\mathbf{U}_{\alpha,\mathbf{q}}(\mathbf{r})$ where $\mathbf{q}$ is the wavevector and α defines the polarization direction of the mode. The steady-state solutions to Maxwell's equations lead to the Helmholtz equation

$$[\nabla^2 + \mathbf{q}^2 n^2(\mathbf{r})]\mathbf{U}_{\alpha,\mathbf{q}}(\mathbf{r}_\parallel, r_\perp) = \mathbf{0}. \tag{6}$$

Here, $n(\mathbf{r})$ is the passive, position dependent refractive index provided by the unexcited semiconductor together with the surrounding passive material such as dielectric mirrors, antireflection coating, barriers, and buffer layers. Since we investigate planar structures, $n(\mathbf{r})$ has only an $r_\perp$-dependence.

The eigenstates are normalized via

$$\int \mathrm{d}^3 r\, n^2(\mathbf{r})\mathbf{U}^\star_{\alpha',\mathbf{q}'}(\mathbf{r}) \cdot \mathbf{U}_{\alpha,\mathbf{q}}(\mathbf{r}) = \delta_{\mathbf{q},\mathbf{q}'}\delta_{\alpha,\alpha'}. \tag{7}$$

For a sufficiently large in-plane extension of the QW and quantization area S, the eigenmode solutions can be separated into in-plane and $r_\perp$-dependent parts

$$\mathbf{U}_{\alpha,\mathbf{q}}(\mathbf{r}) = \frac{1}{\sqrt{\mathsf{S}}}\mathbf{u}_{\alpha,\mathbf{q}}(r_\perp)\,\mathrm{e}^{\mathrm{i}\mathbf{q}_\parallel\cdot\mathbf{r}_\parallel}, \tag{8}$$

where $\mathbf{q} = (\mathbf{q}_\parallel, q_\perp)$. The remaining $r_\perp$-dependent component can be determined with the help of the transfer-matrix technique outlined e.g. in Refs. [26,50]. By using the corresponding complete mode basis, the operator $\mathbf{A}$ can be expressed via the mode expansion

$$\mathbf{A}(\mathbf{r}) = \sum_{\alpha,\mathbf{q}_\parallel,q_\perp} \frac{\mathsf{E}_\mathbf{q}}{\omega_\mathbf{q}}[\mathbf{u}_{\alpha,\mathbf{q}}(r_\perp)\,\mathrm{e}^{\mathrm{i}\mathbf{q}_\parallel\cdot\mathbf{r}_\parallel}B_{\alpha,\mathbf{q}_\parallel,q_\perp} + \text{c.c.}], \tag{9}$$

where the optical frequency $\omega_\mathbf{q} = c|\mathbf{q}|$ is identified together with a constant $\mathsf{E}_\mathbf{q}B_{\alpha,\mathbf{q}_\parallel,q_\perp}$ whose explicit form is defined after the light is quantized.

Altogether, the mode expansion of the vector field leads to a structure that resembles the form of the electronic field operators given in the Bloch basis. In particular, $\mathbf{u}_{\alpha,\mathbf{q}}(r_\perp)$ corresponds to the electronic eigenstate while $B_{\alpha,\mathbf{q}_\parallel,q_\perp}$ is analogous to the electronic operators. Hence, the rigorous quantization procedure of the electromagnetic field [48] replaces the complex-valued expansion coefficients by the photon creation, $B^\dagger$, and

annihilation, B, operators. These operators obey Bosonic commutation relations:

$$[B_{\alpha,\mathbf{q}}, B^{\dagger}_{\alpha',\mathbf{q}'}]_- = B_{\alpha,\mathbf{q}}B^{\dagger}_{\alpha',\mathbf{q}'} - B^{\dagger}_{\alpha',\mathbf{q}'}B_{\alpha,\mathbf{q}} = \delta_{\alpha,\alpha'}\delta_{\mathbf{q}_\parallel,\mathbf{q}'_\parallel}\delta_{q_\perp,q'_\perp},$$

$$[B_{\alpha,\mathbf{q}}, B_{\alpha',\mathbf{q}}]_- = [B^{\dagger}_{\alpha,\mathbf{q}}, B^{\dagger}_{\alpha',\mathbf{q}'}]_- = 0. \tag{10}$$

The quantization procedure also fixes the vacuum-field amplitude

$$\mathsf{E}_{\mathbf{q}} = \sqrt{\hbar\omega_{\mathbf{q}}/(2\varepsilon_0)}. \tag{11}$$

In the literature, the quantization volume V is sometimes defined into $\mathsf{E}_{\mathbf{q}}$ via $\mathsf{E}_{\mathbf{q}} \to \sqrt{\hbar\omega_{\mathbf{q}}/(2\varepsilon_0)\mathsf{V}}$. However, in this review we choose the notation such that V is included with the mode functions by implementing the normalization (7). This way, we not only obtain a formal similarity between the mode and the Bloch functions but we can also address the quantization volume once and for all in the mode function calculations.

The quantization introduces quantum statistics to the light modes $\mathbf{U}_{\alpha,\mathbf{q}_\parallel,q_\perp}(\mathbf{r})$ in the sense that each light mode is characterized by non-trivial quantum fluctuations besides its classical expectation value. The quantized transverse electric and magnetic fields can be evaluated from the general relations

$$\mathbf{E}_{\mathrm{T}} = -\frac{\partial \mathbf{A}}{\partial t}, \quad \mathbf{B} = \nabla \times \mathbf{A}, \tag{12}$$

respectively. As for the carrier system, it is also beneficial to simplify the notation for the light field by introducing an implicit labeling,

$$B_{\mathbf{q}} = B_{\mathbf{q}_\parallel,q_\perp} \equiv B_{\alpha,\mathbf{q}_\parallel,q_\perp}, \tag{13}$$

where the polarization is included with the in-plane momentum $\mathbf{q}_\parallel$.

To treat the lattice vibrations, we introduce the field operator for the quantized displacement of the lattice ion at the position $\mathbf{r}$ as

$$\mathbf{Q}(\mathbf{r}) = \sum_{\alpha,\mathbf{p}_\parallel,p_\perp} \mathsf{Q}_{\alpha,\mathbf{p}_\parallel,p_\perp}[D_{\alpha,\mathbf{p}_\parallel,p_\perp} + D^{\dagger}_{\alpha,-\mathbf{p}_\parallel,-p_\perp}]e^{i(\mathbf{p}_\parallel\cdot\mathbf{r}_\parallel + p_\perp r_\perp)}. \tag{14}$$

Here, $\mathsf{Q}_{\alpha,\mathbf{p}}$ denotes the vacuum-displacement amplitude while the three-dimensional phonon momentum is decomposed into its in-plane, $\mathbf{p}_\parallel$, and perpendicular parts, $p_\perp$. The different phonon branches are labeled by α. The quantized phonon fields are Bosonic such that they obey the commutation relations:

$$[D_{\alpha,\mathbf{p}}, D^{\dagger}_{\alpha',\mathbf{p}'}]_- = D_{\alpha,\mathbf{p}}D^{\dagger}_{\alpha',\mathbf{p}'} - D^{\dagger}_{\alpha',\mathbf{p}'}D_{\alpha,\mathbf{p}} = \delta_{\alpha,\alpha'}\delta_{\mathbf{p}_\parallel,\mathbf{p}'_\parallel}\delta_{p_\perp,p'_\perp},$$
$$[D_{\alpha,\mathbf{p}}, D_{\alpha',\mathbf{p}}]_- = [D^{\dagger}_{\alpha,\mathbf{p}}, D^{\dagger}_{\alpha',\mathbf{p}'}]_- = 0. \tag{15}$$

Similarly to the photons, we also introduce here an implicit notation

$$D_{\mathbf{p}} = D_{\mathbf{p}_\parallel,p_\perp} \equiv D_{\alpha,\mathbf{p}_\parallel,p_\perp}. \tag{16}$$

Besides the momentum $\mathbf{p}$, each phonon mode can be associated with a phonon energy $\hbar\Omega_{\mathbf{p}}$. The acoustical phonons have a liner dispersion while $\Omega_{\mathbf{p}}$ is nearly constant for optical phonons. In general, one always finds three branches α of acoustic phonons in a three-dimensional semiconductor [51] corresponding to the three independent modes of sound waves in a solid. In lattices with more than one atom within a unit cell, additional optical phonon branches are present.

2.2. Many-body Hamiltonian

Since detailed discussions of the system Hamiltonian $H_{\rm sys}$ can be found in Refs. [1,26], we restrict the discussion here to a brief summary of those aspects that are explicitly needed for the subsequent derivations. We write the total Hamiltonian as

$$H_{\rm sys} = H_0 + H_{\rm C} + H_{\rm D} + H_{\rm P}. \tag{17}$$

Here, the non-interacting parts of the carrier–photon–phonon system are contained in H_0. Additionally, we have the Coulomb interaction among the carriers in $H_{\rm C}$, the dipole interaction between light and matter in $H_{\rm D}$, and the phonon interaction in $H_{\rm P}$, respectively.

The explicit form of the different terms is

$$\begin{aligned} H_0 = &\sum_{\lambda,\mathbf{k}_\parallel} \varepsilon^{\lambda}_{\mathbf{k}_\parallel} a^{\dagger}_{\lambda,\mathbf{k}_\parallel} a_{\lambda,\mathbf{k}_\parallel} + \sum_{\mathbf{q}_\parallel,q_\perp} \hbar\omega_{\mathbf{q}} \left[B^{\dagger}_{\mathbf{q}_\parallel,q_\perp} B_{\mathbf{q}_\parallel,q_\perp} + \frac{1}{2} \right] \\ &+ \sum_{\mathbf{p}_\parallel,p_\perp} \hbar\Omega_{\mathbf{p}} \left[D^{\dagger}_{\mathbf{p}_\parallel,p_\perp} D_{\mathbf{p}_\parallel,p_\perp} + \frac{1}{2} \right], \end{aligned} \tag{18}$$

$$H_{\rm C} = \frac{1}{2} \sum_{\lambda,\lambda'} \sum_{\mathbf{k}_\parallel,\mathbf{k}'_\parallel,\mathbf{q}_\parallel \neq 0} V_{\mathbf{q}_\parallel} a^{\dagger}_{\lambda,\mathbf{k}_\parallel+\mathbf{q}_\parallel} a^{\dagger}_{\lambda',\mathbf{k}'_\parallel-\mathbf{q}_\parallel} a_{\lambda',\mathbf{k}'_\parallel} a_{\lambda,\mathbf{k}_\parallel}, \tag{19}$$

$$H_{\rm D} = -{\rm i}\hbar \sum_{\lambda,\mathbf{k}_\parallel,\mathbf{q}_\parallel} [B^{\lambda}_{\mathbf{q}_\parallel,\Sigma} - (B^{\bar{\lambda}}_{-\mathbf{q}_\parallel,\Sigma})^{\dagger}] a^{\dagger}_{\lambda,\mathbf{k}_\parallel} a_{\bar{\lambda},\mathbf{k}_\parallel-\mathbf{q}_\parallel}, \tag{20}$$

$$H_{\rm P} = \hbar \sum_{\lambda,\mathbf{k}_\parallel,\mathbf{p}_\parallel} [D^{\lambda}_{\mathbf{p}_\parallel,\Sigma} + (D^{\lambda}_{-\mathbf{p}_\parallel,\Sigma})^{\dagger}] a^{\dagger}_{\lambda,\mathbf{k}_\parallel} a_{\lambda,\mathbf{k}_\parallel-\mathbf{p}_\parallel}. \tag{21}$$

Here, we used an implicit notation for the indices of the carrier, photon, and phonon operators. The detailed index structure and other formal aspects of the Hamiltonian are discussed in Appendix A. Furthermore, we still have to define the different matrix elements appearing in Eqs. (18)–(21).

The first term in Eq. (18) contains the kinetic energies of the Bloch electrons,

$$\varepsilon^{c}_{\mathbf{k}_\parallel} = \frac{\hbar^2\mathbf{k}_\parallel^2}{2m_{\rm e}}, \quad \varepsilon^{v}_{\mathbf{k}_\parallel} = -\frac{\hbar^2\mathbf{k}_\parallel^2}{2m_{\rm h}} - E_{\rm g}, \tag{22}$$

in the conduction and valence band, respectively. These bands are separated by the band-gap energy $E_{\rm g}$. Close to the band extrema, we may apply a parabolic approximation [1,51] to introduce effective masses $m_{\rm e}$ and $m_{\rm h}$ for the electrons and holes, respectively. For the two-band systems under strong confinement conditions, the envelope functions $\xi_\lambda(r_\perp)$ for electrons and holes are identical, i.e. $\xi_c(r_\perp) = \xi_v(r_\perp) = \xi(r_\perp)$. Thus, the Coulomb-matrix element does not depend on the band and sub-band indices [52],

$$V_{\mathbf{q}_\parallel} = \frac{e^2}{2\varepsilon_0\varepsilon|q_\parallel|} \int {\rm d}r_\perp\, {\rm d}r'_\perp |\xi(r_\perp)|^2\, {\rm e}^{-|\mathbf{q}_\parallel(r_\perp-r'_\perp)|} |\xi(r'_\perp)|^2. \tag{23}$$

Here, ε_0 is the permittivity of the vacuum and ε is the dielectric constant of the semiconductor material. Expression (23) approaches the Fourier transformation of the

two-dimensional Coulomb interaction in the limit when the confinement layer becomes infinitely thin, i.e. $|\xi(r_\perp)|^2 \to \delta(r_\perp)$. The multi-band generalization of Eq. (23) is discussed in Appendix A.

The strength of the light–matter interaction is directly connected to the generalized dipole-matrix element between the two electronic bands,

$$d^{\lambda,\lambda',\sigma,\mathbf{k}_\parallel}_{\alpha,\mathbf{q}_\parallel,q_\perp} = \frac{1}{v_0}\int_{v_0} \mathrm{d}^3 r\, w^{\star}_{\lambda,\sigma,\mathbf{k}_\parallel}(\mathbf{r})\; Q\mathbf{r}\cdot\mathbf{e}_\alpha(\mathbf{q}) w_{\lambda',\sigma,\mathbf{k}_\parallel-\mathbf{q}_\parallel}(\mathbf{r}), \tag{24}$$

where $\mathbf{e}_\alpha(\mathbf{q})$ is the polarization direction of the light mode $\mathbf{q}$ and Q is the electric charge of the electrons. Note, that the dipole-matrix element does not involve the confinement functions since the integration over the unit-cell volume v_0 is sensitive only to the lattice-periodic wavefunctions.

For the two-band systems investigated here, only the contributions for $\lambda \neq \lambda'$ are relevant for optical transitions. Since $d^{\lambda,\lambda',\sigma,\mathbf{k}_\parallel}$ has only a weak $\mathbf{k}_\parallel$ dependence, we set $\mathbf{k}_\parallel = \mathbf{0}$ in the matrix element to obtain

$$d^{\lambda}_{\mathbf{q}_\parallel,q_\perp} \equiv d^{\lambda,\bar{\lambda},\sigma,\mathbf{k}_\parallel}_{\alpha,\mathbf{q}_\parallel,q_\perp} = d^{\lambda,\bar{\lambda},\sigma,\mathbf{0}}_{\alpha,\mathbf{q}_\parallel,q_\perp}, \tag{25}$$

where $\bar{\lambda}$ is defined via

$$\bar{c} = v, \quad \bar{v} = c \tag{26}$$

for our two-band system. The light–matter interaction can be presented in a compact form by introducing the collective photon operator

$$B^{\lambda}_{\mathbf{q}_\parallel,\Sigma} \equiv \sum_{q_\perp} \mathsf{F}^{\lambda}_{\mathbf{q}_\parallel,q_\perp} B_{\mathbf{q}_\parallel,q_\perp} \tag{27}$$

which combines all photon operators with the same in-plane component $\mathbf{q}_\parallel$. The different modes are weighted via the coupling matrix element

$$\mathsf{F}^{\lambda}_{\mathbf{q}_\parallel,q_\perp} \equiv \frac{1}{\hbar} d^{\lambda}_{\mathbf{q}_\parallel,q_\perp} \mathsf{E}_{\mathbf{q}} \tilde{u}_{\mathbf{q}_\parallel,q_\perp}, \tag{28}$$

including the effective mode function obtained from $\mathbf{u}_{\mathbf{q}}(r_\perp) = u_{\mathbf{q}}(r_\perp)\mathbf{e}_{\mathbf{q}}$ using

$$\tilde{u}_{\mathbf{q}_\parallel,q_\perp} = \int \mathrm{d}r_\perp |\xi(r_\perp)|^2 u_{\mathbf{q}_\parallel,q_\perp}(r_\perp). \tag{29}$$

Since we are only interested in planar structures that are much thinner than the typical optical wavelength, we can approximate $\tilde{u}_{\mathbf{q}_\parallel,q_\perp} \approx u_{\mathbf{q}_\parallel,q_\perp}(0)$.

At low temperatures and carrier energies in close vicinity of the band extrema, the coupling to lattice vibrations in GaAs-like systems follows dominantly from the interaction with longitudinal acoustical phonons. While the carriers in the QW are strongly confined, the lattice vibrations extend throughout the entire three-dimensional sample, i.e. QW (or QWI) plus barrier material. When the QW is thin enough, the confined system does not change the properties of the otherwise three-dimensional phonons. Thus, we may use the same phonon dispersion as for the bulk semiconductor. These observations define the strength of the phonon–carrier interaction via [1]

$$\mathsf{G}^{\lambda}_{\mathbf{p}} = F^{\lambda}\sqrt{\frac{\hbar|\mathbf{p}|}{2c_{\mathrm{LA}}\rho_{\mathrm{M}}\mathsf{L}^3}}\int \mathrm{d}r_\perp |\xi(r_\perp)|^2\, \mathrm{e}^{-\mathrm{i}p_\perp\cdot r_\perp} \tag{30}$$

which contains the deformation constant F^{λ}, the speed of sound c_{LA}, the mass density of the lattice ions ρ_{M}, and the quantization volume L^3. In the same way as for the photons, we may also introduce a collective phonon operator

$$D^{\lambda}_{\mathbf{p}_{\parallel},\Sigma} \equiv \sum_{p_{\perp}} \mathsf{G}^{\lambda}_{\mathbf{p}_{\parallel},p_{\perp}} D_{\mathbf{p}_{\parallel},p_{\perp}}. \tag{31}$$

With the help of this definition, we can write the phonon–carrier interaction Hamiltonian in the compact form of Eq. (21).

3. Equations of motion hierarchy

A measurement on a quantum mechanical system, such as a semiconductor QW or QWI interacting with classical or quantum light fields, can determine the expectation value $\langle O\rangle$ of the corresponding operator O. If we want to analyze experimental results by a comparison with our calculations or if we want to predict the outcome of a measurement, we have to compute the relevant expectation values. One systematic way to do this is to derive the dynamical equations for the needed operators and then take the appropriate expectation values.

For this purpose, we start from the Heisenberg equation,

$$\mathrm{i}\hbar\frac{\partial}{\partial t}\langle O\rangle = \langle [O, H_{\mathrm{sys}}]_{-}\rangle, \tag{32}$$

to derive the quantum dynamics for the interacting carrier–photon–phonon system. When we use the many-body Hamiltonian defined in Eqs. (17)–(21) and explicitly evaluate the commutator on the right-hand side of Eq. (32), we obtain an equation of motion for the operator O that contains couplings to new operators which have a significantly more complicated structure than the original operator. This is the beginning of the well-known hierarchy of infinitely many coupled equations that emerges if one continues to generate Heisenberg equations for the newly introduced, more complex operators. In the following, we briefly review how this hierarchy problem and thus the quantum dynamics of the interacting carrier–photon–phonon system can be treated systematically via the so-called cluster expansion [39–46].

3.1. General operator dynamics

Since the entire system of quasi-particle excitations is described quantum mechanically with the help of the Fermionic carrier and the Bosonic photon and phonon operators, it is natural to start from the dynamics of these elementary operators. By evaluating the Heisenberg equation of motion using the system Hamiltonian (17), we obtain the photon-operator dynamics:

$$\mathrm{i}\hbar\frac{\partial}{\partial t} B_{\mathbf{q}_{\parallel},q_{\perp}} = \hbar\omega_{\mathbf{q}} B_{\mathbf{q}_{\parallel},q_{\perp}} + \mathrm{i}\hbar \sum_{\lambda,\mathbf{k}_{\parallel}} [\mathsf{F}^{\lambda}_{\mathbf{q}_{\parallel},q_{\perp}}]^{\star} a^{\dagger}_{\lambda,\mathbf{k}_{\parallel}} a_{\bar{\lambda},\mathbf{k}_{\parallel}+\mathbf{q}_{\parallel}}, \tag{33}$$

$$\mathrm{i}\hbar\frac{\partial}{\partial t} B^{\dagger}_{\mathbf{q}_{\parallel},q_{\perp}} = -\hbar\omega_{\mathbf{q}} B^{\dagger}_{\mathbf{q}_{\parallel},q_{\perp}} + \mathrm{i}\hbar \sum_{\lambda,\mathbf{k}_{\parallel}} \mathsf{F}^{\lambda}_{\mathbf{q}_{\parallel},q_{\perp}} a^{\dagger}_{\bar{\lambda},\mathbf{k}_{\parallel}} a_{\lambda,\mathbf{k}_{\parallel}-\mathbf{q}_{\parallel}}. \tag{34}$$

Similarly, we find for the phonon-operator dynamics:

$$i\hbar\frac{\partial}{\partial t}D_{\mathbf{p}_\parallel,p_\perp} = \hbar\Omega_{\mathbf{p}}D_{\mathbf{p}_\parallel,p_\perp} + \hbar\sum_{\lambda,\mathbf{k}_\parallel}\mathsf{G}^{\lambda}_{\mathbf{p}_\parallel,p_\perp}a^{\dagger}_{\lambda,\mathbf{k}_\parallel}a_{\lambda,\mathbf{k}_\parallel+\mathbf{p}_\parallel}, \tag{35}$$

$$i\hbar\frac{\partial}{\partial t}D^{\dagger}_{\mathbf{p}_\parallel,p_\perp} = -\hbar\Omega_{\mathbf{p}}D^{\dagger}_{\mathbf{p}_\parallel,p_\perp} - \hbar\sum_{\lambda,\mathbf{k}_\parallel}\mathsf{G}^{\lambda}_{\mathbf{p}_\parallel,p_\perp}a^{\dagger}_{\lambda,\mathbf{k}_\parallel}a_{\lambda,\mathbf{k}_\parallel-\mathbf{p}_\parallel}. \tag{36}$$

Clearly, both the phonon and photon equations contain couplings to carrier operators. However, due to the simple form of Eqs. (33) and (35), the photon- and phonon-operator dynamics can be directly integrated to give

$$B_{\mathbf{q}_\parallel,q_\perp}(t) = B_{\mathbf{q}_\parallel,q_\perp}(0)\,\mathrm{e}^{-i\omega_{\mathbf{q}}t} + \sum_{\lambda,\mathbf{k}_\parallel}[\mathsf{F}^{\lambda}_{\mathbf{q}_\parallel,q_\perp}]^{\star}\int_0^t \mathrm{d}u\, a^{\dagger}_{\lambda,\mathbf{k}_\parallel}(u)a_{\bar{\lambda},\mathbf{k}_\parallel+\mathbf{q}_\parallel}(u)\,\mathrm{e}^{-i\omega_q(t-u)}, \tag{37}$$

$$D_{\mathbf{p}_\parallel,p_\perp}(t) = D_{\mathbf{p}_\parallel,p_\perp}(0)\,\mathrm{e}^{-i\Omega_p t} + i\sum_{\lambda,\mathbf{k}_\parallel}\mathsf{G}^{\lambda}_{\mathbf{p}_\parallel,p_\perp}\int_0^t \mathrm{d}u\, a^{\dagger}_{\lambda,\mathbf{k}_\parallel}(u)a_{\lambda,\mathbf{k}_\parallel+\mathbf{p}_\parallel}(u)\,\mathrm{e}^{-i\Omega_p(t-u)}. \tag{38}$$

These results show that both, a single photon or a single phonon operator are formally equivalent to a combination of two carrier operators. We will use this fact later on, when we introduce systematic truncation schemes for the hierarchy problem.

From a purely formal point of view, Eqs. (37)–(38) relate different classes of photon, phonon, and carrier operators. Clearly, a single photon or phonon operator corresponds to a single-particle operator. A general N-particle operator has the form

$$O_N = B^{\dagger}_1\ldots B^{\dagger}_{N_1}D^{\dagger}_1\ldots D^{\dagger}_{N_2}a^{\dagger}_1\ldots a^{\dagger}_{N_3}a_{N_3}\ldots a_1D_{N_4}\ldots D_1B_{N_5}\ldots B_1 \tag{39}$$

with all possible combinations of N_j fulfilling $N_1+N_2+N_3+N_4+N_5=N$. According to this classification, H_{C}, H_{P}, and H_{D} correspond to two-particle interactions. We also notice that the pure photon- and phonon-operator dynamics, Eqs. (33)–(36), involves only single-particle terms.

We find a more complicated dynamical equation for the carrier operators:

$$\begin{aligned} i\hbar\frac{\partial}{\partial t}a_{\lambda,\mathbf{k}_\parallel} = {} & \varepsilon^{\lambda}_{\mathbf{k}_\parallel}a_{\lambda,\mathbf{k}_\parallel} + \sum_{\lambda',\mathbf{k}'_\parallel,\mathbf{l}_\parallel}V_{\mathbf{l}_\parallel}a^{\dagger}_{\lambda',\mathbf{k}'_\parallel+\mathbf{l}_\parallel}a_{\lambda',\mathbf{k}'_\parallel}a_{\lambda,\mathbf{k}_\parallel+\mathbf{l}_\parallel} \\ & - i\hbar\sum_{\mathbf{q}_\parallel}[B^{\lambda}_{\mathbf{q}_\parallel,\Sigma} - (B^{\bar{\lambda}}_{-\mathbf{q}_\parallel,\Sigma})^{\dagger}]\,a_{\bar{\lambda},\mathbf{k}_\parallel-\mathbf{q}_\parallel} \\ & + \hbar\sum_{\mathbf{p}_\parallel}[D^{\lambda}_{\mathbf{p}_\parallel,\Sigma} + (D^{\lambda}_{-\mathbf{p}_\parallel,\Sigma})^{\dagger}]\,a_{\lambda,\mathbf{k}_\parallel-\mathbf{p}_\parallel}, \end{aligned} \tag{40}$$

$$i\hbar\frac{\partial}{\partial t}a^{\dagger}_{\lambda,\mathbf{k}_\parallel} = -\varepsilon^{\lambda}_{\mathbf{k}_\parallel}a^{\dagger}_{\lambda,\mathbf{k}_\parallel} - \sum_{\lambda',\mathbf{k}'_\parallel,\mathbf{l}_\parallel}V_{\mathbf{l}_\parallel}a^{\dagger}_{\lambda,\mathbf{k}_\parallel+\mathbf{l}_\parallel}a^{\dagger}_{\lambda',\mathbf{k}'_\parallel}a_{\lambda',\mathbf{k}'_\parallel+\mathbf{l}_\parallel}$$

$$+ \mathrm{i}\hbar \sum_{\mathbf{q}_\parallel} [B^{\bar{\lambda}}_{\mathbf{q}_\parallel,\Sigma} - (B^{\lambda}_{-\mathbf{q}_\parallel,\Sigma})^\dagger]\, a^\dagger_{\bar{\lambda},\mathbf{k}_\parallel+\mathbf{q}_\parallel}$$
$$- \hbar \sum_{\mathbf{p}_\parallel} [D^{\lambda}_{\mathbf{p}_\parallel,\Sigma} + (D^{\lambda}_{-\mathbf{p}_\parallel,\Sigma})^\dagger]\, a^\dagger_{\lambda,\mathbf{k}_\parallel+\mathbf{p}_\parallel}. \tag{41}$$

If we now analyze the structure of Eqs. (40)–(41) in detail, we notice terms that couple the dynamics of single-carrier operators to: (i) three-carrier operators due to the Coulomb interaction, (ii) a combination of a photon and a carrier operator due to the light–matter interaction, as well as (iii) one phonon and one carrier operator due to the carrier–phonon interaction. Since photon and phonon operators are formally equivalent to two-carrier operators, all these complicated terms effectively lead to the coupling of one-carrier operators to combinations of three-carrier operators. In general, Eqs. (33)–(36) and (40)–(41) can be applied directly to derive the dynamics of any generic N-particle operator (39).

Eqs. (33)–(36) and (40)–(41) are the first step in the infinite hierarchy of equations where the N-particle operator quantity is coupled to $N+1$ operators. Since the equations of motion for expectation values are directly obtained from those of the operators, the expectation values inherit the same hierarchy problem,

$$\mathrm{i}\hbar \frac{\partial}{\partial t} \langle N \rangle = T[\langle N \rangle] + V[\langle N+1 \rangle]. \tag{42}$$

Here, the functional T results mainly from the non-interacting part of the Hamiltonian while V originates from the interactions. These interactions couple the N-particle expectation value $\langle N \rangle$ to $\langle N+1 \rangle$ quantities. Consequently, Eq. (42) cannot be closed and we must resort to a systematic truncation scheme in order to obtain controlled approximations.

3.2. Cluster expansion

One successful approach to deal with the hierarchy problem is to use the so-called cluster-expansion scheme [18,39,43,45]. This approach is well established, e.g. in quantum chemistry where it is used to treat the many-body problems related to molecular eigenstates [40–42]. In semiconductor systems, this method has been used to analyze a variety of many-body and quantum-optical problems [18,26,37,43,45,46,53,54]. In the following, we first review the basic idea behind the cluster expansion and then discuss specific aspects that are relevant for the investigations of our semiconductor system.

The cluster-expansion method is based on a clear physical principle where one determines all consistent factorizations of an N-particle quantity $\langle N \rangle$ in terms of (i) independent single particles (singlets), (ii) correlated pairs (doublets), (iii) correlated three-particle clusters (triplets), up to (iv) correlated N-particle clusters. If we formally know all expectation values from $\langle 1 \rangle$ to $\langle N \rangle$, a specific correlated cluster can be constructed recursively using

$$\langle 2 \rangle = \langle 2 \rangle_{\mathrm{S}} + \Delta\langle 2 \rangle,$$

$$\langle 3 \rangle = \langle 3 \rangle_{\mathrm{S}} + \langle 1 \rangle \Delta\langle 2 \rangle + \Delta\langle 3 \rangle,$$
$$\langle N \rangle = \langle N \rangle_{\mathrm{S}} + \langle N-2 \rangle_{\mathrm{S}} \Delta\langle 2 \rangle + \langle N-4 \rangle_{\mathrm{S}} \Delta\langle 2 \rangle \Delta\langle 2 \rangle$$
$$+ \cdots + \langle N-3 \rangle_{\mathrm{S}} \Delta\langle 3 \rangle + \langle N-5 \rangle_{\mathrm{S}} \Delta\langle 2 \rangle \Delta\langle 3 \rangle + \cdots + \Delta\langle N \rangle. \tag{43}$$

Here, the quantities with the subscript S denote the singlet contributions and the terms $\Delta\langle J\rangle$ contain the purely correlated parts of the J-particle cluster. In Eq. (43), each term includes a sum over all *unique* possibilities to reorganize the N coordinates among singlets, doublets and so on. The different reorganizations are defined by permutations of operator indices. To guarantee the fundamental indistinguishability of particles, one must add up all the permutations. For Fermionic operators, one has to take a positive sign for even permutations and a negative sign for odd permutations. For Bosons, all permutations are added with a positive sign. This way, all cluster groups in Eq. (43) are fully antisymmetric for the Fermionic carriers and fully symmetric for the Bosonic photon and phonon operators, respectively.

To obtain more insights into the different contributions appearing in Eq. (43), we first consider the singlet factorization. For pure carrier-operator terms, we find the *Hartree–Fock factorization*

$$\langle a_1^\dagger \dots a_N^\dagger a_N \dots a_1\rangle_{\mathrm{S}} = \sum_\sigma (-1)^\sigma \prod_{j=1}^{N} \langle a_j^\dagger a_{\sigma[j]}\rangle, \tag{44}$$

where σ is an element of the permutation group with indices $1,\dots,N$. Specifically, $\sigma[j]$ defines the mapping of the index j under the permutation σ. In the sum over all permutations, the even permutations lead to $(-1)^\sigma = +1$ while the odd permutations lead to $(-1)^\sigma = -1$. Eq. (44) can be written in a more compact form by noting that it actually involves the determinant of a matrix, i.e.

$$M_{j,k} \equiv \langle a_j^\dagger a_k\rangle, \quad \langle a_1^\dagger \dots a_N^\dagger a_N \dots a_1\rangle_{\mathrm{S}} = \det(\mathbf{M}). \tag{45}$$

Pure photon or phonon terms or a mixture of them also allow for a simple singlet factorization

$$\langle b_1^\dagger \dots b_M^\dagger b_{M+1} \dots b_N\rangle_{\mathrm{S}} = \langle b_1^\dagger\rangle \dots \langle b_M^\dagger\rangle \langle b_{M+1}\rangle \dots \langle b_N\rangle, \tag{46}$$

where $M \leqslant N$ and b stands for a generic Boson operator (either photon or phonon) identified by its index. Eq. (46) clearly describes a classical factorization since each expectation value of a single Bosonic operator represents a complex-valued quantity, $\beta_j = \langle b_j\rangle$, such that one simply obtains the product of the different β_j. With this observation, we realize that also the combination of carrier and Boson operators produces a simple singlet contribution which is obtained by replacing each Boson operator by the corresponding classical β_j while the remaining pure carrier part can be factorized using Eq. (45).

The systematic cluster expansion is obtained by decomposing any given N-particle quantity into C-particle correlations,

$$\langle N\rangle_{1\dots\mathrm{C}} \equiv \langle N\rangle_{\mathrm{S}} + \langle N\rangle_{\mathrm{D}} + \dots + \langle N\rangle_{\mathrm{C}} = \sum_{J=1}^{C} \langle N\rangle_J, \tag{47}$$

following directly from Eq. (43). Here, $\langle N\rangle_{\mathrm{S}}$ contains only singlets, $\langle N\rangle_{\mathrm{D}}$ contains all combinations of doublets but no higher-order correlations and so on. The nature of the respective physical problem determines the lowest possible level at which one might truncate the cluster expansion. For example, one clearly needs calculations at least up to the doublet level for electron–hole systems containing bound pairs, i.e. excitons [18,29,55]. Increasingly more clusters have to be included if one wants to describe excitonic molecules

or even higher correlations [56,57]. For the light field, the singlet contributions describe the classical part of the field while the quantum fluctuations are determined by the higher order correlations. In many quantum-optical phenomena, decisive contributions result from the doublet correlation terms such as photon number and two-photon absorption correlations.

For many experimentally relevant situations, one can limit the description of the semiconductor system to a phase space where plasma and excitons coexist but higher order cluster are less important. In this regime, the singlet–doublet approximation describes a multitude of microscopic effects via the factorized N-particle expectation value $\langle N\rangle_{\mathrm{SD}}$. At this level of approximation, we need to solve the dynamics of all possible singlets $\langle 1\rangle$ and doublets $\Delta\langle 2\rangle$ because then any arbitrary $\langle N\rangle$ consist only of known combinations of single-particle expectation values and two-particle correlations.

To see the general structure of the relevant singlet–doublet equations, we start from Eq. (42) and apply the truncation (47) up to three-particle correlations (triplets)—i.e. one level higher than a pure singlet–doublet theory since we want to extend some investigations beyond the doublet level. We find the general equation structure

$$\mathrm{i}\hbar\frac{\partial}{\partial t}\langle 1\rangle = T_1[\langle 1\rangle] + V_{1a}[\langle 2\rangle_{\mathrm{S}}] + V_{1b}[\Delta\langle 2\rangle], \tag{48}$$

$$\mathrm{i}\hbar\frac{\partial}{\partial t}\Delta\langle 2\rangle = T_2[\Delta\langle 2\rangle] + V_{2a}[\langle 3\rangle_{\mathrm{SD}}] + V_{2b}[\Delta\langle 3\rangle], \tag{49}$$

$$\mathrm{i}\hbar\frac{\partial}{\partial t}\Delta\langle 3\rangle = T_3[\Delta\langle 3\rangle] + V_3[\langle 4\rangle_{\mathrm{SDT}}], \tag{50}$$

where $T_{1(2,3)}$ and $V_{1(2,3)}$ are known functionals defined by the respective Heisenberg equations of motion. In this form, the structure of the singlet and doublet equations is exact while only the triplet dynamics is approximated. Consequently, the hierarchy is systematically truncated resulting in a finite number of coupled equations.

The evaluation of the full singlet–doublet–triplet approximation, Eqs. (48)–(50), is still beyond current numerical capabilities if one wants to study QW or QWI systems. However, one can find clear physical principles to simplify the triplet dynamics (50) since it contains two distinct classes of contributions: (i) the microscopic processes describing scattering effects between two-particle correlations and single-particle quantities and (ii) interactions which are responsible for the formation of genuine three-particle correlations like trions. To the first category belong effects where correlated electron–hole pairs scatter with an electron, hole, or phonon. These interactions lead to screening of the Coulomb interaction, dephasing of the coherences, and formation or equilibration of exciton populations [18,29,55].

Since the formation of bound three-particle complexes is slow in QWs and QWIs after optical excitations and requires high densities beyond the exciton Mott transition to become relevant [56,57], we omit genuine three-particle correlations from the analysis. Thus, we end up with a consistent singlet–doublet approach where we treat triplet correlations at the scattering level. This leads us to the general equation structure

$$\mathrm{i}\hbar\frac{\partial}{\partial t}\langle 1\rangle = T_1[\langle 1\rangle] + V_1[\langle 2\rangle_{\mathrm{S}}] + V_1[\Delta\langle 2\rangle],$$

$$\mathrm{i}\hbar\frac{\partial}{\partial t}\Delta\langle 2\rangle = T_2[\Delta\langle 2\rangle] + V_2[\langle 3\rangle_{\mathrm{SD}}] + G[\langle 1\rangle, \Delta\langle 2\rangle]. \tag{51}$$

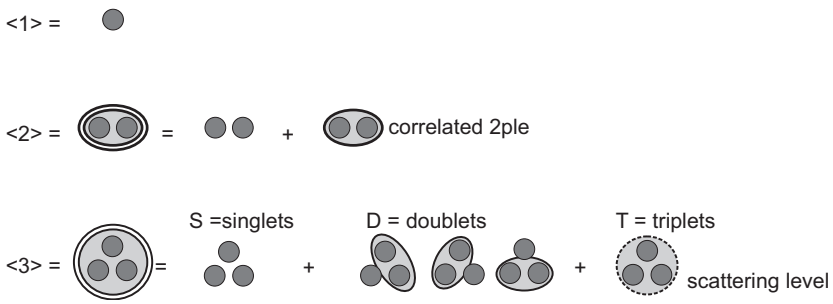

Fig. 1. Visualization of the cluster-expansion approach up to the level where singlets and doublets are fully included and the triplets are treated at the scattering level. The first line defines the singlets, the second line shows how the doublets are decomposed into their singlet contributions and the correlated part, and the third line depicts how the triplets are expanded into products of three singlets, products of correlated doublets and singlets, and correlated triplets which are replaced by the scattering-level approximation.

Here, the functional $G[\langle 1\rangle, \Delta\langle 2\rangle]$ indicates that three-particle correlations are included at the scattering level. The schematical structure of the approximation behind Eq. (51) is depicted in Fig. 1.

The pure one- and two-particle dynamics can now be obtained from Eq. (51) by evaluating the factorizations $\langle 2\rangle_{\mathrm{SD}}$ and $\langle 3\rangle_{\mathrm{SD}}$. For the detailed calculations, we explicitly need the different singlet–doublet factorizations which can be obtained directly by applying Eqs. (43) and (47) for any combination of carrier, photon, or phonon operators. The corresponding derivation of the singlet–doublet dynamics follows a straightforward procedure after one evaluates the explicit forms of the needed factorizations. This is done in Appendices C and D.

4. Singlet–doublet correlations

In this section, we start from Eqs. (48)–(50) and evaluate the general singlet–doublet approximation for the QW and QWI system. In particular, we now have to explicitly determine all functionals and their cluster-expansion factorizations. As discussed in Section 3.2, the closed set of Eqs. (51) truncates the infinite equation hierarchy systematically by including all possibilities to have two-particle correlations in the many-body system.

In practice, we explicitly evaluate the terms appearing in the singlet–doublet dynamics (48)–(49) by using the operator Eqs. (33)–(36) and (40)–(41) as well as the truncation formulas (C.3)–(C.13). The derivations are significantly simplified with the help of the compact-notation formalism introduced in Appendix B where the detailed derivations, definitions, and several useful relations are summarized. In the discussion here, we concentrate on the explicit physical content of the equations and therefore summarize only few important intermediate steps together with the results of the detailed derivations.

4.1. Singlet–doublet quantities for homogeneous excitation

We first set up the dynamical equations for the singlets

$$\langle 1\rangle = \{\langle a^{\dagger}_{\lambda,\mathbf{k}_{\parallel}} a_{\lambda',\mathbf{k}'_{\parallel}}\rangle, \langle B_{\mathbf{q}_{\parallel},q_{\perp}}\rangle, \text{or } \langle D_{\mathbf{p}_{\parallel},p_{\perp}}\rangle\}. \tag{52}$$

Generally, the momenta $\mathbf{k}_\parallel$ and $\mathbf{k}'_\parallel$ can be different. However, in this review we only consider situations where the system is excited with a homogeneous external light pulse propagating perpendicular to the QW (QWI) structure. In this configuration, all quantities are homogeneous and the corresponding two-point expectation values vanish for $\mathbf{k}_\parallel \neq \mathbf{k}'_\parallel$, $\mathbf{q}_\parallel \neq \mathbf{0}$, and $\mathbf{p}_\parallel \neq \mathbf{0}$. Thus, we can only have a difference in the band or spin index in the terms $\langle a^\dagger_{\lambda,\mathbf{k}_\parallel} a_{\lambda',\mathbf{k}'_\parallel}\rangle$, i.e.

$$\langle a^\dagger_{\lambda,\mathbf{k}_\parallel} a_{\lambda',\mathbf{k}'_\parallel}\rangle = \delta_{\mathbf{k}_\parallel,\mathbf{k}'_\parallel}\langle a^\dagger_{\lambda,\mathbf{k}_\parallel} a_{\lambda',\mathbf{k}_\parallel}\rangle. \tag{53}$$

In the same way, the homogeneous coherent light and phonon fields have

$$\langle B_{\mathbf{q}_\parallel,q_\perp}\rangle = \delta_{\mathbf{q}_\parallel,\mathbf{0}}\langle B_{\mathbf{0},q_\perp}\rangle, \quad \langle D_{\mathbf{p}_\parallel,p_\perp}\rangle = \delta_{\mathbf{p}_\parallel,\mathbf{0}}\langle D_{\mathbf{0},p_\perp}\rangle. \tag{54}$$

In order to have a more compact notation, we define

$$P^{\lambda,\lambda'}_{\mathbf{k}_\parallel} = \langle a^\dagger_{\lambda,\mathbf{k}_\parallel} a_{\lambda',\mathbf{k}_\parallel}\rangle, \quad n^\lambda_{\mathbf{k}_\parallel} \equiv P^{\lambda,\lambda}_{\mathbf{k}_\parallel} = \langle a^\dagger_{\lambda,\mathbf{k}_\parallel} a_{\lambda,\mathbf{k}_\parallel}\rangle, \tag{55}$$

where $P^{\lambda,\lambda'\neq\lambda}_{\mathbf{k}_\parallel}$ determines the microscopic polarization and $n^\lambda_{\mathbf{k}_\parallel}$ gives the microscopic carrier occupation probability for the band λ.

On our way to complete the equations for the singlet–doublet approach (48)–(49), we proceed to determine the dynamics of the doublet correlations generated under homogeneous conditions. As a consequence of the system's homogeneity, the combined in-plane momentum of all creation operators has to be equal to that of the annihilation operators in all correlation terms. For two-particle carrier correlations, we therefore have to demand that

$$\begin{aligned}\Delta\langle a^\dagger_{\lambda,\mathbf{k}_\parallel} a^\dagger_{v,\mathbf{k}'_\parallel} a_{v',\mathbf{k}''_\parallel} a_{\lambda',\mathbf{k}'''_\parallel}\rangle &= \delta_{\mathbf{k}_\parallel+\mathbf{k}'_\parallel,\mathbf{k}''_\parallel+\mathbf{k}'''_\parallel}\Delta\langle a^\dagger_{\lambda,\mathbf{k}_\parallel} a^\dagger_{v,\mathbf{k}'_\parallel} a_{v',\mathbf{k}''_\parallel} a_{\lambda',\mathbf{k}'''_\parallel}\rangle \\ &\equiv \delta_{\mathbf{k}''_\parallel,\mathbf{k}'_\parallel+\mathbf{q}_\parallel}\delta_{\mathbf{k}'''_\parallel,\mathbf{k}_\parallel-\mathbf{q}_\parallel}\Delta\langle a^\dagger_{\lambda,\mathbf{k}_\parallel} a^\dagger_{v,\mathbf{k}'_\parallel} a_{v',\mathbf{k}'_\parallel+\mathbf{q}_\parallel} a_{\lambda',\mathbf{k}_\parallel-\mathbf{q}_\parallel}\rangle,\end{aligned} \tag{56}$$

where the last step defines the momentum condition with the help of a new momentum $\mathbf{q}_\parallel$. This is performed because this identification simply presents the general form of the two-particle carrier correlations as they appear in the further derivations. In our subsequent calculations, we will often identify $\mathbf{q}_\parallel$ as the center-of-mass momentum of the correlated two-particle entities.

For later use, we introduce an abbreviation

$$c^{\mathbf{q}_\parallel,\mathbf{k}'_\parallel,\mathbf{k}_\parallel}_{\lambda,v;v',\lambda'} \equiv \Delta\langle a^\dagger_{\lambda,\mathbf{k}_\parallel} a^\dagger_{v,\mathbf{k}'_\parallel} a_{v',\mathbf{k}'_\parallel+\mathbf{q}_\parallel} a_{\lambda',\mathbf{k}_\parallel-\mathbf{q}_\parallel}\rangle \tag{57}$$

for the generic two-particle correlations. Here, the superscripts are arranged such that $\mathbf{q}_\parallel$ indicates the momentum transfer, whereas $\mathbf{k}'_\parallel$ and $\mathbf{k}_\parallel$ are the momentum indices of the second and first creation operator, respectively. The combination of creation and destruction operators in Eq. (57) shows that total momentum conservation is satisfied for all band indices $(\lambda, v, v', \lambda')$.

The doublet correlations with mixed combinations of carrier-, photon-, and phonon operators obey the same conservation law for the in-plane momentum as the pure carrier correlations. Thus, we find that only the combinations

$$\begin{aligned}\Delta\langle 2\rangle_{\mathrm{mix}} = \{&\Delta\langle B^\dagger_{\mathbf{q}_\parallel,q_\perp} a^\dagger_{v,\mathbf{k}_\parallel-\mathbf{q}_\parallel} a_{v',\mathbf{k}_\parallel}\rangle, \Delta\langle D^\dagger_{\mathbf{p}_\parallel,p_\perp} a^\dagger_{v,\mathbf{k}_\parallel-\mathbf{p}_\parallel} a_{v',\mathbf{k}_\parallel}\rangle, \\ &\Delta\langle B^\dagger_{\mathbf{q}_\parallel,q_\perp} D_{\mathbf{q}_\parallel,p_\perp}\rangle, \Delta\langle B_{\mathbf{q}_\parallel,q_\perp} D_{-\mathbf{q}_\parallel,p_\perp}\rangle\}\end{aligned} \tag{58}$$

are allowed. Furthermore, the pure photon and phonon correlations assume the generic form

$$\Delta\langle 2\rangle_{\rm bos} = \{\Delta\langle B^{\dagger}_{\mathbf{q}_\parallel,q_\perp} B_{\mathbf{q}_\parallel,q'_\perp}\rangle, \Delta\langle B_{\mathbf{q}_\parallel,q_\perp} B_{-\mathbf{q}_\parallel,q'_\perp}\rangle, \Delta\langle D^{\dagger}_{\mathbf{p}_\parallel,p_\perp} D_{\mathbf{p}_\parallel,p'_\perp}\rangle, \Delta\langle D_{\mathbf{p}_\parallel,p_\perp} D_{-\mathbf{p}_\parallel,p'_\perp}\rangle\}. \tag{59}$$

Eqs. (57)–(59) define the generic two-particle correlations of homogeneous systems.

4.2. Singlet dynamics

We start the analysis by investigating the singlet dynamics of the photons and phonons. For the situation where the system is excited with a classical light pulse, we can use Maxwell's equations to compute the optical properties. For a quantum-optical description, we have to solve Eqs. (33)–(34) and use the result in the mode expansion (9). If we assume that the light field propagates perpendicular to the planar QW (QWI) and differentiate the vector potential twice with respect to time, we obtain

$$\left[\frac{\partial^2}{\partial r_\perp^2} - \frac{n^2(r_\perp)}{c^2}\frac{\partial^2}{\partial t^2}\right]\langle A(\mathbf{0},r_\perp)\rangle = -\frac{\mu_0|\xi(r_\perp)|^2}{\mathsf{S}}\frac{\partial}{\partial t}\sum_{\mathbf{k}_\parallel,\lambda} d_{\lambda,\bar{\lambda}} P^{\lambda,\bar{\lambda}}_{\mathbf{k}_\parallel}, \tag{60}$$

as derived, e.g. in Refs. [48,26]. Using Eq. (12) we then find the usual wave equation

$$\left[\frac{\partial^2}{\partial r_\perp^2} - \frac{n^2(r_\perp)}{c^2}\frac{\partial^2}{\partial t^2}\right]\langle E(\mathbf{0},r_\perp)\rangle = \frac{\mu_0|\xi(r_\perp)|^2}{\mathsf{S}}\frac{\partial^2}{\partial t^2}\sum_{\mathbf{k}_\parallel,\lambda} d_{\lambda,\bar{\lambda}} P^{\lambda,\bar{\lambda}}_{\mathbf{k}_\parallel}. \tag{61}$$

The explicit mode expansion of the electric field depends on the used gauge [48,26]. However, one has the general expression,

$$E(\mathbf{r}) = \sum_{\mathbf{q}_\parallel,q_\perp}[\mathrm{i}\mathsf{E}_{q_\perp}\mathbf{U}_{\mathbf{q}_\parallel,q_\perp}(r_\perp)B_{\mathbf{0},q_\perp} - \mathrm{i}\mathsf{E}_{q_\perp}U^{\star}_{\mathbf{q}_\parallel,q_\perp}(r_\perp)B^{\dagger}_{\mathbf{0},q_\perp}], \tag{62}$$

for the field outside the QW (QWI). For later reference, it is convenient to define an effective electric field

$$E^{\lambda}_{\mathbf{q}_\parallel} \equiv \frac{d_{\lambda,\bar{\lambda}}}{\mathsf{S}}\int \mathrm{d}^3 r|\xi(r_\perp)|^2 E(\mathbf{r})\,\mathrm{e}^{-\mathrm{i}\mathbf{q}_\parallel\cdot\mathbf{r}_\parallel} = \mathrm{i}\hbar[B^{\lambda}_{\mathbf{q}_\parallel,\Sigma} - (B^{\bar{\lambda}}_{-\mathbf{q}_\parallel,\Sigma})^{\dagger}] \tag{63}$$

which follows directly from Eqs. (27)–(29).

To simplify the notation also for the phonon–carrier interaction problem, we define

$$Q^{\lambda}_{\mathbf{p}_\parallel} \equiv \hbar[D^{\lambda}_{\mathbf{p}_\parallel,\Sigma} + (D^{\lambda}_{-\mathbf{p}_\parallel,\Sigma})^{\dagger}] \tag{64}$$

in analogy to Eq. (63). These effective quantities have the following symmetry relations:

$$(E^{\lambda}_{\mathbf{q}_\parallel})^{\dagger} = E^{\bar{\lambda}}_{-\mathbf{q}_\parallel}, \quad E^{\lambda}_{\mathbf{q}_\parallel} = (E^{\bar{\lambda}}_{-\mathbf{q}_\parallel})^{\dagger}, \tag{65}$$

$$(Q^{\lambda}_{\mathbf{p}_\parallel})^{\dagger} = Q^{\lambda}_{-\mathbf{p}_\parallel}, \quad Q^{\lambda}_{\mathbf{p}_\parallel} = (Q^{\lambda}_{-\mathbf{p}_\parallel})^{\dagger}, \tag{66}$$

which are used frequently in the subsequent derivations.

The solution of the wave equation (61) describes the classical field in the presence of the induced optical polarization. An equivalent, alternative, solution is found by applying

Eq. (33) directly,

$$i\hbar\frac{\partial}{\partial t}\langle B_{\mathbf{0},q_\perp}\rangle = \hbar\omega_{q_\perp}\langle B_{\mathbf{0},q_\perp}\rangle + i\hbar\sum_{\lambda,\mathbf{k}_\parallel}[\mathsf{F}^{\lambda}_{\mathbf{0},q_\perp}]^{\star}P^{\lambda,\bar{\lambda}}_{\mathbf{k}_\parallel}, \tag{67}$$

and by using this result together with the mode expansion (9).

Similarly, the coherent phonon dynamics resulting from Eq. (35) is

$$i\hbar\frac{\partial}{\partial t}\langle D_{\mathbf{0},p_\perp}\rangle = \hbar\Omega_{p_\perp}\langle D_{\mathbf{0},p_\perp}\rangle + \hbar\sum_{\lambda,\mathbf{k}_\parallel} G^{\lambda}_{\mathbf{0},p_\perp} n^{\lambda}_{\mathbf{k}_\parallel}. \tag{68}$$

Since phonons are coupled to the macroscopic environment surrounding the QW (QWI), coherent phonons typically decay rapidly. In this review, we treat phonons only as a bath. This implies that

$$\langle D_{\mathbf{p}}\rangle = \langle D^{\dagger}_{\mathbf{p}}\rangle = 0, \tag{69}$$

i.e. the phonon effects are fully incoherent in all our investigations.

The classical light-field dynamics depends on the optical polarization in the semiconductor. To complete the singlet investigation, we therefore have to solve the $P^{\lambda,\lambda'}_{\mathbf{k}_\parallel}$ dynamics. Evaluating the corresponding Heisenberg equations of motion (40)–(41), we obtain

$$\begin{aligned} i\hbar\frac{\partial}{\partial t}P^{\lambda,\lambda'}_{\mathbf{k}_\parallel} &= (\varepsilon^{\lambda'}_{\mathbf{k}_\parallel} - \varepsilon^{\lambda}_{\mathbf{k}_\parallel})P^{\lambda,\lambda'}_{\mathbf{k}_\parallel} \\ &\quad + \sum_{v,\mathbf{k}'_\parallel,\mathbf{q}_\parallel\neq\mathbf{0}} V_{\mathbf{q}_\parallel}[\langle a^{\dagger}_{\lambda,\mathbf{k}_\parallel}a^{\dagger}_{v,\mathbf{k}'_\parallel}a_{v,\mathbf{k}'_\parallel+\mathbf{q}_\parallel}a_{\lambda',\mathbf{k}_\parallel-\mathbf{q}_\parallel}\rangle - \langle a^{\dagger}_{\lambda,\mathbf{k}_\parallel-\mathbf{q}_\parallel}a^{\dagger}_{v,\mathbf{k}'_\parallel+\mathbf{q}_\parallel}a_{v,\mathbf{k}'_\parallel}a_{\lambda',\mathbf{k}_\parallel}\rangle] \\ &\quad - \sum_{\mathbf{q}_\parallel}[\langle E^{\lambda'}_{\mathbf{q}_\parallel}a^{\dagger}_{\lambda,\mathbf{k}_\parallel}a_{\bar{\lambda}',\mathbf{k}_\parallel-\mathbf{q}_\parallel}\rangle - \langle (E^{\lambda}_{\mathbf{q}_\parallel})^{\dagger}a^{\dagger}_{\bar{\lambda},\mathbf{k}_\parallel-\mathbf{q}_\parallel}a_{\lambda',\mathbf{k}_\parallel}\rangle] \\ &\quad + \sum_{\mathbf{p}_\parallel}[\langle Q^{\lambda'}_{\mathbf{p}_\parallel}a^{\dagger}_{\lambda,\mathbf{k}_\parallel}a_{\lambda',\mathbf{k}_\parallel-\mathbf{p}_\parallel}\rangle - \langle (Q^{\lambda}_{\mathbf{p}_\parallel})^{\dagger}a^{\dagger}_{\lambda,\mathbf{k}_\parallel-\mathbf{p}_\parallel}a_{\lambda',\mathbf{k}_\parallel}\rangle], \end{aligned} \tag{70}$$

where $\bar{\lambda}$ inverts the band index as defined in Eq. (26). Eq. (70) shows that the polarization dynamics has exactly the form of the schematic Eq. (48). Hence, we can directly apply the cluster expansion to isolate the singlet and correlated-doublet contributions. With the help of Eqs. (C.2)–(C.4) we can write Eq. (70) as

$$\begin{aligned} i\hbar\frac{\partial}{\partial t}P^{\lambda,\lambda'}_{\mathbf{k}_\parallel} &= (\tilde{\varepsilon}^{\lambda'}_{\mathbf{k}_\parallel} - \tilde{\varepsilon}^{\lambda}_{\mathbf{k}_\parallel})P^{\lambda,\lambda'}_{\mathbf{k}_\parallel} + \Omega^{\lambda}_{\mathbf{k}_\parallel}P^{\bar{\lambda},\lambda'}_{\mathbf{k}_\parallel} - P^{\lambda,\bar{\lambda}'}_{\mathbf{k}_\parallel}\Omega^{\bar{\lambda}'}_{\mathbf{k}_\parallel} \\ &\quad + \sum_{v,\mathbf{k}'_\parallel,\mathbf{q}_\parallel\neq\mathbf{0}} V_{\mathbf{q}_\parallel}[c^{\mathbf{q}_\parallel,\mathbf{k}'_\parallel,\mathbf{k}_\parallel}_{\lambda,v;v,\lambda'} - (c^{\mathbf{q}_\parallel,\mathbf{k}'_\parallel,\mathbf{k}_\parallel}_{\lambda',v;v,\lambda})^{\star}] \\ &\quad - \sum_{\mathbf{q}_\parallel}[\Delta\langle E^{\lambda'}_{\mathbf{q}_\parallel}a^{\dagger}_{\lambda,\mathbf{k}_\parallel}a_{\bar{\lambda}',\mathbf{k}_\parallel-\mathbf{q}_\parallel}\rangle - \Delta\langle (E^{\lambda}_{\mathbf{q}_\parallel})^{\dagger}a^{\dagger}_{\bar{\lambda},\mathbf{k}_\parallel-\mathbf{q}_\parallel}a_{\lambda',\mathbf{k}_\parallel}\rangle] \\ &\quad + \sum_{\mathbf{q}_\parallel}[\Delta\langle Q^{\lambda}_{\mathbf{q}_\parallel}a^{\dagger}_{\lambda,\mathbf{k}_\parallel}a_{\lambda',\mathbf{k}_\parallel-\mathbf{q}_\parallel}\rangle - \Delta\langle (Q^{\lambda}_{\mathbf{q}_\parallel})^{\dagger}a^{\dagger}_{\lambda,\mathbf{k}_\parallel-\mathbf{q}_\parallel}a_{\lambda',\mathbf{k}_\parallel}\rangle]. \end{aligned} \tag{71}$$

Here, we defined the renormalized kinetic energy

$$\tilde{\varepsilon}^{\lambda}_{\mathbf{k}_\parallel} \equiv \varepsilon^{\lambda}_{\mathbf{k}_\parallel} - \sum_{\mathbf{k}'_\parallel} V_{\mathbf{k}'_\parallel-\mathbf{k}_\parallel}n^{\lambda}_{\mathbf{k}'_\parallel}, \tag{72}$$

and the renormalized Rabi frequency

$$\Omega^{\lambda}_{\mathbf{k}_\parallel} \equiv \langle E^{\lambda}_{\mathbf{0}} \rangle + \sum_{\mathbf{k}'_\parallel} V_{\mathbf{k}'_\parallel - \mathbf{k}_\parallel} P^{\lambda,\bar{\lambda}}_{\mathbf{k}'_\parallel}. \tag{73}$$

Eq. (71) is formally exact, and the quality of our results only depends on how systematically we are able to evaluate the correlated doublets.

4.3. Doublet dynamics

For our systematic treatment of the dynamical evolution of the correlated doublets $\Delta\langle 2\rangle$, we follow a general and straightforward procedure. The equations of motion of the full $\langle 2\rangle$ are obtained from Eqs. (33)–(36) and (40)–(41). Clearly, these equations are coupled to three-particle terms. At the same time, the equation for the correlated part of the doublets can formally be written as

$$\mathrm{i}\hbar \frac{\partial}{\partial t} \Delta\langle 2\rangle = \mathrm{i}\hbar \frac{\partial}{\partial t} \langle 2\rangle - \mathrm{i}\hbar \frac{\partial}{\partial t} \langle 2\rangle_{\mathrm{S}}, \tag{74}$$

where the part $\partial/\partial t\langle 2\rangle_{\mathrm{S}}$ is fully determined by the singlet dynamics. As a next step, we now apply the cluster expansion to the three-particle correlations $\langle 3\rangle$ using Eqs. (C.6)–(C.13). Following this procedure, the consistent singlet–doublet equations are obtained when the truly correlated $\Delta\langle 3\rangle$ are omitted. At this stage, our treatment corresponds to the level defined by Eqs. (48)–(49). As an improvement, we then include the triplets $\Delta\langle 3\rangle$ at the scattering level.

4.3.1. Pure photon and phonon correlations

Eqs. (33)–(36) for the photon and phonon operators couple single-particle operators to other single-particle operators. Thus, also the equations for the pure photon and phonon doublets do not introduce a hierarchy problem. When we apply Eq. (74) together with Eqs. (33)–(34), we find the generic photon-correlation dynamics:

$$\begin{aligned}
\mathrm{i}\hbar \frac{\partial}{\partial t} \Delta\langle B^{\dagger}_{\mathbf{q}_\parallel,q_\perp} B_{\mathbf{q}_\parallel,q'_\perp} \rangle &= \hbar(\omega_{\mathbf{q}'} - \omega_{\mathbf{q}}) \Delta\langle B^{\dagger}_{\mathbf{q}_\parallel,q_\perp} B_{\mathbf{q}_\parallel,q'_\perp} \rangle \\
&\quad + \mathrm{i}\hbar \sum_{\lambda,\mathbf{k}_\parallel} \mathsf{F}^{\lambda}_{\mathbf{q}_\parallel,q_\perp} \Delta\langle a^{\dagger}_{\bar{\lambda},\mathbf{k}_\parallel} a_{\lambda,\mathbf{k}_\parallel - \mathbf{q}_\parallel} B_{\mathbf{q}_\parallel,q'_\perp} \rangle \\
&\quad + \mathrm{i}\hbar \sum_{\lambda,\mathbf{k}_\parallel} [\mathsf{F}^{\lambda}_{\mathbf{q}_\parallel,q'_\perp}]^{\star} \Delta\langle B^{\dagger}_{\mathbf{q}_\parallel,q_\perp} a^{\dagger}_{\lambda,\mathbf{k}_\parallel - \mathbf{q}_\parallel} a_{\bar{\lambda},\mathbf{k}_\parallel} \rangle,
\end{aligned} \tag{75}$$

$$\begin{aligned}
\mathrm{i}\hbar \frac{\partial}{\partial t} \Delta\langle B^{\dagger}_{\mathbf{q}_\parallel,q_\perp} B^{\dagger}_{-\mathbf{q}_\parallel,q'_\perp} \rangle &= -\hbar(\omega_{\mathbf{q}'} + \omega_{\mathbf{q}}) \Delta\langle B^{\dagger}_{\mathbf{q}_\parallel,q_\perp} B^{\dagger}_{-\mathbf{q}_\parallel,q'_\perp} \rangle \\
&\quad + \mathrm{i}\hbar \sum_{\lambda,\mathbf{k}_\parallel} \mathsf{F}^{\lambda}_{\mathbf{q}_\parallel,q_\perp} \Delta\langle a^{\dagger}_{\bar{\lambda},\mathbf{k}_\parallel} a_{\lambda,\mathbf{k}_\parallel - \mathbf{q}_\parallel} B^{\dagger}_{-\mathbf{q}_\parallel,q'_\perp} \rangle \\
&\quad + \mathrm{i}\hbar \sum_{\lambda,\mathbf{k}_\parallel} \mathsf{F}^{\lambda}_{-\mathbf{q}_\parallel,q'_\perp} \Delta\langle B^{\dagger}_{\mathbf{q}_\parallel,q_\perp} a^{\dagger}_{\bar{\lambda},\mathbf{k}_\parallel - \mathbf{q}_\parallel} a_{\lambda,\mathbf{k}_\parallel} \rangle.
\end{aligned} \tag{76}$$

These equations couple the photon correlations to other doublet-correlation terms with mixed photon-carrier operators. Consequently, the quality level of the solutions depends

only on the accuracy with which the mixed carrier–photon terms in Eqs. (75)–(76) can be evaluated.

Using Eqs. (35)–(36) together with Eq. (74), we obtain the dynamics for the pure phonon correlations:

$$\begin{aligned}
\mathrm{i}\hbar\frac{\partial}{\partial t}\Delta\langle D^{\dagger}_{\mathbf{p}_\parallel,p_\perp}D_{\mathbf{p}_\parallel,p'_\perp}\rangle &= \hbar(\Omega_{\mathbf{p}'}-\Omega_{\mathbf{p}})\Delta\langle D^{\dagger}_{\mathbf{p}_\parallel,p_\perp}D_{\mathbf{p}_\parallel,p'_\perp}\rangle \\
&\quad-\hbar\sum_{\lambda,\mathbf{k}_\parallel}\mathsf{G}^{\lambda}_{\mathbf{p}_\parallel,p_\perp}\Delta\langle a^{\dagger}_{\lambda,\mathbf{k}_\parallel}a_{\lambda,\mathbf{k}_\parallel-\mathbf{p}_\parallel}D_{\mathbf{p}_\parallel,p'_\perp}\rangle \\
&\quad+\hbar\sum_{\lambda,\mathbf{k}_\parallel}\mathsf{G}^{\lambda}_{\mathbf{p}_\parallel,p'_\perp}\Delta\langle D^{\dagger}_{\mathbf{p}_\parallel,p_\perp}a^{\dagger}_{\lambda,\mathbf{k}_\parallel}a_{\lambda,\mathbf{k}_\parallel+\mathbf{p}_\parallel}\rangle, \qquad (77)
\end{aligned}$$

$$\begin{aligned}
\mathrm{i}\hbar\frac{\partial}{\partial t}\Delta\langle D^{\dagger}_{\mathbf{p}_\parallel,p_\perp}D^{\dagger}_{-\mathbf{p}_\parallel,p'_\perp}\rangle &= -\hbar(\Omega_{\mathbf{p}'}+\Omega_{\mathbf{p}})\Delta\langle D^{\dagger}_{\mathbf{p}_\parallel,p_\perp}D^{\dagger}_{-\mathbf{p}_\parallel,p'_\perp}\rangle \\
&\quad+\hbar\sum_{\lambda,\mathbf{k}_\parallel}\mathsf{G}^{\lambda}_{\mathbf{p}_\parallel,p_\perp}\Delta\langle a^{\dagger}_{\lambda,\mathbf{k}_\parallel}a_{\lambda,\mathbf{k}_\parallel-\mathbf{p}_\parallel}D^{\dagger}_{-\mathbf{p}_\parallel,p'_\perp}\rangle \\
&\quad+\hbar\sum_{\lambda,\mathbf{k}_\parallel}\mathsf{G}^{\lambda}_{-\mathbf{p}_\parallel,p'_\perp}\Delta\langle D^{\dagger}_{\mathbf{p}_\parallel,p_\perp}a^{\dagger}_{\bar{\lambda},\mathbf{k}_\parallel}a_{\lambda,\mathbf{k}_\parallel+\mathbf{p}_\parallel}\rangle. \qquad (78)
\end{aligned}$$

Due to the structural similarity between the phonon and the photon dynamics, we can immediately draw the corresponding conclusions. In particular, we know that the quality of the phonon correlations depends only on the accuracy of the solutions obtained for the mixed phonon–carrier terms. We can also verify in a straightforward manner that the mixed terms in Eqs. (75)–(78) satisfy the homogeneous conditions (58).

4.3.2. Mixed carrier–photon–phonon correlations

The simplest mixed-operator correlation dynamics is obtained for combinations of a photon and a phonon operator. Using Eqs. (33)–(36), we find

$$\begin{aligned}
\mathrm{i}\hbar\frac{\partial}{\partial t}\Delta\langle B^{\dagger}_{\mathbf{q}_\parallel,q_\perp}D_{\mathbf{q}_\parallel,q'_\perp}\rangle &= \hbar(\Omega_{\mathbf{q}'}-\omega_{\mathbf{q}})\Delta\langle B^{\dagger}_{\mathbf{q}_\parallel,q_\perp}D_{\mathbf{q}_\parallel,q'_\perp}\rangle \\
&\quad+\mathrm{i}\hbar\sum_{\lambda,\mathbf{k}_\parallel}\mathsf{F}^{\lambda}_{\mathbf{q}_\parallel,q_\perp}\Delta\langle a^{\dagger}_{\bar{\lambda},\mathbf{k}_\parallel}a_{\lambda,\mathbf{k}_\parallel-\mathbf{q}_\parallel}D_{\mathbf{q}_\parallel,q'_\perp}\rangle \\
&\quad+\hbar\sum_{\lambda,\mathbf{k}_\parallel}\mathsf{G}^{\lambda}_{\mathbf{p}_\parallel,p'_\perp}\Delta\langle B^{\dagger}_{\mathbf{p}_\parallel,p_\perp}a^{\dagger}_{\lambda,\mathbf{k}_\parallel}a_{\lambda,\mathbf{k}_\parallel+\mathbf{p}_\parallel}\rangle, \qquad (79)
\end{aligned}$$

$$\begin{aligned}
\mathrm{i}\hbar\frac{\partial}{\partial t}\Delta\langle B^{\dagger}_{\mathbf{q}_\parallel,q_\perp}D^{\dagger}_{-\mathbf{q}_\parallel,q'_\perp}\rangle &= -\hbar(\omega_{\mathbf{q}'}+\Omega_{\mathbf{q}})\Delta\langle B^{\dagger}_{\mathbf{q}_\parallel,q_\perp}D^{\dagger}_{-\mathbf{q}_\parallel,q'_\perp}\rangle \\
&\quad+\mathrm{i}\hbar\sum_{\lambda,\mathbf{k}_\parallel}\mathsf{F}^{\lambda}_{\mathbf{q}_\parallel,q_\perp}\Delta\langle a^{\dagger}_{\bar{\lambda},\mathbf{k}_\parallel}a_{\lambda,\mathbf{k}_\parallel-\mathbf{q}_\parallel}D^{\dagger}_{-\mathbf{q}_\parallel,q'_\perp}\rangle \\
&\quad+\hbar\sum_{\lambda,\mathbf{k}_\parallel}\mathsf{G}^{\lambda}_{\mathbf{p}_\parallel,p_\perp}\Delta\langle a^{\dagger}_{\lambda,\mathbf{k}_\parallel}a_{\lambda,\mathbf{k}_\parallel-\mathbf{p}_\parallel}B^{\dagger}_{-\mathbf{p}_\parallel,p'_\perp}\rangle. \qquad (80)
\end{aligned}$$

Again, as in the case of the pure photon and phonon-correlation dynamics, Eqs. (79)–(80) do not directly lead to a hierarchy problem. However, in order to solve Eqs. (75)–(80), we need the explicit equations for the mixed photon–carrier and the phonon–carrier

correlations, i.e.

$$\Pi^{\lambda',\lambda}_{\mathbf{k}_\parallel;\mathbf{q}_\parallel,q_\perp} \equiv \Delta\langle B^\dagger_{\mathbf{q}_\parallel,q_\perp} a^\dagger_{\lambda',\mathbf{k}_\parallel-\mathbf{q}_\parallel} a_{\lambda,\mathbf{k}_\parallel}\rangle, \tag{81}$$

$$\Xi^{\lambda',\lambda}_{\mathbf{k}_\parallel;\mathbf{q}_\parallel,p_\perp} \equiv \Delta\langle D^\dagger_{\mathbf{q}_\parallel,p_\perp} a^\dagger_{\lambda',\mathbf{k}_\parallel-\mathbf{q}_\parallel} a_{\lambda,\mathbf{k}_\parallel}\rangle, \tag{82}$$

respectively. Here, $\Pi^{\lambda',\lambda}$ describes photon-assisted carrier correlations while $\Xi^{\lambda',\lambda}$ is related to phonon-assisted carrier correlations. As we will see, these correlations do involve hierarchy problems.

The photon-assisted carrier correlation dynamics can be obtained in the spirit of Eq. (74) by implementing Eqs. (34) and (40)–(41) together with the singlet–doublet factorizations (C.3)–(C.13). Following this procedure, we find

$$\begin{aligned}
i\hbar\frac{\partial}{\partial t}\Pi^{\lambda',\lambda}_{\mathbf{k}_\parallel;\mathbf{q}_\parallel,q_\perp} &= (\tilde{\varepsilon}^{\lambda}_{\mathbf{k}_\parallel} - \tilde{\varepsilon}^{\lambda'}_{\mathbf{k}_\parallel-\mathbf{q}_\parallel} - \hbar\omega_{\mathbf{q}})\Pi^{\lambda',\lambda}_{\mathbf{k}_\parallel;\mathbf{q}_\parallel,q_\perp} \\
&\quad + (n^{\lambda}_{\mathbf{k}_\parallel} - n^{\lambda'}_{\mathbf{k}_\parallel-\mathbf{q}_\parallel})\sum_{\mathbf{l}_\parallel} V_{\mathbf{l}_\parallel-\mathbf{k}_\parallel}\Pi^{\lambda',\lambda}_{\mathbf{l}_\parallel;\mathbf{q}_\parallel,q_\perp} \\
&\quad + P^{\bar{\lambda},\lambda}_{\mathbf{k}_\parallel}\sum_{\mathbf{l}_\parallel} V_{\mathbf{l}_\parallel-\mathbf{k}_\parallel}\Pi^{\lambda',\bar{\lambda}}_{\mathbf{l}_\parallel;\mathbf{q}_\parallel,q_\perp} - P^{\lambda',\bar{\lambda}'}_{\mathbf{k}_\parallel}\sum_{\mathbf{l}_\parallel} V_{\mathbf{l}_\parallel-\mathbf{k}_\parallel}\Pi^{\bar{\lambda}',\lambda}_{\mathbf{l}_\parallel;\mathbf{q}_\parallel,q_\perp} \\
&\quad + P^{\bar{\lambda}',\lambda}_{\mathbf{k}_\parallel}\Delta\langle B^\dagger_{\mathbf{q}_\parallel,q_\perp} E^{\lambda'}_{\mathbf{q}_\parallel}\rangle - P^{\lambda',\bar{\lambda}}_{\mathbf{k}_\parallel-\mathbf{q}_\parallel}\Delta\langle B^\dagger_{\mathbf{q}_\parallel,q_\perp} E^{\bar{\lambda}}_{\mathbf{q}_\parallel}\rangle \\
&\quad + \Pi^{\bar{\lambda}',\lambda}_{\mathbf{k}_\parallel;\mathbf{q}_\parallel,q_\perp}\Omega^{\lambda'}_{\mathbf{k}_\parallel-\mathbf{q}_\parallel} - \Pi^{\lambda',\bar{\lambda}}_{\mathbf{k}_\parallel;\mathbf{q}_\parallel,q_\perp}\Omega^{\bar{\lambda}}_{\mathbf{k}_\parallel} \\
&\quad + i\hbar\left[\mathsf{F}^{\lambda'}_{\mathbf{q}} P^{\bar{\lambda}',\lambda}_{\mathbf{k}_\parallel}(1-n^{\lambda'}_{\mathbf{k}_\parallel-\mathbf{q}_\parallel}) - \mathsf{F}^{\bar{\lambda}'}_{\mathbf{q}} P^{\lambda',\lambda}_{\mathbf{k}_\parallel} P^{\lambda',\bar{\lambda}'}_{\mathbf{k}_\parallel-\mathbf{q}_\parallel} + \sum_{v,\mathbf{k}'_\parallel}\mathsf{F}^{v}_{\mathbf{q}}(c^{\mathbf{q}_\parallel,\mathbf{k}'_\parallel,\mathbf{k}_\parallel}_{\lambda,v;\bar{v},\lambda'})^\star\right] \\
&\quad + P^{\lambda',\lambda}_{\mathbf{k}_\parallel-\mathbf{q}_\parallel}\Delta\langle B^\dagger_{\mathbf{q}_\parallel,q_\perp} Q^{\lambda}_{\mathbf{q}_\parallel}\rangle - P^{\lambda',\lambda}_{\mathbf{k}_\parallel}\Delta\langle B^\dagger_{\mathbf{q}_\parallel,q_\perp} Q^{\lambda'}_{\mathbf{q}_\parallel}\rangle \\
&\quad + V_{\mathbf{q}_\parallel}(P^{\lambda',\lambda}_{\mathbf{k}_\parallel-\mathbf{q}_\parallel} - P^{\lambda',\lambda}_{\mathbf{k}_\parallel})\sum_{v,\mathbf{l}_\parallel}\Pi^{v,v}_{\mathbf{l}_\parallel;\mathbf{q}_\parallel,q_\perp} + V[\Pi^{\lambda',\lambda}_{\mathbf{k}_\parallel;\mathbf{q}_\parallel,q_\perp}]_{\mathrm{T}}.
\end{aligned} \tag{83}$$

Here, the last term contains the genuine three-particle correlations

$$\begin{aligned}
V[\Pi^{\lambda',\lambda}_{\mathbf{k}_\parallel;\mathbf{q}_\parallel,q_\perp}]_{\mathrm{T}} = &\sum_{v,\mathbf{k}'_\parallel,\mathbf{l}_\parallel}(V_{\mathbf{l}_\parallel}\Delta\langle B^\dagger_{\mathbf{q}_\parallel,q_\perp} a^\dagger_{\lambda',\mathbf{k}_\parallel-\mathbf{q}_\parallel} a^\dagger_{v,\mathbf{k}'_\parallel+\mathbf{q}_\parallel} a_{v,\mathbf{k}'_\parallel+\mathbf{l}_\parallel} a_{\lambda,\mathbf{k}_\parallel-\mathbf{l}_\parallel}\rangle \\
&- V_{\mathbf{l}_\parallel-\mathbf{q}_\parallel}\Delta\langle B^\dagger_{\mathbf{q}_\parallel,q_\perp} a^\dagger_{\lambda',\mathbf{k}_\parallel-\mathbf{l}_\parallel} a^\dagger_{v,\mathbf{k}'_\parallel+\mathbf{l}_\parallel} a_{v,\mathbf{k}'_\parallel} a_{\lambda,\mathbf{k}_\parallel}\rangle) \\
&- \sum_{\mathbf{l}_\parallel}(\Delta\langle B^\dagger_{\mathbf{q}_\parallel,q_\perp} E^{\bar{\lambda}}_{\mathbf{l}_\parallel} a^\dagger_{\lambda',\mathbf{k}_\parallel-\mathbf{q}_\parallel} a_{\bar{\lambda},\mathbf{k}_\parallel-\mathbf{l}_\parallel}\rangle \\
&- \Delta\langle B^\dagger_{\mathbf{q}_\parallel,q_\perp} E^{\lambda'}_{\mathbf{q}_\parallel-\mathbf{l}_\parallel} a^\dagger_{\bar{\lambda}',\mathbf{k}_\parallel-\mathbf{l}_\parallel} a_{\lambda,\mathbf{k}_\parallel}\rangle) \\
&+ \sum_{\mathbf{l}_\parallel}(\Delta\langle B^\dagger_{\mathbf{q}_\parallel,q_\perp} Q^{\lambda}_{\mathbf{l}_\parallel} a^\dagger_{\lambda',\mathbf{k}_\parallel-\mathbf{q}_\parallel} a_{\lambda,\mathbf{k}_\parallel-\mathbf{l}_\parallel}\rangle \\
&- \Delta\langle B^\dagger_{\mathbf{q}_\parallel,q_\perp} Q^{\lambda'}_{\mathbf{q}_\parallel-\mathbf{l}_\parallel} a^\dagger_{\lambda',\mathbf{k}_\parallel-\mathbf{l}_\parallel} a_{\lambda,\mathbf{k}_\parallel}\rangle).
\end{aligned} \tag{84}$$

Clearly, these three-particle correlation terms fully conserve the in-plane momentum as demanded by the homogeneity condition discussed in Section 4.1.

In an analogous way, the dynamics of the phonon-assisted carrier correlations is derived as

$$
\begin{aligned}
\mathrm{i}\hbar\frac{\partial}{\partial t}\,\Xi^{\lambda',\lambda}_{\mathbf{k}_\parallel;\mathbf{q}_\parallel,q_\perp} &= (\tilde{\varepsilon}^{\lambda}_{\mathbf{k}_\parallel}-\tilde{\varepsilon}^{\lambda'}_{\mathbf{k}_\parallel-\mathbf{q}_\parallel}-\hbar\omega_{\mathbf{q}})\Xi^{\lambda',\lambda}_{\mathbf{k}_\parallel;\mathbf{q}_\parallel,q_\perp}\\
&\quad+(n^{\lambda}_{\mathbf{k}_\parallel}-n^{\lambda'}_{\mathbf{k}_\parallel-\mathbf{q}_\parallel})\sum_{\mathbf{l}_\parallel}V_{\mathbf{l}_\parallel-\mathbf{k}_\parallel}\Xi^{\lambda',\lambda}_{\mathbf{l}_\parallel;\mathbf{q}_\parallel,q_\perp}\\
&\quad+P^{\bar{\lambda},\lambda}_{\mathbf{k}_\parallel}\sum_{\mathbf{l}_\parallel}V_{\mathbf{l}_\parallel-\mathbf{k}_\parallel}\Xi^{\lambda',\bar{\lambda}}_{\mathbf{l}_\parallel;\mathbf{q}_\parallel,q_\perp}-P^{\lambda',\bar{\lambda}'}_{\mathbf{k}_\parallel-\mathbf{q}_\parallel}\sum_{\mathbf{l}_\parallel}V_{\mathbf{l}_\parallel-\mathbf{k}_\parallel}\Xi^{\bar{\lambda}',\lambda}_{\mathbf{l}_\parallel;\mathbf{q}_\parallel,q_\perp}\\
&\quad+P^{\bar{\lambda}',\lambda}_{\mathbf{k}_\parallel}\Delta\langle D^{\dagger}_{\mathbf{q}_\parallel,q_\perp}E^{\lambda'}_{\mathbf{q}_\parallel}\rangle-P^{\lambda',\bar{\lambda}}_{\mathbf{k}_\parallel}\Delta\langle D^{\dagger}_{\mathbf{q}_\parallel,q_\perp}E^{\bar{\lambda}}_{\mathbf{q}_\parallel}\rangle\\
&\quad+\Xi^{\bar{\lambda}',\lambda}_{\mathbf{k}_\parallel;\mathbf{q}_\parallel,q_\perp}\Omega^{\lambda'}_{\mathbf{k}_\parallel-\mathbf{q}_\parallel}-\Xi^{\lambda',\bar{\lambda}}_{\mathbf{k}_\parallel;\mathbf{q}_\parallel,q_\perp}\Omega^{\bar{\lambda}}_{\mathbf{k}_\parallel}\\
&\quad-\hbar\left[\mathsf{G}^{\lambda'}_{\mathbf{q}}P^{\lambda',\lambda}_{\mathbf{k}_\parallel}(1-n^{\lambda'}_{\mathbf{k}_\parallel-\mathbf{q}_\parallel})-\mathsf{F}^{\bar{\lambda}'}_{\mathbf{q}}P^{\bar{\lambda}',\lambda}_{\mathbf{k}_\parallel}P^{\lambda',\bar{\lambda}'}_{\mathbf{k}_\parallel-\mathbf{q}_\parallel}+\sum_{\nu,\mathbf{k}'_\parallel}\mathsf{G}^{\nu}_{\mathbf{q}}(c^{\mathbf{q}_\parallel,\mathbf{k}'_\parallel,\mathbf{k}_\parallel}_{\lambda,\nu;\nu,\lambda'})^{\star}\right]\\
&\quad+P^{\lambda',\lambda}_{\mathbf{k}_\parallel-\mathbf{q}_\parallel}\Delta\langle D^{\dagger}_{\mathbf{q}_\parallel,q_\perp}Q^{\lambda}_{\mathbf{q}_\parallel}\rangle-P^{\lambda',\lambda}_{\mathbf{k}_\parallel}\Delta\langle D^{\dagger}_{\mathbf{q}_\parallel,q_\perp}Q^{\lambda'}_{\mathbf{q}_\parallel}\rangle\\
&\quad+V_{\mathbf{q}_\parallel}(P^{\lambda',\lambda}_{\mathbf{k}_\parallel-\mathbf{q}_\parallel}-P^{\lambda',\lambda}_{\mathbf{k}_\parallel})\sum_{\nu,\mathbf{l}_\parallel}\Xi^{\nu,\nu}_{\mathbf{l}_\parallel;\mathbf{q}_\parallel,q_\perp}+V[\Xi^{\lambda',\lambda}_{\mathbf{k}_\parallel;\mathbf{q}_\parallel,q_\perp}]_{\mathrm{T}}. \qquad (85)
\end{aligned}
$$

Here, the triplet scattering terms have the generic form

$$
\begin{aligned}
&V[\Xi^{\lambda',\lambda}_{\mathbf{k}_\parallel;\mathbf{q}_\parallel,q_\perp}]_{\mathrm{T}}\\
&\quad=\sum_{\nu,\mathbf{k}'_\parallel,\mathbf{l}_\parallel}(V_{\mathbf{l}_\parallel}\Delta\langle D^{\dagger}_{\mathbf{q}_\parallel,q_\perp}a^{\dagger}_{\lambda',\mathbf{k}_\parallel-\mathbf{q}_\parallel}a^{\dagger}_{\nu,\mathbf{k}'_\parallel+\mathbf{q}_\parallel}a_{\nu,\mathbf{k}'_\parallel+\mathbf{l}_\parallel}a_{\lambda,\mathbf{k}_\parallel-\mathbf{l}_\parallel}\rangle\\
&\qquad-V_{\mathbf{l}_\parallel-\mathbf{q}_\parallel}\Delta\langle D^{\dagger}_{\mathbf{q}_\parallel,q_\perp}a^{\dagger}_{\lambda',\mathbf{k}_\parallel-\mathbf{l}_\parallel}a^{\dagger}_{\nu,\mathbf{k}'_\parallel+\mathbf{l}_\parallel}a_{\nu,\mathbf{k}'_\parallel}a_{\lambda,\mathbf{k}_\parallel}\rangle)\\
&\qquad-\sum_{\mathbf{l}_\parallel}(\Delta\langle D^{\dagger}_{\mathbf{q}_\parallel,q_\perp}E^{\bar{\lambda}}_{\mathbf{l}_\parallel}a^{\dagger}_{\lambda',\mathbf{k}_\parallel-\mathbf{q}_\parallel}a_{\bar{\lambda},\mathbf{k}_\parallel-\mathbf{l}_\parallel}\rangle-\Delta\langle D^{\dagger}_{\mathbf{q}_\parallel,q_\perp}E^{\lambda'}_{\mathbf{q}_\parallel-\mathbf{l}_\parallel}a^{\dagger}_{\bar{\lambda}',\mathbf{k}_\parallel-\mathbf{l}_\parallel}a_{\lambda,\mathbf{k}_\parallel}\rangle)\\
&\qquad+\sum_{\mathbf{l}_\parallel}(\Delta\langle D^{\dagger}_{\mathbf{q}_\parallel,q_\perp}Q^{\lambda}_{\mathbf{l}_\parallel}a^{\dagger}_{\lambda',\mathbf{k}_\parallel-\mathbf{q}_\parallel}a_{\lambda,\mathbf{k}_\parallel-\mathbf{l}_\parallel}\rangle-\Delta\langle D^{\dagger}_{\mathbf{q}_\parallel,q_\perp}Q^{\lambda'}_{\mathbf{q}_\parallel-\mathbf{l}_\parallel}a^{\dagger}_{\lambda',\mathbf{k}_\parallel-\mathbf{l}_\parallel}a_{\lambda,\mathbf{k}_\parallel}\rangle). \qquad (86)
\end{aligned}
$$

Once again, Eqs. (83) and (85) are formally exact for homogeneous excitation conditions. The quality of the solutions depends only on the accuracy of the results for the triplets.

4.3.3. Pure carrier correlations

For the completion of our singlet–doublet analysis, we still need to determine the explicit form of the pure carrier correlation dynamics. Because of the Fermionic nature of the charge carriers, the pure carrier doublets exhibit an internal antisymmetry with respect to the exchange of any two annihilation or creation operators. Consequently, $c_{\lambda,\nu;\nu',\lambda'}$ satisfies the general symmetries

$$
c^{\mathbf{q}_\parallel,\mathbf{k}'_\parallel,\mathbf{k}_\parallel}_{\lambda,\nu;\nu',\lambda'}=c^{-\mathbf{q}_\parallel,\mathbf{k}_\parallel,\mathbf{k}'_\parallel}_{\nu,\lambda;\lambda',\nu'}, \qquad (87)
$$

$$
c^{\mathbf{q}_\parallel,\mathbf{k}'_\parallel,\mathbf{k}_\parallel}_{\lambda,\nu;\nu',\lambda'}=-c^{-\mathbf{j}_\parallel,\mathbf{k}'_\parallel,\mathbf{k}_\parallel}_{\lambda,\nu;\lambda',\nu'}, \qquad (88)
$$

$$c^{\mathbf{q}_\parallel,\mathbf{k}'_\parallel,\mathbf{k}_\parallel}_{\lambda,v;v',\lambda'} = -c^{\mathbf{j}_\parallel,\mathbf{k}_\parallel,\mathbf{k}'_\parallel}_{v,\lambda;v',\lambda'}, \tag{89}$$

where we have identified a momentum combination

$$\mathbf{j}_\parallel \equiv \mathbf{k}'_\parallel + \mathbf{q}_\parallel - \mathbf{k}_\parallel. \tag{90}$$

Eq. (87) follows from the simultaneous exchange of creation and annihilation operators, whereas Eqs. (89) and (88) are obtained by exchanging either just the annihilation or just the creation operators, respectively.

In general, the symmetry relations (87)–(89) help us to identify the different terms related to the different possibilities of exchanging Fermi operators in the expressions for the doublet dynamics. In fact, it always is a good idea check to verify that the derived singlet–doublet dynamics indeed obeys the conditions (87)–(89) which are required because of the Fermionic antisymmetry of the many-body system. For this check, it is useful to define a *Fermionic antisymmetry operator*

$$\mathrm{Sym_F}([]^{\mathbf{q}_\parallel,\mathbf{k}'_\parallel,\mathbf{k}_\parallel}_{\lambda,v;v',\lambda'}) = []^{\mathbf{q}_\parallel,\mathbf{k}'_\parallel,\mathbf{k}_\parallel}_{\lambda,v;v',\lambda'} + []^{-\mathbf{q}_\parallel,\mathbf{k}_\parallel,\mathbf{k}'_\parallel}_{v,\lambda;\lambda',v'} - []^{-\mathbf{j}_\parallel,\mathbf{k}'_\parallel,\mathbf{k}_\parallel}_{\lambda,v;\lambda',v'} - []^{\mathbf{j}_\parallel,\mathbf{k}_\parallel,\mathbf{k}'_\parallel}_{v,\lambda;v'\lambda'}, \tag{91}$$

for a generic correlation quantity $[]^{\mathbf{q}_\parallel,\mathbf{k}'_\parallel,\mathbf{k}_\parallel}_{\lambda,v;v',\lambda'}$. This operator produces the following properties for two correlations, denoted by c and $\tilde{c}$, yielding

$$\mathrm{Sym_F}(c^{\mathbf{q}_\parallel,\mathbf{k}'_\parallel,\mathbf{k}_\parallel}_{\lambda,v;v',\lambda'}) = 4c^{\mathbf{q}_\parallel,\mathbf{k}'_\parallel,\mathbf{k}_\parallel}_{\lambda,v;v',\lambda'}, \tag{92}$$

$$\begin{aligned}\mathrm{Sym_F}([c+\tilde{c}]^{\mathbf{q}_\parallel,\mathbf{k}'_\parallel,\mathbf{k}_\parallel}_{\lambda,v;v',\lambda'}) &= \mathrm{Sym_F}([c]^{\mathbf{q}_\parallel,\mathbf{k}'_\parallel,\mathbf{k}_\parallel}_{\lambda,v;v',\lambda'} + [\tilde{c}]^{\mathbf{q}_\parallel,\mathbf{k}'_\parallel,\mathbf{k}_\parallel}_{\lambda,v;v',\lambda'}) \\ &= \mathrm{Sym_F}(c^{\mathbf{q}_\parallel,\mathbf{k}'_\parallel,\mathbf{k}_\parallel}_{\lambda,v;v',\lambda'}) + \mathrm{Sym_F}(\tilde{c}^{\mathbf{q}_\parallel,\mathbf{k}'_\parallel,\mathbf{k}_\parallel}_{\lambda,v;v',\lambda'}),\end{aligned} \tag{93}$$

$$\mathrm{Sym_F}(c^{\mathbf{q}_\parallel,\mathbf{k}_\parallel,\mathbf{k}_\parallel}_{\lambda,\lambda;v',\lambda'}) = 0 \;\Leftrightarrow\; c^{\mathbf{q}_\parallel,\mathbf{k}_\parallel,\mathbf{k}_\parallel}_{\lambda,\lambda;v',\lambda'} = 0, \quad \forall \mathbf{q}_\parallel, \mathbf{k}_\parallel, \tag{94}$$

$$\mathrm{Sym_F}(c^{-\mathbf{q}_\parallel,\mathbf{k}_\parallel+\mathbf{q},\mathbf{k}_\parallel-\mathbf{q}_\parallel}_{\lambda,v;\lambda',\lambda'}) = 0 \;\Leftrightarrow\; c^{-\mathbf{q}_\parallel,\mathbf{k}_\parallel+\mathbf{q},\mathbf{k}_\parallel-\mathbf{q}}_{\lambda,v;\lambda',\lambda'} = 0, \quad \forall \mathbf{q}_\parallel, \mathbf{k}_\parallel. \tag{95}$$

The first relation, Eq. (92), verifies that the doublet correlation is an eigenstate of $\mathrm{Sym_F}(c)$, and the following equations show that the Fermionic antisymmetry operation is additive and that the doublet correlations vanish for identical indices of two creation or annihilation operators.

It turns out that we may actually use $\mathrm{Sym_F}(c)$ to identify different classes of effects in the correlation dynamics since each physically different contribution to $c_{\lambda,v;v'\lambda'}$ must be an eigenstate of $\mathrm{Sym_F}$ in the same way as $c_{\lambda,v;v'\lambda'}$. This observation allows for a compact presentation of the singlet–doublet dynamics because we have to identify only one of the four possible terms generated by Eq. (91).

For the explicit construction of the doublet equations, we use Eqs. (40)–(41) for the individual carrier creation and destruction operators to evaluate the contributions to Eq. (74). Then we implement the singlet–doublet factorizations (C.3)–(C.13) and sort the resulting terms according to the different classes of physical effects. By applying Eq. (91) to

the different terms, we then obtain a set of contributions according to

$$\begin{aligned} i\hbar\frac{\partial}{\partial t}c^{\mathbf{q}_\parallel,\mathbf{k}'_\parallel,\mathbf{k}_\parallel}_{\lambda,\nu;\nu',\lambda'} &= (\tilde{\varepsilon}^{\lambda'}_{\mathbf{k}_\parallel-\mathbf{q}_\parallel}+\tilde{\varepsilon}^{\nu'}_{\mathbf{k}'_\parallel+\mathbf{q}_\parallel}-\tilde{\varepsilon}^{\nu}_{\mathbf{k}'_\parallel}-\tilde{\varepsilon}^{\lambda}_{\mathbf{k}_\parallel})\, c^{\mathbf{q}_\parallel,\mathbf{k}'_\parallel,\mathbf{k}_\parallel}_{\lambda,\nu;\nu',\lambda} + \mathrm{Sym}_F([\tfrac{1}{2}S^{(1)}-S^{(2)}]^{\mathbf{q}_\parallel,\mathbf{k}'_\parallel,\mathbf{k}_\parallel}_{\lambda,\nu;\nu',\lambda'}) \\ &\quad + \mathrm{Sym}_F([D_{\mathrm{Scr}}+\tfrac{1}{4}D^{(0)}_{\mathrm{Coul}}-\tfrac{1}{2}D^{(1)}_{\mathrm{Coul}}+D^{(2)}_{\mathrm{Coul}}]^{\mathbf{q}_\parallel,\mathbf{k}'_\parallel,\mathbf{k}_\parallel}_{\lambda,\nu;\nu',\lambda'}) \\ &\quad + \mathrm{Sym}_F([\tfrac{1}{2}D_{\mathrm{clas}}+D_{\mathrm{QED}}+D_{\mathrm{phon}}]^{\mathbf{q}_\parallel,\mathbf{k}'_\parallel,\mathbf{k}_\parallel}_{\lambda,\nu;\nu',\lambda'}) + V_2[c^{\mathbf{q}_\parallel,\mathbf{k}'_\parallel,\mathbf{k}_\parallel}_{\lambda,\nu;\nu',\lambda'}]_T. \end{aligned} \tag{96}$$

Here, the second line contains only singlet terms $S^{(j)}$, the third and fourth lines contain the correlated doublets D, and the last term consists only of correlated triplets.

In order to get a feeling for the physical processes represented by the individual terms in Eq. (96), we consider different idealized situations. For example, if we start from a mean-field electron–hole plasma, we have singlet contributions in the carrier system but the two- and three-particle correlations initially vanish. The two-particle correlations can then be generated only via the pure singlet sources:

$$[S^{(1)}]^{\mathbf{q}_\parallel,\mathbf{k}'_\parallel,\mathbf{k}_\parallel}_{\lambda,\nu;\nu',\lambda'} \equiv V_{\mathbf{q}_\parallel}(P^{\lambda,\lambda'}_{\mathbf{k}_\parallel}P^{\nu,\nu'}_{\mathbf{k}'_\parallel}-P^{\lambda,\lambda'}_{\mathbf{k}_\parallel-\mathbf{q}_\parallel}P^{\nu,\nu'}_{\mathbf{k}'+\mathbf{q}_\parallel}), \tag{97}$$

$$[S^{(2)}]^{\mathbf{q}_\parallel,\mathbf{k}'_\parallel,\mathbf{k}_\parallel}_{\lambda,\nu;\nu',\lambda'} \equiv V_{\mathbf{q}_\parallel}\sum_\beta P^{\lambda,\beta}_{\mathbf{k}_\parallel}P^{\beta,\lambda'}_{\mathbf{k}_\parallel-\mathbf{q}_\parallel}(P^{\nu,\nu'}_{\mathbf{k}'_\parallel}-P^{\nu,\nu'}_{\mathbf{k}'_\parallel+\mathbf{q}_\parallel}). \tag{98}$$

These terms originate from the singlet parts of the Coulomb-interaction terms. The first one results from the Hartree–Fock factorization of two-particle expectation values and the second term is obtained from the singlet contribution of three-particle expectation values. It is straightforward to see that $\mathrm{Sym}_F(S^{(1)})$ produces the same contributions twice. As a consequence of this degeneracy, the factor $\frac{1}{2}$ appears in Eq. (96).

To gain some insight into the three-particle factorization terms, $S^{(2)}$, and the various Coulomb-induced contributions D, we present them via diagrams. Here, we consider the general situation that the Coulomb interaction produces three-particle terms with the indices (β,λ,ν) for the creation operators and (β,ν',λ') for the annihilation operators. We adopt the convention that the indices (λ,ν) and (ν',λ') stem from the original two-particle correlation, whereas the common index β, referred to as the "interaction" index, is related to the different possibilities to change and add correlations via the Coulomb interaction. The diagrams representing the different configurations of creation and annihilation operators are then constructed according to the following rules:

(1) each Fermi creation operator is indicated by a filled circle and each annihilation operator is symbolized by an open circle,
(2) operators that appear within a doublet correlation are surrounded by a line (shaded ellipse in Fig. 2),
(3) operators with an "interaction" index are indicated by a short line attached to the circle,
(4) those diagrams, which are obtained via the exchange $\lambda\leftrightarrow\nu$ or $\lambda'\leftrightarrow\nu'$, are identical due to the symmetry operation, Eq. (91).

With the help of the diagram rules, we find five different classes of contributions to the singlet–doublet factorization of the three-particle terms appearing in Eq. (49), see Fig. 2. The diagram in the top line of Fig. 2 follows from Eq. (98). It contains only singlet

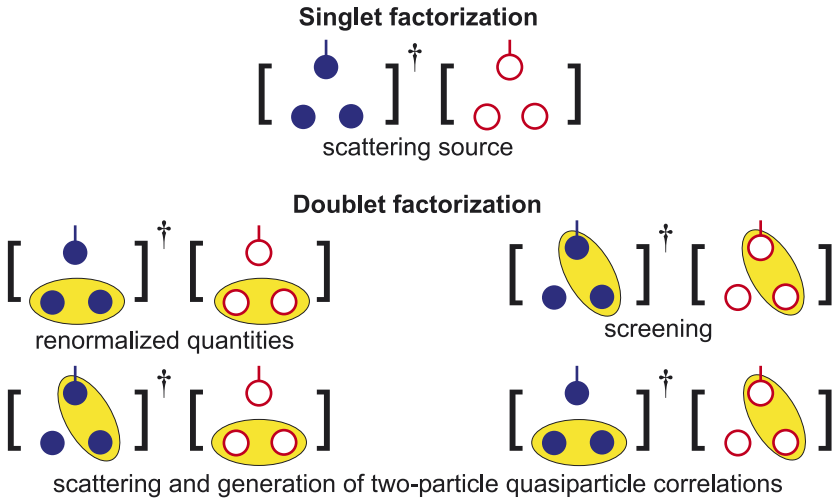

Fig. 2. Diagrammatic presentation of the singlet–doublet factorization for the Coulomb-induced three-particle terms in the hierarchy problem, Eq. (49). The creation (annihilation) operators are depicted as filled (open) circles. Operators with an "interaction" index, i.e. an index not appearing in the original doublet (see text), are marked by a line attached to the circle. Operator pairs that appear inside correlated doublets are grouped within an ellipse.

contributions, such as

$$\begin{aligned} &n_1 n_2(1-n_3-n_4)-(1-n_1-n_2)n_3 n_4 \\ &\quad = n_1 n_2(1-n_3)(1-n_4)-(1-n_1)(1-n_2)n_3 n_4, \end{aligned} \tag{99}$$

times a prefactor containing the Coulomb-matrix element which is responsible for the momentum exchange between the carrier occupations n_j. Eq. (99) has the typical form of a Boltzmann scattering term. Hence, we can say that the singlet sources (97)–(98) represent in- and out-scattering contributions of the different single-particle quantities. With this scattering interpretation for the singlet terms, we identify the different index combinations as density–density [as presented in Eq. (99)], polarization–density, or as polarization–polarization scattering.

It is interesting to note that if we only include the singlet diagram depicted in the top line of Fig. 2 to the doublet dynamics, the steady-state result of the corresponding Eq. (96) produces exactly the same equations as the well-known (unscreened) second-Born scattering approximation [1,22,52]. Thus, the full dynamic solution of Eqs. (96) with just the simplest diagram is already a quantum-kinetic approximation beyond the Markov limit. We can therefore generally conclude that *the singlet terms*, Eqs. (97)–(98), *act as scattering sources* which spontaneously generate two-particle correlations.

Once correlation contributions exist, they are modified by the terms corresponding to the diagrams in the second and third line of Fig. 2. All these terms contain products of correlated doublets. The simplest doublet diagram consists of singlet terms that carry both of the interaction indices times correlated pairs that have the same index combinations as those in the original $c_{\lambda,\nu;\nu',\lambda'}$. Physically, these terms represent renormalizations of the kinetic energy and the Rabi frequency entering the contribution

$$[D_{\text{clas}}]^{\mathbf{q}_\parallel,\mathbf{k}'_\parallel,\mathbf{k}_\parallel}_{\lambda,\nu;\nu',\lambda'} \equiv \Omega^{\lambda}_{\mathbf{k}_\parallel} c^{\mathbf{q}_\parallel,\mathbf{k}'_\parallel,\mathbf{k}_\parallel}_{\bar{\lambda},\nu;\nu',\lambda'} - \Omega^{\bar{\lambda}'}_{\mathbf{k}_\parallel-\mathbf{q}_\parallel} c^{\mathbf{q}_\parallel,\mathbf{k}'_\parallel,\mathbf{k}_\parallel}_{\bar{\lambda},\nu;\nu',\bar{\lambda}'}. \tag{100}$$

Again, $\mathrm{Sym}_{\mathrm{F}}(D_{\mathrm{clas}})$ produces the same term twice such that the factor $\frac{1}{2}$ has to appear for this contribution in Eq. (96).

The third diagram in Fig. 2 identifies contributions where both interaction indices appear within the correlation terms, i.e.

$$[D_{\mathrm{scr}}]^{\mathbf{q}_\parallel,\mathbf{k}'_\parallel,\mathbf{k}_\parallel}_{\lambda,v;v',\lambda'} \equiv V_{\mathbf{q}_\parallel}(P^{\lambda,\lambda'}_{\mathbf{k}_\parallel} - P^{\lambda,\lambda'}_{\mathbf{k}_\parallel-\mathbf{q}_\parallel}) \sum_{\beta,\mathbf{l}_\parallel} c^{\mathbf{q}_\parallel,\mathbf{k}'_\parallel,\mathbf{l}_\parallel}_{\beta,v;v',\beta}. \tag{101}$$

Here, the β and $\mathbf{l}_\parallel$ sums indicate that all possibilities to alter the correlations are included within this class of diagrams. The Coulomb-matrix element is outside the sum together with a difference between singlet terms.

If only $S^{(1)}$ and D_{scr} are included to Eq. (96) together with the kinetic-energy terms, we would have an equation such as

$$\begin{aligned} \mathrm{i}\hbar\frac{\partial}{\partial t} c^{\mathbf{q}_\parallel,\mathbf{k}'_\parallel,\mathbf{k}_\parallel}_{\lambda,v;v,\lambda}\Big|_{\mathrm{Lind}} &= (\tilde{\varepsilon}^{\lambda}_{\mathbf{k}_\parallel-\mathbf{q}_\parallel} + \tilde{\varepsilon}^{v}_{\mathbf{k}'_\parallel+\mathbf{q}_\parallel} - \tilde{\varepsilon}^{v}_{\mathbf{k}'_\parallel} - \tilde{\varepsilon}^{\lambda}_{\mathbf{k}_\parallel} - \mathrm{i}\gamma) c^{\mathbf{q}_\parallel,\mathbf{k}'_\parallel,\mathbf{k}_\parallel}_{\lambda,v;v,\lambda'} \\ &\quad + V_{\mathbf{q}_\parallel} n^{v}_{\mathbf{k}'_\parallel}(n^{\lambda}_{\mathbf{k}_\parallel} - n^{\lambda}_{\mathbf{k}_\parallel-\mathbf{q}_\parallel}) \\ &\quad + V_{\mathbf{q}_\parallel}(n^{\lambda}_{\mathbf{k}_\parallel} - n^{\lambda}_{\mathbf{k}_\parallel-\mathbf{q}_\parallel}) \sum_{\mathbf{l}_\parallel} c^{\mathbf{q}_\parallel,\mathbf{k}'_\parallel,\mathbf{l}_\parallel}_{\lambda,v;v,\lambda}. \end{aligned} \tag{102}$$

Here, we added a phenomenological dephasing and, for simplicity, we included only a part of the possible $S^{(1)}$ and did not symmetrize D_{scr}. Eq. (102) has the steady-state solution

$$c^{\mathbf{q}_\parallel,\mathbf{k}'_\parallel,\mathbf{k}_\parallel}_{\lambda,v;v,\lambda}\Big|_{\mathrm{Lind}} = \frac{n^{v}_{\mathbf{k}_\parallel}(n^{\lambda}_{\mathbf{k}_\parallel-\mathbf{q}_\parallel} - n^{\lambda}_{\mathbf{k}_\parallel}) W_{\mathbf{q}_\parallel}(\varepsilon^{v}_{\mathbf{k}'_\parallel+\mathbf{q}_\parallel} - \varepsilon^{v}_{\mathbf{k}'_\parallel})}{\varepsilon^{\lambda}_{\mathbf{k}_\parallel-\mathbf{q}_\parallel} + \varepsilon^{v}_{\mathbf{k}'_\parallel+\mathbf{q}_\parallel} - \varepsilon^{v}_{\mathbf{k}'_\parallel} - \varepsilon^{\lambda}_{\mathbf{k}_\parallel} - \mathrm{i}\gamma}, \tag{103}$$

$$W_{\mathbf{q}_\parallel}(\Delta E) \equiv \frac{V_{\mathbf{q}_\parallel}}{1 - V_{\mathbf{q}_\parallel} L_{\mathbf{q}_\parallel}(\Delta E)},$$

$$L_{\mathbf{q}_\parallel}(\Delta E) \equiv \sum_{\mathbf{k}_\parallel} \frac{(n^{\lambda}_{\mathbf{k}_\parallel-\mathbf{q}_\parallel} - n^{\lambda}_{\mathbf{k}_\parallel})}{\varepsilon^{\lambda}_{\mathbf{k}_\parallel-\mathbf{q}_\parallel} + \varepsilon^{\lambda}_{\mathbf{k}_\parallel} + \Delta E - \mathrm{i}\gamma}, \tag{104}$$

where we have identified the screened Coulomb interaction W and the Lindhard sum $L(\Delta E)$. Without D_{scr}, the steady-state solution, Eq. (103), has W replaced by V in the numerator. Hence, we can conclude that D_{scr} *produces terms which lead to screening of the interaction potential*. More precisely, these doublet contributions introduce Lindhard-type screening for the singlet dynamics via the hierarchical coupling of singlets to doublets. As long as we do not make a steady-state assumption, the dynamic build up of the singlet screening is fully included via the doublet dynamics (96). At the next level, the doublet-correlations are dynamically screened by specific triplet contributions, and so on. In other words, the screening of the interaction potential in a given level of the cluster expansion is always provided by contributions from the next higher cluster level.

The analysis of Eqs. (102)–(103) concentrated only on a subset of terms. In general, $\mathrm{Sym}_{\mathrm{F}}$ introduces exchange terms influencing screening [58–61]. In addition, the β sum may lead to coupling between coherent and incoherent quantities via polarization. Thus, the most general form of D_{scr} contains screening, Fermionic exchange, and coherent–incoherent coupling dynamics.

The fourth and fifth diagrams in Fig. 2 can be written explicitly as

$$[D^{(1)}_{\mathrm{Coul}}]^{\mathbf{q}_\parallel,\mathbf{k}'_\parallel,\mathbf{k}_\parallel}_{\lambda,\nu;\nu',\lambda'} \equiv \sum_{\beta,\mathbf{l}_\parallel} V_{\mathbf{l}_\parallel-\mathbf{q}_\parallel}(P^{\lambda,\beta}_{\mathbf{k}_\parallel}[c^{-\mathbf{l}_\parallel,\mathbf{k}'_\parallel+\mathbf{q}_\parallel,\mathbf{k}_\parallel-\mathbf{q}_\parallel}_{\lambda',\nu';\nu,\beta}]^\star - P^{\beta,\lambda'}_{\mathbf{k}_\parallel-\mathbf{q}_\parallel} c^{\mathbf{l}_\parallel,\mathbf{k}'_\parallel,\mathbf{k}_\parallel}_{\lambda,\nu;\nu',\beta}),$$

$$[D^{(2)}_{\mathrm{Coul}}]^{\mathbf{q}_\parallel,\mathbf{k}'_\parallel,\mathbf{k}_\parallel}_{\lambda,\nu;\nu',\lambda'} \equiv \sum_{\beta,\mathbf{l}_\parallel} V_{\mathbf{l}_\parallel-\mathbf{k}_\parallel}(P^{\lambda,\beta}_{\mathbf{k}_\parallel} c^{\mathbf{q}_\parallel,\mathbf{k}'_\parallel,\mathbf{l}_\parallel}_{\beta,\nu';\nu,\lambda} - P^{\beta,\lambda'}_{\mathbf{k}_\parallel-\mathbf{q}_\parallel} c^{\mathbf{q}_\parallel,\mathbf{k}'_\parallel,\mathbf{l}_\parallel}_{\lambda,\nu;\nu',\beta}). \tag{105}$$

Here, both a singlet and a doublet term, as well as the Coulomb-matrix element carry an interaction index, rendering these contributions the most complicated class of diagrams. Actually, there is a similar contribution

$$[D^{(0)}_{\mathrm{Coul}}]^{\mathbf{q}_\parallel,\mathbf{k}'_\parallel,\mathbf{k}_\parallel}_{\lambda,\nu;\nu',\lambda'} \equiv \sum_{\mathbf{l}_\parallel} V_{\mathbf{l}_\parallel-\mathbf{q}_\parallel}([c^{-\mathbf{l}_\parallel,\mathbf{k}'_\parallel+\mathbf{q}_\parallel,\mathbf{k}_\parallel-\mathbf{q}_\parallel}_{\lambda,\nu;\nu',\lambda'}]^\star - c^{\mathbf{l}_\parallel,\mathbf{k}'_\parallel,\mathbf{k}_\parallel}_{\lambda,\nu;\nu',\lambda'}) \tag{106}$$

that only involves doublets and no singlets. Expressions (105)–(106) describe a class of processes where the Coulomb interaction can add or change correlations. In other words, the $D^{(j)}_{\mathrm{Coul}}$ terms *can generate new two-particle quasi-particles*, *such as excitons*, *in the many-body system and they describe the scattering of these quasi-particles with singlets*. Since the symmetrization produces the same term four times for $D^{(0)}$ and twice for $D^{(1)}$, they are divided by 4 and 2, respectively, in Eq. (96).

The terms

$$\begin{aligned}[D_{\mathrm{QED}}]^{\mathbf{q}_\parallel,\mathbf{k}'_\parallel,\mathbf{k}_\parallel}_{\lambda,\nu;\nu',\lambda'} \equiv\ & P^{\lambda,\bar{\lambda}'}_{\mathbf{k}_\parallel} \Delta\langle[E^{\bar{\lambda}'}_{\mathbf{q}_\parallel}]^\dagger a^\dagger_{\nu,\mathbf{k}'_\parallel} a_{\nu',\mathbf{k}'_\parallel+\mathbf{q}_\parallel}\rangle \\ & - P^{\bar{\lambda},\lambda'}_{\mathbf{k}_\parallel-\mathbf{q}_\parallel} \Delta\langle[E^{\lambda}_{\mathbf{q}_\parallel}]^\dagger a^\dagger_{\nu,\mathbf{k}'_\parallel} a_{\nu',\mathbf{k}'_\parallel+\mathbf{q}_\parallel}\rangle\end{aligned} \tag{107}$$

in Eq. (96) describe quantum-optical contributions to the pure carrier doublets. The corresponding phonon contributions follow from

$$\begin{aligned}[D_{\mathrm{phon}}]^{\mathbf{q}_\parallel,\mathbf{k}'_\parallel,\mathbf{k}_\parallel}_{\lambda,\nu;\nu',\lambda'} \equiv\ & P^{\lambda,\lambda'}_{\mathbf{k}_\parallel} \Delta\langle[Q^{\lambda'}_{\mathbf{q}_\parallel}]^\dagger a^\dagger_{\nu,\mathbf{k}'_\parallel} a_{\nu',\mathbf{k}'_\parallel+\mathbf{q}_\parallel}\rangle \\ & - P^{\lambda,\lambda'}_{\mathbf{k}_\parallel-\mathbf{q}_\parallel} \Delta\langle[Q^{\lambda}_{\mathbf{q}_\parallel}]^\dagger a^\dagger_{\nu,\mathbf{k}'_\parallel} a_{\nu',\mathbf{k}'_\parallel+\mathbf{q}_\parallel}\rangle.\end{aligned} \tag{108}$$

These quantum-optical and phonon terms basically *describe all possibilities to correlate either the light field or the phonons with the carrier system in ways that create and modify pure carrier correlations*.

At this stage, we have now discussed all singlet–doublet contributions entering into the carrier-doublet dynamics (96). Since all these contributions together drive and modify the carrier correlations, and since Eq. (96) is non-linear, the different effects are clearly not additive. Instead, one finds a complicated interplay between all the contributions such that they usually cannot be separated. Thus, one has to perform a careful analysis for each given excitation configuration to determine which particular many-body and/or quantum-optical effect may be dominant.

As the last remaining element, we need to evaluate the three-particle scattering terms appearing in Eq. (96). We obtain

$$
\begin{aligned}
V_2[c^{\mathbf{q}_\parallel,\mathbf{k}'_\parallel,\mathbf{k}_\parallel}_{\lambda,\nu;\nu',\lambda'}] \equiv\ & + \sum_{\beta,\mathbf{k}''_\parallel,\mathbf{l}_\parallel} V_{\mathbf{l}_\parallel}(\Delta\langle a^\dagger_{\lambda,\mathbf{k}_\parallel} a^\dagger_{\nu,\mathbf{k}'_\parallel} a^\dagger_{\beta,\mathbf{k}''_\parallel} a_{\beta,\mathbf{k}''_\parallel} a_{\nu',\mathbf{k}'_\parallel+\mathbf{q}_\parallel} a_{\lambda',\mathbf{k}_\parallel-\mathbf{q}_\parallel+\mathbf{l}_\parallel}\rangle \\
& + \Delta\langle a^\dagger_{\lambda,\mathbf{k}_\parallel} a^\dagger_{\nu,\mathbf{k}'_\parallel} a^\dagger_{\beta,\mathbf{k}''_\parallel} a_{\beta,\mathbf{k}''_\parallel} a_{\nu',\mathbf{k}'_\parallel+\mathbf{q}_\parallel+\mathbf{l}_\parallel} a_{\lambda',\mathbf{k}_\parallel-\mathbf{q}_\parallel}\rangle \\
& - \Delta\langle a^\dagger_{\lambda,\mathbf{k}_\parallel} a^\dagger_{\nu,\mathbf{k}'_\parallel+\mathbf{l}_\parallel} a^\dagger_{\beta,\mathbf{k}''_\parallel-\mathbf{l}_\parallel} a_{\beta,\mathbf{k}''_\parallel} a_{\nu',\mathbf{k}'_\parallel+\mathbf{q}_\parallel} a_{\lambda',\mathbf{k}_\parallel-\mathbf{q}_\parallel}\rangle \\
& - \Delta\langle a^\dagger_{\lambda,\mathbf{k}_\parallel-\mathbf{l}_\parallel} a^\dagger_{\nu,\mathbf{k}'_\parallel} a^\dagger_{\beta,\mathbf{k}''_\parallel} a_{\beta,\mathbf{k}''_\parallel-\mathbf{l}_\parallel} a_{\nu',\mathbf{k}'_\parallel+\mathbf{q}_\parallel} a_{\lambda',\mathbf{k}_\parallel-\mathbf{q}_\parallel}\rangle) \\
& + \sum_{\mathbf{l}_\parallel} (\Delta\langle E^{\bar{\lambda}}_{-\mathbf{l}_\parallel} a^\dagger_{\bar{\lambda},\mathbf{k}_\parallel-\mathbf{l}_\parallel} a^\dagger_{\nu,\mathbf{k}'_\parallel} a_{\nu',\mathbf{k}'_\parallel+\mathbf{q}_\parallel} a_{\lambda',\mathbf{k}_\parallel-\mathbf{q}_\parallel}\rangle \\
& + \Delta\langle E^{\bar{\nu}}_{\mathbf{l}_\parallel} a^\dagger_{\lambda,\mathbf{k}_\parallel} a^\dagger_{\bar{\nu},\mathbf{k}'_\parallel+\mathbf{l}_\parallel} a_{\nu',\mathbf{k}'_\parallel+\mathbf{q}_\parallel} a_{\lambda',\mathbf{k}_\parallel-\mathbf{q}_\parallel}\rangle \\
& - \Delta\langle E^{\nu'}_{-\mathbf{l}_\parallel} a^\dagger_{\lambda,\mathbf{k}_\parallel} a^\dagger_{\nu,\mathbf{k}'_\parallel} a_{\bar{\nu}',\mathbf{k}'_\parallel+\mathbf{q}_\parallel+\mathbf{l}_\parallel} a_{\lambda',\mathbf{k}_\parallel-\mathbf{q}_\parallel}\rangle \\
& - \Delta\langle E^{\lambda'}_{\mathbf{l}_\parallel} a^\dagger_{\lambda,\mathbf{k}_\parallel} a^\dagger_{\nu,\mathbf{k}'_\parallel} a_{\nu',\mathbf{k}'_\parallel+\mathbf{q}_\parallel} a_{\bar{\lambda}',\mathbf{k}_\parallel-\mathbf{q}_\parallel-\mathbf{l}_\parallel}\rangle) \\
& - \sum_{\mathbf{l}_\parallel} (\Delta\langle Q^{\lambda}_{-\mathbf{l}_\parallel} a^\dagger_{\lambda,\mathbf{k}_\parallel-\mathbf{l}_\parallel} a^\dagger_{\nu,\mathbf{k}'_\parallel} a_{\nu',\mathbf{k}'_\parallel+\mathbf{q}_\parallel} a_{\lambda',\mathbf{k}_\parallel-\mathbf{q}_\parallel}\rangle \\
& + \Delta\langle Q^{\nu}_{\mathbf{l}_\parallel} a^\dagger_{\lambda,\mathbf{k}_\parallel} a^\dagger_{\nu,\mathbf{k}'_\parallel+\mathbf{l}_\parallel} a_{\nu',\mathbf{k}'_\parallel+\mathbf{q}_\parallel} a_{\lambda',\mathbf{k}_\parallel-\mathbf{q}_\parallel}\rangle \\
& - \Delta\langle Q^{\nu'}_{-\mathbf{l}_\parallel} a^\dagger_{\lambda,\mathbf{k}_\parallel} a^\dagger_{\nu,\mathbf{k}'_\parallel} a_{\nu',\mathbf{k}'_\parallel+\mathbf{q}_\parallel+\mathbf{l}_\parallel} a_{\lambda',\mathbf{k}_\parallel-\mathbf{q}_\parallel}\rangle \\
& - \Delta\langle Q^{\lambda'}_{\mathbf{l}_\parallel} a^\dagger_{\lambda,\mathbf{k}_\parallel} a^\dagger_{\nu,\mathbf{k}'_\parallel} a_{\nu',\mathbf{k}'_\parallel+\mathbf{q}_\parallel} a_{\lambda',\mathbf{k}_\parallel-\mathbf{q}_\parallel-\mathbf{l}_\parallel}\rangle)). \qquad (109)
\end{aligned}
$$

Here, the first four lines result from the Coulomb interaction, the next four lines are due to the light–matter interaction, and the last four lines are a consequence of the carrier–phonon coupling. The systematic derivation of these different three-particle scattering terms is discussed in the Appendices.

When the triplet terms are added to Eq. (96), the singlet–doublet dynamics is formally exact and the quality of the results depends only on the accuracy with which we are able to evaluate the three-particle correlation terms. The combination of Eqs. (67)–(68), (71), (75)–(78), (79)–(80), (83), (85), and (96) is therefore the general starting point of any singlet–doublet analysis.

5. Excitonic effects in semiconductor optics

Semiconductor optical experiments with coherent laser sources can access a wide variety of intriguing many-body phenomena. By suitably choosing the intensity, spectrum, temporal duration, and/or the direction of the laser pulse or the pulse sequence, one can realize many fundamentally different excitation conditions. Current experiments utilize a large variety of laser sources ranging from ultrafast sub-picosecond pulsed systems [62–65] all the way to continuous-wave (cw) operation. More and more sophisticated experiments are done using coherent light in a wide range of the electromagnetic spectrum, covering the THz and far-infrared [19,66–70] into the visible up to the ultra violet (uv) regime.

By choosing the appropriate excitation conditions, both the concentration and the character of the excited quasi-particles can be manipulated. One can apply different measurement schemes to detect the excitation-induced changes in the optical response such as light transmission, reflection, and absorption [10–14,71,72] as well as light scattering and wave-mixing signatures [73–83]. This coherent laser excitation approach is widely used not only to explore quantum-mechanical properties of many-body systems but also with the goal to develop practical devices.

5.1. Maxwell-semiconductor Bloch equations

An ideal, coherent laser generates a quantum field that is as close as possible to classical light. Therefore, the interaction of laser light and matter can often be described at the semiclassical level. Here, one uses the classical electrodynamic theory in conjunction with a quantum-mechanical approach to analyze the creation, annihilation and interaction of the different material excitations. In this spirit, we now specialize the general singlet–doublet formalism of Section 4 to the case of a classical light field.

As discussed in Section 4.2, the classical light field is described by the single-particle part, $\langle B_{\mathbf{q}}\rangle$, of the photon operators when they appear inside any expectation value. In this classical factorization, $B_{\mathbf{q}}$ is taken out of the expectation values as a complex-valued field. Since this field can be decomposed into an amplitude and a phase, the classical part of the light field is referred to as *coherent* while the remaining quantum-optical fluctuations are incoherent if they exist without the classical field.

Based on the formal equivalence of light and particle correlations, the classical excitations should—in first order—generate single-particle carrier quantities. Thus, we have to solve the full singlet dynamics in order to determine the principal effects of classical optical excitations. In particular, we have to evaluate the dynamics of the microscopic polarization and the carrier occupations during and after the excitation. For this purpose, we introduce a simplifying notation for the microscopic polarization

$$P_{\mathbf{k}_\parallel} \equiv P^{v,c}_{\mathbf{k}_\parallel} = \langle a^\dagger_{v,\mathbf{k}_\parallel} a_{c,\mathbf{k}_\parallel}\rangle, \tag{110}$$

and for the electron and hole occupations

$$f^{\mathrm{e}}_{\mathbf{k}_\parallel} \equiv n^c_{\mathbf{k}_\parallel} = P^{c,c}_{\mathbf{k}_\parallel} = \langle a^\dagger_{c,\mathbf{k}_\parallel} a_{c,\mathbf{k}_\parallel}\rangle, \tag{111}$$

$$f^{\mathrm{h}}_{\mathbf{k}_\parallel} \equiv 1 - n^v_{\mathbf{k}_\parallel} = 1 - P^{v,v}_{\mathbf{k}_\parallel} = 1 - \langle a^\dagger_{v,\mathbf{k}_\parallel} a_{v,\mathbf{k}_\parallel}\rangle = \langle a_{v,\mathbf{k}_\parallel} a^\dagger_{v,\mathbf{k}_\parallel}\rangle. \tag{112}$$

Using these notations in Eq. (71), we can write the general *semiconductor Bloch equations* (SBE) [1,84]

$$\mathrm{i}\hbar\frac{\partial}{\partial t} P_{\mathbf{k}_\parallel} = \tilde{\varepsilon}_{\mathbf{k}_\parallel} P_{\mathbf{k}_\parallel} - [1 - f^{\mathrm{e}}_{\mathbf{k}_\parallel} - f^{\mathrm{h}}_{\mathbf{k}_\parallel}]\Omega_{\mathbf{k}_\parallel} + \Gamma^{v,c}_{\mathbf{k}_\parallel} + \Gamma^{\mathrm{QED}}_{v,c;\mathbf{k}_\parallel}, \tag{113}$$

$$\hbar\frac{\partial}{\partial t} f^{\mathrm{e}}_{\mathbf{k}_\parallel} = 2\,\mathrm{Im}[P_{\mathbf{k}_\parallel}\Omega^\star_{\mathbf{k}_\parallel} + \Gamma^{c,c}_{\mathbf{k}_\parallel} + \Gamma^{\mathrm{QED}}_{c,c;\mathbf{k}_\parallel}], \tag{114}$$

$$\hbar\frac{\partial}{\partial t} f^{\mathrm{h}}_{\mathbf{k}_\parallel} = 2\,\mathrm{Im}[P_{\mathbf{k}}\Omega^\star_{\mathbf{k}_\parallel} - \Gamma^{v,v}_{\mathbf{k}_\parallel} - \Gamma^{\mathrm{QED}}_{v,v;\mathbf{k}_\parallel}]. \tag{115}$$

Here, we introduced the renormalized kinetic electron–hole-pair energy and the renormalized Rabi frequency,

$$\tilde{\varepsilon}_{\mathbf{k}_\parallel} \equiv \varepsilon^c_{\mathbf{k}_\parallel} - \varepsilon^v_{\mathbf{k}_\parallel} - \sum_{\mathbf{k}'_\parallel} V_{\mathbf{k}_\parallel - \mathbf{k}'_\parallel}(f^{\mathrm{e}}_{\mathbf{k}'_\parallel} + f^{\mathrm{h}}_{\mathbf{k}'_\parallel}),$$

$$\Omega_{\mathbf{k}_\parallel} \equiv d_{c,v}\langle E(0,t)\rangle + \sum_{\mathbf{k}'_\parallel} V_{\mathbf{k}_\parallel - \mathbf{k}'_\parallel} P_{\mathbf{k}'_\parallel}, \tag{116}$$

respectively. These familiar forms are obtained directly by combining Eqs. (62)–(63) and (72)–(73) with the new definitions (110)–(112).

In Eqs. (113)–(115), the doublet contributions show up as quantum-optical correlations Γ^{QED} and as microscopic scattering terms

$$\Gamma^{\lambda,\lambda'}_{\mathbf{k}_\parallel} \equiv \sum_{v,\mathbf{k}'_\parallel,\mathbf{q}_\parallel \neq \mathbf{0}} V_{\mathbf{q}_\parallel}[c^{\mathbf{q}_\parallel,\mathbf{k}'_\parallel,\mathbf{k}_\parallel}_{\lambda,v;v,\lambda'} - (c^{\mathbf{q}_\parallel,\mathbf{k}'_\parallel,\mathbf{k}_\parallel}_{\lambda',v;v,\lambda})^\star] + \sum_{\mathbf{q}_\parallel}[\Delta\langle Q^{\lambda'}_{\mathbf{q}_\parallel} a^\dagger_{\lambda,\mathbf{k}_\parallel} a_{\lambda',\mathbf{k}_\parallel - \mathbf{q}_\parallel}\rangle - \Delta\langle (Q^{\lambda}_{\mathbf{q}_\parallel})^\dagger a^\dagger_{\lambda,\mathbf{k}_\parallel - \mathbf{q}_\parallel} a_{\lambda',\mathbf{k}_\parallel}\rangle] \tag{117}$$

due to the Coulomb (first line) and the phonon–carrier (second line) interactions. In general, the doublet terms $\Gamma^{\lambda,\lambda'}$ introduce microscopic couplings to the two-particle Coulomb and phonon correlations, which describe dephasing, energy renormalizations, and screening, as well as relaxation of the carrier densities toward steady-state distributions.

The quantum-optical two-particle correlations have the explicit form

$$\Gamma^{\mathrm{QED}}_{\lambda,\lambda';\mathbf{k}_\parallel} \equiv -\sum_{\mathbf{q}_\parallel}[\Delta\langle E^{\lambda'}_{\mathbf{q}_\parallel} a^\dagger_{\lambda,\mathbf{k}_\parallel} a_{\tilde{\lambda}',\mathbf{k}_\parallel - \mathbf{q}_\parallel}\rangle - \Delta\langle (E^{\lambda}_{\mathbf{q}_\parallel})^\dagger a^\dagger_{\tilde{\lambda},\mathbf{k}_\parallel - \mathbf{q}_\parallel} a_{\lambda',\mathbf{k}_\parallel}\rangle]. \tag{118}$$

They introduce all combinations of photon-assisted correlations which describe the spontaneous recombination of carriers, entanglement effects, or the generation of densities via quantum-light absorption. Since these effects often play a minor role in typical classical optical experiments, we omit the Γ^{QED} contributions for this discussion.

For a classical light field, it is often sufficient to evaluate the self-consistent coupling of the SBE to Maxwell's wave equation (61)

$$\left[\frac{\partial^2}{\partial r_\perp^2} - \frac{n^2(r_\perp)}{c^2}\frac{\partial^2}{\partial t^2}\right]\langle E(r_\perp,t)\rangle = \mu_0|\xi(r_\perp)|^2\frac{\partial^2}{\partial t^2}P, \tag{119}$$

where the classical light field is directly influenced by the macroscopic optical polarization given by

$$P = \frac{d_{vc}}{\mathsf{S}}\sum_{\mathbf{k}_\parallel} P_{\mathbf{k}_\parallel} + \mathrm{c.c.}, \tag{120}$$

with the quantization area S. Since the macroscopic polarization follows from the singlet term $P_{\mathbf{k}_\parallel}$, the wave equation involves only single-particle contributions without the hierarchy problem. The classical field $\langle E(r_\perp,t)\rangle$ can equivalent be computed directly from the operator-singlet Eq. (67). To obtain the wave equation in the form of Eq. (119), we

assumed that the light field propagates in the direction $r_\perp$ perpendicular to a planar structure with the background refractive index $n(r_\perp)$.

Eqs. (113)–(115) and (119) constitute the MSBE [1,84] which can be used as a general starting point to investigate excitations induced by classical light fields in direct-gap semiconductors. The form of the MSBE is formally exact and the quality of the results depends only on how accurately $\Gamma^{\lambda,\lambda'}$ and Γ^{QED} can be evaluated.

In the remainder of this section, we concentrate on situations where the Coulomb and classical light induced effects dominate and the photon-assisted correlation terms can be omitted. In particular, we are interested to see which physical effects can be described via the MSBE by including $\Gamma^{\lambda,\lambda'}$ at different levels.

5.2. Excitonic states

The homogeneous solution of Eq. (113) without the two-particle correlations defines the eigen-value problem known as the *Wannier equation*

$$\tilde{\varepsilon}_{\mathbf{k}_\parallel}\phi^{\mathrm{R}}_\lambda(\mathbf{k}_\parallel) - (1 - f^{\mathrm{e}}_{\mathbf{k}_\parallel} - f^{\mathrm{h}}_{\mathbf{k}_\parallel}) \sum_{\mathbf{k}'_\parallel} V_{\mathbf{k}_\parallel - \mathbf{k}'_\parallel}\phi^{\mathrm{R}}_\lambda(\mathbf{k}'_\parallel) = E_\lambda \phi^{\mathrm{R}}_\lambda(\mathbf{k}_\parallel) \tag{121}$$

which, for vanishing densities, has a one-to-one correspondence to the Schrödinger equation for the relative-motion problem of atomic hydrogen [1]. The solutions of Eq. (121) define the *exciton* states which describe how electrons and holes are bound together due to the attractive Coulomb interaction of these oppositely charged quasi-particles.

As soon as carrier populations are present, $f^{\mathrm{e}}_{\mathbf{k}_\parallel}$ and $f^{\mathrm{h}}_{\mathbf{k}_\parallel}$ assume finite values with the consequence that Eq. (121) deviates from the original hydrogen problem and becomes a non-Hermitean equation. Consequently, Eq. (121) has both left-handed, $\phi^{\mathrm{L}}_\lambda(\mathbf{k}_\parallel)$, and right-handed, $\phi^{\mathrm{R}}_\lambda(\mathbf{k}_\parallel)$, solutions connected via

$$\phi^{\mathrm{L}}_\lambda(\mathbf{k}_\parallel) = \frac{\phi^{\mathrm{R}}_\lambda(\mathbf{k}_\parallel)}{1 - f^{\mathrm{e}}_{\mathbf{k}_\parallel} - f^{\mathrm{h}}_{\mathbf{k}_\parallel}}. \tag{122}$$

These left- and right-handed solutions are normalized such that

$$\sum_{\mathbf{k}_\parallel} \phi^{\mathrm{L}}_\lambda(\mathbf{k}_\parallel)\phi^{\mathrm{R}}_\nu(\mathbf{k}_\parallel) = \delta_{\lambda,\nu}. \tag{123}$$

Since Eq. (121) defines a real-valued eigen-value problem, we may choose the eigenstates to be real-valued in momentum space.

When we take another look at the term

$$(1 - f^{\mathrm{e}}_{\mathbf{k}_\parallel} - f^{\mathrm{h}}_{\mathbf{k}_\parallel}) V_{\mathbf{k}_\parallel - \mathbf{k}'_\parallel} \equiv V^{\mathrm{eff}}_{\mathbf{k}_\parallel - \mathbf{k}'_\parallel}, \tag{124}$$

we notice that it can be viewed as an effective interaction. Since the phase-space filling factor, $(1 - f^{\mathrm{e}} - f^{\mathrm{h}})$, becomes negative for elevated densities, V^{eff} changes its sign for a certain range of momentum values as the density is increased. Consequently, the effective Coulomb interaction changes from attractive for low densities to repulsive for sufficiently large densities due to the Fermionic Pauli-blocking effects. The resulting Fermi pressure prevents the existence of bound excitons in the many-body system, i.e. the excitonic Mott transition is then reached [1,56,85–87].

5.3. Coherent excitonic polarization

As a next step, we discuss now characteristic signatures of the exciton states in semiclassical semiconductor spectroscopy. Using these states as a basis, we expand the polarization

$$P_{\mathbf{k}_\parallel} = \sum_\lambda p_\lambda \phi^{\mathrm{R}}_\lambda(\mathbf{k}_\parallel), \quad p_\lambda = \sum_{\mathbf{k}_\parallel} \phi^{\mathrm{L}}_\lambda(\mathbf{k}_\parallel) P_{\mathbf{k}_\parallel}. \tag{125}$$

This way, Eq. (113) is converted into

$$\mathrm{i}\hbar \frac{\partial}{\partial t} p_\lambda = E_\lambda p_\lambda - d_{vc}\sqrt{\mathsf{S}}\phi^{\mathrm{R}}_\lambda(\mathbf{r}_\parallel = 0)\langle E(t)\rangle - \mathrm{i}\Gamma_\lambda, \tag{126}$$

which shows that optical excitations involve only *s*-like states. For any other symmetry, the exciton wavefunction in real space,

$$\phi^{\mathrm{R}}_\lambda(\mathbf{r}_\parallel) \equiv \frac{1}{\sqrt{\mathsf{S}}} \sum_{\mathbf{k}_\parallel} \phi^{\mathrm{R}}_\lambda(\mathbf{k}_\parallel)\, \mathrm{e}^{\mathrm{i}\mathbf{k}_\parallel \cdot \mathbf{r}_\parallel} \tag{127}$$

vanishes at $\mathbf{r}_\parallel = 0$. Even though Eq. (126) has a seemingly simple form, the consistent solution with the two-particle correlation terms Γ_λ is highly non-trivial. Due to the relatively difficult mathematical structure of the exciton eigenfunctions, it is often advantageous in practice to numerically evaluate the full problem in the original electron–hole picture.

When the two-particle correlation terms in Eqs. (113)–(115), e.g. the Γ term in Eq. (113), can be neglected, the system is in the so-called coherent limit [1], where the excitation does not suffer from irreversible decay. In this limit, we have the strict conservation law

$$(f_{\mathbf{k}_\parallel} - \tfrac{1}{2})^2 + |P_{\mathbf{k}_\parallel}|^2 = \tfrac{1}{4}, \tag{128}$$

where $f_{\mathbf{k}_\parallel} \equiv f^{\mathrm{e}}_{\mathbf{k}_\parallel} = f^{\mathrm{h}}_{\mathbf{k}_\parallel}$. Since this ideally coherent system does not have correlations, the Hartree–Fock factorization is exact and we should be able to find the many-body wavefunction in the form of a Slater determinant. Thus, we look for a wavefunction in the form

$$|\Psi_{\mathrm{coh}}\rangle = \prod_{\mathbf{k}_\parallel} L^\dagger_{\mathbf{k}_\parallel} |\Psi_0\rangle, \tag{129}$$

where $|\Psi_0\rangle$ is the state of the completely empty semiconductor and $L^\dagger_{\mathbf{k}_\parallel}$ is a Fermionic creation operator such that $|\Psi_{\mathrm{coh}}\rangle$ is a Slater determinant. Since $|\Psi_{\mathrm{coh}}\rangle$ does not involve any correlations, the only constraint is that it should produce the correct $f_{\mathbf{k}_\parallel}$ and $P_{\mathbf{k}_\parallel}$ satisfying the condition (128).

We can choose the operator as

$$L^\dagger_{\mathbf{k}_\parallel} = \mathrm{e}^{\mathrm{i}\psi_{\mathbf{k}_\parallel}} \sin\beta_{\mathbf{k}_\parallel} a^\dagger_{c,\mathbf{k}_\parallel} + \cos\beta_{\mathbf{k}_\parallel} a^\dagger_{v,\mathbf{k}_\parallel} \tag{130}$$

which has indeed a Fermionic character since

$$[L_{\mathbf{k}_\parallel}, L_{\mathbf{k}'_\parallel}]_+ = [L^\dagger_{\mathbf{k}_\parallel}, L^\dagger_{\mathbf{k}'_\parallel}]_+ = 0, \quad [L_{\mathbf{k}_\parallel}, L^\dagger_{\mathbf{k}'_\parallel}]_+ = \delta_{\mathbf{k}_\parallel,\mathbf{k}'_\parallel}. \tag{131}$$

Evaluating the expectation values with the coherent-state wavefunction (129), we directly see that only diagonal contributions exist, i.e.

$$\langle a^\dagger_{c,\mathbf{k}_\parallel} a_{c,\mathbf{k}'_\parallel}\rangle_{\mathrm{coh}} = \langle a_{v,\mathbf{k}'_\parallel} a^\dagger_{v,\mathbf{k}_\parallel}\rangle_{\mathrm{coh}} = \delta_{\mathbf{k}_\parallel,\mathbf{k}'_\parallel} \sin^2\beta_{\mathbf{k}_\parallel} \equiv \delta_{\mathbf{k}_\parallel,\mathbf{k}'_\parallel} f_{\mathbf{k}_\parallel}, \tag{132}$$

$$\langle a^{\dagger}_{v,\mathbf{k}_\parallel} a_{c,\mathbf{k}'_\parallel}\rangle_{\rm coh} = \delta_{\mathbf{k}_\parallel,\mathbf{k}'_\parallel} \sin\beta_{\mathbf{k}_\parallel} \cos\beta_{\mathbf{k}_\parallel} e^{i\psi_{\mathbf{k}_\parallel}} \equiv \delta_{\mathbf{k}_\parallel,\mathbf{k}'_\parallel} P_{\mathbf{k}_\parallel}. \tag{133}$$

Using the basic properties of the trigonometric functions, it is easy to verify that Eqs. (132)–(133) satisfy the coherent-limit condition (128). The explicit values of $\beta_{\mathbf{k}_\parallel}$ and $\psi_{\mathbf{k}_\parallel}$ are then fixed by the inverse of Eqs. (132)–(133), i.e.

$$\beta_{\mathbf{k}_\parallel} = \arcsin\sqrt{f_{\mathbf{k}_\parallel}}, \tag{134}$$

$$e^{i\psi_{\mathbf{k}_\parallel}} = \frac{P_{\mathbf{k}_\parallel}}{|P_{\mathbf{k}_\parallel}|}, \tag{135}$$

which now defines uniquely the many-body wavefunction (129).

Since the coherent limit can also be discussed in the exciton basis, Eq. (125), it is worthwhile to study how excitonic features enter the exact wavefunction, Eq. (129). For this purpose, it is convenient to introduce an exciton operator

$$X_{\lambda,\mathbf{q}_\parallel} \equiv \sum_{\mathbf{k}_\parallel} \phi^{\rm R}_{\lambda}(\mathbf{k}_\parallel) a^{\dagger}_{v,\mathbf{k}_\parallel-\mathbf{q}_{\rm h}} a_{c,\mathbf{k}_\parallel+\mathbf{q}_{\rm e}}, \tag{136}$$

containing the center-of-mass momentum $\mathbf{q}_\parallel$ and

$$\mathbf{q}_{\rm e} = \frac{m_{\rm e}}{m_{\rm e}+m_{\rm h}}\mathbf{q}_\parallel, \quad \mathbf{q}_{\rm h} = \frac{m_{\rm h}}{m_{\rm e}+m_{\rm h}}\mathbf{q}_\parallel. \tag{137}$$

The inverse transformation from the exciton to the electron–hole picture follows from

$$a^{\dagger}_{v,\mathbf{k}_\parallel-\mathbf{q}_{\rm h}} a_{c,\mathbf{k}_\parallel+\mathbf{q}_{\rm e}} = \sum_{\lambda} \phi^{\rm L}_{\lambda}(\mathbf{k}_\parallel) X_{\lambda,\mathbf{q}_\parallel}, \tag{138}$$

where we used the completeness relation,

$$\sum_{\lambda} \phi^{\rm L}_{\lambda}(\mathbf{k}'_\parallel)\phi^{\rm R}_{\lambda}(\mathbf{k}_\parallel) = \delta_{\mathbf{k}_\parallel,\mathbf{k}'_\parallel}, \tag{139}$$

to simplify the λ sum.

Sometimes, the optical properties of semiconductors are modeled by treating $X_{\lambda,\mathbf{q}_\parallel}$ as a Bosonic operator. However, this approximation can seriously compromise the validity of the description since exciton operators have a Fermionic substructure [18,23,88–90], which cannot be ignored in most of the relevant semiconductor investigations. Thus, we always perform our explicit calculations in the electron–hole picture. This way, we not only include the correct Fermionic properties but we can also evaluate the excitonic features by using the transformations (136) and (138).

Next, we introduce the operator

$$S = \sum_{\lambda} [c^{\star}_{\lambda} X_{\lambda,0} - c_{\lambda} X^{\dagger}_{\lambda,0}] \tag{140}$$

which has the interesting property

$$\begin{aligned} e^{S} a^{\dagger}_{v,\mathbf{k}_\parallel} e^{-S} &= a^{\dagger}_{v,\mathbf{k}_\parallel} + [S, a^{\dagger}_{v,\mathbf{k}_\parallel}]_- + \frac{1}{2!}[S,[S,a^{\dagger}_{v,\mathbf{k}_\parallel}]_-]_- + \cdots \\ &= e^{i\psi_{\mathbf{k}_\parallel}} \sin\beta_{\mathbf{k}_\parallel} a^{\dagger}_{c,\mathbf{k}_\parallel} + \cos\beta_{\mathbf{k}_\parallel} a^{\dagger}_{v,\mathbf{k}_\parallel} = L^{\dagger}_{\mathbf{k}_\parallel}. \end{aligned} \tag{141}$$

This transformation produces the Fermionic $L^{\dagger}_{\mathbf{k}_\parallel}$ operator when we make the identification

$$e^{i\psi_{\mathbf{k}_\parallel}}\beta_{\mathbf{k}_\parallel} \equiv \sum_{\lambda} c_\lambda \phi^{R}_{\lambda}(\mathbf{k}_\parallel). \tag{142}$$

The inverse relation is

$$c_\lambda = \sum_{\mathbf{k}_\parallel} \phi^{L}_{\lambda}(\mathbf{k}_\parallel)\, e^{i\psi_{\mathbf{k}_\parallel}}\beta_{\mathbf{k}_\parallel}. \tag{143}$$

Consequently, we can write $L^{\dagger}_{\mathbf{k}_\parallel} = e^{S} a^{\dagger}_{v,\mathbf{k}_\parallel} e^{-S}$. Using this general connection, the coherent-limit wavefunction can be expressed as

$$\begin{aligned} |\Psi_{\mathrm{coh}}\rangle &= \prod_{\mathbf{k}_\parallel} (e^{S} a^{\dagger}_{v,\mathbf{k}_\parallel} e^{-S})|\Psi_0\rangle \\ &= e^{S}\left(\prod_{\mathbf{k}_\parallel} a^{\dagger}_{v,\mathbf{k}_\parallel}\right) e^{-S}|\Psi_0\rangle = e^{S}\prod_{\mathbf{k}_\parallel} a^{\dagger}_{v,\mathbf{k}_\parallel}|\Psi_0\rangle \end{aligned} \tag{144}$$

since $e^{S}e^{-S} = 1$ and $e^{-S}|\Psi_0\rangle = |\Psi_0\rangle$. With the help of this form, we see that $\prod_{\mathbf{k}_\parallel} a^{\dagger}_{v,\mathbf{k}_\parallel}|\Psi_0\rangle \equiv |G\rangle$ is the ground state of a semiconductor where the valence band is completely filled. Thus, the coherent-limit state can equivalently be presented as

$$|\Psi_{\mathrm{coh}}\rangle = e^{S}|G\rangle, \tag{145}$$

showing that the classical excitation generates a well-defined many-body state which is known analytically before the scattering Γ^{λ} sets in.

To study the coherent limit in more detail, we define the functional

$$D[c] \equiv e^{S[c]} = e^{\sum_{\lambda}(c^{\star}_{\lambda} X_{\lambda,0} - c_\lambda X^{\dagger}_{\lambda,0})} \tag{146}$$

which creates the coherent-limit wavefunction, $|\Psi_{\mathrm{coh}}\rangle = D[c]|G\rangle$, according to Eq. (145). The functional form of D resembles the displacement operator generating coherent states for fully Bosonic fields [49]. Based on this formal analogy, we can argue that $|\Psi_{\mathrm{coh}}\rangle$ describes *coherent exciton states*. However, we should always keep in mind that the operator $X_{\lambda,0}$ is fundamentally non-Bosonic [88] such that $|\Psi_{\mathrm{coh}}\rangle$ should not be interpreted as a Bosonic exciton. Moreover, $|\Psi_{\mathrm{coh}}\rangle$ is still a Slater determinant of single-electron functions in a conduction–valence-band superposition state. Hence, such a coherent exciton state is fundamentally different from an incoherent population of truly bound excitons which consists of strongly correlated two-particle electron–hole-pair states.

A proper interpretation of coherent excitons is obtained via Eqs. (129)–(130) showing the full Fermionic substructure. Hence, such a coherent exciton is nothing but a state where any single carrier with momentum $\mathbf{k}_\parallel$ is in a superposition state between the conduction and valence band. The different carriers are completely uncorrelated; only the conduction–valence band mixture of each carrier state is given by a collective phase and an amplitude determined by β and ψ.

5.4. Linear optical response

Conceptually, the simplest experiment is to probe the linear response of the excited semiconductor with a weak classical probe spectrally overlapping the interesting transitions in the vicinity of the band-gap energy. The basic measurable quantities in

this setup follow from the linear susceptibility:

$$\chi(\omega) \equiv \frac{P(\omega)}{\varepsilon_0 E(\omega)} \tag{147}$$

which is obtained as the probe-induced macroscopic polarization, $P(\omega)$, divided by the probe field, $E(\omega)$. Later on, we discuss how $\chi(\omega)$ defines transmission, reflection, and absorption of the light field. In these investigations, the influence of scattering events on P becomes very important since the system may contain a large concentration of incoherent quasi-particles which may lead to strong and non-trivial scattering effects. Since these contributions cannot be described by coherent excitons alone, we have to revert to the full MSBE (113)–(119).

5.5. Elliott formula

Before we discuss the full microscopic correlation contributions to the SBE, we first summarize the analytic solution of the linear problem. As a simplification, we use a phenomenological expression for Γ [1] since this allows us to identify the principal effects beyond the coherent limit. To simplify the analysis, we start from an incoherent semiconductor system, i.e. all polarizations vanish before the system is excited. In this linear limit, $f^{e}_{\mathbf{k}_\parallel}$ and $f^{h}_{\mathbf{k}_\parallel}$ remain zero while only a small—linear—polarization $P_{\mathbf{k}_\parallel}$ is generated. When the microscopic Γ is replaced by a phenomenological value $-i\gamma p_\lambda$, Eq. (126) becomes

$$\hbar\omega p_\lambda(\omega) = (E_\lambda - i\gamma)p_\lambda(\omega) - d_{vc}\sqrt{S}\phi^{R}_\lambda(r=0)\langle E(\omega)\rangle, \tag{148}$$

where we Fourier transformed to the frequency space. The solution of Eq. (148) determines the macroscopic polarization according to

$$\begin{aligned} P(\omega) &= \frac{d_{c,v}}{S}\sum_{\mathbf{k}_\parallel} P_{\mathbf{k}_\parallel}(\omega) = \frac{d_{c,v}}{S}\sum_\lambda \sum_{\mathbf{k}_\parallel} \phi^{R}_\lambda(\mathbf{k}_\parallel)p_\lambda(\omega) \\ &= \frac{d_{c,v}}{\sqrt{S}}\sum_\lambda \phi^{R}_\lambda(\mathbf{r}_\parallel = 0)p_\lambda(\omega) = |d_{cv}|^2 \sum_\lambda \frac{|\phi^{R}_\lambda(\mathbf{r}_\parallel = 0)|^2}{E_\lambda - \hbar\omega - i\gamma}\langle E(\omega)\rangle, \end{aligned} \tag{149}$$

where the last step follows from the solution of Eq. (148). Inserting (149) into Eq. (147), we find the famous *Elliott formula* [5] for the linear semiconductor susceptibility

$$\chi(\omega) = \frac{|d_{cv}|^2}{\varepsilon_0}\sum_\lambda \frac{|\phi^{R}_\lambda(r=0)|^2}{E_\lambda - \hbar\omega - i\gamma}. \tag{150}$$

Since the linear absorption is basically proportional to the imaginary part of the susceptibility [1], the semiconductor absorption shows resonances at the frequencies $\omega = E_\lambda/\hbar$ corresponding to excitonic energies.

The presence of excitonic resonances in $\chi(\omega)$ should not be taken as evidence for the existence of exciton populations in the probed systems. In fact, the largest and best defined resonances are observed for an originally unexcited low-temperature semiconductor. In this case, the linear response does not involve any populations and the weak probe field merely tests the transition possibilities of the interacting system. In other words, the linear response is exclusively determined by the linear polarization that defines the strengths of the different allowed optical transitions. When the linear response shows well defined,

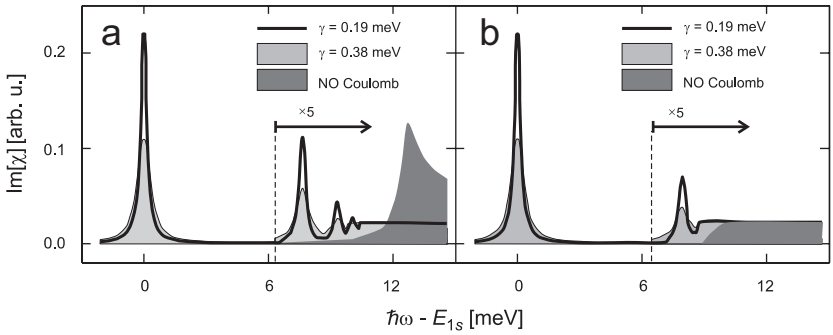

Fig. 3. Imaginary part of the susceptibility, $\mathrm{Im}[\chi(\omega)]$, obtained by evaluating the Elliott formula with a constant dephasing γ. Results for (a) a quantum-wire (QWI) system and (b) a quantum well (QW) are shown; to enhance the visibility of higher excitonic resonances, the corresponding spectrum is multiplied by 5. The calculated spectra for $\gamma = 0.19\,\mathrm{meV}$ are plotted as a solid line, whereas the light shaded area presents the results for $\gamma = 0.38\,\mathrm{meV}$. For comparison, we plot as a dark shaded area the spectra obtained from a calculation without Coulomb interaction ($\gamma = 0.38\,\mathrm{meV}$). The frequency detuning is chosen with respect to the lowest exciton resonance at the energy E_{1s}.

pronounced excitonic resonance, this only means that the light–matter-coupling induced transitions are particularly strong at these frequencies.

To illustrate the basic features of the linear optical properties, we present in Fig. 3 the computed $\mathrm{Im}[\chi(\omega)]$ for an unexcited QWI and QW system. We assumed phenomenological dephasing constants for which we took the values $\gamma = 0.19$ and $0.38\,\mathrm{meV}$. Comparing the QW and the QWI results, we immediately notice that the spectra look very similar. In both cases, they are dominated by excitonic resonances whose spectral width is determined by the phenomenological dephasing constant. From the energetically higher excitons, only the $n = 2$-state is well resolved. The other resonances merge with the onset of the continuum absorption. A more pronounced difference between the QW and QWI systems is visible in the results where we switched off the Coulomb interaction. Here, we obtain a peak just above the band-gap energy ($12\,\mathrm{meV}$ above the $1s$ resonance) for the QWI case as a consequence of the broadened $1/\sqrt{\hbar\omega}$ singularity of the one-dimensional density of states. For the QW system, the density of states is a step function.

5.6. Self-consistent transmission and reflection

In the derivation of the Elliott formula, we treated the optical field as an unmodified external field by solving the SBE without the coupling to the wave equation. If we want to fully account for the self-consistent coupling between the polarization and the light field, we additionally have to include the wave equation (119) into our analysis. A typical QW thickness is around 10 nm while the wavelength of the light is hundreds of nanometers. Therefore, for normal incidence of the light field, the QW practically acts as a δ-function sheet. Thus, Eq. (119) can be reduced to

$$\left[\frac{\partial^2}{\partial r_\perp^2} - \frac{n^2}{c^2}\frac{\partial^2}{\partial t^2}\right]\langle E(r_\perp, t)\rangle = \mu_0 \delta(r_\perp)\frac{\partial^2}{\partial t^2} P, \tag{151}$$

where the confinement function $|\xi(r_\perp)|^2$ is replaced by $\delta(r_\perp)$ at the QW position $r_\perp = 0$.

The self-consistent coupling between light and matter can be solved numerically [91,92]. To gain analytic insight, we next assume that the QW and the barrier materials have a negligible difference in their background refractive index, such that we can take everywhere the same value for n. With these simplifying assumptions, one can show [52], that the light field is determined by the equation

$$\langle E(r_\perp,t)\rangle = \langle E(r_\perp,t)\rangle_0 - \mu_0 \frac{c}{2n}\frac{\partial}{\partial u} P(u)\Big|_{u=t-|nr_\perp|/c}, \tag{152}$$

where $\langle E(r_\perp,t)\rangle_0$ is the incoming laser pulse that approaches the QW system from left to right. The transmitted and reflected fields are then given by

$$\langle E_{\rm R}(r_\perp,t)\rangle = -\mu_0 \frac{c}{2n}\frac{\partial}{\partial u} P(u)\Big|_{u=t-|nr_\perp|/c}, \quad r_\perp \leqslant 0, \tag{153}$$

$$\langle E_{\rm T}(r_\perp,t)\rangle = \langle E(r_\perp,t)\rangle_0 - \mu_0 \frac{c}{2n}\frac{\partial}{\partial u} P(u)\Big|_{u=t-|nr_\perp|/c}, \quad r_\perp \geqslant 0, \tag{154}$$

respectively. Taking the Fourier transform of both expressions at the QW position $r_\perp = 0$, we find the spectrum of the reflected and transmitted fields

$$\langle E_{\rm R}(\omega)\rangle = {\rm i}\mu_0 \frac{c}{2n}\,\omega P(\omega), \tag{155}$$

$$\langle E_{\rm T}(\omega)\rangle = \langle E(\omega)\rangle_0 + {\rm i}\mu_0 \frac{c}{2n}\,\omega P(\omega), \tag{156}$$

which establishes exact relations for both, linear and non-linear excitation conditions. In the linear case, we have $P(\omega) = \varepsilon_0\chi(\omega)\langle E_{\rm T}(\omega)\rangle$ since the macroscopic polarization is directly proportional to the field $\langle E_{\rm T}(\omega)\rangle$ at the QW position, see Eq. (147). Inserting these relations into Eqs. (155)–(156), we find the explicit form for the linear reflection and transmission spectra,

$$\langle E_{\rm R}(\omega)\rangle = \frac{{\rm i}\xi(\omega)}{1-{\rm i}\xi(\omega)}\langle E(\omega)\rangle_0, \tag{157}$$

$$\langle E_{\rm T}(\omega)\rangle = \frac{1}{1-{\rm i}\xi(\omega)}\langle E(\omega)\rangle_0, \tag{158}$$

$$\xi(\omega) \equiv \frac{1}{2}\frac{\omega}{nc}\,\chi(\omega) = \sum_\lambda \frac{\Gamma^{\rm rad}_{\lambda,\lambda}}{E_\lambda - \hbar\omega - {\rm i}\gamma}, \tag{159}$$

where $c = 1/\sqrt{\mu_0\varepsilon_0}$ is the speed of light in vacuum. We have also defined the radiative coupling constant

$$\Gamma^{\rm rad}_{\lambda,v} \equiv \frac{1}{2}\frac{|d_{v,c}|^2}{\varepsilon_0}\frac{\omega_0}{nc}\,\phi^{\rm R}_\lambda(\mathbf{r}_\parallel = 0)\phi^{\rm R}_v(\mathbf{r}_\parallel = 0). \tag{160}$$

In principle, $\Gamma^{\rm rad}_{\lambda,v}$ should contain the frequency ω instead of $\omega_0 \equiv E_{\rm g}/\hbar$ corresponding to the band-gap energy. However, since all interesting band-to-band transitions are within few percent of ω_0, we may ignore the full frequency dependency in Eq. (160). For a QWI

system, also the density of wires, $n_{\rm wire}$, has to be included to provide

$$\Gamma^{\rm rad}_{\lambda,\nu} \equiv \frac{1}{2}\frac{|d_{v,c}|^2}{\varepsilon_0}\frac{\omega_0}{nc}\, n_{\rm wire}\phi^{\rm R}_{\lambda}(\mathbf{r}_{\parallel}=0)\phi^{\rm R}_{\nu}(\mathbf{r}_{\parallel}=0). \tag{161}$$

In our numerical evaluations, we adjust $n_{\rm wire}$ such that the QWI array produces the same $\Gamma^{\rm rad}_{1s,1s}$ as the corresponding QW system.

Along the lines of these arguments, we can now identify the reflection and transmission coefficients in the linear regime as

$$R(\omega) \equiv \frac{\langle E_{\rm R}(\omega)\rangle}{\langle E(\omega)\rangle_0} = \frac{{\rm i}\xi(\omega)}{1-{\rm i}\xi(\omega)}, \tag{162}$$

$$T(\omega) \equiv \frac{\langle E_{\rm T}(\omega)\rangle}{\langle E(\omega)\rangle_0} = \frac{1}{1-{\rm i}\xi(\omega)}, \tag{163}$$

respectively. From these, we obtain the linear absorption as

$$\alpha(\omega) \equiv 1-|R(\omega)|^2-|T(\omega)|^2 = \frac{2\,{\rm Im}[\xi(\omega)]}{1+|\xi(\omega)|^2+2\,{\rm Im}[\xi(\omega)]}, \tag{164}$$

which defines the scaled intensity difference of the incoming and the sum of the reflected and the transmitted fields.

For sufficiently low densities, $\xi(\omega)$ is clearly dominated by the $1s$ resonance as shown in Fig. 3. Consequently, in the spectral range of the $1s$-exciton resonance $\xi(\omega)$ can often be approximated by the first term in the sum (159). This approximation produces

$$R(\omega) = \frac{{\rm i}\Gamma^{\rm rad}_{1s,1s}}{E_{1s}-\hbar\omega-{\rm i}(\gamma+\Gamma^{\rm rad}_{1s,1s})}, \tag{165}$$

$$T(\omega) = \frac{E_{1s}-\hbar\omega-{\rm i}\gamma}{E_{1s}-\hbar\omega-{\rm i}(\gamma+\Gamma^{\rm rad}_{1s,1s})}, \tag{166}$$

$$\alpha(\omega) \equiv \frac{2\gamma\Gamma^{\rm rad}_{1s,1s}}{(E_{1s}-\hbar\omega)^2+(\gamma+\Gamma^{\rm rad}_{1s,1s})^2}, \tag{167}$$

showing that the self-consistent light–matter coupling introduces an additional broadening $\Gamma^{\rm rad}_{1s,1s}$ of the absorption resonance [52,93–96].

If we assume that ${\rm Im}[\xi(\omega)]$ and $|\xi(\omega)|^2$ are small in magnitude ($\ll 1$), we find that the absorption spectrum reduces to the form

$$\alpha_{\rm Elliott}(\omega) = 2\,{\rm Im}[\xi(\omega)] = \frac{\omega}{nc}\,{\rm Im}[\chi(\omega)] = \sum_{\lambda}\frac{2\gamma\Gamma^{\rm rad}_{\lambda,\lambda}}{(E_{\lambda}-\hbar\omega)^2+\gamma^2} \tag{168}$$

which connects the Elliott formula and the QW absorption. In the Elliott result, the light–matter coupling is not included fully self-consistently since the excitonic resonances are not additionally broadened by $\Gamma^{\rm rad}_{\lambda,\lambda}$. Nevertheless, $\alpha_{\rm Elliott}(\omega)$ should describe the QW absorption accurately as long as the non-radiative homogeneous dephasing strongly exceeds the radiative dephasing, i.e. $\gamma \gg \Gamma^{\rm rad}_{\lambda,\lambda}$, which often is the case in real semiconductor structures.

Eqs. (162)–(164) present general relations for the linear reflection, transmission, and absorption for a thin QW even when the response function $\xi(\omega)$ does not have a Lorentzian form. In particular, these relations tell us how the self-consistent light–matter coupling transforms the linear susceptibility $\chi(\omega)$ into measurable quantities. For example, the true single QW absorption, Eq. (164), can deviate significantly from its inconsistent counterpart, $\alpha_{\text{Elliott}}(\omega) = 2\text{Im}[\xi(\omega)] = (\omega/nc)\,\text{Im}[\chi(\omega)]$, for situations where the radiative coupling is dominant.

It is interesting to note that the Eqs. (162)–(164) suggest a scheme to extract both γ and $\Gamma_{1s,1s}$ using the measured width of the $1s$ resonance and the measured value of the peak absorption, transmission, or reflection. As an illustration, we consider a case where the strongest $1s$ resonance has a dominantly Lorentzian lineshape. In this situation, we may directly apply the relations (165)–(167) to obtain

$$\alpha_{1s} \equiv \frac{2\gamma\Gamma^{\text{rad}}_{1s,1s}}{(\gamma+\Gamma^{\text{rad}}_{1s,1s})^2}, \quad T_{1s} = \frac{\gamma}{\gamma+\Gamma^{\text{rad}}_{1s,1s}}, \quad R_{1s} = -\frac{\Gamma^{\text{rad}}_{1s,1s}}{\gamma+\Gamma^{\text{rad}}_{1s,1s}} \tag{169}$$

at $\hbar\omega = E_{1s}$. If we now take the measured values of the $1s$-peak absorption, α_{meas}, and its width γ_{meas}, Eq. (169) implies that the actual γ and $\Gamma_{1s,1s}$ are determined by the simple pair of equations,

$$\alpha_{\text{meas}} = \frac{2\gamma\Gamma^{\text{rad}}_{1s,1s}}{(\gamma+\Gamma^{\text{rad}}_{1s,1s})^2}, \quad \gamma_{\text{meas}} = \gamma + \Gamma^{\text{rad}}_{1s,1s}. \tag{170}$$

The solutions are

$$\Gamma^{\text{rad}}_{1s,1s} = \frac{\gamma_{\text{meas}}(1 \pm \sqrt{1-2\alpha_{\text{meas}}})}{2}, \quad \gamma = \frac{\gamma_{\text{meas}}(1 \mp \sqrt{1-2\alpha_{\text{meas}}})}{2}. \tag{171}$$

Similarly, we obtain

$$\Gamma^{\text{rad}}_{1s,1s} = \gamma_{\text{meas}}(1-|T_{1s}|), \quad \gamma = \gamma_{\text{meas}}|T_{1s}|, \tag{172}$$

$$\Gamma^{\text{rad}}_{1s,1s} = \gamma_{\text{meas}}|R_{1s}|, \quad \gamma = \gamma_{\text{meas}}(1-|R_{1s}|), \tag{173}$$

from either the experimental transmission or reflection. Thus, the measurement of the single-QW absorption, transmission, or reflection spectra in absolute units can be used to extract the actual values of the radiative and non-radiative dephasing constants.

To investigate how the self-consistent light–matter coupling changes the usual Elliott absorption, we compute the actual absorption for a QW and a QWI system using Eq. (164). The results are presented in Fig. 4 and compared with those obtained from Eq. (168) using different phenomenological dephasings γ. In Figs. 4a and d, we see that for γ close to or smaller than the radiative damping, the light–matter coupling strongly modifies the absorption at the $1s$ resonance. The true $1s$ absorption becomes considerably smaller in magnitude and broader in width as predicted by Eq. (167). The radiative coupling reduces α mostly at the $1s$ peak; for the higher excitonic states, the coupling effects are much weaker. These features are still clearly observable for the case of larger dephasing, $\gamma = 10\Gamma_{1s,1s}$, presented in Figs. 4b and e.

In Figs. 4c and f, the computed full $1s$-absorption peak and the analytic result from Eq. (169) are plotted as function of γ. Even though the analytic formula includes only the $1s$ state, it reproduces the full result with great accuracy even for elevated γ. The Elliott

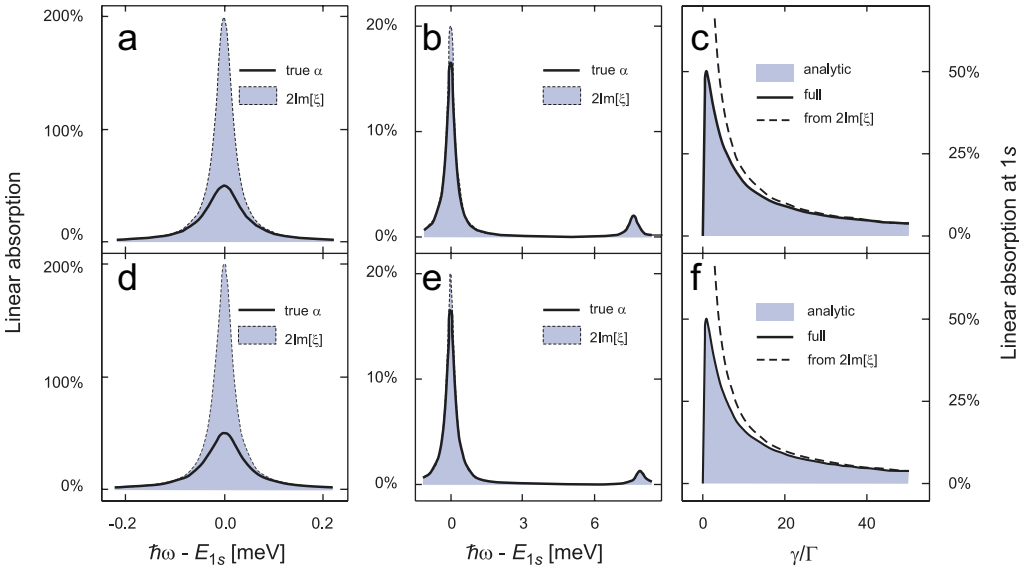

Fig. 4. Influence of the self-consistent light–matter coupling effects on the linear absorption. The true absorption (solid line) is compared with α_{Elliott} (dashed, shaded area) which does not include radiative coupling. Frames (a), (b), and (c) [(d), (e), and (f)] present the results for a QWI [QW] system using $\Gamma^{\text{rad}}_{1s,1s} = 20\,\mu\text{eV}$. The phenomenological dephasing is taken as $\gamma = \Gamma^{\text{rad}}_{1s,1s}$ in (a) and (d), and as $\gamma = 10\Gamma^{\text{rad}}_{1s,1s}$ in (b) and (e). Frames (c) and (f) compare the dephasing dependence of the peak absorption at the $1s$ resonance for the full calculation (solid line) with the analytic result from Eq. (169) (shaded area) and the Elliott result, $\text{Im}[\xi]_{1s} = \Gamma^{\text{rad}}_{1s,1s}/\gamma$ (dashed line).

result $\text{Im}[\xi]$ approaches the full α_{1s} only for large dephasing values. The level of deviation between $\text{Im}[\xi]$ and α_{1s} gives an estimate how accurately the absorption peak height must be measured in order to accurately construct the actual γ and $\Gamma_{1s,1s}$ from Eqs. (171). We also notice that the linear absorption is maximized when γ is equal to the radiative dephasing. For this case, 50% of the light is absorbed because only the cosine part (antinode at the QW) of the plane wave can be absorbed. This maximum absorption is naturally changed in we include, e.g. an air–QW–air index step to the analysis since then the structure acts as an optical cavity where the light is multiply reflected resulting in standing-wave contributions.

5.7. Radiative polarization decay

The exact solution (152) for the classical field allows us to fully include the self-consistent light–matter coupling to the SBE. In particular, applying Eq. (152) at the QW position $r_\perp = 0$, we obtain

$$\begin{aligned}\langle E(0,t)\rangle &= \langle E(0,t)\rangle_0 - \mu_0 \frac{c}{2n}\frac{\partial}{\partial t} P(t),\\ &= \langle E(0,t)\rangle_0 - \frac{1}{2n\varepsilon_0 c}\frac{d_{v,c}}{\sqrt{S}}\sum_\lambda \phi^{\text{R}}_\lambda(\mathbf{r}_\parallel = 0)\frac{\partial}{\partial t} p_\lambda,\end{aligned} \tag{174}$$

where $\langle E(0,t)\rangle_0$ is the incoming laser field and the macroscopic polarization is expressed in the exciton basis (125). We notice from Eq. (126) that each different exciton component

has its eigenfrequency $\omega_\lambda = E_\lambda/\hbar$. However, since these frequencies and the excitation frequency are all within a few percent of the band-gap frequency

$$\omega_0 \equiv \frac{E_g}{\hbar}, \tag{175}$$

we may use $(\partial/\partial t)p_\lambda = -i\omega_0 p_\lambda$ to simplify (174),

$$\langle E(0,t)\rangle = \langle E(0,t)\rangle_0 + i\frac{1}{\sqrt{S}2\varepsilon_0 n}\frac{d_{v,c}\omega_0}{c}\sum_\lambda \phi_\lambda^R(\mathbf{r}_\parallel = 0)p_\lambda(t), \tag{176}$$

just as in Eq. (160). If we now insert this solution back into Eq. (126), we obtain

$$i\hbar\frac{\partial}{\partial t}p_\lambda = E_\lambda p_\lambda - d_{vc}\sqrt{S}\phi_\lambda^R(\mathbf{r}_\parallel = 0)\langle E(t)\rangle_0 - i\sum_\beta \Gamma_{\lambda,\beta}^{rad}p_\beta - i\Gamma_\lambda. \tag{177}$$

Here, the radiative decay constant Γ^{rad} appears according to Eq. (160). If the excitation is resonant with a particular exciton energy E_λ, we may approximately assume that only the component $p_\nu = \delta_{\nu,\lambda}p_\lambda$ is excited. In this case, Eq. (177) predicts that this polarization component decays exponentially with the rate $\Gamma_{\lambda,\lambda}^{rad}/\hbar$ when the additional scattering Γ_λ can be omitted. This radiative decay of the QW polarization [97] is a consequence of the lacking momentum conservation in the $r_\perp$ direction between the photon and the polarization. For an infinite bulk material, this radiative decay is replaced by polariton oscillations resulting from the self-consistent coupling between the polarization and the light field [1,97–100].

An obvious way to improve the Elliott formula for a QW is to include the radiative decay constant $\Gamma_{\lambda,\lambda}^{rad}$ of each exciton state in Eq. (150), as suggested by our earlier result, Eq. (167). As a consequence, each exciton resonance then experiences a different broadening. To analyze the characteristic behavior of this radiative decay, we plot $\Gamma_{\lambda,\lambda}^{rad}$ in Fig. 5a and the radiative decay time,

$$\tau_\lambda = \frac{\hbar}{2\Gamma_{\lambda,\lambda}^{rad}}, \tag{178}$$

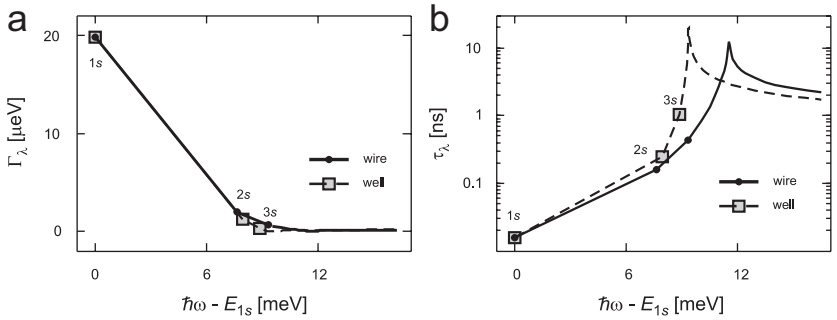

Fig. 5. Radiative decay rate for the *s*-like exciton states. (a) The computed $\Gamma_{\lambda,\lambda}^{rad}$ and (b) the radiative decay time are presented as function of exciton energy. These quantities have been evaluated using Eqs. (161) and (178), respectively. The QWI results (solid line) are compared to those for a QW (dashed line). The filled circles (QWI) and squares (QW) indicate the three first bound states. The line between these points is only a guide to the eye since there are no real states in between these points.

for $|p_\lambda|^2$ in Fig. 5b as function of exciton energy. The results are presented for the optically active s-like excitons in the generic GaAs QW (solid line) and QWI (dashed line) system used in all our computations. We see that the radiative decay constant decreases strongly with increasing exciton quantum number.The 1s-exciton lifetime is roughly 15 ps for the QWI and the QW system used in this review. For the other states, the lifetime approaches the nanosecond range which clearly indicates that these states are only weakly coupled to the light field. In Fig. 5b, we note that the transition to the continuum states is indicated by a sharp increase of τ_λ.

So far, our analysis shows that the coherent optical polarization vanishes from the system either via radiative decay or non-radiatively via scattering-induced Γ_λ contributions. These effects can in principle be observed as spectral changes in the linear absorption (see Fig. 4). One can also show that the Elliott formula remains structurally unchanged even when the correlation contributions Γ in Eq. (126) are included microscopically. However, in this case we have to allow for a more general interpretation of the terms appearing in the Elliott formula. In particular, γ then depends on both ω and the exciton state λ, and one finds density-, exciton-index-, and frequency-dependent renormalizations of both E_λ and $\phi_\lambda(\mathbf{r}_\parallel = 0)$ [22,31,101].

5.8. Coherent and incoherent carrier correlations

Our analysis shows that it is natural to separate the singlet contributions into coherent and incoherent parts, i.e. into the optical polarization and the carrier populations, respectively. As shown in the previous section, the coherently induced polarization $P_{\mathbf{k}_\parallel}$ decays on a picosecond time scale, whereas the characteristic lifetime of the incoherent densities $f^{\mathrm{e}}_{\mathbf{k}_\parallel}$ and $f^{\mathrm{h}}_{\mathbf{k}_\parallel}$ is in the range of several nanoseconds.

In the same way as the singlets, also the carrier doublets can be divided into coherent and incoherent correlations depending on their characteristic decay times. The character of a generic two-particle correlation can be deduced from its singlet–doublet dynamics (96). As a general starting point, the unexcited semiconductor has vanishing polarization, densities, and correlations. As the excitation is applied, the field induces a polarization which then can be converted into different quasi-particle excitations and correlations. The structure of Eq. (96) shows that a generic correlation is generated via the single-particle source term

$$S^{\mathbf{q}_\parallel,\mathbf{k}'_\parallel,\mathbf{k}_\parallel}_{\lambda,\nu;\nu',\lambda'} \equiv \mathrm{Sym}_{\mathrm{F}}([\tfrac{1}{2}S^{(1)} - S^{(2)}]^{\mathbf{q}_\parallel,\mathbf{k}'_\parallel,\mathbf{k}_\parallel}_{\lambda,\nu;\nu',\lambda'}). \tag{179}$$

If $S_{\lambda,\nu;\nu',\lambda'}$ exists only as long as the coherent polarization is present, this correlation is *coherent*; otherwise it is *incoherent*. With this analysis, we find that

$$\Delta\langle 2\rangle_{\mathrm{coh}} = \{c^{\mathbf{q}_\parallel,\mathbf{k}'_\parallel,\mathbf{k}_\parallel}_{c,c,c,v}, c^{\mathbf{q}_\parallel,\mathbf{k}'_\parallel,\mathbf{k}_\parallel}_{v,v,v,c}, c^{\mathbf{q}_\parallel,\mathbf{k}'_\parallel,\mathbf{k}_\parallel}_{v,v,c,c}\} \tag{180}$$

represent the coherent correlations whereas

$$\Delta\langle 2\rangle_{\mathrm{inc}} = \{c^{\mathbf{q}_\parallel,\mathbf{k}'_\parallel,\mathbf{k}_\parallel}_{c,c,c,c}, c^{\mathbf{q}_\parallel,\mathbf{k}'_\parallel,\mathbf{k}_\parallel}_{v,v,v,v}, c^{\mathbf{q}_\parallel,\mathbf{k}'_\parallel,\mathbf{k}_\parallel}_{c,v,c,v}\} \tag{181}$$

are the incoherent correlations, respectively.

5.9. Linear optical polarization

Before we investigate the non-linear optical properties, we first study the response of a semiconductor to a weak optical excitation. Even though we allow for the presence of finite densities, we still include only contributions that are linear in the optical probe induced polarization. Since we assume classical fields, we can omit the quantum-optical correction in Eq. (113), i.e.

$$i\hbar\frac{\partial}{\partial t}P_{\mathbf{k}_\parallel}=\tilde{\varepsilon}_{\mathbf{k}_\parallel}P_{\mathbf{k}_\parallel}-[1-f^{e}_{\mathbf{k}_\parallel}-f^{h}_{\mathbf{k}_\parallel}]\Omega_{\mathbf{k}_\parallel}+\Gamma^{v,c}_{\mathbf{k}_\parallel}, \tag{182}$$

$$\Gamma^{v,c}_{\mathbf{k}_\parallel}\equiv\sum_{v,\mathbf{k}'_\parallel,\mathbf{q}_\parallel\neq\mathbf{0}}V_{\mathbf{q}_\parallel}[c^{\mathbf{q}_\parallel,\mathbf{k}'_\parallel,\mathbf{k}_\parallel}_{v,v;v,c}+c^{\mathbf{q}_\parallel,\mathbf{k}'_\parallel,\mathbf{k}_\parallel}_{v,c;c,c}-(c^{\mathbf{q}_\parallel,\mathbf{k}'_\parallel,\mathbf{k}_\parallel}_{c,v;v,v}+c^{\mathbf{q}_\parallel,\mathbf{k}'_\parallel,\mathbf{k}_\parallel}_{c,c;c,v})^{\star}]. \tag{183}$$

In this form, the self-consistent light–matter coupling follows as we use the result (174) to define the renormalized Rabi frequency $\Omega_{\mathbf{k}_\parallel}$. Furthermore, the carrier densities are not changed by the weak probe field.

To solve Eqs. (182)–(183), we have to evaluate the dynamics of the coherent carrier correlations $c_{v,v;v,c}$, $c_{v,c;c,c}$, $c_{c,v;v,v}$, and $c_{c,c;c,v}$. Since the formal dynamics of all of these terms is very similar, the full singlet–doublet equations are presented only for $c_{v,v;v,c}$ in the Appendix G. Furthermore, we elaborate here only those parts of $c_{v,v;v,c}$ that are important for the linear response.

In general, $c_{v,v;v,c}$ couples also to incoherent density–density correlations $c_{\lambda,\lambda;\lambda,\lambda}$ and we define

$$c^{\mathbf{q}_\parallel,\mathbf{k}'_\parallel,\mathbf{k}_\parallel}_{X}\equiv c^{\mathbf{q}_\parallel,\mathbf{k}'_\parallel,\mathbf{k}_\parallel}_{c,v;c,v} \tag{184}$$

which we will later relate to correlations of true exciton populations. We show in the Appendices that also c_X and $c_{\lambda,\lambda;\lambda,\lambda}$ are driven by the coherent light. However, these contributions are non-linear such that c_X and $c_{\lambda,\lambda;\lambda,\lambda}$, if it exists, only contributes as constant source to the linear response. In addition to these, $c_{v,v;v,c}$ also couples to the coherent biexciton amplitude

$$c^{\mathbf{q}_\parallel,\mathbf{k}'_\parallel,\mathbf{k}_\parallel}_{\mathrm{BiX}}\equiv c^{\mathbf{q}_\parallel,\mathbf{k}'_\parallel,\mathbf{k}_\parallel}_{v,v;c,c} \tag{185}$$

which is a coherent correlation. However, c_{BiX} is irrelevant for the linear response since it produces only non-linear contributions to the dynamics of $c_{v,v;v,c}$.

We may now unravel the dynamics of $c_{v,v;v,c}$ with the help of Eqs. (96)–(109). The details are given in the Appendices such that we can here directly apply the results by including only those terms that are relevant for the linear response to a classical field. We obtain

$$\begin{aligned}i\hbar\frac{\partial}{\partial t}c^{\mathbf{q}_\parallel,\mathbf{k}'_\parallel,\mathbf{k}_\parallel}_{v,v;v,c}&=(\tilde{\varepsilon}^{e}_{\mathbf{k}_\parallel-\mathbf{q}_\parallel}+\tilde{\varepsilon}^{h}_{\mathbf{k}_\parallel}-\tilde{\varepsilon}^{h}_{\mathbf{k}'_\parallel+\mathbf{q}_\parallel}+\tilde{\varepsilon}^{h}_{\mathbf{k}'_\parallel}-i\gamma)c^{\mathbf{q}_\parallel,\mathbf{k}'_\parallel,\mathbf{k}_\parallel}_{v,v;v,c}\\&\quad+S^{\mathbf{q}_\parallel,\mathbf{k}'_\parallel,\mathbf{k}_\parallel}_{v,v;v,c}+[D^{\mathbf{q}_\parallel,\mathbf{k}'_\parallel,\mathbf{k}_\parallel}_{v,v;v,c}]_{\mathrm{coh}}+[D^{\mathbf{q}_\parallel,\mathbf{k}'_\parallel,\mathbf{k}_\parallel}_{v,v;v,c}]_{\mathrm{inc}},\end{aligned} \tag{186}$$

where the triplet scattering is replaced by a phenomenological dephasing constant γ. The fully microscopic description of the triplets is discussed in the Appendices.

In general, $S_{v,v;v,c}$ results from the singlet factorization of the Coulomb-induced three-particle terms, i.e. from the terms represented by the simplest diagram in Fig. 2. Physically, $S_{v,v;v,c}$ acts as a source that generates $c_{v,v;v,c}$ even when the doublet correlations initially

vanish. Explicitly, we can write

$$\begin{aligned}\mathrm{S}^{\mathbf{q}_\parallel,\mathbf{k}'_\parallel,\mathbf{k}_\parallel}_{\lambda,\nu;\nu',\lambda'} \equiv{}& \delta_{\sigma,\sigma'} V_{\mathbf{j}_\parallel}[P_{\mathbf{k}_\parallel-\mathbf{q}_\parallel}(f^{\mathrm{h}}_{\mathbf{k}_\parallel} f^{\mathrm{h}}_{\mathbf{k}'_\parallel} \bar{f}^{\mathrm{h}}_{\mathbf{k}'_\parallel+\mathbf{q}_\parallel})_\Sigma - P_{\mathbf{k}'_\parallel}(f^{\mathrm{h}}_{\mathbf{k}_\parallel} f^{\mathrm{e}}_{\mathbf{k}_\parallel-\mathbf{q}_\parallel} \bar{f}^{\mathrm{h}}_{\mathbf{k}'_\parallel+\mathbf{q}_\parallel})_\Sigma] \\ &+ V_{\mathbf{q}_\parallel}[P_{\mathbf{k}_\parallel}(f^{\mathrm{h}}_{\mathbf{k}'_\parallel} f^{\mathrm{e}}_{\mathbf{k}_\parallel-\mathbf{q}_\parallel} \bar{f}^{\mathrm{h}}_{\mathbf{k}'_\parallel+\mathbf{q}_\parallel})_\Sigma - P_{\mathbf{k}_\parallel-\mathbf{q}_\parallel}(f^{\mathrm{h}}_{\mathbf{k}_\parallel} f^{\mathrm{h}}_{\mathbf{k}'_\parallel} \bar{f}^{\mathrm{h}}_{\mathbf{k}'_\parallel+\mathbf{q}_\parallel})_\Sigma], \end{aligned} \tag{187}$$

where we have denoted the explicit spin-index dependency for the combination that is relevant for optical excitations, i.e.

$$c_{v,v;v,c} \equiv c_{(v,\sigma),(v,\sigma');(v,\sigma'),(c,\sigma)}, \quad S_{v,v;v,c} \equiv S_{(v,\sigma),(v,\sigma');(v,\sigma'),(c,\sigma)}. \tag{188}$$

We have also introduced the abbreviations

$$\bar{f}^{\lambda}_{\mathbf{k}_\parallel} = 1 - f^{\lambda}_{\mathbf{k}_\parallel}, \tag{189}$$

$$(f^{\lambda}_{\mathbf{k}_\parallel} f^{\lambda'}_{\mathbf{k}'_\parallel} \bar{f}^{\lambda''}_{\mathbf{k}''_\parallel})_\Sigma \equiv f^{\lambda}_{\mathbf{k}_\parallel} f^{\lambda'}_{\mathbf{k}'_\parallel}(1 - f^{\lambda''}_{\mathbf{k}''_\parallel}) + (1 - f^{\lambda}_{\mathbf{k}_\parallel})(1 - f^{\lambda'}_{\mathbf{k}'_\parallel}) \bar{f}^{\lambda''}_{\mathbf{k}''_\parallel}, \tag{190}$$

$$\mathbf{j}_\parallel \equiv \mathbf{k}'_\parallel + \mathbf{q}_\parallel - \mathbf{k}_\parallel. \tag{191}$$

Since $\mathrm{S}_{v,v;v,c}$ is the only term which drives the initially non-existing correlation, we conclude that $c_{v,v;v,c}$ is generated only via polarization transfer because all terms in $\mathrm{S}_{v,v;v,c}$ contain P. This observation also verifies that $c_{v,v;v,c}$ is a coherent correlation as classified earlier in Section 5.8.

Once $c_{v,v;v,c}$ is generated, it is modified by more complicated terms that contain the Coulomb-matrix element and correlated doublets in the singlet–doublet factorization of the hierarchy problem. Already in Section 4.3.3, we have shown that these contributions can be subdivided into terms related to screening-type effects and build-up of new quasi-particle states. By using the results derived in the Appendices, we obtain the contributions for the linear response,

$$\begin{aligned}[D^{\mathbf{q}_\parallel,\mathbf{k}'_\parallel,\mathbf{k}_\parallel}_{v,v;v,c}]_{\mathrm{coh}} = {}& V_{\mathbf{q}_\parallel}(f^{\mathrm{h}}_{\mathbf{k}'_\parallel+\mathbf{q}_\parallel} - f^{\mathrm{h}}_{\mathbf{k}'_\parallel}) \sum_{\mathbf{l}_\parallel} (c^{\mathbf{q}_\parallel,\mathbf{l}_\parallel,\mathbf{k}_\parallel}_{v,c;c,c} + c^{\mathbf{q}_\parallel,\mathbf{l}_\parallel,\mathbf{k}_\parallel}_{v,v;v,c}) \\ &+ V_{\mathbf{j}_\parallel}(f^{\mathrm{h}}_{\mathbf{k}_\parallel} - f^{\mathrm{h}}_{\mathbf{k}_\parallel+\mathbf{j}_\parallel}) \sum_{\mathbf{l}_\parallel} (c^{-\mathbf{j}_\parallel,\mathbf{k}'_\parallel,\mathbf{l}_\parallel}_{c,v;c,c} + c^{-\mathbf{j}_\parallel,\mathbf{k}'_\parallel,\mathbf{l}_\parallel}_{v,v;c,v}) \\ &+ (1 - f^{\mathrm{h}}_{\mathbf{k}_\parallel} - f^{\mathrm{h}}_{\mathbf{k}'_\parallel}) \sum_{\mathbf{l}_\parallel} V_{\mathbf{l}_\parallel+\mathbf{q}_\parallel} [c^{\mathbf{l}_\parallel,\mathbf{k}'_\parallel+\mathbf{q}_\parallel,\mathbf{k}_\parallel-\mathbf{q}_\parallel}_{c,v;v,v}]^\star \\ &- (1 - f^{\mathrm{e}}_{\mathbf{k}_\parallel-\mathbf{q}_\parallel} - f^{\mathrm{h}}_{\mathbf{k}_\parallel}) \sum_{\mathbf{l}_\parallel} V_{\mathbf{l}-\mathbf{k}_\parallel} c^{\mathbf{q}_\parallel,\mathbf{k}'_\parallel,\mathbf{l}_\parallel}_{v,v;v,c} \\ &+ (1 - f^{\mathrm{e}}_{\mathbf{k}_\parallel-\mathbf{q}_\parallel} - f^{\mathrm{h}}_{\mathbf{k}'_\parallel}) \sum_{\mathbf{l}_\parallel} V_{\mathbf{l}-\mathbf{k}'_\parallel} c^{\mathbf{j}_\parallel,\mathbf{l}_\parallel,\mathbf{k}_\parallel}_{v,v;v,c} \\ &+ (f^{\mathrm{h}}_{\mathbf{k}'_\parallel+\mathbf{q}_\parallel} - f^{\mathrm{h}}_{\mathbf{k}_\parallel}) \sum_{\mathbf{l}_\parallel} V_{\mathbf{l}-\mathbf{k}_\parallel} c^{-\mathbf{j}_\parallel,\mathbf{k}'_\parallel,\mathbf{l}_\parallel}_{v,v;c,v} + (f^{\mathrm{h}}_{\mathbf{k}'_\parallel} - f^{\mathrm{h}}_{\mathbf{k}'_\parallel+\mathbf{q}_\parallel}) \sum_{\mathbf{l}_\parallel} V_{\mathbf{l}_\parallel-\mathbf{k}'_\parallel} c^{\mathbf{q}_\parallel,\mathbf{l}_\parallel,\mathbf{k}_\parallel}_{v,v;v,c} \\ &- (f^{\mathrm{e}}_{\mathbf{k}_\parallel-\mathbf{q}_\parallel} - f^{\mathrm{h}}_{\mathbf{k}'_\parallel+\mathbf{q}_\parallel}) \sum_{\mathbf{l}_\parallel} V_{\mathbf{l}_\parallel-\mathbf{q}_\parallel} c^{\mathbf{l}_\parallel,\mathbf{k}'_\parallel,\mathbf{k}_\parallel}_{v,v;v,c}, \end{aligned} \tag{192}$$

$$
\begin{aligned}
[D^{\mathbf{q}_\parallel,\mathbf{k}'_\parallel,\mathbf{k}_\parallel}_{v,v;v,c}]_{\mathrm{inc}} = {} & V_{\mathbf{q}_\parallel}(P_{\mathbf{k}_\parallel} - P_{\mathbf{k}_\parallel-\mathbf{q}_\parallel}) \sum_{\mathbf{l}_\parallel} (c^{\mathbf{q}_\parallel,\mathbf{k}'_\parallel,\mathbf{l}_\parallel}_{c,v;v,c} + c^{\mathbf{q}_\parallel,\mathbf{k}'_\parallel,\mathbf{l}_\parallel}_{v,v;v,v}) \\
& - V_{\mathbf{j}_\parallel}(P_{\mathbf{k}'_\parallel} - P_{\mathbf{k}'_\parallel-\mathbf{j}_\parallel}) \sum_{\mathbf{l}_\parallel} (c^{-\mathbf{j}_\parallel,\mathbf{l}_\parallel,\mathbf{k}_\parallel}_{v,c;c,v} + c^{-\mathbf{j}_\parallel,\mathbf{l}_\parallel,\mathbf{k}_\parallel}_{v,v;v,v}) \\
& + \sum_{\mathbf{l}_\parallel} V_{\mathbf{l}-\mathbf{k}_\parallel}(P_{\mathbf{k}_\parallel-\mathbf{q}_\parallel} c^{\mathbf{q}_\parallel,\mathbf{k}'_\parallel,\mathbf{l}_\parallel}_{v,v;v,v} - P_{\mathbf{k}_\parallel}[c^{\mathbf{q}_\parallel,\mathbf{k}'_\parallel,\mathbf{l}_\parallel}_{c,v;v,c} - c^{-\mathbf{j}_\parallel,\mathbf{k}'_\parallel,\mathbf{l}_\parallel}_{c,v;c,v}]) \\
& - \sum_{\mathbf{l}_\parallel} V_{\mathbf{l}_\parallel-\mathbf{k}'_\parallel}(P_{\mathbf{k}'_\parallel}[c^{\mathbf{q}_\parallel,\mathbf{l}_\parallel,\mathbf{k}_\parallel}_{v,c;v,c} - c^{-\mathbf{j}_\parallel,\mathbf{l}_\parallel,\mathbf{k}_\parallel}_{v,c;c,v}] + P_{\mathbf{k}_\parallel-\mathbf{q}_\parallel} c^{\mathbf{j}_\parallel,\mathbf{k}_\parallel,\mathbf{l}_\parallel}_{v,v;v,v}) \\
& + \sum_{\mathbf{l}_\parallel} V_{\mathbf{l}_\parallel+\mathbf{q}_\parallel}[P^\star_{\mathbf{k}_\parallel} c^{\mathbf{l}_\parallel,\mathbf{k}'_\parallel+\mathbf{q}_\parallel,\mathbf{k}_\parallel-\mathbf{q}_\parallel}_{c,v;v,c} + P^\star_{\mathbf{k}'_\parallel} c^{\mathbf{l}_\parallel,\mathbf{k}'_\parallel+\mathbf{q}_\parallel,\mathbf{k}_\parallel-\mathbf{q}_\parallel}_{c,v;c,v}]^\star \\
& - \sum_{\mathbf{l}_\parallel} V_{\mathbf{l}_\parallel-\mathbf{q}_\parallel} P_{\mathbf{k}_\parallel-\mathbf{q}_\parallel} c^{\mathbf{l}_\parallel,\mathbf{k}'_\parallel,\mathbf{k}_\parallel}_{v,v;v,v}. \qquad (193)
\end{aligned}
$$

The close inspection shows that the first two lines of Eqs. (192) and (193) contain terms where the Coulomb-matrix element appears outside the sum. As discussed in Section 4.3.3, such contributions yield Lindhard-type screening to the polarization dynamics while the remaining, more complicated terms may lead to the formation of new quasi-particle correlations.

When we solve Eqs. (182)–(183) and (186)–(193), we obtain a fully microscopic description for the linear response to a classical probe. We have presented here only the dynamics of $c_{v,v;v,c}$. However, the other correlations can be obtained from Eqs. (186)–(193) using the simple substitution rules

$$
v \leftrightarrow c, \quad f^{\mathrm{e}} \to 1 - f^{\mathrm{h}}, \quad f^{\mathrm{h}} \to 1 - f^{\mathrm{e}} \qquad (194)
$$

and/or complex conjugation.

The incoherent quantities, such as f^{e}, f^{h}, $c_{c,v;c,v}$, $c_{v,v;v,v}$, and $c_{c,c;c,c}$, are not changed by the weak probe pulse such that they drive coherent correlations only as external sources defined by the excitation state of the semiconductor at the time when the system is probed. Hence, when one uses ultrafast probe pulses, the system of incoherent quasi-particle excitations can be regarded as quasi-stationary. Consequently, we take in the following f^{e}, f^{h}, $c_{c,v;c,v}$, $c_{v,v;v,v}$, and $c_{c,c;c,c}$ as stationary quantities determined by the incoherent excitation state of the system.

Since single-particle carrier densities are present when one probes an excited incoherent semiconductor many-body state, they always contribute to the Coulomb induced scattering via Eq. (187). At the same time, there exists a large phase space of semiconductor states where the incoherent correlations are infinitesimally small even when large concentrations of incoherent quasi-particle excitations are present. For example, an uncorrelated electron–hole plasma produces only vanishingly small correlation contributions (193) to the scattering of polarization.

As the most prominent correlated state, the semiconductor may contain true excitons, i.e. the Coulomb bound electron–hole pairs described by c_X. Such terms enter to the polarization dynamics exclusively via the $[D_{v,v;v,c}]_{\mathrm{inc}}$ term. Also different configurations of incoherent quantities can alter the non-radiative scattering and dephasing experienced by the optical polarization. Thus, the presence of carrier densities or incoherent correlations introduces *excitation induced dephasing* to the coherences [1,52,81,102–104]. In the

following, we investigate this phenomenon for various carrier concentrations using the full microscopic theory.

5.10. Excitation induced dephasing

The essence of excitation induced dephasing can be understood as we investigate the linear response of a semiconductor under quasi-stationary plasma conditions, i.e. we assume that both exciton populations and density–density correlations are negligibly small. In practice, this situation can be realized for elevated lattice temperatures and/or elevated carrier densities [31]. Under these conditions, $[D_{v,v;v,c}]_{\mathrm{inc}}$ can be omitted from the analysis such that only the carrier densities determine the initial state of the probed semiconductor.

In simplified treatments, the full $c_{v,v;v,c}$ dynamics, Eq. (186), has been reduced further by omitting also $[D_{v,v;v,c}]_{\mathrm{coh}}$. This can be justified if coherences live only for much shorter times than it takes to build up new quasi-particles via $[D_{v,v;v,c}]_{\mathrm{coh}}$. In this case, the steady-state result of Eq. (186), without the coherent or incoherent $[D_{v,v;v,c}]$, produces the well-known second-Born scattering approximation [1,52] where one typically uses the steady-state solution of $c_{v,v;v,c}$ within the Markov limit. At this level, one obtains a computationally feasible scheme for semiconductor systems of any dimensionality. Since the second Born linear response results have already shown excellent agreement between theory and experiments for a wide range of parameters [1,22,105], it can be concluded that the underlying assumptions represent a good approximation to the conditions realized in the respective experiments.

For our numerical evaluations, we assume that we probe a system in which we have an incoherent electron–hole plasma with Fermi–Dirac quasi-equilibrium distributions of electrons and holes at the lattice temperature, $T = 40\,\mathrm{K}$. Figs. 6a and c, respectively, present the computed absorption spectra for a QWI and a QW for three representative

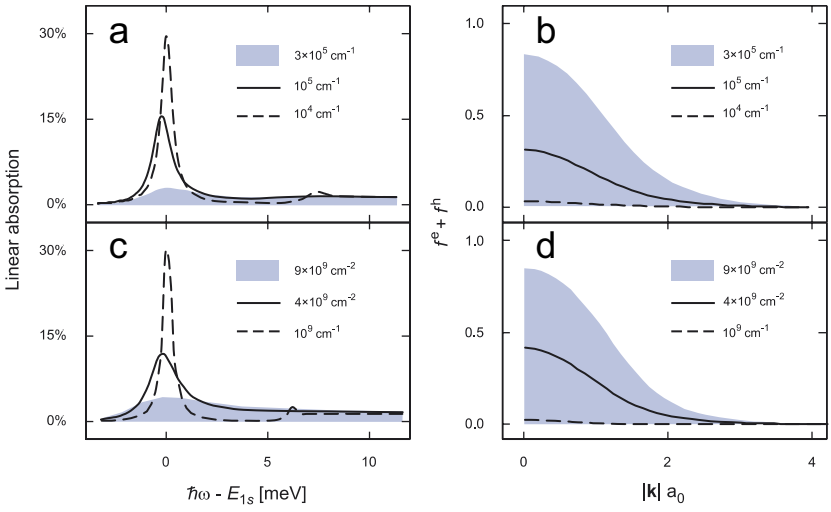

Fig. 6. Fully microscopically computed self-consistent absorption spectra. The QWI and QW spectra for three different carrier densities are shown in (a) and (c), respectively. Frames (b) and (d) show the assumed Fermi–Dirac quasi-equilibrium distributions ($f^{\mathrm{e}} + f^{\mathrm{h}}$) for the temperature 40 K.

carrier densities. Figs. 6b and d show $(f^{e}_{\mathbf{k}_\parallel}+f^{h}_{\mathbf{k}_\parallel})$ to quantify the level of excitation. For the lowest density, the population factor $(f^{e}_{\mathbf{k}_\parallel}+f^{h}_{\mathbf{k}_\parallel})$ is way below unity. Consequently, in the corresponding spectra we observe clear absorption resonances at the 1*s* and the 2*s* energy. A closer look reveals that the 2*s* resonance is spectrally broader than the 1*s* peak. This shows one of the basic features of Coulomb interaction induced dephasing, i.e. the higher excitonic states experience more dephasing than the lower ones. This trend is clearly opposite to that of pure radiative dephasing. We can estimate from Fig. 6 that the excitation induced dephasing produces a broadening in the range of $\gamma = 1\,\mathrm{meV}$ for the highest density used. Thus, even moderate densities already lead to dephasing rates which largely exceed the radiative decay $\Gamma^{\mathrm{rad}}_{1s,1s} = 20\,\mu\mathrm{eV}$. Hence, for these conditions the self-consistent light–matter coupling effects become less prominent. As a general trend, we observe that the QW system experiences a bit larger excitation-induced dephasing than the QWI since the phase-space for Coulomb scattering events is larger in two dimensions than in one.

For elevated densities, also the 1*s* resonance is broadened and the absorption dip between the bound and continuum states is gradually filled. This absorption increase is not a consequence of the band-gap shift but is caused by the excitation induced resonance broadening, i.e. the frequency dependent scattering [101]. Even for situations where $(f^{e}_{\mathbf{k}_\parallel}+f^{h}_{\mathbf{k}_\parallel})$ is still relatively low, the 2*s* and higher excitons are already bleached. As a general feature for both well and wire systems, we see that the spectral position of the 1*s* resonance remains basically unchanged for different carrier densities, indicating that the microscopic scattering leads to energy renormalizations which compensate the Hartree–Fock shifts. As the density is increased, we see that the 1*s* resonance is nearly completely bleached. The corresponding $(f^{e}_{\mathbf{k}_\parallel}+f^{h}_{\mathbf{k}_\parallel})$ is close to unity, indicating strong phase-space filling effects which eventually eliminate the bound exciton states. Only ionized excitons exist beyond this Mott transition [56,86,106]. As the density is increased further, the system enters to the regime of negative absorption, i.e. optical gain [107–110].

Our numerical evaluations show that the full QWI computation and the second Born results are very similar for the investigated conditions. Hence, we conclude that the contributions of $[D_{v,v;v,c}]_{\mathrm{coh}}$ are not significant for the plasma conditions analyzed here. However, in cases where quasi-particle correlations are present, both the $[D_{v,v;v,c}]_{\mathrm{coh}}$ and $[D_{v,v;v,c}]_{\mathrm{inc}}$ contributions become important.

To obtain a deeper understanding of the excitation-induced dephasing effects, we introduce an analytic model. For this purpose, we start from Eqs. (182) to (183) and see that we have the general conservation law

$$\sum_{\mathbf{k}_\parallel} \Gamma^{v,c}_{\mathbf{k}_\parallel} = 0. \tag{195}$$

This result suggests that the total polarization is conserved in the presence of pure excitation-induced dephasing. As a result, the Coulomb scattering has a diffusive character in the sense that it redistributes the microscopical polarization without changing the total macroscopic polarization.

For a simple model where $\Gamma^{v,c}_{\mathbf{k}_\parallel}$ is approximated by the constant dephasing $-\mathrm{i}\gamma P_{\mathbf{k}_\parallel}$, the condition (195) cannot be satisfied since the diffusive scattering is replaced by a genuine decay. To improve this approximation, we introduce a diffusive dephasing model

$$\Gamma^{\mathrm{diff}}_{\mathbf{k}_\parallel} = -\mathrm{i}\gamma[P_{\mathbf{k}_\parallel} - \tfrac{1}{2}(P_{\mathbf{k}_\parallel+\mathbf{K}_\parallel} + P_{\mathbf{k}_\parallel-\mathbf{K}_\parallel})], \tag{196}$$

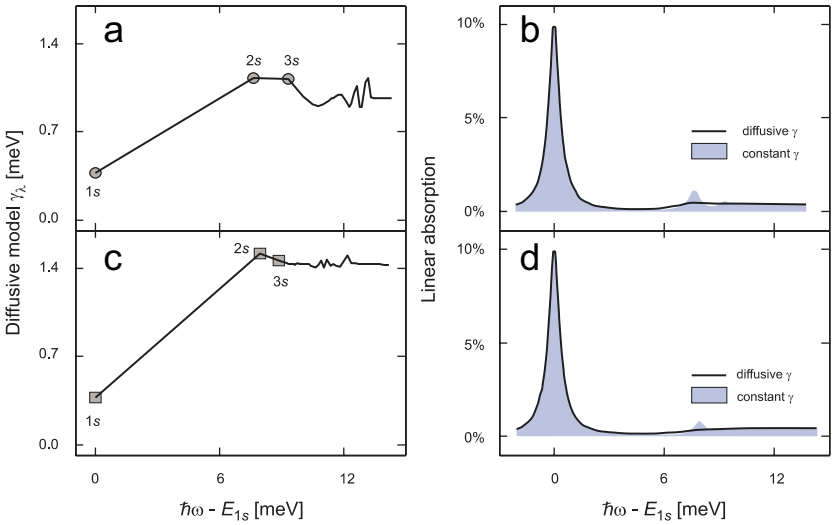

Fig. 7. Excitation induced dephasing via diffusive model. (a) Computed γ_λ for a QWI system according to Eq. (198); circles indicate the positions of the three lowest bound exciton states; the lines connecting bound states are just a guide to the eye since there are no actual states in between. (b) The corresponding absorption (solid line) is compared with a constant γ computation (shaded area). The same analysis for a QW system is presented in frames (c) and (d). The scattering parameters: $\mathbf{K}_\parallel a_0 = 1.25$ and γ are chosen to produce $\gamma_{1s} = 380\,\mu\text{eV}$ for both systems.

where $\mathbf{K}_\parallel$ is a typical momentum exchange in a Coulomb scattering process. This form clearly satisfies the fundamental relation (195).

When we use the ansatz (196) in the exciton basis Eq. (177), we obtain

$$i\hbar\frac{\partial}{\partial t}p_\lambda = (E_\lambda - i\Gamma^{\text{rad}}_{\lambda,\lambda} - i\gamma_\lambda)p_\lambda - d_{vc}\sqrt{S}\phi^{R}_\lambda(\mathbf{r}=0)\langle E(t)\rangle_0, \tag{197}$$

$$\gamma_\lambda \equiv \gamma\left[1 - \sum_{\mathbf{k}_\parallel}\phi^{L}_\lambda(\mathbf{k}_\parallel)\phi^{R}_\lambda(\mathbf{k}_\parallel \pm \mathbf{K}_\parallel)\right], \tag{198}$$

where we have assumed that only the exciton state p_λ is excited. This result nicely explains the exciton-index dependent dephasing observed in the full microscopic description. As an illustration, we present in Figs. 7a and c results for γ_λ obtained by evaluating Eq. (198) for a QWI and a QW system, respectively. We clearly see the strong variation of the dephasing for the different exciton states. The dephasing constant is several times larger for the $2s$ than for the $1s$ state which suffers the weakest excitation induced dephasing effects. According to our simplified model, the precise value of the dephasing for the energetically higher states shows some non-monotonic variations which can be partly attributed to the discrete nature of the diffusive model where only one scattering momentum is included. Inserting the computed dephasing into the Elliott formula, we obtain the results shown in Figs. 7b and d which qualitatively reproduce the main features of the full calculations, Fig. 6. In particular, we immediately understand why the $1s$ state shows a clear resonance while higher excitonic resonances merge into one common resonance close to the $2s$ state.

Our investigations so far concentrate exclusively on the linear response of the potentially pre-excited system to the optical probe fields. However, the underlying singlet–doublet analysis can be directly extended to the non-linear regime. For these situations, the influence of non-linear polarization terms (e.g. polarization–polarization scattering), coupling to all classes of correlations, as well as non-Markovian features can become important [27,52,104,111–114]. One can also extend this treatment to cover different experimental geometries such as multiple wave-mixing configurations. For these situations, one has to generalize the homogeneous equations to allow for spatially inhomogeneous excitations, but the cluster-expansion scheme works also in that case.

If one limits the wave-mixing investigations to the coherent regime, one can introduce an alternative systematic method, the so-called dynamical truncation scheme [115,116] where the semiconductor response is presented via a power expansion in terms of the exciting coherent field. This approach produces a set of non-linearly coupled equations which can be applied to determine, e.g. a non-linear susceptibility $\chi^{(N)}$ where N refers to the power of $\langle E\rangle^N$. It is straightforward to show that the cluster expansion, performed up to N-particle clusters, fully describes all microscopic contributions provided by the $\chi^{(2N-1)}$-level approach while it simultaneously contains self-consistent contributions to all orders of $\langle E\rangle$. Since the cluster expansion also includes, e.g. the second Born approach, we may conclude that it provides a unifying systematic generalization of both $\chi^{(N)}$ and the second Born scattering schemes. Moreover, the cluster expansion contains a much more complete equation structure than either one of the other schemes.

6. From polarization to incoherent populations

In the previous section, where we discussed coherent exciton states and their properties, we concluded that these states do not describe truly bound electron–hole-pair populations. Instead, the coherent exciton states correspond to the interband polarization that defines the strength of the optical transitions. Furthermore, the polarization decays on a picosecond or even sub-picosecond time scale due to radiative and excitation-induced dephasing such that coherent excitons have a relatively short lifetime.

In this section, we now investigate how the transition from the coherent to the incoherent regime takes place after classical optical excitation. In particular, we investigate the conditions under which the system contains *incoherent excitons*, i.e. Coulomb-bound electron–hole-pair states which describe genuine two-particle objects. For this purpose, we apply the full singlet–doublet theory at the level discussed in Section 4.

6.1. Energy transfer in the carrier system

In order to study the quasi-particle populations generated in the non-radiative decay of the optically induced polarization, we follow the relevant processes by mapping how energy is transferred between coherent and incoherent states. For this purpose, we start from the pure carrier part of the system Hamiltonian (17)–(21),

$$H_{\mathrm{carr}} = \sum_{\lambda,\mathbf{k}_\parallel} \varepsilon^{\lambda}_{\mathbf{k}_\parallel} a^{\dagger}_{\lambda,\mathbf{k}_\parallel} a_{\lambda,\mathbf{k}_\parallel} + \frac{1}{2}\sum_{\lambda,\lambda'} \sum_{\mathbf{k}_\parallel,\mathbf{k}'_\parallel,\mathbf{q}_\parallel\neq 0} V_{\mathbf{q}_\parallel} a^{\dagger}_{\lambda,\mathbf{k}_\parallel+\mathbf{q}_\parallel} a^{\dagger}_{\lambda',\mathbf{k}'_\parallel-\mathbf{q}_\parallel} a_{\lambda',\mathbf{k}'_\parallel} a_{\lambda,\mathbf{k}_\parallel}. \tag{199}$$

Roughly, each electron–hole-pair excitation process increases the system energy by E_g since an electron is moved across the band gap from the valence into the conduction band. Thus, using E_g as the zero energy level, we define the average carrier energy as

$$E_{\text{carr}} \equiv \langle H_{\text{carr}} \rangle - E_g \sum_{\mathbf{k}_\parallel} f^{\text{h}}_{\mathbf{k}_\parallel} = E^{\text{S}}_{\text{carr}} + E^{\text{D}}_{\text{carr}}, \tag{200}$$

$$\begin{aligned} E^{\text{S}}_{\text{carr}} = & \sum_{\mathbf{k}_\parallel} [\varepsilon^{\text{e}}_{\mathbf{k}_\parallel} f^{\text{e}}_{\mathbf{k}_\parallel} + \varepsilon^{\text{h}}_{\mathbf{k}_\parallel} f^{\text{h}}_{\mathbf{k}_\parallel}] \\ & + \frac{1}{2} \sum_{\mathbf{k}_\parallel, \mathbf{k}'_\parallel} V_{\mathbf{k}_\parallel - \mathbf{k}'_\parallel} [f^{\text{e}}_{\mathbf{k}_\parallel} f^{\text{e}}_{\mathbf{k}'_\parallel} + f^{\text{h}}_{\mathbf{k}_\parallel} f^{\text{h}}_{\mathbf{k}'_\parallel}] - \sum_{\mathbf{k}_\parallel, \mathbf{k}'_\parallel} V_{\mathbf{k}_\parallel - \mathbf{k}'_\parallel} P^{\star}_{\mathbf{k}_\parallel} P_{\mathbf{k}'_\parallel}, \end{aligned} \tag{201}$$

$$E^{\text{D}}_{\text{carr}} = \sum_{\mathbf{k}_\parallel, \mathbf{k}'_\parallel, \mathbf{q}_\parallel} [\tfrac{1}{2} V_{\mathbf{q}_\parallel} (c^{\mathbf{q}_\parallel, \mathbf{k}'_\parallel, \mathbf{k}_\parallel}_{c,c;c,c} + c^{\mathbf{q}_\parallel, \mathbf{k}'_\parallel, \mathbf{k}_\parallel}_{v,v;v,v}) - V_{\mathbf{k}'_\parallel + \mathbf{q}_\parallel - \mathbf{k}_\parallel} c^{\mathbf{q}_\parallel, \mathbf{k}'_\parallel, \mathbf{k}_\parallel}_{X}], \tag{202}$$

where we assumed that the system is homogeneous. For this situation, the sum of the singlet $E^{\text{S}}_{\text{carr}}$ and doublet $E^{\text{D}}_{\text{carr}}$ energy contributions determines the total energy of the carrier system. While all singlets add to the energy of the system, it is interesting to see that only the incoherent two-particle correlations appear in Eq. (202). Thus, the energy transfer from the decaying polarization only occurs into incoherent quantities.

We now apply the microscopic equations at the singlet–doublet level to analyze the energy redistribution due to the different scattering mechanisms. We furthermore investigate which quasi-particle states are created or destroyed during the quantum-dynamical processes. To monitor the energy transfer, we introduce scaled energies:

$$\bar{E} \equiv \bar{E}^{\text{S}} + \bar{E}^{\text{D}}, \tag{203}$$

$$\bar{E}^{\text{S}} \equiv \frac{E^{\text{S}}_{\text{carr}}}{\sum_{\mathbf{k}_\parallel} f^{\text{e}}_{\mathbf{k}_\parallel}}, \quad \bar{E}^{\text{D}} \equiv \frac{E^{\text{D}}_{\text{carr}}}{\sum_{\mathbf{k}_\parallel} f^{\text{e}}_{\mathbf{k}_\parallel}}, \tag{204}$$

where $\sum_{\mathbf{k}_\parallel} f^{\text{e}}_{\mathbf{k}_\parallel} = \sum_{\mathbf{k}_\parallel} f^{\text{h}}_{\mathbf{k}_\parallel}$ defines the total number of optically excited carriers and $\bar{E}$ defines the total energy per particle.

6.2. From coherent to incoherent excitations

We focus our analysis on situations where a relatively short optical pulse induces a polarization P in the semiconductor. To describe the subsequent interaction induced temporal decay of this polarization, we clearly have to go beyond the linear limit. Even though a linear optical field can induce a linear polarization, the generation of incoherent quantities requires interactions that appear in the equations only when we consider effects that are non-linear with respect to the exciting field. These non-linear contributions become critically important especially in the long-time regime where all coherences have vanished. Hence, a consistent analysis has to include higher orders of the exciting light field and at least the full dynamics of carriers and the two-particle correlations.

We start our analysis using the full MSBE (113)–(115) and (119) with the scattering contributions

$$i\hbar\frac{\partial}{\partial t}P_{\mathbf{k}_\parallel}\bigg|_{\text{scatt}} = \Gamma^{v,c}_{\mathbf{k}_\parallel,\text{Coul}} + \Gamma^{v,c}_{\mathbf{k}_\parallel,\text{phon}}, \tag{205}$$

$$\hbar\frac{\partial}{\partial t}f^{\text{e}}_{\mathbf{k}_\parallel}\bigg|_{\text{scatt}} = 2\,\text{Im}[\Gamma^{c,c}_{\mathbf{k}_\parallel,\text{Coul}} + \Gamma^{c,c}_{\mathbf{k}_\parallel,\text{phon}}], \tag{206}$$

$$\hbar\frac{\partial}{\partial t}f^{\text{h}}_{\mathbf{k}_\parallel}\bigg|_{\text{scatt}} = -2\,\text{Im}[\Gamma^{v,v}_{\mathbf{k}_\parallel,\text{Coul}} + \Gamma^{v,v}_{\mathbf{k}_\parallel,\text{phon}}]. \tag{207}$$

The explicit form of the Coulomb and phonon-induced scattering terms can be obtained by identifying

$$\Gamma^{\lambda,\lambda'}_{\mathbf{k}_\parallel,\text{Coul}} \equiv \sum_{v,\mathbf{k}'_\parallel,\mathbf{q}_\parallel\neq\mathbf{0}} V_{\mathbf{q}_\parallel}[c^{\mathbf{q}_\parallel,\mathbf{k}'_\parallel,\mathbf{k}_\parallel}_{\lambda,v;v,\lambda'} - (c^{\mathbf{q}_\parallel,\mathbf{k}'_\parallel,\mathbf{k}_\parallel}_{\lambda',v;v,\lambda})^\star], \tag{208}$$

$$\Gamma^{\lambda,\lambda'}_{\mathbf{k}_\parallel,\text{phon}} \equiv \sum_{\mathbf{q}_\parallel}[\Delta\langle Q^{\lambda'}_{\mathbf{q}_\parallel} a^\dagger_{\lambda,\mathbf{k}_\parallel} a_{\lambda',\mathbf{k}_\parallel-\mathbf{q}_\parallel}\rangle - \Delta\langle (Q^{\lambda}_{\mathbf{q}_\parallel})^\dagger a^\dagger_{\lambda,\mathbf{k}_\parallel-\mathbf{q}_\parallel} a_{\lambda',\mathbf{k}_\parallel}\rangle], \tag{209}$$

from Eq. (117).

To analyze the states that are generated via classical excitation of the originally unexcited semiconductor, we compare the results of two calculations at different levels of approximation for our QWI system. In one case, we perform the analysis only at the singlet level. Here, we just solve the MSBE without the scattering terms. In the other case, we evaluate the full singlet–doublet dynamics with the scattering terms (205)–(207) fully included. We always assume a relatively weak excitation with a 500 fs pulse that is resonant with the excitonic 1*s*-absorption peak. This way, we have strong absorption and at the same time we can keep the excitation level sufficiently low such that most of the interpretations used for the linear absorption case are still relevant. The phonons are treated as a bath with a lattice temperature of 10 K. In this situation, only the acoustical phonons are relevant [117]; only these are included in the computations.

The upper panels of Fig. 8 present the laser pulse $I(t)$ (dashed line), the generated macroscopic polarization $|P|^2$ (shaded area), and the total carrier density n_{eh} (solid line) according to the following definitions:

$$I(t) \equiv |\langle E(t)\rangle|^2, \tag{210}$$

$$P \equiv \frac{d_{v,c}}{\mathsf{L}}\sum_{k_\parallel} P_{k_\parallel}, \tag{211}$$

$$n_{\text{eh}} \equiv \frac{1}{\mathsf{L}}\sum_{k_\parallel} f^{\text{e}}_{k_\parallel} = \frac{1}{\mathsf{L}}\sum_{k_\parallel} f^{\text{h}}_{k_\parallel}, \tag{212}$$

for the QWI system with normalization length L. The lower panels of Fig. 8 show the total average energy per particle $\bar{E}$ (solid line) and its subdivision into singlet $\bar{E}^{\text{S}}$ (dashed line) and doublet $\bar{E}^{\text{D}}$ (dotted line) energies. The result of the full singlet–doublet analysis is

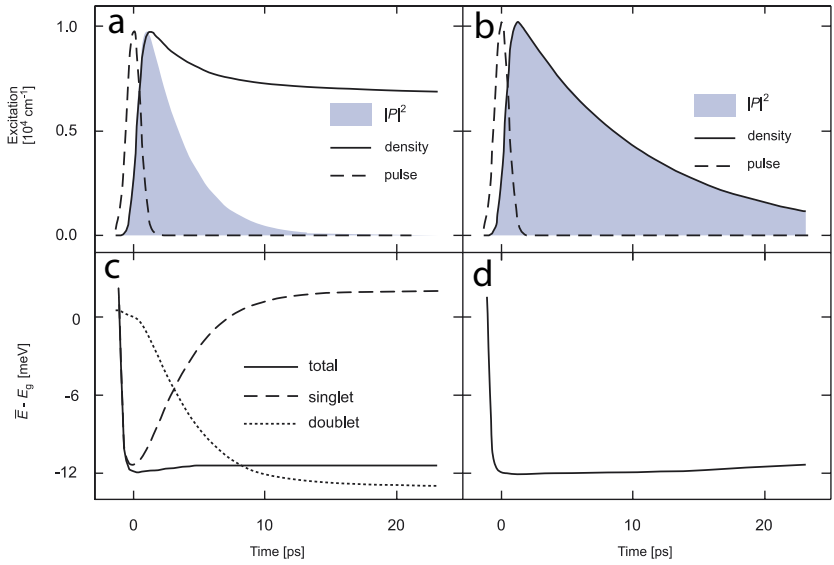

Fig. 8. Comparison of the consistent singlet–doublet and singlet computations for a resonantly excited quantum wire (QWI). The optical polarization (shaded area), the carrier density (solid line), and the excitation pulse (dashed line) are shown for (a) the full singlet–doublet computation and (b) the singlet computation. Also the corresponding energy per particle is shown; (c) the total energy (solid line) of the full singlet–doublet is also split into its singlet (dashed line) and doublet (dotted line) contributions according to Eq. (204). (d) The energy for the singlet computation consists only of the singlet part.

presented in the left column while the singlet computation is presented in the right column of Fig. 8.

We notice that the optically generated polarization in the singlet analysis vanishes purely radiatively with the decay constant corresponding to the radiative decay time $\tau_{1s} = 15\,\text{ps}$ determined earlier, see Fig. 5. The polarization falls off much faster for the full scattering computation which yields an approximately 4 ps decay time for the chosen conditions. Since the radiative decay is the same in both cases, the faster decrease in the full singlet–doublet analysis is clearly a consequence of non-radiative processes.

We also notice significant differences in the temporal evolution of the densities. In the pure singlet analysis the density decays precisely with the same rate as $|P|^2$. This can be easily understood since in the singlet solution, i.e. without scattering, the system always produces the coherent limit implying the strict connection, $f_{k_\parallel} \propto |P_{k_\parallel}|^2 \propto \mathrm{e}^{-t/\tau_{1s}}$, see Eq. (128). This behavior is drastically changed as soon as microscopic scattering is included. In this case, the polarization and the densities display significantly different dynamic behaviors. While the polarization decays rather rapidly, a large fraction of the carriers remains in the system long after the coherences have vanished. In fact, we do not note any appreciable carrier-density decay within the 20 ps time window shown in Fig. 8. This demonstrates the general trend that incoherent quasi-particle excitations in semiconductors exist much longer than the coherent quantities. This explains e.g. why semiconductors can spontaneously emit light for very long times after the excitation.

Having seen that the scattering changes the quasi-particle excitations from purely coherent to incoherent, it is interesting to analyze how the singlet and doublet components

of the carrier energy evolve. Fig. 8 shows that, after the pulse, both the singlet and the full singlet–doublet analysis yield a total energy per particle that is close to the 1*s*-exciton energy. Since this is also the average energy of the excitation, both computations fully conserve the total energy. However, in the pure singlet analysis the doublet energy (thick solid line) is always zero by definition. In other words, the coherent-limit quasi-particles exhibit full energy conservation exclusively via the singlet contributions. When the scattering is systematically included, we see in Fig. 8d that the light pulse first pumps energy into the singlets which then transfer their energy almost completely to the doublets during the decay time of the polarization. As we see from Eq. (202), these doublets consist of incoherent quasi-particle correlations besides the long-living densities.

To get more detailed information about the relevant incoherent correlations, we take a closer look at the effects of $\Gamma^{v,c}_{\text{Coul}}$ and $\Gamma^{v,c}_{\text{phon}}$. First of all, we notice that $\Gamma^{v,c}_{\text{Coul}}$ contains only coherent carrier correlations. In the same way, also

$$\Delta\langle 2\rangle^{\text{phon}}_{\text{coh}} = \{\Delta\langle Q^{\lambda} a^{\dagger}_{v} a_{c}\rangle, \Delta\langle Q^{\lambda} a^{\dagger}_{c} a_{v}\rangle\} \tag{213}$$

represents coherent phonon-assisted correlations while the remaining group

$$\Delta\langle 2\rangle^{\text{phon}}_{\text{inc}} = \{\Delta\langle Q^{\lambda} a^{\dagger}_{c} a_{c}\rangle, \Delta\langle Q^{\lambda} a^{\dagger}_{v} a_{v}\rangle\} \tag{214}$$

belongs to the class of incoherent phonon-assisted contributions. These groups are analogous to Eqs. (180)–(181) for the pure carrier correlations.

In order to track how the energy transfer between singlets and doublets, we evaluate the dynamics of $E^{\text{D}}_{\text{carr}}$ and investigate how it is changed by the coherent correlations $\Delta\langle 2\rangle_{\text{coh}}$. For this purpose, we have to solve the equations of motion for $c_{c,c;c,c}$, $c_{v,v;v,v}$, and $c_{c,v;c,v} \equiv c_X$, which is done in Appendices D–F. Using these results, we can write

$$\mathrm{i}\hbar \frac{\partial}{\partial t} E^{\text{D}}_{\text{carr}}\bigg|_{\text{coh}} = -\sum_{\mathbf{k}_{\parallel},\mathbf{k}'_{\parallel},\mathbf{q}_{\parallel}} V_{\mathbf{k}'_{\parallel}+\mathbf{q}_{\parallel}-\mathbf{k}_{\parallel}} \mathrm{i}\hbar \frac{\partial}{\partial t} c_X^{\mathbf{q}_{\parallel},\mathbf{k}'_{\parallel},\mathbf{k}_{\parallel}}\bigg|_{\text{coh}}, \tag{215}$$

where the subindex "coh" means that only coherent correlations are included in the equations of motion. We notice that only the excitonic correlations c_X appear whereas the carrier correlations $c_{c,c,c,c}$ and $c_{v,v,v,v}$ do not contribute in Eq. (215).

The explicit dynamics of c_X is given in Appendix F. There we show that the c_X dynamics in Eq. (215) can be replaced by

$$\mathrm{i}\hbar \frac{\partial}{\partial t} c_X^{\mathbf{q}_{\parallel},\mathbf{k}'_{\parallel},\mathbf{k}_{\parallel}}\bigg|_{\text{coh}} \to G^{\mathbf{q}_{\parallel},\mathbf{k}'_{\parallel},\mathbf{k}_{\parallel}}_{X,\text{Coul}} + G^{\mathbf{q}_{\parallel},\mathbf{k}'_{\parallel},\mathbf{k}_{\parallel}}_{X,\text{phon}}, \tag{216}$$

where we separate the Coulomb and phonon contributions according to

$$\begin{aligned} G^{\mathbf{q}_{\parallel},\mathbf{k}'_{\parallel},\mathbf{k}_{\parallel}}_{X,\text{Coul}} \equiv{}& V_{\mathbf{q}_{\parallel}}(P^{\star}_{\mathbf{k}_{\parallel}} - P^{\star}_{\mathbf{k}_{\parallel}-\mathbf{q}_{\parallel}}) \sum_{\mathbf{l}_{\parallel}} (c^{\mathbf{q}_{\parallel},\mathbf{k}'_{\parallel},\mathbf{l}_{\parallel}}_{c,v;c,c} + c^{\mathbf{q}_{\parallel},\mathbf{k}'_{\parallel},\mathbf{l}_{\parallel}}_{v,v;c,v}) \\ &- V_{\mathbf{q}_{\parallel}}(P_{\mathbf{k}'_{\parallel}+\mathbf{q}_{\parallel}} - P_{\mathbf{k}'_{\parallel}}) \sum_{\mathbf{l}_{\parallel}} (c^{\mathbf{q}_{\parallel},\mathbf{l}_{\parallel},\mathbf{k}_{\parallel}}_{c,c;c,v} + c^{\mathbf{q}_{\parallel},\mathbf{l}_{\parallel},\mathbf{k}_{\parallel}}_{c,v;v,v}), \end{aligned} \tag{217}$$

$$\begin{aligned} G^{\mathbf{q}_{\parallel},\mathbf{k}'_{\parallel},\mathbf{k}_{\parallel}}_{X,\text{phon}} \equiv{}& P^{\star}_{\mathbf{k}_{\parallel}} \Delta\langle [Q^{v}_{\mathbf{q}_{\parallel}}]^{\dagger} a^{\dagger}_{v,\mathbf{k}'_{\parallel}} a_{c,\mathbf{k}'_{\parallel}+\mathbf{q}_{\parallel}}\rangle - P^{\star}_{\mathbf{k}_{\parallel}-\mathbf{q}_{\parallel}} \Delta\langle [Q^{c}_{\mathbf{q}_{\parallel}}]^{\dagger} a^{\dagger}_{v,\mathbf{k}'_{\parallel}} a_{c,\mathbf{k}'_{\parallel}+\mathbf{q}_{\parallel}}\rangle \\ &+ P_{\mathbf{k}'_{\parallel}} \Delta\langle Q^{c}_{\mathbf{q}_{\parallel}} a^{\dagger}_{c,\mathbf{k}_{\parallel}} a_{v,\mathbf{k}_{\parallel}-\mathbf{q}_{\parallel}}\rangle - P_{\mathbf{k}'_{\parallel}+\mathbf{q}_{\parallel}} \Delta\langle Q^{v}_{\mathbf{q}_{\parallel}} a^{\dagger}_{c,\mathbf{k}_{\parallel}} a_{v,\mathbf{k}_{\parallel}-\mathbf{q}_{\parallel}}\rangle, \end{aligned} \tag{218}$$

respectively. If one inspects the full form of the coherent contributions in Eqs. (F.7) and (F.10), one notices that $G_{X,\mathrm{phon}}$ contains all coherent phonon-assisted correlations while $G_{X,\mathrm{Coul}}$ contains only a subset of the coherent carrier correlations. The other coherent carrier correlations do not participate in the energy transfer related to the non-radiative scattering of the polarization. In addition, we notice that $G_{X,\mathrm{Coul}}$ and $G_{X,\mathrm{phon}}$ contain exactly the same coherent correlations as those appearing in the polarization scattering terms $\Gamma^{v,c}_{\mathbf{k}_\parallel,\mathrm{Coul}}$ and $\Gamma^{v,c}_{\mathbf{k}_\parallel,\mathrm{phon}}$ in Eqs. (208)–(209). Since essentially the same coherent correlations determine both processes, i.e. the polarization decay and the correlation build-up, we can conclude that *the source of the c_X correlations, G_X, and the polarization scattering contributions, Γ, are intimately related.*

To fully appreciate the consequences of this relation, we now apply Eq. (216) in Eq. (215) and obtain

$$\begin{aligned}
\mathrm{i}\hbar\frac{\partial}{\partial t}E^{\mathrm{D}}_{\mathrm{carr}}\bigg|_{\mathrm{coh}} &= \sum_{\mathbf{k}_\parallel,\mathbf{k}'_\parallel} V_{\mathbf{k}'_\parallel-\mathbf{k}_\parallel}P^{\star}_{\mathbf{k}_\parallel}\Bigg[\sum_{\mathbf{l}_\parallel,\mathbf{q}_\parallel,\beta} V_{\mathbf{q}_\parallel}[c^{\mathbf{q}_\parallel,\mathbf{l}_\parallel,\mathbf{k}'_\parallel}_{v,\beta;\beta,c}-(c^{\mathbf{q}_\parallel,\mathbf{l}_\parallel,\mathbf{k}'_\parallel}_{c,\beta;\beta,v})^{\star}] \\
&\quad+\sum_{\mathbf{q}_\parallel}(\Delta\langle Q^{c}_{\mathbf{q}_\parallel}a^{\dagger}_{v,\mathbf{k}'_\parallel}a_{c,\mathbf{k}'_\parallel-\mathbf{q}_\parallel}\rangle-\Delta\langle(Q^{v}_{\mathbf{q}_\parallel})^{\dagger}a^{\dagger}_{v,\mathbf{k}_\parallel-\mathbf{q}_\parallel}a_{c,\mathbf{k}'_\parallel}\rangle)\Bigg] \\
&\quad+\sum_{\mathbf{k}_\parallel,\mathbf{k}'_\parallel} V_{\mathbf{k}'_\parallel-\mathbf{k}_\parallel}P_{\mathbf{k}'_\parallel}\Bigg[\sum_{\mathbf{l}_\parallel,\mathbf{q}_\parallel,\beta} V_{\mathbf{q}_\parallel}[c^{\mathbf{q}_\parallel,\mathbf{l}_\parallel,\mathbf{k}_\parallel}_{c,\beta;\beta,v}-(c^{\mathbf{q}_\parallel,\mathbf{l}_\parallel,\mathbf{k}_\parallel}_{v,\beta;\beta,c})^{\star}] \\
&\quad+\sum_{\mathbf{q}_\parallel}(\Delta\langle Q^{v}_{\mathbf{q}_\parallel}a^{\dagger}_{c,\mathbf{k}_\parallel}a_{v,\mathbf{k}_\parallel-\mathbf{q}_\parallel}\rangle-\Delta\langle(Q^{c}_{\mathbf{q}_\parallel})^{\dagger}a^{\dagger}_{c,\mathbf{k}_\parallel-\mathbf{q}_\parallel}a_{v,\mathbf{k}_\parallel}\rangle)\Bigg],
\end{aligned} \tag{219}$$

after suitable exchanges of the summation variables, as shown in Appendix F.3. With the help of Eqs. (208)–(209), this relation can be simplified to

$$\begin{aligned}
\mathrm{i}\hbar\frac{\partial}{\partial t}E^{\mathrm{D}}_{\mathrm{carr}}\bigg|_{\mathrm{coh}} &= \sum_{\mathbf{k}_\parallel,\mathbf{k}'_\parallel} V_{\mathbf{k}'_\parallel-\mathbf{k}_\parallel}P^{\star}_{\mathbf{k}_\parallel}[\Gamma^{v,c}_{\mathbf{k}'_\parallel,\mathrm{Coul}}+\Gamma^{v,c}_{\mathbf{k}'_\parallel,\mathrm{phon}}] \\
&\quad+\sum_{\mathbf{k}_\parallel,\mathbf{k}'_\parallel} V_{\mathbf{k}'_\parallel-\mathbf{k}_\parallel}P_{\mathbf{k}'_\parallel}[\Gamma^{c,v}_{\mathbf{k}_\parallel,\mathrm{Coul}}+\Gamma^{c,v}_{\mathbf{k}_\parallel,\mathrm{phon}}] \\
&= \mathrm{i}\hbar\frac{\partial}{\partial t}\sum_{\mathbf{k}_\parallel,\mathbf{k}'_\parallel} V_{\mathbf{k}'_\parallel-\mathbf{k}_\parallel}P_{\mathbf{k}'_\parallel}P^{\star}_{\mathbf{k}_\parallel}\bigg|_{\mathrm{scatt}},
\end{aligned} \tag{220}$$

where Eq. (205) has been used in the final step. We now recognize that the right-hand side of Eq. (220) is identical to the negative time derivative of the coherent singlet energy (201), i.e.

$$\frac{\partial}{\partial t}E^{\mathrm{D}}_{\mathrm{carr}}\bigg|_{\mathrm{coh}} = -\frac{\partial}{\partial t}E^{\mathrm{S,coh}}_{\mathrm{carr}}\bigg|_{\mathrm{scatt}}. \tag{221}$$

It is interesting to note that this general relation is independent of the detailed form of the coherent correlations. Hence, we can conclude that the decay of the polarization via $\Gamma^{c,v}$ leads to the generation of incoherent c_X correlations via the $G_{X,\mathrm{Coul}}$ and $G_{X,\mathrm{phon}}$ terms. As we discuss later in this review, c_X fully includes the description of incoherent exciton

populations. Thus, our analysis here precisely describes the microscopic mechanism responsible for the conversion of coherent polarization into incoherent exciton populations via Coulomb- and phonon-induced scattering.

6.3. Dynamics of exciton correlations

In this section, we take a closer look at the correlations included in c_X. For this purpose, we write the singlet–doublet equations in the form

$$\begin{aligned}
i\hbar\frac{\partial}{\partial t}c_X^{\mathbf{q}_\parallel,\mathbf{k}'_\parallel,\mathbf{k}_\parallel} &= (\tilde{\varepsilon}^{e}_{\mathbf{k}'_\parallel+\mathbf{q}_\parallel}+\tilde{\varepsilon}^{h}_{\mathbf{k}'_\parallel}-\tilde{\varepsilon}^{e}_{\mathbf{k}_\parallel}-\tilde{\varepsilon}^{h}_{\mathbf{k}_\parallel-\mathbf{q}_\parallel})c_X^{\mathbf{q}_\parallel,\mathbf{k}'_\parallel,\mathbf{k}_\parallel}+S_X^{\mathbf{q}_\parallel,\mathbf{k}'_\parallel,\mathbf{k}_\parallel}\\
&\quad+(1-f^{e}_{\mathbf{k}_\parallel}-f^{h}_{\mathbf{k}_\parallel-\mathbf{q}_\parallel})\sum_{\mathbf{l}_\parallel}V_{\mathbf{l}_\parallel-\mathbf{k}_\parallel}c_X^{\mathbf{q}_\parallel,\mathbf{k}'_\parallel,\mathbf{l}_\parallel}\\
&\quad-(1-f^{e}_{\mathbf{k}'_\parallel+\mathbf{q}_\parallel}-f^{h}_{\mathbf{k}'_\parallel})\sum_{\mathbf{l}_\parallel}V_{\mathbf{l}_\parallel-\mathbf{k}'_\parallel}c_X^{\mathbf{q}_\parallel,\mathbf{l}_\parallel,\mathbf{k}_\parallel}\\
&\quad+G_{X,\mathrm{Coul}}^{\mathbf{q}_\parallel,\mathbf{k}'_\parallel,\mathbf{k}_\parallel}+G_{X,\mathrm{phon}}^{\mathbf{q}_\parallel,\mathbf{k}'_\parallel,\mathbf{k}_\parallel}+D_{X,\mathrm{rest}}^{\mathbf{q}_\parallel,\mathbf{k}'_\parallel,\mathbf{k}_\parallel}+T_X^{\mathbf{q}_\parallel,\mathbf{k}'_\parallel,\mathbf{k}_\parallel}. \qquad (222)
\end{aligned}$$

Here, the first line is the sum of the renormalized kinetic energy of the particles plus the singlet source

$$\begin{aligned}
S_X^{\mathbf{q}_\parallel,\mathbf{k}'_\parallel,\mathbf{k}_\parallel} &\equiv \delta_{\sigma,\sigma'}V_{\mathbf{j}_\parallel}[(f^{e}_{\mathbf{k}'_\parallel+\mathbf{q}_\parallel}f^{h}_{\mathbf{k}'_\parallel}\bar{f}^{e}_{\mathbf{k}_\parallel}\bar{f}^{h}_{\mathbf{k}_\parallel-\mathbf{q}_\parallel})_\Sigma\\
&\quad+P^{\star}_{\mathbf{k}_\parallel}P_{\mathbf{k}'_\parallel+\mathbf{q}_\parallel}(f^{h}_{\mathbf{k}_\parallel-\mathbf{q}_\parallel}-f^{h}_{\mathbf{k}'_\parallel})+P^{\star}_{\mathbf{k}_\parallel-\mathbf{q}_\parallel}P_{\mathbf{k}'_\parallel}(f^{e}_{\mathbf{k}_\parallel}-f^{e}_{\mathbf{k}'_\parallel+\mathbf{q}_\parallel})]\\
&\quad+V_{\mathbf{q}_\parallel}[P^{\star}_{\mathbf{k}_\parallel}P_{\mathbf{k}'_\parallel}(f^{h}_{\mathbf{k}_\parallel-\mathbf{q}_\parallel}-f^{e}_{\mathbf{k}'_\parallel+\mathbf{q}_\parallel})-P^{\star}_{\mathbf{k}_\parallel-\mathbf{q}_\parallel}P_{\mathbf{k}'_\parallel+\mathbf{q}_\parallel}(f^{h}_{\mathbf{k}'_\parallel}-f^{e}_{\mathbf{k}_\parallel})\\
&\quad-P^{\star}_{\mathbf{k}_\parallel-\mathbf{q}_\parallel}P_{\mathbf{k}'_\parallel}(f^{e}_{\mathbf{k}_\parallel}-f^{e}_{\mathbf{k}'_\parallel+\mathbf{q}_\parallel})+P^{\star}_{\mathbf{k}_\parallel}P_{\mathbf{k}'_\parallel+\mathbf{q}_\parallel}(f^{h}_{\mathbf{k}'_\parallel}-f^{h}_{\mathbf{k}_\parallel-\mathbf{q}_\parallel})]. \qquad (223)
\end{aligned}$$

This expression contains the singlet factorization of the Coulomb-induced two- and three-particle terms, i.e. the simplest diagram in Fig. 2. For clarity, we explicitly write here the spin dependence following from the sequence $c_X \equiv c_{(c,\sigma),(v,\sigma');(c,\sigma'),(v,\sigma)}$. Additionally, we introduce the abbreviation

$$(f^{\lambda}_{\mathbf{k}_\parallel}f^{\lambda'}_{\mathbf{k}'_\parallel}\bar{f}^{\lambda''}_{\mathbf{k}''_\parallel}\bar{f}^{\lambda'''}_{\mathbf{k}'''_\parallel})_\Sigma \equiv f^{\lambda}_{\mathbf{k}_\parallel}f^{\lambda'}_{\mathbf{k}'_\parallel}(1-f^{\lambda''}_{\mathbf{k}''_\parallel})(1-f^{\lambda'''}_{\mathbf{k}'''_\parallel})-(1-f^{\lambda}_{\mathbf{k}_\parallel})(1-f^{\lambda'}_{\mathbf{k}'_\parallel})f^{\lambda''}_{\mathbf{k}''_\parallel}f^{\lambda'''}_{\mathbf{k}'''_\parallel} \qquad (224)$$

which identifies the in- and out-scattering terms discussed earlier in connection with the second-Born approximation, see Section 5.10. These terms act as a source to the c_X dynamics also in the purely incoherent regime, verifying once again that c_X is fundamentally an incoherent correlation.

The second and third lines of Eq. (222) contain the two most important contributions of the incoherent Coulomb-induced correlations $[D_X]_{\mathrm{inc}}$. The complete form of $[D_X]_{\mathrm{inc}}$ is derived in Appendix F and presented in Eq. (F.6). In general, $[D_X]_{\mathrm{inc}}$ consists of terms such as $(n^{\lambda}-n^{\nu})\sum Vc_{\lambda,\nu;\nu',\lambda'}$. As a result, $[D_X]_{\mathrm{inc}}$ can be considered as a systematic generalization of the single-particle scattering S_X because it involves higher-order clusters as scattering partners. More specifically, these can be interpreted as microscopic processes where a correlated two-particle quantity scatters from an incoherent carrier occupation $n^{\lambda}=f^{e}$ or $n^{\lambda}=1-f^{h}$.

When the carrier densities are relatively low, the dominant scattering contributions originate from those terms which contain a phase-space filling term $(1-f^{e}-f^{h})$. This

allows us to introduce the so-called *main-sum approximation* [18,29], where only these dominant contributions of $[D_X]_{\rm inc}$ are included. This approach proves to be very useful once we look for analytic solutions to Eq. (222). For this reason, we explicitly present only the main-sum structure in the second and third lines of Eq. (222). These main-sum terms describe the attractive interaction between electrons and holes, allowing them to become truly bound electron–hole pairs, i.e. *incoherent excitons*.

Note that *we include the full structure of* $[D_X]_{\rm inc}$ *in all our numerical evaluations*. This way, the analysis fully incorporates e.g. the microscopic restrictions for exciton populations as a consequence of Pauli-blocking effects and scattering with electrons and holes.

The fourth line of Eq. (222) contains $G_{X,\rm Coul}$ and $G_{X,\rm phon}$ which are responsible for the generation of incoherent excitons via polarization scattering as discussed before. The remaining two-particle contributions are denoted as $D_{\rm rest}$. They contain the terms beyond the main-sum contributions as well as those coherent correlations that do not contribute to the energy transfer between polarization and c_X (see Eqs. (F.6)–(F.7) for the full forms). As a last contribution, the c_X dynamics contains T_X which symbolizes the three-particle Coulomb and phonon terms. As presented here, the c_X dynamics (222) is formally exact and the accuracy of the numerical solutions depends only on the accuracy with which the three-particle correlation terms can be included to the analysis.

The dynamical equations for the correlations $c^{\mathbf{q},\mathbf{k}',\mathbf{k}}_{\lambda,\nu,\nu',\lambda'}$ are structurally similar to Eq. (222). In the numerical solutions, we treat all of these equations together with the corresponding equations for the singlets. This way, we fully include one- and two-particle correlations and obtain a closed set of equations providing a consistent description of optical excitations in semiconductors up to the level of three-particle correlations. In the following, we will introduce different levels of approximations for these triplet contributions. Our most sophisticated and still numerically feasible approximation describes the triplet terms at the level where we include microscopic scattering among singlets and doublets. As we will show, this is a very reasonable approximation for many interesting semiconductor excitation conditions.

6.4. Incoherent excitons

As a very broad definition, an incoherent exciton is a quasi-particle that consists of a Coulomb-bound electron–hole pair. Even though this statement seems simple and straightforward, once one seriously considers the Fermionic nature of the constituent electron and hole, one cannot simply define a pure Bosonic exciton operator or a rigorous number operator for excitons in a Fermionic many-body system [88]. For the purposes of this review, we need to develop a systematic definition for true excitons. In particular, we may speak of exciton populations in a system only when we have correlations between at least one electron and hole. Furthermore, excitons exhibit the *correlation in the relative coordinate between the electron and hole* and the dependency of the pair wavefunction is governed by *the generalized Wannier equation*. The *bound* (*ionized*) *state solutions* define *bound* (*ionized*) *excitons*.

We find a natural way to identify incoherent excitons once we evaluate the electron–hole pair-correlation function

$$g_{\rm eh}(\mathbf{r}_\parallel) \equiv \langle \Psi^\dagger_{\rm e}(\mathbf{r}_\parallel)\Psi^\dagger_{\rm h}(0)\Psi_{\rm h}(0)\Psi_{\rm e}(\mathbf{r}_\parallel)\rangle, \tag{225}$$

$$\Psi_{\mathrm{e}}(\mathbf{r}_{\parallel}) = \frac{1}{\sqrt{\mathsf{S}}}\sum_{\mathbf{k}_{\parallel}} a_{c,\mathbf{k}_{\parallel}} \mathrm{e}^{\mathrm{i}\mathbf{k}_{\parallel}\cdot\mathbf{r}_{\parallel}}, \quad \Psi_{\mathrm{h}}^{\dagger}(\mathbf{r}_{\parallel}) = \frac{1}{\sqrt{\mathsf{S}}}\sum_{\mathbf{k}_{\parallel}} a_{v,\mathbf{k}_{\parallel}} \mathrm{e}^{\mathrm{i}\mathbf{k}_{\parallel}\cdot\mathbf{r}_{\parallel}}. \tag{226}$$

Here, only the envelope part of the field operator $\hat{\Psi}_{\lambda}(\mathbf{r}_{\parallel})$ is included since the characteristic dimensions of Wannier excitons involve length scales much longer than the lattice periodic part of the Bloch functions. In general, $g_{\mathrm{eh}}(\mathbf{r}_{\parallel})$ defines the conditional probability to find an electron at position $\mathbf{r}_{\parallel}$ when the hole is positioned at the origin. Thus, $g_{\mathrm{eh}}(\mathbf{r}_{\parallel})$ allows us to identify what kind of correlations one can observe in the relative coordinate between the electrons and holes in the many-body system.

It is useful to divide the pair-correlation function into singlet and doublet contributions. Assuming homogeneous excitation conditions, we can write

$$g_{\mathrm{eh}}(\mathbf{r}_{\parallel}) \equiv g_{\mathrm{eh}}^{\mathrm{S}}(\mathbf{r}_{\parallel}) + \Delta g_{\mathrm{eh}}(\mathbf{r}_{\parallel}), \tag{227}$$

$$g_{\mathrm{eh}}^{\mathrm{S}}(\mathbf{r}_{\parallel}) \equiv n_{\mathrm{e}} n_{\mathrm{h}} + |P_{\mathrm{eh}}(\mathbf{r}_{\parallel})|^2, \quad P_{\mathrm{eh}}(\mathbf{r}_{\parallel}) \equiv \frac{1}{\mathsf{S}}\sum_{\mathbf{k}_{\parallel}} P_{\mathbf{k}_{\parallel}} \mathrm{e}^{\mathrm{i}\mathbf{k}_{\parallel}\cdot\mathbf{r}_{\parallel}}, \tag{228}$$

$$\Delta g_{\mathrm{eh}}(\mathbf{r}_{\parallel}) \equiv \frac{1}{\mathsf{S}^2}\sum_{\mathbf{k}_{\parallel},\mathbf{k}'_{\parallel},\mathbf{q}_{\parallel}} c_X^{\mathbf{q}_{\parallel},\mathbf{k}'_{\parallel},\mathbf{k}_{\parallel}} \mathrm{e}^{\mathrm{i}(\mathbf{k}'_{\parallel}+\mathbf{q}_{\parallel}-\mathbf{k}_{\parallel})\cdot\mathbf{r}_{\parallel}}. \tag{229}$$

We observe that the singlet part, $g_{\mathrm{eh}}^{\mathrm{S}}(\mathbf{r}_{\parallel})$, consists of a background contribution, $n_{\mathrm{e}}n_{\mathrm{h}}$, which expresses the fact that the probability of simultaneously finding and electron and a hole has a simple contribution which is nothing but the product of their densities. This density product is $\mathbf{r}_{\parallel}$ independent, in contrast to the second singlet contribution $|P_{\mathrm{eh}}(\mathbf{r}_{\parallel})|^2$ which expresses the fact that optical transitions connect those electrons and holes that are spatially close to each other. This can be seen by transforming the SBE (113) into $\mathbf{r}_{\parallel}$-space. This procedure yields

$$\mathrm{i}\hbar\frac{\partial}{\partial t}P_{\mathrm{eh}}(\mathbf{r}_{\parallel}) = \left[-\frac{\hbar^2}{2\mu}\nabla_{\parallel}^2 + E_{\mathrm{g}} - \frac{e^2}{4\pi\varepsilon_0\varepsilon_r|r_{\parallel}|}\right]P_{\mathrm{eh}}(\mathbf{r}_{\parallel}) - \delta(\mathbf{r}_{\parallel})d_{v,c}\langle E(t)\rangle + \mathrm{i}\hbar\frac{\partial}{\partial t}P_{\mathrm{eh}}(\mathbf{r}_{\parallel})\Big|_{\mathrm{scatt}}, \tag{230}$$

where we have applied the low-density limit and the effective-mass approximation, for simplicity. We see from Eq. (230) that the optical field generates electron–hole transitions at $\mathbf{r}_{\parallel} = 0$ even in the artificial case without Coulomb interaction. Hence, the resulting enhancement of $|P_{\mathrm{eh}}(\mathbf{r}_{\parallel})|^2$ close to the origin is a general consequence of optical excitations in direct-gap semiconductors, not a signature for the presence of excitons. As a result, true exciton populations can be described only by the correlated two-particle contributions $\Delta g_{\mathrm{eh}}(\mathbf{r}_{\parallel})$. Since these contributions are determined by the c_X correlations, we clearly need those to obtain a microscopic description of incoherent exciton populations in the many-body system.

We now come back to the question which incoherent quasi-particles are generated by the non-radiative scattering of the polarization. As the polarization decays, we enter into the incoherent regime where the singlet part of the pair-correlation function reduces to $g_{\mathrm{eh}}^{\mathrm{S}}(\mathbf{r}_{\parallel}) = n_{\mathrm{e}}n_{\mathrm{h}}$ such that it does not exhibit any $\mathbf{r}_{\parallel}$ dependence. However, since the coherent polarization may also be converted into incoherent c_X correlations, the corresponding pair-correlation function, $\Delta g_{\mathrm{eh}}(\mathbf{r}_{\parallel})$, may also show a genuine $\mathbf{r}_{\parallel}$ dependence. Thus, we

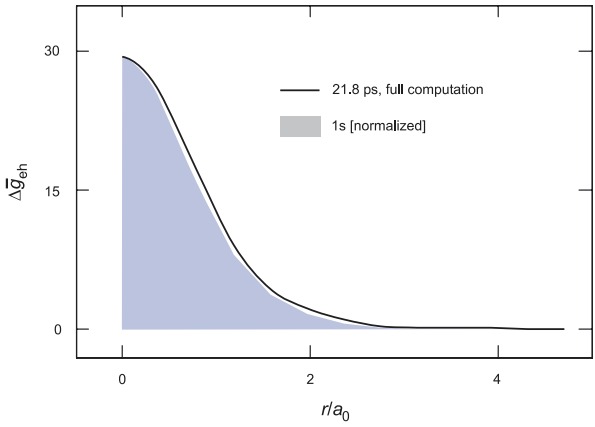

Fig. 9. The pair-correlation function (solid line) after the decay of polarization via non-radiative scattering. The shaded area shows the extension of $|\phi^{R}_{1s}(\mathbf{r}_{\parallel})|^2$ for a 1s-exciton state. The pair-correlation function is determined at 21.8 ps, i.e. the final time in Fig. 8.

argue that the polarization can be directly converted into incoherent excitons under suitable conditions.

To confirm this conclusion, we analyze again Fig. 8 and plot the normalized

$$\Delta\bar{g}_{eh}(\mathbf{r}_{\parallel}) \equiv \Delta g_{eh}(\mathbf{r}_{\parallel})/(n_e n_h), \tag{231}$$

in Fig. 9 as solid line at the final time $t = 21.8$ ps. At this moment, the polarization-to-population conversion is completed as can be seen in Fig. 8. We also plot $|\phi^{R}_{1s}(\mathbf{r}_{\parallel})|^2$ (shaded area) defined by the Wannier Eq. (121) in order to show the spatial dependency of the 1s exciton polarization. We observe a perfect match between $\Delta\bar{g}_{eh}(\mathbf{r}_{\parallel})$ and the 1s-exciton state demonstrating that electrons and holes are correlated to the degree described by the 1s-exciton wavefunction. Since all criteria for a true exciton are satisfied, we have shown that non-radiative scattering can convert a coherent polarization, i.e. coherent excitons into true incoherent exciton populations. As a further evidence, we observe in Fig. 8 that incoherent excitons can have an energy per particle that corresponds to the 1s-exciton binding energy.

6.5. Correlated electron–hole plasma

In the previous section, we have shown that the c_X correlation dynamics can be used to microscopically describe the generation of incoherent excitons. At the same time, we know that c_X involves a set of features such as scattering and screening as well as true excitons. Thus, it is interesting to study what is the most general class of incoherent quasi-particle excitations described by c_X. With this knowledge, we can then precisely specify the incoherent many-body states that can be observed in semiconductors as long as no clusters occur that are of higher order than doublets. In other words, we are then able to define the full phase-space of singlet–doublet quasi-particle excitations and their relevance under different physical conditions.

We start this investigation by taking another look at $\Delta g_{\rm eh}(\mathbf{r}_\parallel)$. For this purpose, we transform it into an exciton basis using

$$\Delta\langle X^\dagger_{\lambda,\mathbf{q}_\parallel} X_{v,\mathbf{q}_\parallel}\rangle = \sum_{\mathbf{k}_\parallel,\mathbf{k}'_\parallel} \phi^{\rm L}_\lambda(\mathbf{k}_\parallel)\phi^{\rm L}_v(\mathbf{k}'_\parallel) c_{\rm X}^{\mathbf{q}_\parallel,\mathbf{k}'_\parallel-\mathbf{q}_{\rm h},\mathbf{k}_\parallel+\mathbf{q}_{\rm e}} \equiv \Delta N_{\lambda,v}(\mathbf{q}_\parallel), \tag{232}$$

$$c_{\rm X}^{\mathbf{q}_\parallel,\mathbf{k}'_\parallel-\mathbf{q}_{\rm h},\mathbf{k}_\parallel+\mathbf{q}_{\rm e}} = \sum_{\lambda,v} \phi^{\rm R}_\lambda(\mathbf{k}_\parallel)\phi^{\rm R}_v(\mathbf{k}'_\parallel)\Delta N_{\lambda,v}(\mathbf{q}_\parallel), \tag{233}$$

where we have applied the definition (136) for the exciton operator. In our investigations, we use real-valued exciton functions in the momentum space. Consequently, we do not have to keep track of complex conjugation, which simplifies the notation in the forthcoming investigations.

This exciton-basis representation can now be inserted into Eq. (229), which gives

$$\Delta g_{\rm eh}(\mathbf{r}_\parallel) = \sum_{\lambda,v}\left(\frac{1}{\mathsf{S}}\sum_{\mathbf{q}_\parallel}\Delta N_{\lambda,v}(\mathbf{q}_\parallel)\right)\phi^{\rm R}_\lambda(\mathbf{r}_\parallel)\phi^{\rm R}_v(\mathbf{r}_\parallel). \tag{234}$$

In situations where $\Delta g_{\rm eh}(\mathbf{r}_\parallel)$ exclusively displays a $|\phi^{\rm R}_\beta(\mathbf{r}_\parallel)|^2$ dependence, it is obvious that the $\sum_{\lambda,v}$ sum is dominated by the element $\lambda = v = \beta$. Since this corresponds to the case where only β excitons exist, we conclude that

$$\Delta n_\beta = \Delta n_{\beta,\beta} \equiv \frac{1}{\mathsf{S}}\sum_{\mathbf{q}_\parallel}\Delta N_{\beta,\beta}(\mathbf{q}_\parallel) \tag{235}$$

defines the density of β excitons in the system and

$$\Delta N_\beta(\mathbf{q}_\parallel) \equiv \Delta N_{\beta,\beta}(\mathbf{q}_\parallel) \tag{236}$$

is their momentum distribution. The physical relevance of these quantities is shown even more clearly in Section 6.6 where we discuss how individual Δn_β can be measured experimentally.

Since only the diagonal part of $\Delta\langle X^\dagger_\lambda X_v\rangle$ corresponds to excitons, the off-diagonal contributions must correspond to some other correlated quasi-particle states. To resolve the character and relevance of these many-body states, we apply Eq. (233) to Eq. (222) and obtain

$$\begin{aligned} i\hbar\frac{\partial}{\partial t}\Delta N_{\lambda,v}(\mathbf{q}_\parallel) &= (E_v - E_\lambda)\Delta N_{\lambda,v}(\mathbf{q}_\parallel) \\ &\quad + (E_v - E_\lambda)N_{\lambda,v}(\mathbf{q}_\parallel)_{\rm S} + S^{\lambda,v}_{\rm coh}(\mathbf{q}_\parallel) \\ &\quad + iG^{\lambda,v}(\mathbf{q}_\parallel) + D^{\lambda,v}_{\rm rest}(\mathbf{q}_\parallel) + T^{\lambda,v}(\mathbf{q}_\parallel), \end{aligned} \tag{237}$$

where the incoherent part of the singlet scattering, S_X, in Eq. (222) produces a source

$$N_{\lambda,v}(\mathbf{q}_\parallel)_{\rm S} \equiv \langle X^\dagger_{\lambda,\mathbf{q}_\parallel} X_{v,\mathbf{q}_\parallel}\rangle_{\rm S} = \sum_{\mathbf{k}_\parallel}\phi^{\rm L}_\lambda(\mathbf{k}_\parallel) f^{\rm e}_{\mathbf{k}_\parallel+\mathbf{q}_{\rm e}} f^{\rm h}_{\mathbf{k}_\parallel-\mathbf{q}_{\rm h}}\phi^{\rm L}_v(\mathbf{k}_\parallel). \tag{238}$$

This contribution has a finite value in the incoherent regime whenever we have any quasi-particle excitation in the system. Particularly, it drives exclusively the non-diagonal $\Delta\langle X^\dagger_\lambda X_v\rangle$ since it exists in Eq. (237) only when $\lambda \neq v$. Thus, we can already conclude at this

point that the incoherent part of the singlet scattering generates new correlated quasi-particles that do not have the character of excitons.

The other sources to c_X are expressed symbolically as $S^{\lambda,\nu}_{\rm coh}(\mathbf{q}_\parallel)$ containing the coherent contributions of the singlet scattering. The polarization-to-population scattering is determined by $G^{\lambda,\nu}(\mathbf{q}_\parallel) \equiv G^{\lambda,\nu}_{X,\rm Coul}(\mathbf{q}_\parallel) + G^{\lambda,\nu}_{X,\rm phon}(\mathbf{q}_\parallel)$. The contributions $D^{\lambda,\nu}_{\rm rest}(\mathbf{q}_\parallel)$ result from the remaining doublet correlations and the triplet-scattering term is denoted as $T^{\lambda,\nu}(\mathbf{q}_\parallel)$. Since these remaining terms are cumbersome to write down in the exciton basis, it is beneficial to perform the fully systematic calculations in the original electron–hole picture as given by Eq. (222). The exciton basis is useful mostly for the interpretation of the results.

Our previous discussion in Sections 6.1–6.4 shows that polarization-to-population conversion can lead to a semiconductor state consisting mainly of incoherent exciton populations. Thus, it is obvious that $G^{\lambda,\nu}(\mathbf{q}_\parallel)$ can be dominantly diagonal. We also see from the structure of Eq. (237) that the generated $\Delta\langle X^\dagger_\beta X_\beta\rangle$ changes only due to the $D^{\beta,\beta}_{\rm rest}$ and $T^{\beta,\beta}$ scattering terms as the incoherent regime is reached. We will show in our further analysis that this scattering becomes weak for low enough densities and lattice temperatures such that we can identify a physically relevant phase space where true excitons exist in the system for very long times.

Since the nature of the other class of incoherent quasi-particles is still unknown, we next try to determine when and how these quasi-particles are generated. For this purpose, we assume completely incoherent conditions such that $S^{\lambda,\nu}_{\rm coh}(\mathbf{q}_\parallel)$ and $G^{\lambda,\nu}(\mathbf{q})$ vanish for all times. In addition, if we introduce an approximation where $D^{\lambda,\nu}_{\rm rest}(\mathbf{q})$ is neglected while the triplet scattering is described phenomenologically via $T^{\lambda,\nu}(\mathbf{q}) = -{\rm i}\gamma\Delta\langle X^\dagger_{\lambda,\mathbf{q}} X_{\nu,\mathbf{q}}\rangle$ in Eq. (237), we obtain a simple steady-state solution

$$\Delta N_{\lambda,\nu}(\mathbf{q}_\parallel) = \frac{E_\nu - E_\lambda}{E_\nu - E_\lambda - {\rm i}\gamma}\langle X^\dagger_{\lambda,\mathbf{q}_\parallel} X_{\nu,\mathbf{q}_\parallel}\rangle_{\rm S}, \tag{239}$$

whenever the carrier densities remain constant. In this form, we observe clearly that the new class of incoherent excitations excludes excitons and depends only on carrier densities. Thus, this part of the many-body state can be referred to as *correlated electron–hole plasma* which is a state where electrons and holes attract each other without forming excitons.

The principal characteristics of the correlated electron–hole plasma is visualized in Fig. 10 for the QWI and QW systems. These results are obtained by inserting Eq. (239) into Eq. (234) for the dilute carrier densities of $n_{\rm eh} = 10^4\,{\rm cm}^{-1}$ for the wire and $n_{\rm eh} = 2\times 10^9\,{\rm cm}^{-2}$ for the QW, respectively. In the numerical evaluations we used 40 K Fermi–Dirac distributions for the electrons and holes in both cases. We notice in Fig. 10 that the pair-correlation functions of the QW and the QWI systems are qualitatively similar. In particular, $\Delta\bar{g}_{\rm eh}(r_\parallel)$ shows an elevated probability to find electron and hole close together. This probability is only weakly dependent on the precise value of the dephasing constant γ.

As a distinctive difference between the correlated plasma and the results for exciton populations (see Fig. 9), we note that $\Delta\bar{g}_{\rm eh}(r_\parallel)$ for the correlated plasma becomes negative for larger distances. This indicates that the electron–hole pairs reduce their average separation by reorganizing the long and short-range parts of the joint probability distribution. In the integrals $\int {\rm d}r_\parallel \Delta\bar{g}_{\rm eh}(r_\parallel)$ in one-dimensional and $\int {\rm d}r_\parallel r_\parallel \Delta\bar{g}_{\rm eh}(r_\parallel)$ in two-dimensional the negative and the positive valued parts compensate each other to yield a vanishing result.

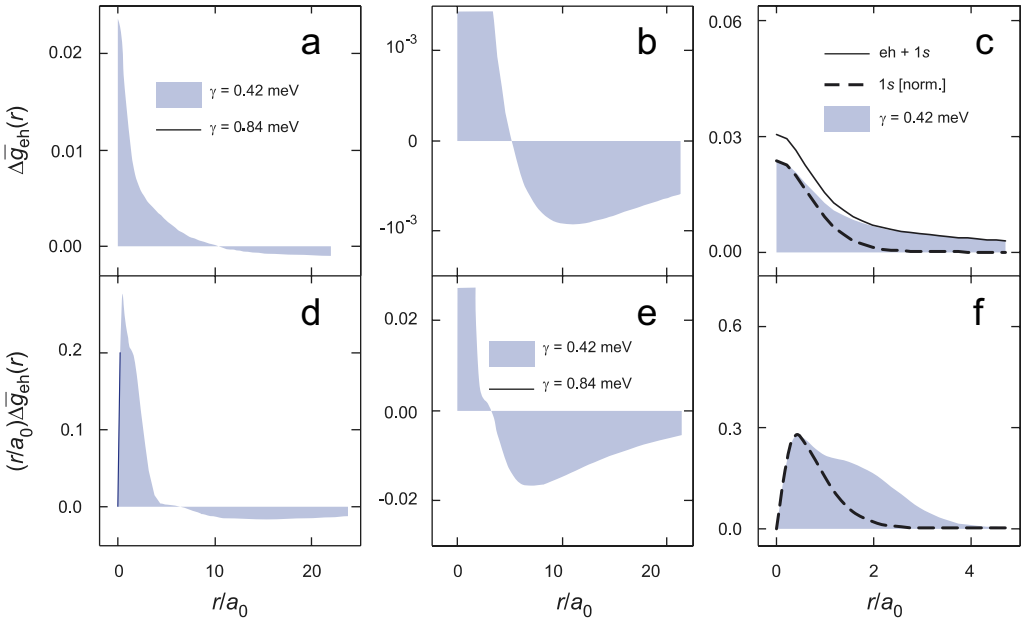

Fig. 10. Pair-correlation function for a correlated electron–hole plasma obtained by evaluating Eqs. (234) with (239). (a) The normalized $\Delta\bar{g}_{eh}$ is show for the QWI system with the carrier density $10^4\,cm^{-1}$ at 40 K. The results are obtained for the two dephasing constants, $\gamma = 0.42\,meV$ (shaded area) and $\gamma = 0.84\,meV$ (solid line). (b) Magnification of the large distance part of frame (a). (c) The influence of real exciton populations is analyzed by evaluating $\Delta\bar{g}_{eh}$. Here, a fraction of 0.16–0.8% (from bottom to top) of 1*s*-excitons is added to the correlated electron–hole plasma. Also $|\phi_{1s}(r)|^2$ (dashed line) and the correlated plasma result (shaded area) are shown. (d)–(f) The same analysis as in (a)–(c) is presented for a QW system with $2 \times 10^9\,cm^{-2}$ carrier density at 40 K. Here, $\Delta\bar{g}_{eh}$ has been multiplied by r to obtain the radial probability distribution.

We see in Figs. 10c and f that already the addition of a small amount of exciton populations to the correlated plasma modifies $\Delta\bar{g}_{eh}(r_\parallel)$ toward a pronounced 1*s*-like shape, which produces an overall positive integration area. This indicates that $\Delta\bar{g}_{eh}(r_\parallel)$ provides a sensitive measure for the presence of truly bound excitons.

In order to understand the energetic differences between the correlated electron–hole plasma and the exciton populations for a general incoherent many-body state, we analyze the total average energy by expressing Eq. (200) in the exciton basis

$$
\begin{aligned}
E_{\mathrm{carr}} = & \sum_{\mathbf{k}_\parallel} [\varepsilon^{\mathrm{e}}_{\mathbf{k}_\parallel} f^{\mathrm{e}}_{\mathbf{k}_\parallel} + \varepsilon^{\mathrm{h}}_{\mathbf{k}_\parallel} f^{\mathrm{h}}_{\mathbf{k}_\parallel}] + \sum_{\mathbf{k}_\parallel,\mathbf{k}'_\parallel} V_{\mathbf{k}_\parallel - \mathbf{k}'_\parallel} [f^{\mathrm{e}}_{\mathbf{k}_\parallel} f^{\mathrm{e}}_{\mathbf{k}'_\parallel} + f^{\mathrm{h}}_{\mathbf{k}_\parallel} f^{\mathrm{h}}_{\mathbf{k}'_\parallel}] \\
& + \sum_{\lambda,\mathbf{q}_\parallel} \left[E_\lambda(\mathbf{q}_\parallel) - \sum_{\mathbf{k}_\parallel} (\varepsilon^{\mathrm{e}}_{\mathbf{k}_\parallel} + \varepsilon^{\mathrm{h}}_{\mathbf{k}_\parallel}) \phi^{\mathrm{L}}_\lambda(\mathbf{k}_\parallel) \phi^{\mathrm{R}}_\lambda(\mathbf{k}_\parallel) \right] \Delta N_\lambda(\mathbf{q}_\parallel) \\
& - \sum_{\lambda \neq \nu,\mathbf{q}_\parallel} \left[\sum_{\mathbf{k}_\parallel} (\varepsilon^{\mathrm{e}}_{\mathbf{k}_\parallel} + \varepsilon^{\mathrm{h}}_{\mathbf{k}_\parallel}) \phi^{\mathrm{L}}_\lambda(\mathbf{k}_\parallel) \phi^{\mathrm{R}}_\nu(\mathbf{k}_\parallel) \right] \Delta N_{\lambda,\nu}(\mathbf{q}_\parallel) \rangle \\
& + \sum_{\mathbf{k}_\parallel,\mathbf{k}'_\parallel,\mathbf{q}_\parallel} \frac{1}{2} V_{\mathbf{q}_\parallel} (c^{\mathbf{q}_\parallel,\mathbf{k}'_\parallel,\mathbf{k}_\parallel}_{c,c;c,c} + c^{\mathbf{q}_\parallel,\mathbf{k}'_\parallel,\mathbf{k}_\parallel}_{v,v;v,v}),
\end{aligned}
\tag{240}
$$

$$E_\lambda(\mathbf{q}_\parallel) \equiv E_\lambda + \frac{\hbar^2 \mathbf{q}_\parallel^2}{2(m_e + m_h)}. \tag{241}$$

Here, $E_\lambda(\mathbf{q}_\parallel)$ defines the energy of an exciton with a center-of-mass momentum $\mathbf{q}_\parallel$. When the incoherent carrier system exists dominantly in the form of an exciton population $\Delta N_{\lambda,\mathbf{q}_\parallel}$, we may omit the non-diagonal $\Delta\langle X_\lambda^\dagger X_\nu\rangle$ contributions to obtain

$$\begin{aligned} E_{\text{carr}}|_{\lambda\text{-pop}} = & \sum_{\mathbf{k}_\parallel} \varepsilon^e_{\mathbf{k}_\parallel} \left[f^e_{\mathbf{k}_\parallel} - \sum_{\mathbf{q}_\parallel} \phi^L_\lambda(\mathbf{k}_\parallel)\phi^R_\lambda(\mathbf{k}_\parallel)\Delta N_\lambda(\mathbf{q}_\parallel) \right] \\ & + \sum_{\mathbf{k}_\parallel} \varepsilon^h_{\mathbf{k}_\parallel} \left[f^h_{\mathbf{k}_\parallel} - \sum_{\mathbf{q}_\parallel} \phi^L_\lambda(\mathbf{k}_\parallel)\phi^R_\lambda(\mathbf{k}_\parallel)\Delta N_\lambda(\mathbf{q}_\parallel) \right] + \sum_{\mathbf{q}_\parallel} E_\lambda(\mathbf{q}_\parallel)\Delta N_\lambda(\mathbf{q}_\parallel) \\ & + \sum_{\mathbf{k}_\parallel,\mathbf{k}'_\parallel} V_{\mathbf{k}_\parallel - \mathbf{k}'_\parallel} [f^e_{\mathbf{k}_\parallel} f^e_{\mathbf{k}'_\parallel} + f^h_{\mathbf{k}_\parallel} f^h_{\mathbf{k}'_\parallel}] \\ & + \sum_{\mathbf{k}_\parallel,\mathbf{k}'_\parallel,\mathbf{q}_\parallel} \frac{1}{2} V_{\mathbf{q}_\parallel} (c^{\mathbf{q}_\parallel,\mathbf{k}'_\parallel,\mathbf{k}_\parallel}_{c,c;c,c} + c^{\mathbf{q}_\parallel,\mathbf{k}'_\parallel,\mathbf{k}_\parallel}_{v,v;v,v}). \end{aligned} \tag{242}$$

For the pure exciton case, the carrier distributions produce the same density as the $\sum_{\mathbf{q}_\parallel}\Delta N_\lambda(\mathbf{q}_\parallel)$ term. In addition, these distributions very closely follow the shape of the exciton wavefunction product, $\phi^L_\lambda(\mathbf{k}_\parallel)\phi^R_\lambda(\mathbf{k}_\parallel)$. Consequently, the first two kinetic energy terms practically compensate each other. Since the remaining terms also vanish for sufficiently dilute densities, we find

$$\lim_{n_{e,h}\to 0} E_{\text{carr}}|_{\lambda\text{-pop}} = \sum_{\mathbf{q}_\parallel} E_\lambda(\mathbf{q}_\parallel)\Delta N_\lambda(\mathbf{q}_\parallel). \tag{243}$$

Hence, the average energy per particle is close to E_λ which can be significantly below the band-gap energy, see Fig. 8. Due to the energy difference between the uncorrelated electron–hole plasma ($E_{\text{carr}} > 0$) and the exciton populations ($E_{\text{carr}} < 0$), the formation of excitons in an electron–hole plasma requires significant dynamical rearrangements between these two many-body states. Hence, we conclude from Eq. (237) that the phenomenological scattering model for $T^{\lambda,\nu}(\mathbf{q})$ is not good enough to describe formation of excitons in the incoherent regime since such an approach only produces a correlated electron–hole plasma.

If the system only contains the correlated electron–hole plasma, we have

$$\begin{aligned} E_{\text{carr}}|_{\text{corr. plasma}} = & \sum_{\mathbf{k}_\parallel} [\varepsilon^e_{\mathbf{k}_\parallel} f^e_{\mathbf{k}_\parallel} + \varepsilon^h_{\mathbf{k}_\parallel} f^h_{\mathbf{k}_\parallel}] + \sum_{\mathbf{k}_\parallel,\mathbf{k}'_\parallel} V_{\mathbf{k}_\parallel - \mathbf{k}'_\parallel} [f^e_{\mathbf{k}_\parallel} f^e_{\mathbf{k}'_\parallel} + f^h_{\mathbf{k}_\parallel} f^h_{\mathbf{k}'_\parallel}] \\ & - \sum_{\lambda \neq \nu,\mathbf{q}_\parallel} \left[\sum_{\mathbf{k}_\parallel} (\varepsilon^e_{\mathbf{k}_\parallel} + \varepsilon^h_{\mathbf{k}_\parallel}) \phi^L_\lambda(\mathbf{k}_\parallel)\phi^R_\nu(\mathbf{k}_\parallel) \right] \Delta N_{\lambda,\nu}(\mathbf{q}_\parallel) \\ & + \sum_{\mathbf{k}_\parallel,\mathbf{k}'_\parallel,\mathbf{q}_\parallel} \frac{1}{2} V_{\mathbf{q}_\parallel} (c^{\mathbf{q}_\parallel,\mathbf{k}'_\parallel,\mathbf{k}_\parallel}_{c,c;c,c} + c^{\mathbf{q}_\parallel,\mathbf{k}'_\parallel,\mathbf{k}_\parallel}_{v,v;v,v}). \end{aligned} \tag{244}$$

Since here all correlation terms are non-linear with respect to the carrier density, we can understand that the formation of such a correlated electron–hole plasma yields only a very small energy reduction compared to the uncorrelated plasma state. Since the correlated and

uncorrelated electron–hole plasma have a very similar, positively valued energy the uncorrelated electron–hole plasma can be converted rather easily into a correlated state where electrons and holes attract each other without true exciton formation. This small scale rearrangement can be well modeled by implementing a phenomenological dephasing $T^{\lambda,\nu}(\mathbf{q}_\parallel)$.

6.6. Terahertz spectroscopy and excitons

In dilute gas spectroscopy, one often detects small concentrations of a particular species of atoms or molecules by using an optical probe that is sensitive to transitions between the eigenstates of the respective species. If the characteristic absorption resonances are observed in the probe spectrum, the atoms or molecules must be present, and one can deduce their relative concentration through proper normalization of the respective transition strength. To understand why this simple scenario does not apply for interband optics in semiconductors, we have to remember that the interband transitions in semiconductors do not conserve the number of electron–hole pairs. In other words, each interband absorption process creates an electron–hole pair while an interband emission process destroys such a pair. As a result, interband absorption or emission leads to transitions that connect semiconductor eigenstates with different numbers of electron–hole pairs.

In order to find a direct analog between semiconductor optics and atomic spectroscopy, we have to consider an energy range of light that does not change the number of electron–hole-pair excitations, i.e. we need to consider intraband transitions where electron–hole pairs are neither created nor destroyed. In particular, we want to look for transitions between the exciton levels [16,17,118,119] to identify the presence of exciton quasi-particles in semiconductors. Here, the most pronounced resonance is expected at $\hbar\omega_t = \hbar\omega_{2p} - \hbar\omega_{1s}$ corresponding to the excitation of the exciton from its lowest, $1s$, state to the next higher, $2p$, state. For many of the commonly studied direct-gap compound semiconductors, the excitonic binding energies are in the range of a few meV such that the transition energy $\hbar\omega_t$ is in the THz part of the electromagnetic spectrum [16,17].

We next discuss the direct correspondence between atomic spectroscopy and THz spectroscopy in semiconductors. A particular interest is here to find a direct way to detect the exciton number as defined in Section 6.4. The theory for THz spectroscopy can be described microscopically with the same precision as the optical interband spectroscopy by applying the same cluster-expansion approach as we have used so far. However, here we do not elaborate on the details of the calculations and emphasize only the fact that THz spectroscopy can unambiguously identify true exciton populations. For this purpose, we only briefly summarize the main steps [18,30,33,34,44,120] needed to understand linear THz absorption features.

In order to keep the analysis as simple as possible and to concentrate on the precise identification of genuine exciton populations, we focus here on a situation where all interband coherences have decayed, i.e. $\mathbf{P}$ and all other coherent quantities vanish. Furthermore, we consider here only classical THz fields described by the vector potential $\langle\mathbf{A}\rangle \equiv \langle A(t)\rangle\mathbf{e}_A$. Under these conditions, the response of a semiconductor to a THz field follows from the current

$$J = \frac{1}{\mathsf{S}}\sum_{\mathbf{k}_\parallel,\lambda}[j_\lambda(\mathbf{k}_\parallel) - e^2\langle A(t)\rangle/m_0]f^\lambda_{\mathbf{k}_\parallel}, \tag{245}$$

with the free-electron mass m_0 and the current-matrix element

$$j_\lambda(\mathbf{k}_\parallel) \equiv -|e|\hbar\mathbf{k}_\parallel \cdot \mathbf{e}_A/m_\lambda, \tag{246}$$

where $\mathbf{e}_A$ is the polarization direction of the THz field. If we assume that the classical THz field propagates perpendicular to the QW or QWI system, the interaction of the carriers with the THz field is governed by the Hamiltonian

$$H_{\mathrm{THz}} = -\sum_{\mathbf{k}_\parallel} j_\lambda(\mathbf{k}_\parallel) a^\dagger_{\lambda,\mathbf{k}_\parallel} a_{\lambda,\mathbf{k}_\parallel} \langle A(t)\rangle, \tag{247}$$

as discussed in Refs. [18,37,120]. It can be shown that the pure THz absorption properties follow entirely from the carrier-density dependent part of J [33,120], i.e.

$$J_{\mathrm{THz}} = \frac{1}{\mathsf{S}} \sum_{\mathbf{k},\lambda} j_\lambda(\mathbf{k}) f^\lambda_{\mathbf{k}}. \tag{248}$$

To compute J_{THz}, we have to evaluate the dynamics of the densities

$$\frac{\partial}{\partial t} f^{\mathrm{e}}_{\mathbf{k}_\parallel} = -\frac{2}{\hbar}\,\mathrm{Im}\left[\sum_{\mathbf{q}_\parallel,\mathbf{k}'_\parallel} V_{\mathbf{k}'_\parallel+\mathbf{q}_\parallel-\mathbf{k}_\parallel} c_X^{\mathbf{q}_\parallel,\mathbf{k}'_\parallel,\mathbf{k}_\parallel} - \sum_{\mathbf{q}_\parallel,\mathbf{k}'_\parallel} V_{\mathbf{q}_\parallel} c_{c,c,c,c}^{\mathbf{q}_\parallel,\mathbf{k}'_\parallel,\mathbf{k}_\parallel}\right], \tag{249}$$

$$\frac{\partial}{\partial t} f^{\mathrm{h}}_{\mathbf{k}_\parallel} = +\frac{2}{\hbar}\,\mathrm{Im}\left[\sum_{\mathbf{q}_\parallel,\mathbf{k}'_\parallel} V_{\mathbf{k}'_\parallel+\mathbf{q}_\parallel-\mathbf{k}_\parallel} c_X^{-\mathbf{q}_\parallel,\mathbf{k}_\parallel,\mathbf{k}'_\parallel} - \sum_{\mathbf{q}_\parallel,\mathbf{k}'_\parallel} V_{\mathbf{q}_\parallel} c_{v,v,v,v}^{\mathbf{q}_\parallel,\mathbf{k}'_\parallel,\mathbf{k}_\parallel}\right], \tag{250}$$

where we have assumed that the incoherent and homogeneous carrier system interacts with a THz field while phonon-coupling effects are neglected for simplicity. Eqs. (249)–(250) show that the single-particle densities do not couple directly to the THz light. Thus, THz absorption must involve at least two-particle correlations, which identifies *THz absorption as a uniquely qualified method to directly detect many-body correlations for incoherent quasi-particle excitations*.

Starting from Eq. (247), we can easily convince ourselves that also $c_{c,c,c,c}$ and $c_{v,v,v,v}$ are not directly coupled to the THz fields. Furthermore, we can show that the exciton correlation is directly driven by

$$\mathrm{i}\hbar\frac{\partial}{\partial t} c_{\mathrm{X}}^{\mathbf{q}_\parallel,\mathbf{k}'_\parallel,\mathbf{k}_\parallel}\bigg|_{\mathrm{THz}} = -j(\mathbf{k}'_\parallel + \mathbf{q}_\parallel - \mathbf{k}_\parallel)\langle A(t)\rangle c_{\mathrm{X}}^{\mathbf{q}_\parallel,\mathbf{k}'_\parallel,\mathbf{k}_\parallel}, \tag{251}$$

where we have identified the reduced current-matrix element,

$$j(\mathbf{k}_\parallel) \equiv j_{\mathrm{e}}(\mathbf{k}_\parallel) + j_{\mathrm{h}}(\mathbf{k}_\parallel). \tag{252}$$

The THz contribution (251) now has to be added to the dynamics of c_X, Eq. (222). With the help of the transformation (233), we can express this THz contribution as

$$\mathrm{i}\hbar\frac{\partial}{\partial t}\Delta N_{\lambda,\nu}(\mathbf{q}_\parallel)\bigg|_{\mathrm{THz}} = \sum_\beta [J_{\lambda,\beta}\Delta N_{\beta,\nu}(\mathbf{q}_\parallel) - J_{\nu,\beta}\Delta N_{\lambda,\beta}(\mathbf{q}_\parallel)]\langle A(t)\rangle, \tag{253}$$

where we identified the transition-matrix element between two exciton states,

$$J_{\alpha,\beta} \equiv \sum_{\mathbf{k}_\parallel} \phi^{\mathrm{L}}_\alpha(\mathbf{k}_\parallel) j(\mathbf{k}_\parallel) \phi^{\mathrm{R}}_\beta(\mathbf{k}_\parallel). \tag{254}$$

As Eq. (253) is added to Eq. (237), the THz transitions can be studied self-consistently in the exciton basis. We evaluate the excitonic signatures in the THz current by taking a time derivative of J_{THz}. Using Eqs. (248)–(250) and (233), we obtain

$$\frac{\partial}{\partial t}J_{\mathrm{THz}} = \frac{2}{\hbar}\,\mathrm{Im}\left[\frac{1}{\mathsf{S}}\sum_{\mathbf{q}_\parallel,\mathbf{k}'_\parallel,\mathbf{k}_\parallel} V_{\mathbf{q}_\parallel}\left(j_{\mathrm{e}}(\mathbf{k}_\parallel)c^{\mathbf{q}_\parallel,\mathbf{k}'_\parallel,\mathbf{k}_\parallel}_{c,c,c,c} - j_{\mathrm{h}}(\mathbf{k}_\parallel)c^{\mathbf{q}_\parallel,\mathbf{k}'_\parallel,\mathbf{k}_\parallel}_{v,v,v,v}\right)\right] + \frac{1}{\hbar}\,\mathrm{Im}\left[\frac{1}{\mathsf{S}}\sum_{\mathbf{q}_\parallel,\lambda,v}(E_v - E_\lambda)J_{\lambda,v}\Delta N_{\lambda,v}(\mathbf{q}_\parallel)\right], \tag{255}$$

where the property (121) of the exciton states has been used to simplify the matrix elements related to the exciton contributions. In general, $c_{c,c,c,c}$ and $c_{v,v,v,v}$ provide electron and hole scattering to the THz currents, which essentially leads to a damping of J_{THz}.

At this stage, we can perform a full numerical analysis of Eqs. (237) and (253)–(255). Even though we do this and present the results later, we first want to gain some analytic insight into the THz response. For this purpose, *and not for the full numerical evaluations*, we now introduce a few simplifications that do not compromise the essential aspects of THz physics. First, we assume that the incoherent semiconductor state is quasi-stationary. This means that f^{e}, f^{h} and c_X are known and stationary before the weak THz excitation of the system. Since such weak THz fields induce only small currents which are damped as a consequence of carrier scattering, it is reasonable to approximate the full microscopic scattering by a phenomenological damping. In other words, for the analytic evaluations we replace the contributions of $c_{c,c,c,c}$ and $c_{v,v,v,v}$ by $-\gamma_J J_{\mathrm{THz}}$ in Eq. (255). We also limit the investigations to the linear response. Here, the exciton correlation can be split into two parts,

$$\Delta N_{\lambda,v}(\mathbf{q}_\parallel) = \Delta N_{\lambda,v}(\mathbf{q}_\parallel)_{(0)} + \Delta N_{\lambda,v}(\mathbf{q}_\parallel)_{(1)}, \tag{256}$$

where $\Delta\langle N\rangle_{(0)}$ is the quasi-stationary exciton correlation and $\Delta\langle N\rangle_{(1)}$ is the linear response to $\langle A\rangle$.

Under these conditions, the exciton correlation dynamics can be linearized such that Eqs. (237) and (253) together produce

$$\mathrm{i}\hbar\frac{\partial}{\partial t}\Delta N_{\lambda,v}(\mathbf{q}_\parallel)_{(1)} = (E_v - E_\lambda - \mathrm{i}\gamma)\Delta N_{\lambda,v}(\mathbf{q}_\parallel)_{(1)} + \sum_\beta [J_{\lambda,\beta}\Delta N_{\beta,v}(\mathbf{q}_\parallel)_{(0)} - J_{v,\beta}\Delta N_{\lambda,\beta}(\mathbf{q}_\parallel)_{(0)}]\langle A(t)\rangle, \tag{257}$$

where the main-sum approximation has been used. Furthermore, in the THz generated contributions, $\Delta\langle N\rangle_{(1)}$ we have replaced the influence of three-particle scattering by a constant dephasing rate [121].

Defining the total density of exciton correlations as

$$\Delta n^{(j)}_{\lambda,v} \equiv \frac{1}{\mathsf{S}}\sum_{\mathbf{q}_\parallel}\Delta N_{\lambda,v}(\mathbf{q}_\parallel)_{(j)}, \tag{258}$$

we may sum Eq. (257) over $\mathbf{q}_\parallel$ and take the Fourier transformation to obtain

$$\hbar\omega\Delta n^{(1)}_{\lambda,v}(\omega) = (E_v - E_\lambda - \mathrm{i}\gamma)\Delta n^{(1)}_{\lambda,v}(\omega) + \sum_\beta [J_{\lambda,\beta}\Delta n^{(0)}_{\beta,v} - J_{v,\beta}\Delta n^{(0)}_{\lambda,\beta}]\langle A(\omega)\rangle. \tag{259}$$

Note that $\Delta n^{(0)}_{\beta,\nu}$ is quasi-stationary such that only the Fourier transform of the THz field appears in the last term. In the same way, we Fourier transform also Eq. (255) to obtain

$$-\mathrm{i}\hbar\omega J_{\mathrm{THz}}(\omega) = -\gamma_J J_{\mathrm{THz}}(\omega) + \frac{1}{2\mathrm{i}}\sum_{\lambda,\nu}(E_\nu - E_\lambda)J_{\lambda,\nu}[\Delta n^{(1)}_{\lambda,\nu}(\omega) - (\Delta n^{(1)}_{\lambda,\nu}(-\omega))^\star], \tag{260}$$

where we replaced the microscopic scattering of the current by a decay constant γ_J and noticed that the quasi-stationary $\Delta n^{(0)}_{\lambda,\nu}$ cannot contribute to the current.

Eqs. (259)–(260) are now closed and yield the solution

$$J_{\mathrm{THz}}(\omega) = \frac{1}{\hbar\omega + \mathrm{i}\gamma_J}\sum_{\nu,\lambda}(S^{\nu,\lambda}(\omega)\Delta n^{(0)}_{\nu,\lambda} - [S^{\nu,\lambda}(-\omega)\Delta n^{(0)}_{\nu,\lambda}]^\star)\langle A(\omega)\rangle. \tag{261}$$

From this expression, we see that the THz current only depends on the initial state of the incoherent quasi-particle excitations, the spectrum of the THz field, and the generic THz response function

$$S^{\nu,\lambda}(\omega) = \sum_\beta \frac{(E_\beta - E_\nu)J_{\nu,\beta}J_{\beta,\lambda}}{E_\beta - E_\nu - \hbar\omega - \mathrm{i}\gamma}. \tag{262}$$

The denominator of this response function introduces resonances corresponding to transitions between different exciton states, whereas the product of the matrix elements $J_{\nu,\beta}J_{\beta,\lambda}$ provides the selection rules.

Just as in the case of linear interband absorption, the result (261) can be directly applied to produce the linear susceptibility

$$\chi_{\mathrm{THz}} \equiv \frac{P_{\mathrm{THz}}(\omega)}{\varepsilon_0\langle E(\omega)\rangle} = \frac{J_{\mathrm{THz}}(\omega)}{\varepsilon_0\omega^2\langle A(\omega)\rangle}, \tag{263}$$

where we used the general relations, $\langle E(t)\rangle = -(\partial/\partial t)\langle A(t)\rangle$ and $J_{\mathrm{THz}}(t) \equiv (\partial/\partial t)P_{\mathrm{THz}}(t)$ to evaluate $\langle E(\omega)\rangle = \mathrm{i}\omega\langle A(\omega)\rangle$ and $P_{\mathrm{THz}}(\omega) = (\mathrm{i}/\omega)J_{\mathrm{THz}}(\omega)$, respectively. Since the QW is thin compared with the THz wavelength (we have assumed that the planar confinement is much smaller than the optical wavelength), we may directly solve the linear propagation problem via the analysis performed in Section 5.6. By applying Eqs. (159) and (164), we obtain

$$\xi_{\mathrm{THz}}(\omega) = \frac{1}{2}\frac{\omega}{nc}\chi_{\mathrm{THz}}(\omega), \quad \alpha_{\mathrm{THz}}(\omega) = 2\,\mathrm{Im}[\xi_{\mathrm{THz}}(\omega)], \tag{264}$$

which provides the linear THz absorption for $|\xi_{\mathrm{THz}}| \ll 1$, as discussed earlier in Section 5.6. As we insert the result (261) into Eq. (264), we find

$$\alpha_{\mathrm{THz}}(\omega) = \mathrm{Im}\left[\sum_{\nu,\lambda}\frac{S^{\nu,\lambda}(\omega)\Delta n^{(0)}_{\nu,\lambda} - [S^{\nu,\lambda}(-\omega)\Delta n^{(0)}_{\nu,\lambda}]^\star}{\varepsilon_0 nc\omega(\hbar\omega + \mathrm{i}\gamma_J)}\right] \tag{265}$$

which gives the THz absorption from a generic incoherent quasi-particle state.

To gain some more detailed insights, we first analyze the THz absorption for the limiting case where only diagonal correlations exist, i.e. $\Delta n^{(0)}_{\nu,\lambda} = \delta_{\nu,\lambda}\Delta n^{(0)}_{\nu,\nu} \equiv \delta_{\nu,\lambda}\Delta n_\nu$. In this

situation, Eq. (265) reduces to

$$\alpha_{\text{atom}}(\omega) = \frac{\omega}{\varepsilon_0 nc}\,\text{Im}\left[\sum_v (S^v_{\text{atom}}(\omega) - [S^v_{\text{atom}}(-\omega)]^\star)\Delta n_v\right], \tag{266}$$

$$S^v_{\text{atom}}(\omega) = \sum_\beta \frac{|D_{v,\beta}|^2}{E_\beta - E_v - \hbar\omega - \text{i}\gamma}. \tag{267}$$

Here, we defined the excitonic dipole-matrix element

$$D_{\lambda,v} \equiv \langle \phi^{\text{L}}_\lambda | e\mathbf{r}\cdot\mathbf{e}_P | \phi^{\text{R}}_v \rangle = \frac{\text{i}\hbar}{E_v - E_\lambda} J_{\lambda,v}, \tag{268}$$

using the general connection of dipole- and current-matrix elements [1]. We have also assumed that the $(E_v - E_\lambda)$ in Eq. (268) as well as in the nominator of Eq. (262) can be replaced by $\hbar\omega$ due to the narrow enough Lorentzian resonances in $S^{\lambda,v}$. With these assumptions, which are typical in atom optics, we find that our THz analysis produces an atom-like absorption spectrum for the case where different atomic levels are populated according to Δn_v. This results clearly establishes the close relation between excitonic THz and atomic spectroscopy helping us to give physical support to our concept of exciton populations.

To illustrate the principal features of the correlated electron–hole plasma and the presence of exciton populations, we compute the THz absorption spectrum for different experimentally relevant combinations. Examples for the results are summarized in Fig. 11. In Fig. 11a we show a contour plot of the correlation function $|\Delta N_{v,\lambda}(0)|$, evaluated from Eq. (239) using the same $\gamma = 1.7\,\text{meV}$ as in Fig. 10. We observe clear plasma properties, i.e. $|\Delta N_{v,\lambda}|$ extends over a large space of exciton states and it has no diagonal contributions, signifying the absence of true exciton populations.

In Fig. 11b we show the same results as in Fig. 11a, however, for a situation where we added a 5% fraction of 1*s* excitons. We observe that $|\Delta N_{v,\lambda}|$ now exhibits a dominant peak at the 1*s* state. In Fig. 11c we plot the induced THz response for the correlated electron–hole plasma with different percentages of 1*s*-excitons. We note that the pure plasma produces a rather featureless THz response without resonances. Only when 1*s*-exciton populations are present, a pronounced 1*s*-to-2*p* transition resonance appears. This resonance, which is located at the energy difference $E_{2p1s} \equiv E_{2p} - E_{1s}$, can therefore be used as a qualitative signature in calculations as well as in real experiments, indicating the presence of 1*s*-exciton populations.

Repeating the analysis for a QW, we obtain the results in Figs. 11d–f. Even though we note some minor quantitative differences, the overall results are qualitatively the same for QW and QWI systems. Hence, we can conclude that the THz response is excellently suited to sensitively detect 1*s*-exciton population features.

So far, we have compared the pure correlated electron–hole plasma with configurations where we have an admixture of bound 1*s*-exciton populations. Additionally, the phase-space of possible quasi-particle states includes also ionized excitons. Since these ionized states form a continuum, one can excite them only collectively. As a simple example, we consider a Gaussian distribution,

$$\Delta n^{\text{Gauss}}_{v,\lambda} \equiv N_0 \text{e}^{-((E_v - E_0)^2/\Delta E^2)} \text{e}^{-((E_\lambda - E_0)^2/\Delta E^2)}, \tag{269}$$

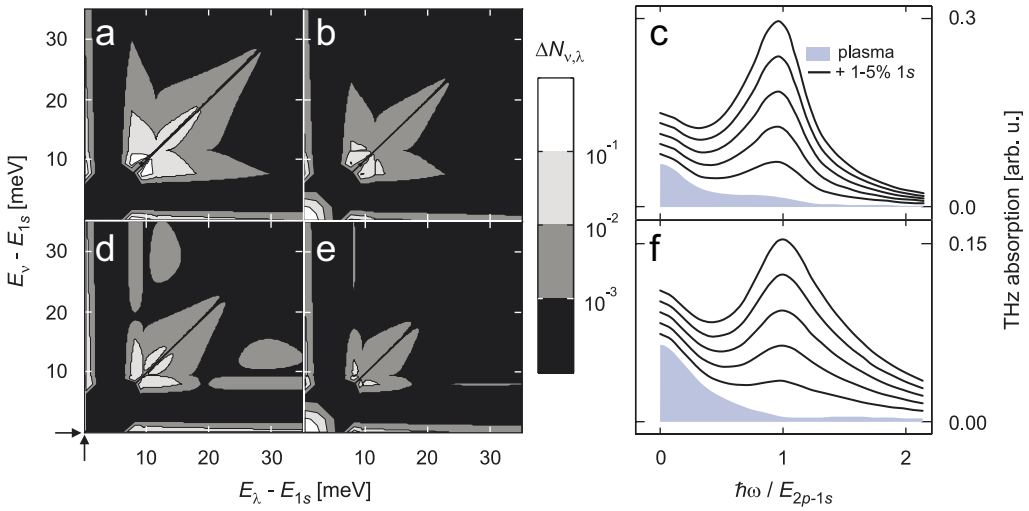

Fig. 11. The contour plot of the exciton correlation, $|\Delta N_{v,\lambda}(0)|$ for the *s*-like states is presented for (a) the correlated electron–hole plasma and (b) an electron–hole plasma with 5% 1*s* excitons in a QWI system. The contour lines are defined with respect to the maximum value of $|\Delta N_{v,\lambda}|$. Here, we represented the discrete states as a 2 meV wide area in order to increase their visibility; otherwise, $|\Delta N_{v,\lambda}|$ would just show discrete points at the bound states. The arrows in the lower left corner indicate the actual position of the 1*s* state. (c) The corresponding THz response is shown for the correlated electron–hole plasma (shaded area) and for the cases where the plasma coexists with 1–5% 1*s*-exciton fraction (solid lines, from bottom to top). The same analysis for the QW system is presented in frames (d)–(f). The carrier densities are chosen as in Fig. 10 and we use $\gamma = \gamma_J = 1.7$ and 2.2 meV in Eq. (265) for the QWI and the QW, respectively.

where $E_0 > E_g$ is the central energy and ΔE is the width of the ionized-state distribution. The total number of ionized electron–hole pairs follows from $\sum_\lambda \Delta n_{\lambda,\lambda}$.

Fig. 12 compares the correlated electron–hole-plasma state of Fig. 11 to the results for the Gaussian ionized-exciton state for both QWI and QW systems. The comparison of frames (a) and (b) for the QWI, respectively (d) and (e) for the QW, clearly demonstrates that the correlated electron–hole plasma and the ionized exciton states look very different once they are presented via a $\Delta N_{v,\lambda}$ contour plot. These drastic deviations clearly show the need to distinguish between both cases. In particular, a Gaussian ionized-exciton state is well-focused around its central energy leaving most of the exciton correlation combinations unoccupied, in contrast to the correlated electron–hole plasma.

In Figs. 12c and f, we compare the THz response of the ionized exciton and the correlated plasma states. In particular, we observe monotonously decaying and featureless responses for both the QW and the QWI system. As a quantitative signature, the correlated electron–hole plasma response extends toward larger frequencies and contains some small but non-trivial oscillations. In contrast to this, ionized populations display a smooth and much faster decaying THz response.

The THz response of the ionized exciton state exhibits a typical Drude-like variation with a $\propto (\omega^2 + \gamma^2)^{-1}$ dependence while the correlated electron–hole plasma obeys such a relation only approximatively. Thus, the presence or absence of a clear Drude-like response can be taken as a signature whether one is dealing with either a correlated electron–hole plasma or an ensemble of ionized exciton states.

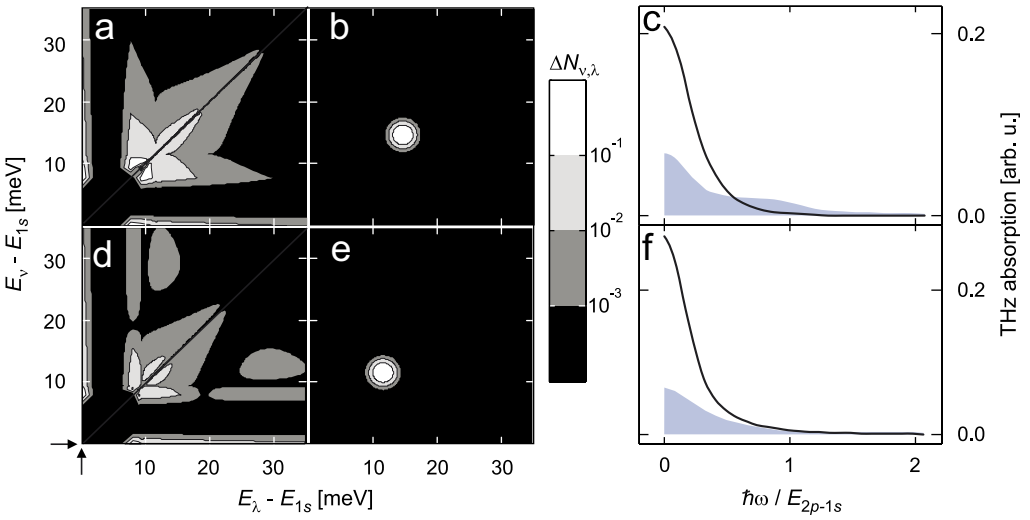

Fig. 12. The results of Figs. 11a and d, are repeated in frames (a) and (d) for the comparison with an ionized *s*-exciton population (b) and (e) in a Gaussian state according to Eq. (269). The ionized state is centered at $E_0 = 2\,\text{meV}$ above the band gap. Its energetic width is $\Delta E = 1\,\text{meV}$ and the total population $\sum_\lambda \Delta N_{\lambda,\lambda}$ corresponds to a 5% fraction of excitons. In frames (c) and (f), the corresponding THz response is shown for the bare correlated electron–hole plasma (shaded area) and the bare Gaussian ionized-exciton state (solid line). The results for the QWI system are shown in frames (a)–(c) and for the QW system in frames (d)–(f), respectively.

Many text-book examples derive the Drude absorption for an electron gas by introducing a phenomenological dephasing. This clearly is the simplest approximation for the microscopic scattering of electrons from other objects. The physical assumptions behind such a discussion are the correlation of the electrons with other quasi-particles. This is clearly the fundamental requirement for the Drude absorption. The examples for the electron–hole system discussed here show how a Drude response emerges when the electrons are correlated with holes via the Coulomb interaction. However, the other quasi-particles could also be phonons, or even doping centers. Thus, the presented microscopic THz theory can be directly generalized to compute THz and conductivity responses for a wide variety of solid-state systems.

In general terms, the incoherent quasi-particle state $\Delta N_{v,\lambda}$ can have a very complicated form. Especially, if one wants to determine its many-body dynamics, one needs the phase informations of the off-diagonal terms $\Delta N_{v\neq\lambda}$ as well as the admixture of *p*-like and higher states. This complicated problem clearly requires a fully self-consistent solution of the many-body problem. In the following sections, we present examples for such solutions. There, we will use the idealized results of the present sections for comparison purposes allowing us to identify the special characteristics of bound and ionized excitons and of the correlated plasma contributions.

7. Optical semiconductor excitations

In this section, we study the resonant optical excitation of a semiconductor QW or QWI system for a variety of experimentally relevant conditions. We place special emphasis to

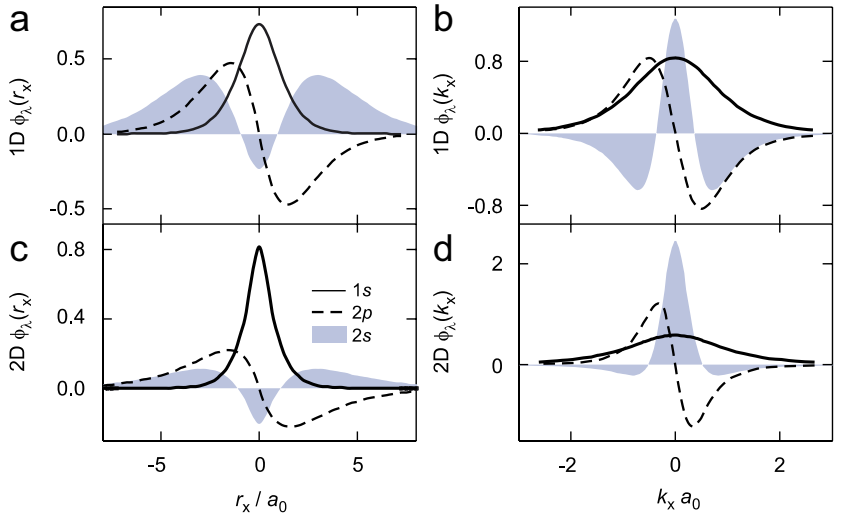

Fig. 13. Wavefunction of three lowest exciton states. The wavefunctions are presented (a) in the real-space and (b) in the momentum space for the QWI system used in this review. Corresponding QW wavefunctions are shown in frames (c) and (d) as cross-sections along the r_x and k_x axes.

resolve how incoherent exciton and/or unbound electron–hole plasma populations emerge. In particular, we carefully characterize the generated quasi-particle states and study their dependency on intensity, and energy of the exciting field. We use the quantity

$$x_\lambda \equiv \frac{\Delta n_\lambda}{n_{\mathrm{eh}}} = \frac{\sum_{\mathbf{q}_\parallel} \Delta\langle X^\dagger_{\lambda,\mathbf{q}_\parallel} X_{\lambda,\mathbf{q}_\parallel}\rangle}{\sum_{\mathbf{k}_\parallel} f^{\mathrm{e(h)}}_{\mathbf{k}_\parallel}} \tag{270}$$

to characterize the concentration of excitons in the state λ relative to the total number of excited carriers. Due to the numerical complexity of the coupled equations, we perform the full computations for the QWI system but the presented results are qualitatively also valid for QWs.

As an important piece of background information, we show in Fig. 13 the exciton wavefunctions of the $1s$ (solid line), $2p$ (dashed line), and $2s$ (shaded area) states in both real space and momentum space representation. These wavefunctions are computed in the low-density limit assuming GaAs-like material parameters for the QWI (upper row) and QW systems (lower row). The QW wavefunctions are presented as cross-sections along the r_x and k_x axes. The corresponding $2p$ energy is approximately 7.6 meV above the $1s$ state while the $2s$ energy is approximately 7.9 meV above the $1s$ state. Even though the $2s$ and $2p$ states are energetically very close, it is interesting to notice that the realistic QW confinement, i.e. the quasi-two dimensional configuration, lifts the energetic degeneracy which is observed for the strictly two-dimensional system [1].

For the QWI system, the $2p$ state is the energetically lowest exciton configuration with an odd parity, i.e. $\phi_{2p}(-\mathbf{k}_\parallel) = -\phi_{2p}(\mathbf{k}_\parallel)$. In analogy to the QW case, the QWI system has similar but less degenerate $2p$ and $2s$ states than the QW system. Here, the used wire confinement produces $2p$ and $2s$ resonance at 5.8 and 7.7 meV above the $1s$ state,

respectively. We also notice that the wavefunctions for the QW and the QWI are very similar, especially, with respect to nodes and symmetry characteristics. For example, the s-like states are (radially) symmetric while the p-like state has an odd parity $\phi_{2p}(-\mathbf{k}_\parallel) = -\phi_{2p}(\mathbf{k}_\parallel)$.

7.1. *Resonant* 1s*-excitation*

We start our analysis by assuming a resonant excitation at the lowest bound exciton energy, i.e. we extend the studies of Section 6.2 where we have already seen that such an excitation can lead to the generation of a considerable concentration of incoherent excitons for not too high intensities, see Figs. 8–10. Fig. 14 presents results of our full numerical calculations. Fig. 14a shows the 0.9 ps long excitation pulse (scaled, dashed line), the generated optical polarization $|P|^2$ (scaled, shaded area), and the excited carrier density n_{eh} (solid line). Fig. 14b compares the dynamical evolution of $|P|^2$ (scaled, shaded area) with the total fraction of 1s-exciton populations x_{1s} (solid line), 2s-exciton populations x_{2s} (dashed line), and 2p-exciton populations x_{2p} (dotted line). Fig. 14c shows the

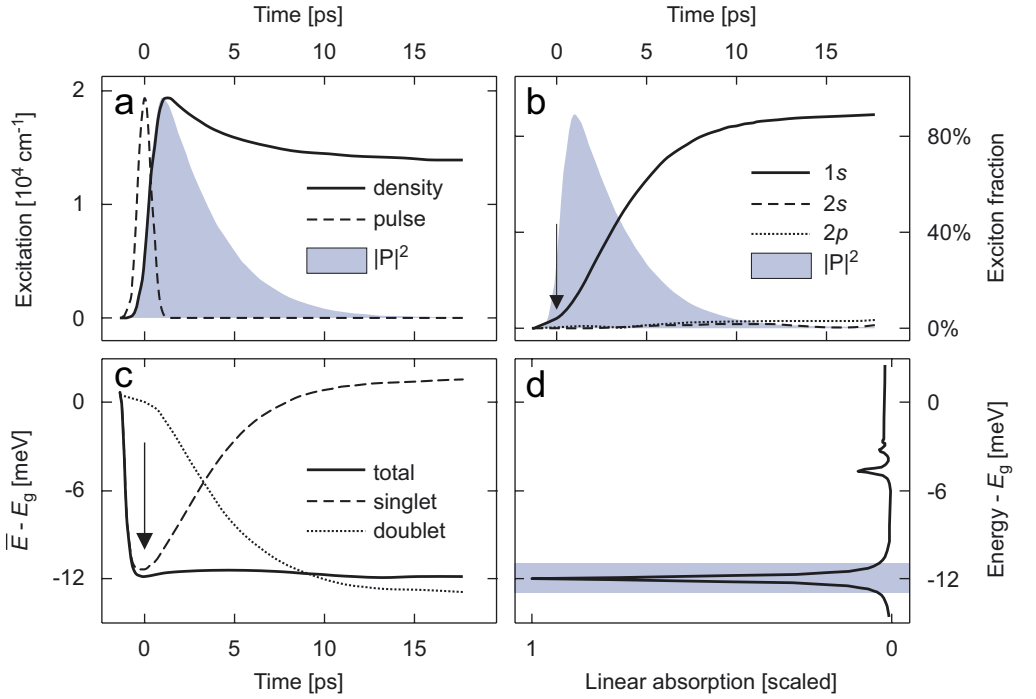

Fig. 14. Excitation at the 1s-exciton resonance. (a) The time-dependent excitation pulse (scaled, dashed line) is compared with the generated optical polarization $|P|^2$ (scaled, shaded area) and the excited carrier density (solid line). (b) The dynamical evolution of $|P|^2$ (scaled, shaded area) is compared with the total fraction of 1s (solid line), 2s (dashed line), and 2p (dotted line) exciton populations. (c) The average energy per particle (solid line) is presented together with the single-particle energy (dashed line) and the correlated two-particle energy (dotted line). (d) The linear absorption spectrum; the spectral extension of the pulse (full width half maximum) is indicated as shaded area. The arrows in panels (b) and (c) mark the temporal position of the pulse maximum.

average energy per particle (solid line) as well as its subdivision into the corresponding single-particle (dashed line) and correlated two-particle energy (dotted line). These quantities are computed by evaluating Eqs. (201)–(204). In Fig. 14d we plot the linear absorption spectrum. The center of the shaded rectangle denotes the central energetic position of the Gaussian excitation pulse and its vertical extension indicates the position of the half-maximum contour lines. The 0.9 ps excitation pulse corresponds to a 2 meV broad (full-width half-maximum value) spectrum.

As we can see in Figs. 14a and b, the decay of the polarization is accompanied by the generation of a carrier population where close to 90% of the electrons and holes are bound into 1*s* excitons. We have already discussed earlier that this polarization-to-population conversion is mediated by the coherent two-particle scattering terms resulting from both the phonon and Coulomb interactions. Fig. 14c indicates a nearly perfect energy conservation between the exciting pulse and the generated incoherent quasi-particle state. This energy is 12 meV below the band gap. Note, that the unexcited system is defined to have a vanishing energy per particle. We see in Fig. 14c that the pulse first transfers its energy to the singlets who then release their energy to the two-particle correlations as the coherences vanish.

7.1.1. Weak excitation

To obtain a more complete picture of the correlated electron–hole pairs, we now project the exciton correlations into the exciton basis using Eq. (233). In particular, we investigate the low-momentum exciton states

$$\Delta N_{\lambda,\nu}(0) = \Delta\langle X^{\dagger}_{\lambda,0} X_{\nu,0}\rangle = \sum_{\mathbf{k}_\parallel,\mathbf{k}'_\parallel} \phi^{\mathrm{L}}_{\lambda}(\mathbf{k}_\parallel)\phi^{\mathrm{L}}_{\nu}(\mathbf{k}'_\parallel) c_{\mathrm{X}}^{\mathbf{q}_\parallel,\mathbf{k}'_\parallel,\mathbf{k}_\parallel}. \tag{271}$$

As discussed already in Section 6.4, the diagonal elements, $\Delta N_{\lambda,\lambda}(0)$, identify the genuine exciton populations while the off-diagonal elements, $\Delta N_{\lambda,\nu\neq\lambda}(0)$, define exciton transition amplitudes. Since exciton correlations can be directly measured via a weak THz probe, we also present the THz absorption spectra, Eq. (264), corresponding to the momentary quasi-particle states. This way, we can identify the characteristic signatures of the particular exciton states in THz measurements.

The left column of Fig. 15 shows $\Delta N_{\lambda,\nu}(0)$ for *s*-like states as function of the exciton energies E_λ and E_ν for the same excitation conditions as in Fig. 14. The right column of Fig. 15 shows the corresponding THz absorption spectra. At the early times, $\Delta N_{\lambda,\nu}(0)$ extends over a relatively large portion of all bound and unbound exciton states and significant non-diagonal correlations are generated. With increasing time, $\Delta N_{\lambda,\nu}(0)$ rapidly develops such that the dominant contribution is centered at the position of the 1*s*-exciton population. The extension of $\Delta N_{\nu,\lambda}$ resembles that of a correlated electron–hole plasma indicating that the discussed excitation scheme generates a mix of correlated electron–hole plasma and a dominant 1*s* population.

The THz absorption qualitatively looks similar to that of the mixture of correlated electron–hole plasma and 1*s*-exciton population, presented in Fig. 11. Checking the absolute values of the induced THz absorption signal, we note that with increasing time the strength of the 1*s*–2*p* resonance in the THz spectrum grows considerably in accordance with the increasing number of 1*s*-excitons in the system.

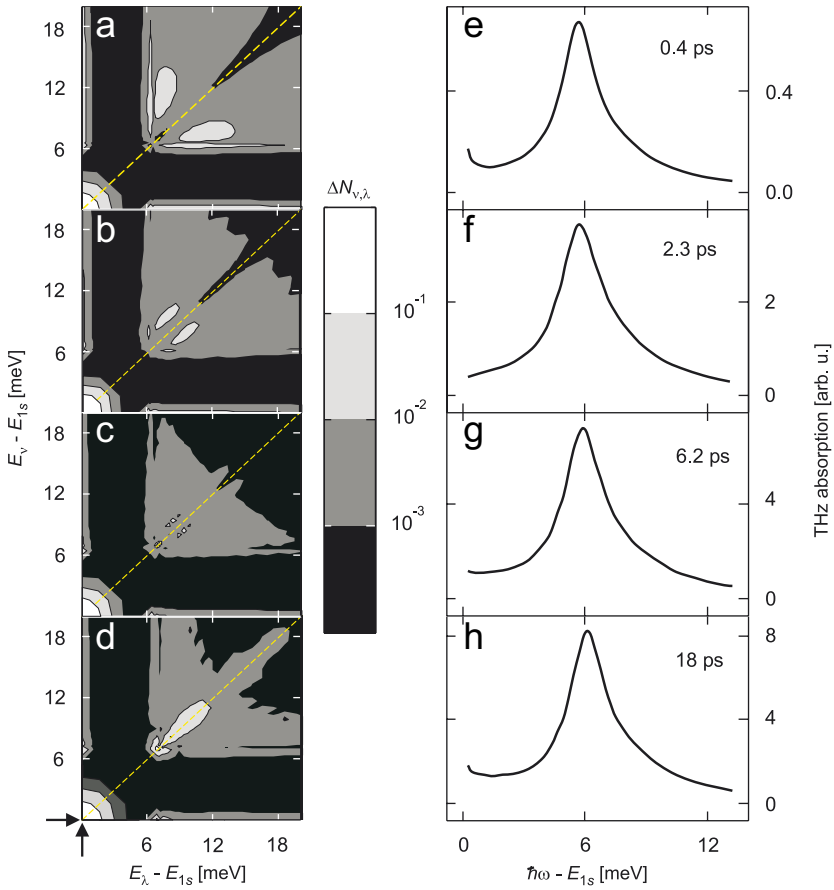

Fig. 15. Analysis of the excitonic correlations generated by the resonant 1*s* excitation of Fig. 14. The left column presents the contour plots of the generated $|\Delta N_{\nu,\lambda}(0)|$ for *s*-like states at different times after the excitation and the right column shows the corresponding THz absorption spectra. The dashed line along the diagonal of the contour plots indicates the location of true exciton populations. The arrows in the lower left corner mark the central energy of the excitation.

7.1.2. Strong excitation

We now repeat our calculations for resonant 1*s*-excitation but this time we assume an increased pump intensity. To characterize the resulting situation, we plot $f^{e}_{\mathbf{k}_\parallel} + f^{h}_{\mathbf{k}_\parallel}$, i.e. the sum of the single-particle carrier distributions, in Fig. 16. As a consequence of the stronger excitation this population factor now reaches values around 0.5 indicating significant phase-space filling effects. Hence, one can expect that the Fermionic substructure of the 1*s* excitons should become relevant.

The generated many-body state is analyzed in Fig. 17 by comparing $|\Delta N_{\nu,\lambda}(0)|$ and the induced THz absorption spectra for the strong and the weak excitation cases. We see that qualitatively very different states are generated. For the weak excitation case, a significant population is observed at the discrete 1*s* state. In contrast, $\Delta N_{\lambda,\nu}(0)$ extends over several energetically different states for the strong excitation. In fact, here the excitonic energies

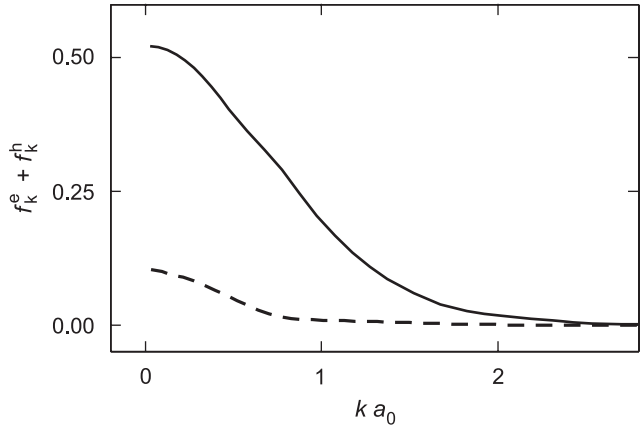

Fig. 16. The sum of the final electron and hole distributions are compared for strong (solid line) and weak (dashed line) excitations.

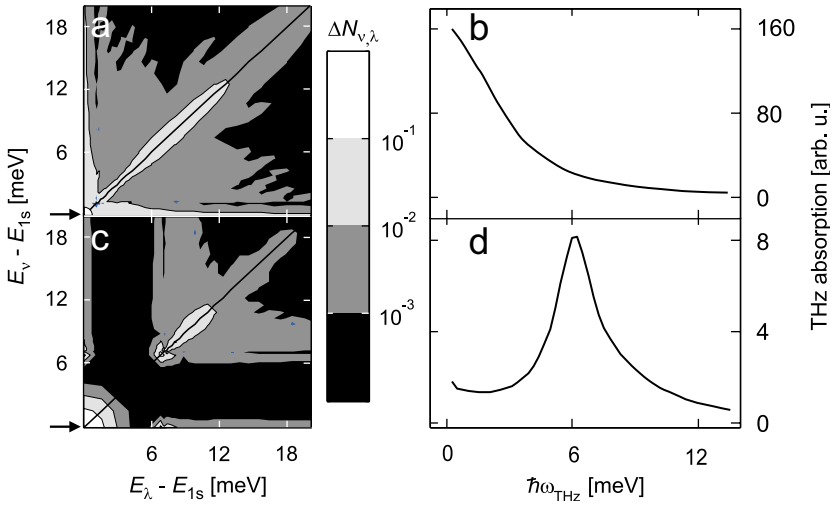

Fig. 17. Quasi-particle state and THz response after resonant 1*s*-excitation using strong [frames (a) and (b)] and weak [frames (c) and (d)] excitation pulses. Frames (a) and (c) show the contour plots of the excitonic correlations $|\Delta N_{v,\lambda}(0)|$; the arrows indicate the energetic position of the excitation. Frames (b) and (d) present the corresponding THz absorption spectra.

almost completely loose their discrete character, which implies that the 1*s*-exciton state is almost ionized as a consequence of the Pauli-exclusion principle [56,30].

The differences between the weak and strong excitation scenarios also show up in their respective THz responses. Whereas a pronounced 1*s* to 2*p* resonance is observed under weak excitation conditions when the 1*s*-exciton state is populated, the strong excitation produces a characteristic Drude-like response of an ionized plasma. Nevertheless, even the ionized electron–hole pairs remain correlated as discussed in Ref. [56]. This conclusion is supported by Fig. 17a which shows a pronounced maximum along the diagonal line indicating the presence of a correlated ionized exciton population.

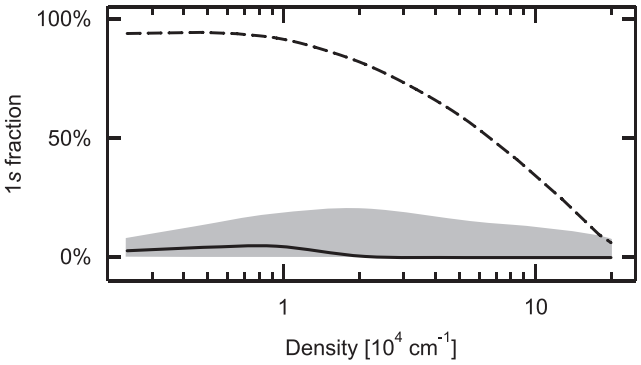

Fig. 18. The polarization-to-population conversion efficiency for 1s (dashed line) and 2p excitons (solid line) is plotted as function of excitation density n. The shaded area represents the result obtained without the phonon scattering (after Ref. [30]).

In Fig. 18, we summarize a series of many resonant 1s-excitation studies by presenting the relative percentage of excitons in the different quantum states as function of the total generated carrier density n_{eh} which in turn monotonously increases with the excitation intensity. We note again, that for low carrier densities the optically induced polarization is mainly converted into incoherent 1s excitons. However, the generated exciton population drops well below 40% already at moderate densities above $10^5\,\mathrm{cm}^{-1}$ where the phase-space-filling factor $(1-f^{\mathrm{e}}-f^{\mathrm{h}})$ still has a peak around 0.5. For even higher densities, $\Delta n_{\nu}/n_{\mathrm{eh}}$ vanishes since the excitons become completely ionized. A test computation where we omit the phonon scattering contributions, Γ_{phon}, indicates that Coulomb scattering alone would only be able to generated up to 15% of excitons. This switch-off analysis confirms that polarization-to-population conversion at sufficiently low densities is dominated by phonon-induced scattering for resonant 1s excitations.

7.2. *Resonant* 2s*-excitation*

So far, we have seen that the resonant 1s excitation generates quasi-particle states where the average energy per particle equals the mean photon energy. Thus, it is logical to check to which degree one can control the quasi-particle states via excitation with different mean frequencies. As an example, we simulate a situation where the optical excitation is resonant with the 2s-exciton state. Otherwise, we assume the same pulse duration as for the 1s excitation. The spectral width of the Gaussian pulse is $\approx 0.5\,\mathrm{meV}$, such that one has essentially no energetic overlap with the 1s state. Since the optical absorption at the 2s energy is roughly 20 times smaller than at the 1s energy, we increased the pulse intensity to generate electron–hole densities comparable to those obtained for the resonant 1s excitation.

The resulting dynamics is presented in Fig. 19, where Fig. 19a shows the excitation pulse (scaled, dashed line), the generated optical polarization $|P|^2$ (scaled, shaded area), and the generated carrier density n_{eh} (solid line). Fig. 19b compares the evolution of $|P|^2$ (scaled, shaded area) with the total fractions for three different exciton populations: x_{1s} (dotted line), x_{2s} (dashed line), and x_{2p} (solid line). Fig. 19c shows the average energy per particle (solid line), together with the single-particle (dashed line) and correlated two-particle

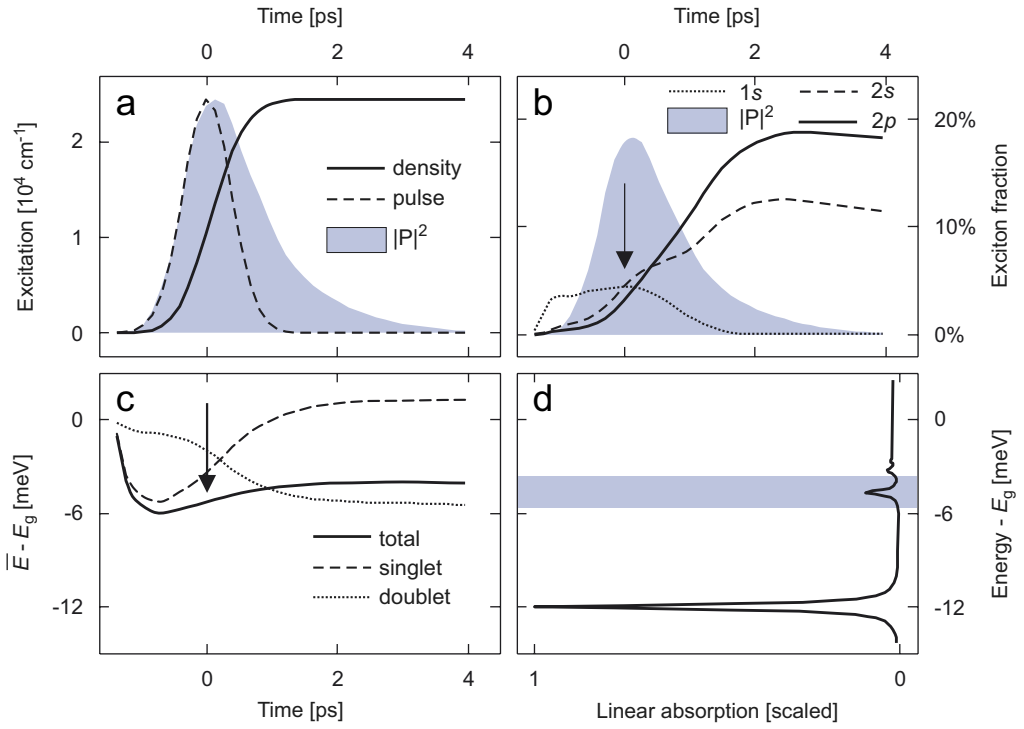

Fig. 19. Excitation at the 2s-exciton resonance. (a) The time-dependent excitation pulse (scaled, dashed line) is compared with the generated optical polarization $|P|^2$ (scaled, shaded area) and the excited carrier density (solid line). (b) The dynamical evolution of $|P|^2$ (scaled, shaded area) is compared with the total fraction of 1*s* (dotted line), 2*s* (dashed line), and 2*p* (solid line) exciton populations. (c) The average energy per particle (solid line) is presented together with the single-particle energy (dashed line) and the correlated two-particle energy (dotted line). (d) The linear absorption spectrum; the spectral extension of the pulse (full width half maximum) is indicated as shaded area. The arrows in panels (b) and (c) mark the temporal position of the pulse maximum.

(dotted line) energies determined using Eqs. (201)–(204). The middle of the shaded rectangle in Fig. 19d indicates the central energetic position of the Gaussian excitation pulse with respect to the linear absorption spectrum. The width of the rectangle symbolizes the half-width of the excitation.

We observe in Fig. 19a that for the chosen conditions the 2*s* excitation generates roughly the same amount of carriers than the 1*s* excitation in Fig. 14a, however, the polarization decays much faster. This phenomenon is directly related to the elevated excitation-induced dephasing for the excited 2*s*-like polarization in comparison with the 1*s*-like polarization in Fig. 14a. As the polarization decays, it transfers its energy to incoherent correlations.

In Fig. 19b we note the surprising result that *the 2s-polarization is converted into a mix of 2s and 2p populations*. This is clearly possible from the energy conservation point of view, however, the direct optical generation of *p*-type excitons is unexpected at first sight since it involves a symmetry change of the optically induced 2*s*-type polarization. As we discuss below, in Section 7.2.2, this symmetry breaking is directly related to the diffusive character of the Coulomb-induced scattering. The energy conservation aspects of this process can be

seen in Fig. 19c showing that the average energy per particle is very close to the energy of the excitation.

7.2.1. Terahertz gain

To better characterize the state that is generated by exciting at the 2*s*-exciton resonance, we assume the same excitation conditions as in Fig. 19 and present in Fig. 20 contour plots of $|\Delta N_{\lambda,v}(0)|$ for *s*-like states in the plane of exciton energies E_v and E_λ. At the early times, this correlation function extends over a broad energy range, similar to the case of the 1*s* excitation. However, with increasing time, $|\Delta N_{\lambda,v}(0)|$ develops its maximum at the 2*s* energy. Furthermore, we observe that the electron–hole quasi-particle state contains significant off-diagonal contributions and populations at elevated energies.

The right column of Fig. 20 contains the THz absorption spectra computed at the respective times. As an important feature, we note that the THz absorption becomes negative around the 2*p*–1*s* transition energy. In other words, the generated quasi-particle

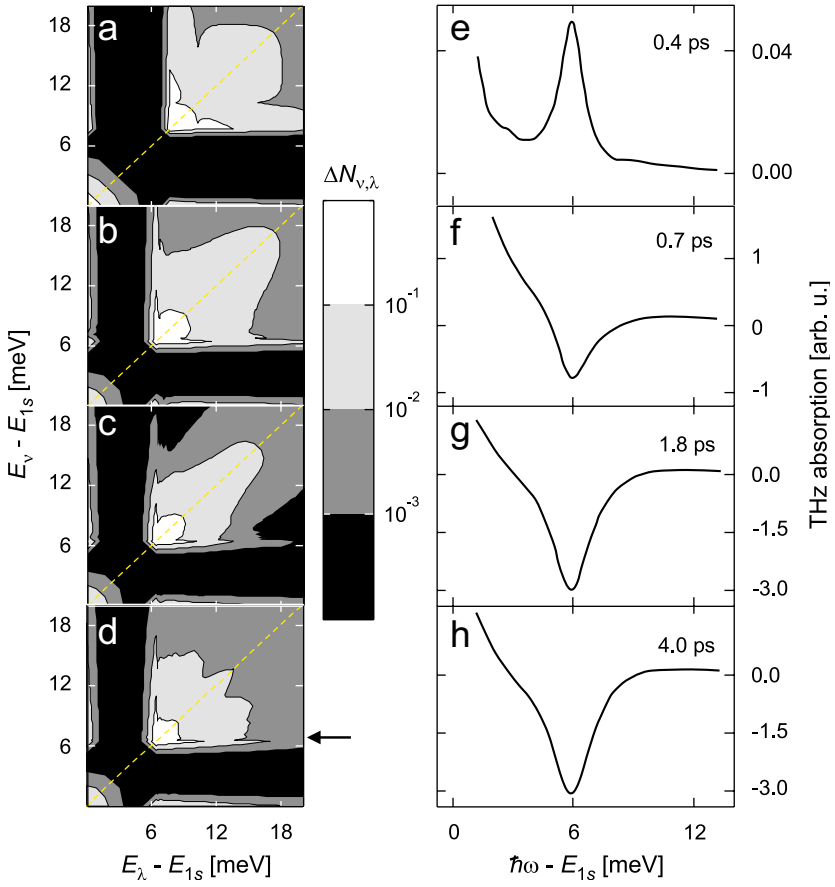

Fig. 20. Analysis of the many-body state generated by the resonant 2*s* excitation shown in Fig. 19. The left (right) column presents the contour plot of $|\Delta N_{\lambda,v}(0)|$ for *s*-like states (the THz absorption spectra). The dashed line at the diagonal indicates the location of true exciton populations and the arrow at frame (d) indicates the central energy of the excitation pulse.

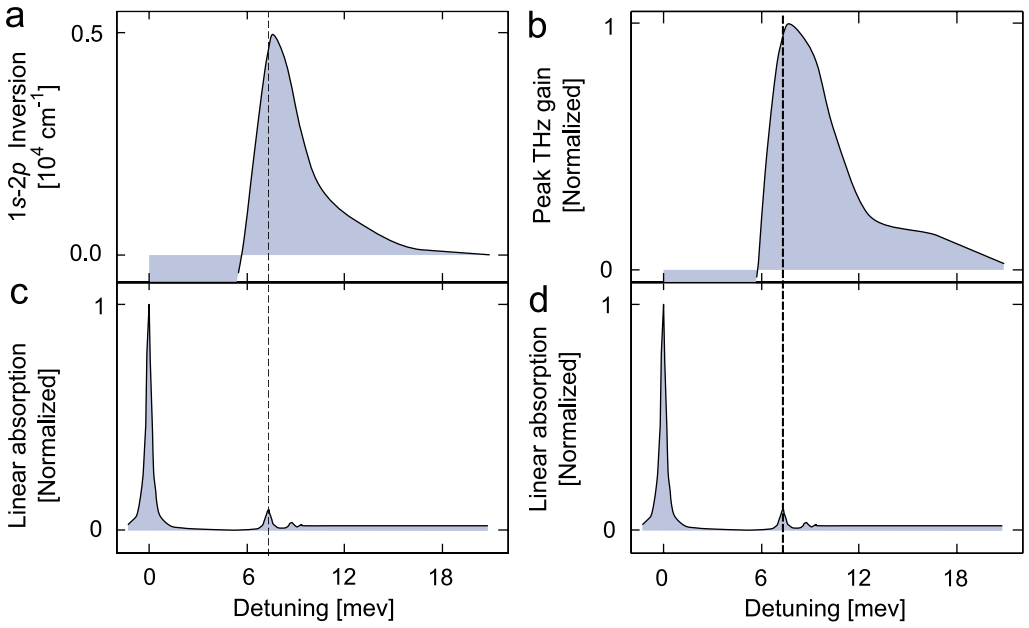

Fig. 21. Exciton 1*s*–2*p* population inversion and THz gain. The population inversion (a) and the THz peak gain (b) are shown as function of the excitation energy as it is tuned across the 2*s* resonance. The linear low-density optical absorption spectrum is plotted in frames (c) and (d) for comparison and the dashed line marks the peak of the 2*s*-exciton resonance.

state exhibits THz gain as a consequence of the population inversion between the 1*s* and 2*p* states [30]. Very similar THz gain features have been observed in recent experiments [122] performed with indirect semiconductors. This gain opens up the possibility to generate THz lasers using the semiconductor as the active THz-gain medium. We notice in Fig. 20 that the THz spectrum is positive for small frequencies close to $\omega = 0$, except for the early times that are dominated by dynamical transients. These positive contributions stem from the excitation of ionized populations together with the electron–hole plasma.

To check the detuning dependence of the predicted THz gain, we analyze the level of population inversion $\Delta n_{\mathrm{inv}} = \Delta n_{2p} - \Delta n_{1s}$ as function of the excitation frequency around the 2*s* resonance. The result is plotted in Fig. 21 together with the THz peak gain. For the assumed pumping strengths, the population inversion has a maximum around $5 \times 10^3\,\mathrm{cm}^{-1}$ for resonant 2*s* excitation. This level can be increased to some extent by elevating the intensity of the excitation. Ultimately, however, the maximum 2*p*-excitation level is restricted by the eventual ionization of the 2*s* and 2*p* exciton states. From an application point of view, it is encouraging to note from Fig. 21 that population inversion and THz gain are obtained for a relatively large range of frequencies which extends to detunings well above the 2*s* state.

Clearly, the excitation induced ionization of the 2*s* and 2*p* states sets limits to the amount of obtainable THz gain and 1*s*–2*p* population inversion. The dependency of these effects on the excitation intensity is investigated in Fig. 22. Here, we have kept the center frequency at the 2*s* resonance and increased the pump intensity. We have then determined the corresponding concentrations for 1*s* excitons (dashed line), 2*s* excitons (shaded area),

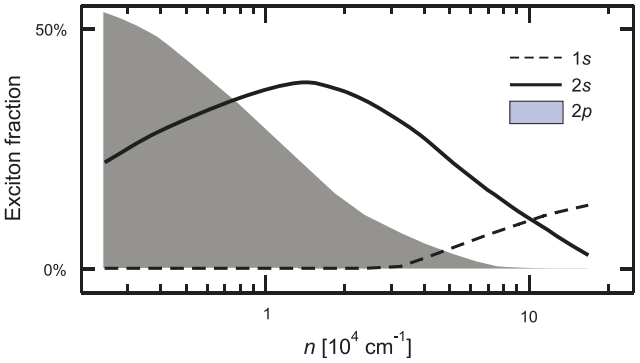

Fig. 22. Optically generated population of 1*s* (dashed line), 2*p* (solid line), and 2*s* (shaded area) excitons as function of excitation density *n* for pumping at the 2*s* resonance. According to Ref. [30].

and 2*p* excitons (solid line). We observe that THz gain is reached for densities up to approximately $7 \times 10^4\,\mathrm{cm}^{-1}$. Due to their weaker binding and enhanced excitation induced dephasing, the 2*s* and 2*p* excitons are ionized for lower densities than the 1*s* excitons.

7.2.2. Formation of 2p-excitons

The question remains why a substantial amount of population in the 2*p*-exciton state is generated after pumping at the 2*s* resonance. Comparing calculations with and without the inclusion of phonon scattering, we can conclude that the 2*p*-exciton generation is dominated by the Coulomb scattering [30]. To understand how the Coulomb interaction induces such symmetry changes in the polarization-to-population conversion, we take a closer look at the scattering (Γ) and the conversion (G) mechanisms in Eqs. (205) and (216)–(218), which both stem from the same basic Fermionic correlation $c_{v,\lambda,\lambda,c} = \Delta\langle a_v^\dagger a_\lambda^\dagger a_\lambda a_c\rangle$. To get a feeling for the principle microscopic mechanism behind the conversion, we consider a few analytic approximations that simplify $c_{v,\lambda,\lambda,c}$ but still preserve the general character of the excitation-induced dephasing [46,30].

The simplest possible approximation,

$$\left[V_{\mathbf{q}_\parallel}\sum_{\mathbf{n}_\parallel,\lambda} c_{v,\lambda,\lambda,c}^{\mathbf{q}_\parallel,\mathbf{n}_\parallel,\mathbf{k}_\parallel}\right]_{\mathrm{app}} = \mathrm{i}\frac{\gamma}{2}P_{\mathbf{k}_\parallel}\delta_{\mathbf{q}_\parallel,0}, \tag{272}$$

introduces a phenomenological dephasing to the polarization Eq. (205), compare Section 6.2. Inserting this into Eqs. (205) and (216)–(217), we arrive at a decay model

$$\mathrm{i}\Gamma_{\mathbf{k}_\parallel}^{\mathrm{app}} = \sum_{\mathbf{q}_\parallel}\left[V_{\mathbf{q}_\parallel}\sum_{\mathbf{n}_\parallel,\lambda} c_{v,\lambda,\lambda,c}^{\mathbf{q}_\parallel,\mathbf{n}_\parallel,\mathbf{k}_\parallel}\right]_{\mathrm{app}} - [c\leftrightarrow v]^\star = \mathrm{i}\gamma P_{\mathbf{k}_\parallel}, \tag{273}$$

$$\mathrm{i}G_{\mathrm{app}}^{\mathbf{q}_\parallel,\mathbf{k}'_\parallel,\mathbf{k}_\parallel} = 2P_{\mathbf{k}_\parallel}^\star \Gamma P_{\mathbf{k}'_\parallel}\delta_{\mathbf{q}_\parallel,0}. \tag{274}$$

These approximations conserve the property that $[P_{\mathbf{k}_\parallel}^\star P_{\mathbf{k}'_\parallel} + \sum_{\mathbf{q}_\parallel} c_X^{\mathbf{q}_\parallel,\mathbf{k}'_\parallel,\mathbf{k}_\parallel}]$ is a constant of motion with respect to the scattering. However, this model only allows for conversion of *s*-type polarization to *s*-like exciton populations, in contrast to our microscopic results.

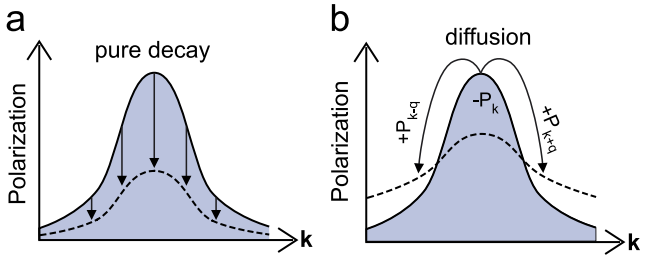

Fig. 23. Schematic presentation of two polarization-to-population conversion schemes: (a) via the dephasing model described by Eqs. (273)–(274) and (b) via the diffusive model described by Eqs. (278)–(279).

The corresponding polarization-to-population conversion is schematically illustrated in Fig. 23a.

For a better approximation, we look at the process of excitation-induced dephasing. We notice that Coulomb-induced dephasing is actually a diffusive redistribution of the microscopic **k**-state polarizations since it satisfies strict conservation laws

$$\sum_{\mathbf{k}_\parallel} \Gamma_{\mathbf{k}_\parallel} = 0, \tag{275}$$

$$\sum_{\mathbf{k}_\parallel,\mathbf{k}'_\parallel,\mathbf{q}_\parallel} G^{\mathbf{q}_\parallel,\mathbf{k}'_\parallel,\mathbf{k}_\parallel} = 0. \tag{276}$$

Clearly, our first approximation violates these conditions. Therefore, we now introduce a model which has the same structural form as the second-Born solution of $c_{v,\lambda,\lambda,c}$ [52]. For this purpose, we approximate

$$\left[V_{\mathbf{q}_\parallel} \sum_{\mathbf{n}_\parallel,\lambda} c^{\mathbf{q}_\parallel,\mathbf{n}_\parallel,\mathbf{k}_\parallel}_{v,\lambda,\lambda,c} \right]_{\mathrm{red}} = \mathrm{i} U_{\mathbf{q}_\parallel} (P_{\mathbf{k}_\parallel} - P_{\mathbf{k}_\parallel - \mathbf{q}_\parallel})/2, \tag{277}$$

where $U_{\mathbf{q}_\parallel}$ is chosen to be a real-valued, non-linear functional of f and P. By inserting this into Eqs. (205) and (216)–(217), we find a diffusive model,

$$\begin{aligned} \mathrm{i}\Gamma^{\mathrm{red}}_{\mathbf{k}_\parallel} &= \sum_{\mathbf{q}_\parallel} \left[V_{\mathbf{q}_\parallel} \sum_{\mathbf{n}_\parallel,\lambda} c^{\mathbf{q}_\parallel,\mathbf{n}_\parallel,\mathbf{k}_\parallel}_{v,\lambda,\lambda,c} \right]_{\mathrm{red}} - [c \leftrightarrow v]^\star \\ &= \mathrm{i} \sum_{\mathbf{q}_\parallel} U_{\mathbf{q}_\parallel} (P_{\mathbf{k}_\parallel - \mathbf{q}_\parallel} - P_{\mathbf{q}_\parallel}), \end{aligned} \tag{278}$$

$$\begin{aligned} \mathrm{i}G^{\mathbf{q}_\parallel,\mathbf{k}'_\parallel,\mathbf{k}_\parallel}_{\mathrm{red}} &= (P^\star_{\mathbf{k}_\parallel} - P^\star_{\mathbf{k}_\parallel - \mathbf{q}_\parallel}) \left[V_{\mathbf{q}_\parallel} \sum_{\mathbf{n}_\parallel,\lambda} c^{-\mathbf{q}_\parallel,\mathbf{n}_\parallel,\mathbf{k}'_\parallel}_{v,\lambda,\lambda,c} \right]_{\mathrm{red}} \\ &\quad - (P_{\mathbf{k}'_\parallel + \mathbf{q}_\parallel} - P_{\mathbf{k}'_\parallel}) \left[V_{\mathbf{q}_\parallel} \sum_{\mathbf{n}_\parallel,\lambda} c^{\mathbf{q}_\parallel,\mathbf{n}_\parallel,\mathbf{k}_\parallel}_{v,\lambda,\lambda,c} \right]^\star_{\mathrm{red}} \\ &= \mathrm{i}(P^\star_{\mathbf{k}_\parallel} - P^\star_{\mathbf{k}_\parallel - \mathbf{q}_\parallel}) U_{\mathbf{q}_\parallel} (P_{\mathbf{k}'_\parallel + \mathbf{q}_\parallel} - P_{\mathbf{k}'_\parallel}), \end{aligned} \tag{279}$$

which obeys the conservation laws (275)–(276). The corresponding polarization-to-population conversion is schematically illustrated in Fig. 23b. We observe that $\Gamma^{\rm red}_{\mathbf{k}_\parallel}$ removes polarization from the state $P_{\mathbf{k}_\parallel}$ and redistributes it to $P_{\mathbf{k}_\parallel-\mathbf{q}_\parallel}$. A slightly more complicated redistribution is obtained for the populations.

The relatively simple form of $G_{\rm red}$, allows us to transform it into the exciton basis. We find that the conversion rate to the exciton state v is

$$G^{v,v}_{\rm red}(\mathbf{q}_\parallel)=\sum_{\mathbf{k}_\parallel,\mathbf{k}'_\parallel}\phi^{\rm L}_v(\mathbf{k}_\parallel)\phi^{\rm L}_v(\mathbf{k}'_\parallel)G^{\mathbf{q}_\parallel,\mathbf{k}'_\parallel-\mathbf{q}_{\rm h},\mathbf{k}_\parallel+\mathbf{q}_{\rm e}}_{\rm red}=|M_v(\mathbf{q}_\parallel)|^2U_{\mathbf{q}}, \tag{280}$$

$$M_v(\mathbf{q}_\parallel)\equiv\sum_{\mathbf{k}_\parallel}\phi^{\rm L}_v(\mathbf{k}_\parallel)\left[P_{\mathbf{k}_\parallel+\mathbf{q}_{\rm e}}-P_{\mathbf{k}_\parallel-\mathbf{q}_{\rm h}}\right], \tag{281}$$

indicating that Coulomb scattering leads to the generation of excitons with finite momenta. However, no population in the $\mathbf{q}_\parallel=0$ state is produced. For low to moderate $2s$-excitation, we may use the approximation $P_{\mathbf{k}_\parallel}\propto\phi^{\rm R}_{2s}(\mathbf{k}_\parallel)$. With the help of the symmetries $\phi^{\rm R}_{2s}(-\mathbf{k}_\parallel)=\phi^{\rm R}_{2s}(\mathbf{k}_\parallel)$ and $\phi^{\rm R}_{2p}(-\mathbf{k}_\parallel)=-\phi^{\rm R}_{2p}(\mathbf{k}_\parallel)$, we find that $2s$- and $2p$-generation rates follow from

$$M_{2s}(\mathbf{q}_\parallel)\propto\sum_{\mathbf{k}_\parallel}\phi^{\rm L}_{2p}(\mathbf{k}_\parallel)[\phi^{\rm R}_{2s}(\mathbf{k}_\parallel+\mathbf{q}_{\rm e})-\phi^{\rm R}_{2s}(\mathbf{k}_\parallel+\mathbf{q}_{\rm h})], \tag{282}$$

$$M_{2p}(\mathbf{q}_\parallel)\propto\sum_{\mathbf{k}_\parallel}\phi^{\rm L}_{2p}(\mathbf{k}_\parallel)[\phi^{\rm R}_{2s}(\mathbf{k}_\parallel+\mathbf{q}_{\rm e})+\phi^{\rm R}_{2s}(\mathbf{k}_\parallel+\mathbf{q}_{\rm h})] \tag{283}$$

which both vanish for $\mathbf{q}_\parallel=0$ but become clearly non-zero for $\mathbf{q}_\parallel\neq0$.

For pumping at the $2s$-resonance, the energy conservation aspects of $U_{\mathbf{q}}$ are practically the same for $2s$ and $2p$ since these states are nearly degenerate. As a result, the overlap of the wavefunctions with shifted arguments in $M_v(\mathbf{q}_\parallel)$ determines the conversion rate such that $|M_v(\mathbf{q}_\parallel)|^2$ can be used to estimate the ratio of generated $2s$ and $2p$ populations. The $\mathbf{q}_\parallel$-dependency of $|M_{2s}(\mathbf{q}_\parallel)|^2$ (dashed line) and $|M_{2p}(\mathbf{q}_\parallel)|^2$ (solid line) is shown in Fig. 24a (b) for the QW (QWI), where we used the low-density exciton wavefunctions in the evaluation. The computed $2p$-distribution is plotted in Fig. 24c for the QWI after the polarization-to-population conversion is complete. We observe that the approximative analysis produces qualitatively similar distributions as the full computation. In addition, the QW and QWI estimates are very close to each other. If we assume that the $\mathbf{q}_\parallel$-dependence of $U_{\mathbf{q}_\parallel}$ can be ignored, $\sum_{\mathbf{q}_\parallel}|M_{2s}(\mathbf{q}_\parallel)|^2$ and $\sum_{\mathbf{q}_\parallel}|M_{2p}(\mathbf{q}_\parallel)|^2$ describes the relative conversion into $2s$ and $2p$ excitons, respectively. The discussed approximative analysis of the conversion produces a ratio of 1.36 of $2s$ over $2p$ population for the QWI, which is close to the fully numerical result. Repeating the same calculations for the QW, we get a ratio 0.99 showing that the generation of p-like states is strong and qualitatively similar for QWs and QWIs.

Since the Coulomb interaction conserves the angular momentum, one may ask how this conservation law is fulfilled when a $2s$-polarization is converted into $2p$-excitons. This problem is easily answered by noting that we have a many-body system where only the total angular momentum and not that of any individual electron–hole pair is conserved. As a simplified example, we can consider a many-body state consisting of two perfect $2p$ excitons. Thus, one exciton may be in a quantum state $|\phi_{n,m}\rangle$ with the usual quantum

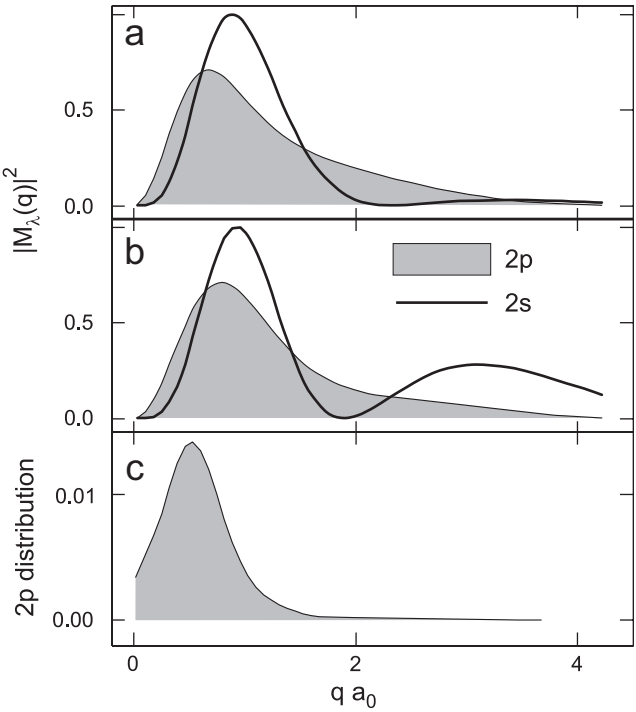

Fig. 24. Analytically computed $|M_{2s}(\mathbf{q}_\parallel)|^2$ (solid line) and $|M_{2p}(\mathbf{q}_\parallel)|^2$ (shaded area) for (a) a QW and (b) a QWI. (c) The numerically computed $2p$ distribution at the final time moment of Fig. 19 (after Ref. [46]).

numbers $n = 1$, $m = \pm 1$ for $2p$-excitons. Using the Clebsch–Gordan coefficients for a two-dimensional system, we may construct a two-exciton state with total ($J = 0$, $J_z = 0$)

$$|\Psi_{0,0}\rangle = \frac{1}{\sqrt{2}}[|\phi_{1,m=+1}\rangle_1|\phi_{1,m=-1}\rangle_2 + |\phi_{1,m=-1}\rangle_1|\phi_{1,m=+1}\rangle_2], \tag{284}$$

showing that the many-body system can contain individual p excitons even though the total angular momentum remains in an s-like state.

7.3. Nonresonant excitation

So far, our analysis has shown that the increase of the excitation frequency from the $1s$- to the $2s$-resonance leads to the generation of correlated electron–hole-pairs which are less strongly bound, i.e. where the attractive interband Coulomb interaction plays a less dominating role. If one continues to elevate the excitation frequency further, the light eventually becomes energetically resonant with the ionized exciton states. Thus, we may anticipate that in this situation the optically induced polarization leads to the creation of incoherent many-body states where the mutual motion of carriers is completely unbound.

To keep the analysis as simple as possible, we consider continuum-excitation conditions where the difference between the $1s$-exciton state and the excitation energy is lower than the longitudinal-optical (LO) phonon energy. Consequently, LO-phonons do not significantly contribute to the polarization-to-population conversion and the LO-phonon

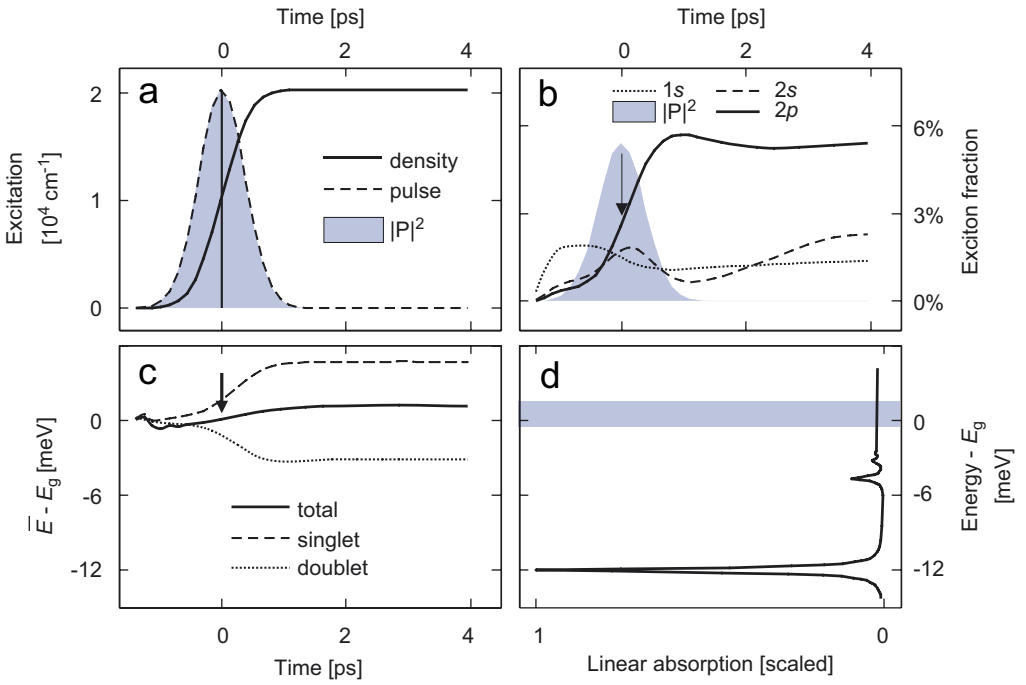

Fig. 25. Non-resonant excitation 12 meV above the 1*s* resonance. (a) The time-dependent excitation pulse (scaled, dashed line) is shown together with the generated optical polarization $|P|^2$ (scaled, shaded area) and the excited carrier density (solid line). (b) The dynamical evolution of $|P|^2$ (scaled, shaded area) is compared with the total fraction of 1*s* (dotted line), 2*s* (dashed line), and 2*p* (solid line) exciton populations. (c) The average energy per particle (solid line) is presented together with the single-particle energy (dashed line) and the correlated two-particle energy (dotted line). (d) The linear absorption spectrum; the spectral extension of the pulse (full width half maximum) is indicated as shaded area. The arrows in panels (b) and (c) mark the temporal position of the pulse maximum.

assisted formation of 1*s*-excitons is negligible. Consequently, we may limit our investigations to effects solely caused by the Coulomb and the acoustic-phonon induced scatterings.

Since in GaAs type systems the LO-phonon energy is roughly 36.5 meV, we start our analysis assuming an excitation frequency of 12 meV above the 1*s*-resonance. This energy is still relatively close to the unrenormalized band. To compensate for the fact that the continuum absorption is significantly weaker than the excitonic absorption, we have to use a correspondingly larger intensity to generate a density comparable to the case of the 1*s* excitation in Fig. 14.

The resulting dynamics is shown in Fig. 25. Here, we plot in Fig. 25a, the excitation pulse (scaled, dashed line), the induced optical polarization $|P|^2$ (scaled, shaded area), and the generated carrier density n_{eh} (solid line). Fig. 25b, compares the dynamical evolution of $|P|^2$ (scaled, shaded area) to that of the total fractions of bound 1*s* (dotted line), 2*s* (dashed line), and 2*p* (solid line) exciton populations. Fig. 25c presents the average energy per particle (solid line) and the corresponding single-particle (dotted line) and correlated two-particle (dashed line) energies which are evaluated using Eqs. (201)–(204). The center of the

shaded rectangle in Fig. 25d indicates the central energetic position of the Gaussian excitation pulse and its width corresponds to the half-maximum contour lines.

In Fig. 25a, we see that $|P|^2$ has virtually the same temporal dynamics as the exciting pulse, which shows that the induced optical polarization more or less follows the pulse adiabatically for the non-resonant excitation conditions used. As long as the polarization exists, it can be converted into correlated incoherent populations. The resulting exciton fractions are plotted in Fig. 25b indicating that even though the excitation frequency is only slightly above the unrenormalized band gap, we only generate approximately 1%, 2%, and 5% of 1*s*, 2*s*, and 2*p* excitons, respectively. For excitation higher into the continuum, these exciton fractions continue to decrease. Thus, we confirm the expectation that non-resonant excitation generates incoherent quasi-particle states with a significantly reduced amount of excitons. In fact, the degree of bound-state populations can be decreased even further for all detunings simply by increasing the excitation intensity.

We can also conclude from Fig. 25c that the generated incoherent quasi-particle state has an average energy per particle that matches the excitation. Furthermore, part of the system energy is stored in the two-particle correlations (dotted line). However, the amount of correlated energy is clearly smaller than for the cases of 1*s*- and 2*s*-excitations studied previously. In addition, the correlated energy decreases as the excitation frequency is increased. Thus, we see that under non-resonant excitation conditions we obtain an electron–hole plasma, i.e. a quasi-particle state with a reduced amount of two-particle correlations.

To quantify how the generation of bound states depends on the excitation frequency, we evaluate the total fraction,

$$x_{\text{sum}} \equiv x_{1s} + x_{2s} + x_{2p}, \tag{285}$$

of 1*s*, 2*s*, and 2*p* excitons for pumping with different detunings. Otherwise, we assume the same material and excitation parameters as in Figs. 14 and 19–25. The result is presented in Fig. 26 for pumping frequencies ranging from resonant 1*s*-excitation to non-resonant excitation 20 meV above the 1*s* state. As a general trend, we notice that the resonant 1*s* excitation produces large fractions of bound exciton populations and an exponential decrease of the total number of excitons, x_{sum}, with increasing detuning.

It is also interesting to analyze the electron–hole quasi-particle state generated via continuum pumping by looking at its exciton basis representation $\Delta N_{\lambda,v}$. In the left column of Fig. 27 we present a contour plot of $|\Delta N_{\lambda,v}(0)|$ for the *s*-like states. At the early times, we notice that $|\Delta N_{\lambda,v}(0)|$ initially spreads over many exciton states before it then narrows somewhat with a peak centered around the ionized exciton state that is resonant with the central energy of the exciting field. However, the correlations extend very far away from the diagonal, $E_v = E_\lambda$, at which we find the true exciton populations.

For all the correlation-function plots, the corresponding THz absorption spectra are presented on the RHS of Fig. 27. We notice a qualitatively different THz response compared to that obtained under resonant 1*s*- and 2*s*-excitation, Figs. 15 and 20, respectively. For the continuum excitation, the THz absorption gradually develops a strong positive peak around $\omega = 0$ and a decay for positive frequencies roughly corresponding to the Drude response, which is characteristic for the plasma nature of the probed electron–hole-pair state. We also observe a small THz gain feature at the 1*s*–2*p* transition. This gain is a consequence of the small population inversion between the 2*p* and 1*s* states (see also Fig. 25) generated under the positively detuned non-resonant excitation.

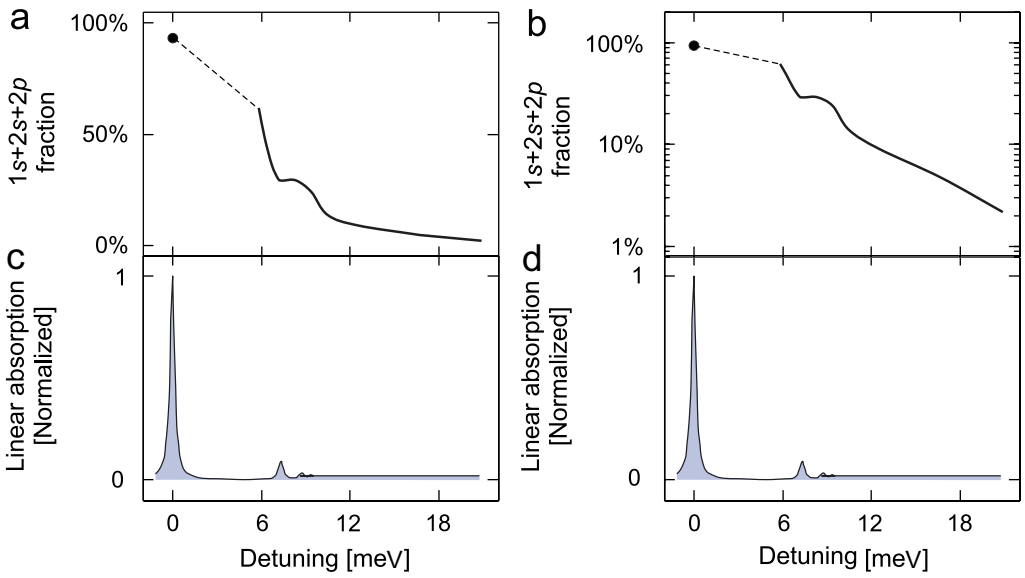

Fig. 26. The population of different bound exciton states is shown as function of excitation frequency. (a) The total fraction of 1*s*, 2*p*, and 2*s* excitons is presented for different pump pulse detunings. The excitation intensity is kept constant except for the isolated 1*s* excitation (filled circle) obtained from Fig. 14. (b) The same data as in (a) are shown on a logarithmic scale. The linear low-density optical absorption spectrum is plotted in frames (c) and (d).

Repeating the non-resonant excitation studies for higher frequencies or increased intensities, most of the interesting features disappear and only the Drude-like behavior remains. To see these effects, we compare the THz absorption spectra for the weak excitation case at 12 meV above the 1*s* state (Fig. 28a), with the result after weak excitation centered at 17 meV (21 meV) above the 1*s* state, Fig. 28c (d). We also show in Fig. 28b the spectra computed for a situation with an excitation configuration where we assume an eight times higher pump intensity but otherwise the same parameters as in Fig. 28a. All the THz spectra are evaluated after the initial coherences have vanished. We clearly note the predominantly Drude-like response in Figs. 28b and d and the additional small gain at the 1*s*–2*p* transition in Figs. 28a and c.

8. Exciton formation

In the previous section, we have seen that non-resonant optical excitation energetically well below the LO-phonon frequency produces an incoherent quasi-particle state that has a vanishingly small level of electron–hole correlations. In other words, we have basically no bound excitons. An interesting follow-up question is then if and how bound excitons are formed at later times after such a non-resonant excitation.

Different aspects of exciton formation have been investigated with several phenomenological models [116,123,124]. In those studies, excitons are often treated as bosonic entities and exciton formation processes are discussed via rate equations and perturbative scattering contributions to produce excitons out of the electron–hole system. Such an

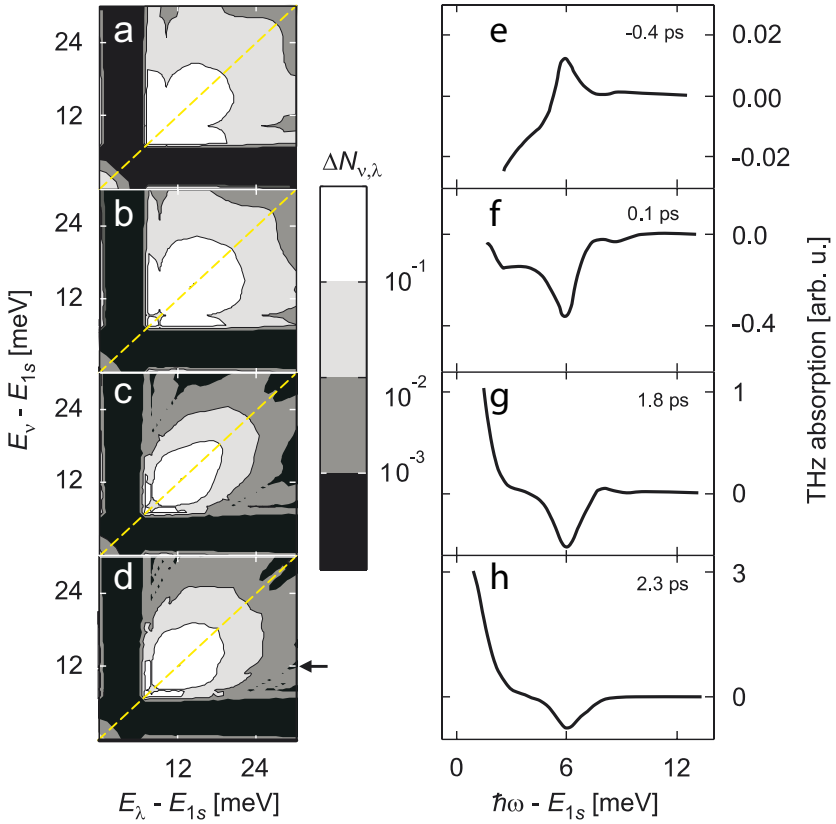

Fig. 27. (a)–(d) The correlation function $|\Delta N_{\nu,\lambda}(0)|$ for *s*-like states and the corresponding THz response (e)–(h) is shown at different times after a continuum excitation. The central frequency of the pump pulse is indicated by the arrow on the RHS of frame (d).

analysis may be helpful to understand some aspects of the exciton formation such as why optical phonons become less important for low temperatures and excitations below the LO-phonon frequency. However, most of these theories do not account for the genuine Fermionic nature of the electron–hole pairs and/or do not systematically treat the different microscopic processes on an equivalent level.

In this section, we study exciton formation fully microscopically by applying the full singlet–doublet approach including the triplets at the scattering level. Since electrons, holes, and excitons are treated at the same fundamentally correct level, we are able to identify the relevant sequence of microscopic processes influencing the exciton formation for conditions where optical phonons are not relevant.

8.1. Numerical studies

Our non-resonant excitation studies show that the generated incoherent quasi-particle state has an average energy per particle that is well above the electron–hole binding energy. Hence, in order to form bound exciton populations this average energy has to be reduced significantly. The best candidate for the necessary transfer out of the carrier system is the

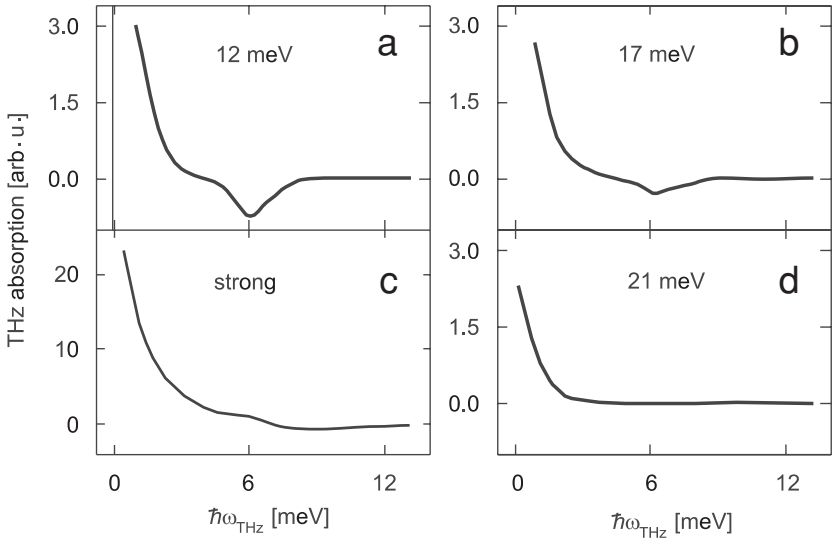

Fig. 28. The induced terahertz absorption after non-resonant excitation is plotted for: (a) weak excitation 12 meV above 1*s* resonance, (b) weak excitation 17 meV above 1*s* resonance, (c) strong excitation 12 meV above 1*s* resonance, and (d) weak excitation 21 meV above 1*s* resonance.

coupling to the reservoir of phonon excitations. Possible mechanisms are LO- and acoustic-phonon-assisted exciton-formation processes. In GaAs type materials, the coupling to LO-phonons is relatively strong, however, for detunings well below the energy of exciton plus LO-phonon, only acoustic phonons are relevant. Since the coupling of the electron–hole excitations to these acoustic phonons is relatively weak, this relaxation channel usually leads to a slow exciton-formation process which is efficient only when the correlated electrons and holes are relatively close to each other.

To study details of this acoustic phonon mediated exciton formation, we perform two independent series of computations. The first one is the full analysis where a QWI is non-resonantly excited above the 1*s* resonance. The obtained results are then compared to those of a calculation where a postulated uncorrelated electron–hole plasma at a given density and temperature is used as an initial state. For this postulated state, we then evolve the full incoherent singlet–doublet dynamics including triplet scattering terms. For discussional simplicity, we call the first analysis the ''full computation'' and the second investigation the ''plasma computation'', even though also this computation correctly includes formation of all correlations via acoustic-phonon and Coulomb-induced effects.

In the full computation, we assume a 0.9 ps long excitation pulse centered 15 meV above the 1*s* resonance. For the plasma calculation, we choose the initial state such that the Fermi–Dirac distributions have matching temperature and density as those generated by the optical excitation. In both computations, we assume 10 K lattice temperature.

Fig. 29 presents the evolution of the 1*s*-exciton fraction as function of time after the excitation, both for the full analysis (solid line) and the plasma computation (shaded area). We see that the full computation directly generates only a very insignificant amount of 1*s* excitons. After some small initial transients related to the rearrangement of the correlated electron–hole configuration, at about 50 ps the 1*s*-exciton fraction starts to grow steadily.

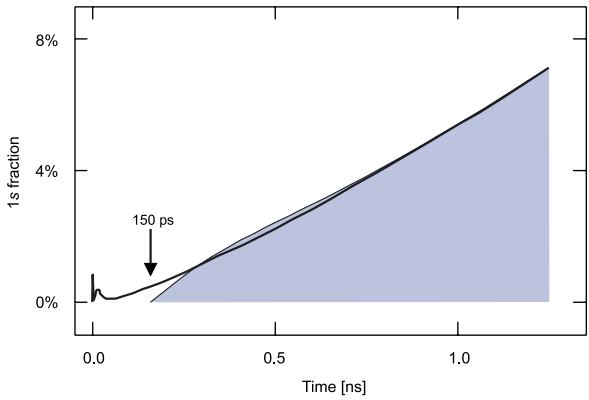

Fig. 29. The percentage of electron–hole pairs bound into 1*s* excitons is plotted as function of time. The result obtained for the full calculation assuming non-resonant excitation is shown as solid line. The shaded area indicates the exciton percentage produced from an incoherently seeded uncorrelated plasma state.

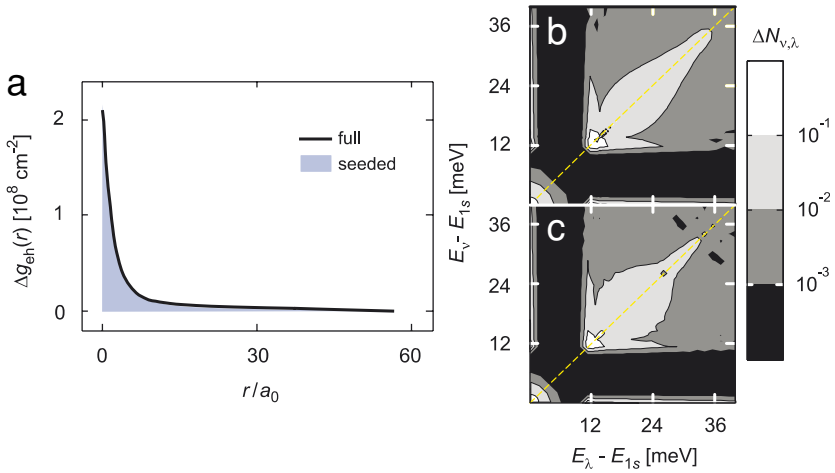

Fig. 30. Electron–hole quasi-particle dynamics: full vs. plasma computation. (a) The electron–hole pair-correlation function is shown for the full (solid line) and the plasma computation (shaded area). These are evaluated at 1.2 ns for the excitations used in Fig. 29. The corresponding $|\Delta N_{\nu,\lambda}|$ states are shown for (b) the full and (c) the plasma computation.

To omit the initial transients, the plasma computation is chosen to match the conditions at the time of 150 ps after the excitation used in the full computation. This time serves as the initial moment of the plasma computation. We see in Fig. 29 that the plasma computation quickly evolves toward the steady exciton-formation curve of the full computation. The generated 1*s*-fraction becomes nearly identical for both cases after about 300 ps. Thus, we conclude that the uncorrelated electron–hole state determines how the subsequent exciton formation proceeds while the correlation effects and the ionized exciton populations are less important.

To confirm this important result in another way, Fig. 30a presents the pair-correlation function Δg_{eh} 1.2 ns after the excitation for the full (solid line) and the plasma calculations

(shaded area). The corresponding exciton correlations $|\Delta N_{\nu,\lambda}(0)|$ are presented in Figs. 30b and c. We clearly see that both results are very similar. Hence, as long as we are only interested in the quasi-stationary results, we may limit our investigations to the plasma calculation. This approximation considerably simplifies the numerical efforts but still contains the relevant microscopic contributions.

8.2. Microscopic analysis

For the microscopic analysis of exciton formation out of an electron–hole plasma, we need to systematically include phonon-assisted three-particle scattering processes. According to Eq. (109), these phonon-induced three-particle correlations result from

$$\begin{aligned} i\hbar\frac{\partial}{\partial t}c_X^{\mathbf{q}_\parallel,\mathbf{k}'_\parallel,\mathbf{k}_\parallel}\Big|_{\text{phon}} = &-\sum_{\mathbf{l}_\parallel}\big(\Delta\langle Q^c_{-\mathbf{l}_\parallel}a^\dagger_{c,\mathbf{k}_\parallel-\mathbf{l}_\parallel}a^\dagger_{v,\mathbf{k}'_\parallel}a_{c,\mathbf{k}'_\parallel+\mathbf{q}_\parallel}a_{v,\mathbf{k}_\parallel-\mathbf{q}_\parallel}\rangle \\ &+\Delta\langle Q^v_{\mathbf{l}_\parallel}a^\dagger_{c,\mathbf{k}_\parallel}a^\dagger_{v,\mathbf{k}'_\parallel+\mathbf{l}_\parallel}a_{c,\mathbf{k}'_\parallel+\mathbf{q}_\parallel}a_{v,\mathbf{k}_\parallel-\mathbf{q}_\parallel}\rangle \\ &-\Delta\langle Q^c_{-\mathbf{l}_\parallel}a^\dagger_{c,\mathbf{k}_\parallel}a^\dagger_{v,\mathbf{k}'_\parallel}a_{c,\mathbf{k}'_\parallel+\mathbf{q}_\parallel+\mathbf{l}_\parallel}a_{v,\mathbf{k}_\parallel-\mathbf{q}_\parallel}\rangle \\ &-\Delta\langle Q^v_{\mathbf{l}_\parallel}a^\dagger_{c,\mathbf{k}_\parallel}a^\dagger_{v,\mathbf{k}'_\parallel}a_{c,\mathbf{k}'_\parallel+\mathbf{q}_\parallel}a_{v,\mathbf{k}_\parallel-\mathbf{q}_\parallel-\mathbf{l}_\parallel}\rangle\big). \end{aligned} \tag{286}$$

The explicit form of the phonon-assisted terms, $\Delta\langle Qa^\dagger a^\dagger aa\rangle$ including single- and two-particle scattering, are derived in Refs. [18,29]. They describe phonon-assisted carrier scattering and two-particle correlation contributions, including excitons. In the exciton-formation process, the phonons remove the energy from the correlated electron–hole plasma such that the scattering can generate bound exciton populations.

Based on the results discussed so far, we may anticipate that electrons and holes must first come close to each other in real space, before they can form bound excitons. Thus, it is natural to follow how the electron–hole-pair correlation function evolves in time as the exciton formation proceeds. Fig. 31 shows a computed sequence of $\Delta g_{\text{eh}}(r)$ as a function of electron–hole distance r for a low carrier density of $n^{\text{e/h}} = 2\times10^4\,\text{cm}^{-1}$. Already at early

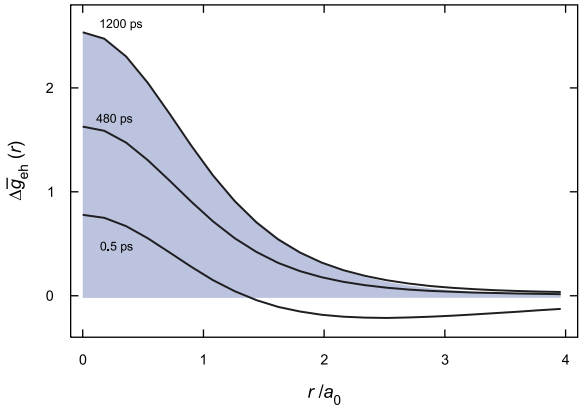

Fig. 31. Pair-correlation function $\Delta g_{\text{eh}}(r)$ for the lattice temperature of $T = 10\,\text{K}$ and carrier density $n = 2\times10^4\,\text{cm}^{-1}$ at different times. The absolute square of the 1s-exciton wavefunction is shown as shaded area (from Ref. [29]).

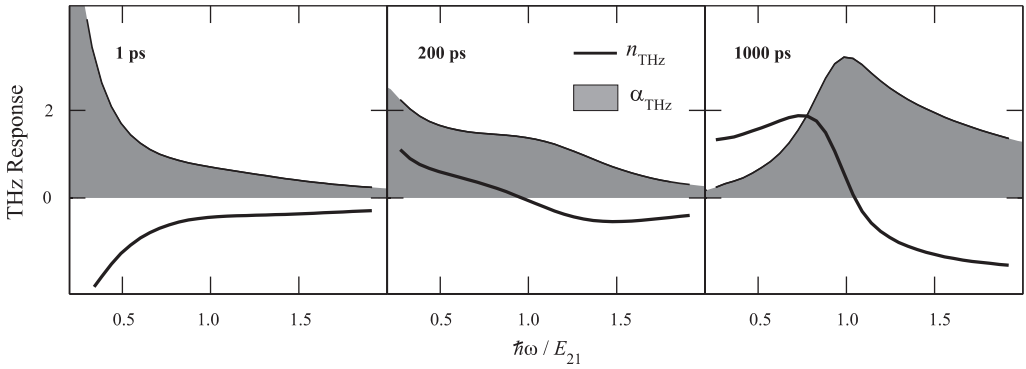

Fig. 32. Computed THz absorption (shaded area) and refractive index changes (solid line) for different THz probe delays after non-resonant excitation. Here, $E_{2p-1s} = 5$ is the energy difference between $1s$ and $2p$ states. From Ref. [30].

times around $t = 0.5$ ps, we see that the probability of finding electrons and holes close to each other increases as a consequence of the Coulomb attraction. We also notice that the correlated Δg_{eh} at early times has clearly negative parts indicating a transient depletion caused by the overall reduction of the electron–hole separation. This form corresponds to the generation of a correlated electron–hole plasma as seen in Section 6.5. At later times, $\Delta g_{eh}(r)$ becomes entirely positive and grows linearly in magnitude. In particular, $\Delta g_{eh}(r)$ then assumes the shape of the probability distribution of $1s$ excitons (shaded area). Thus, the formation of truly bound $1s$-excitons proceeds in the sequence that (i) a correlated plasma is built up on a sub-picosecond time scale due to Coulomb interaction; (ii) in the next step, phonon-assisted scattering forms excitons out of the correlated plasma on a nanosecond time scale.

To illustrate how the exciton formation can be directly detected experimentally, we compute the THz absorption spectrum resulting from non-resonant excitation with a 500 fs excitation pulse energetically 16 meV above the $1s$-exciton resonance. The pulse intensity is chosen such that it generates a moderate $6 \times 10^4\,\mathrm{cm}^{-1}$ carrier density. In Fig. 32, we see that the computed $\alpha_{THz}(\omega)$ is very broad and shows no resonances at 1 ps after the excitation. Even after 200 ps, the THz response has changed only slightly due to the slow phonon scattering from electron–hole plasma to excitons. However, roughly 1 ns after the excitation $\alpha_{THz}(\omega)$ develops a pronounced resonance at the energy corresponding exactly to the difference between the two lowest exciton states. The asymmetric shape of $\alpha_{THz}(\omega)$ is a consequence of transitions between the lowest and all other exciton states. These results are in good qualitative agreement with recent experiments [19].

8.3. Phase space

We next investigate how the exciton formation proceeds under different incoherent excitation conditions determined by the lattice temperature and the carrier density. This analysis allows us to define the phase space of exciton formation [18,29].

Fig. 33 shows the dynamics of the $1s$-exciton fraction, x_{1s}, for different lattice temperatures, always starting from an uncorrelated electron–hole plasma with initial electron and hole distributions at a temperature of $T = 60$ K. Fig. 33 clearly demonstrates

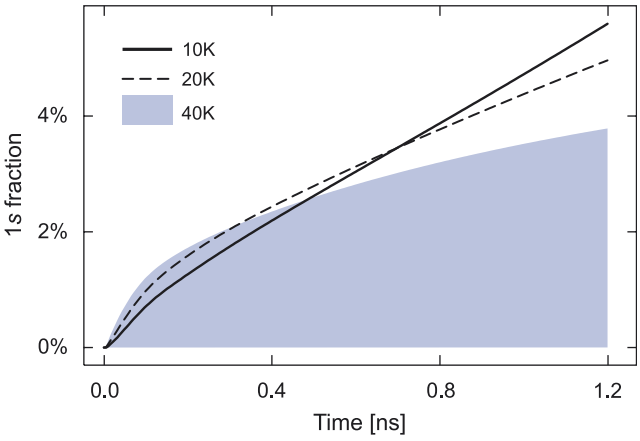

Fig. 33. Exciton-formation dynamics of 1s populations out of an electron–hole plasma with $n = 2 \times 10^4\,\mathrm{cm}^{-1}$ at an initial temperature of $T = 60\,\mathrm{K}$. The generated 1s-exciton fraction, x_{1s}, is presented as function of time for 10 K (solid line), 20 K (dashed line), and 40 K (shaded area) lattice temperature. According to Ref. [29].

how the formation rate of 1s excitons quickly drops with increasing lattice temperatures such that we do not expect any significant formation for temperatures above 40 K.

We repeat this analysis for different initial carrier densities, n_{eh}, and lattice temperatures, T. In each case, we evaluate the exciton-formation rate,

$$r_{1s} \equiv \frac{\partial x_{1s}}{\partial t}, \tag{287}$$

at 1.2 ns after the initialization of the computations. At this time, the exciton formation proceeds almost linearly in time, see Fig. 33. Physically, r_{1s}, determines the fraction of 1s excitons formed per unit time assuming that depletion effects are unimportant.

The basic results of our studies are summarized in Fig. 34 where we plot contour lines indicating the percentage of electron–hole pairs that are bound into 1s-excitons per nanosecond. We clearly see that exciton formation is only significant for cold lattice temperatures below 30 K and rather low densities. However, once the densities are too low, the formation rate drops because it becomes increasingly improbable for electrons and holes to find the scattering partners necessary for the formation process [18]. Hence, there is an optimum density–temperature range where the scattering probability between electrons and holes is sufficiently large to enable exciton formation.

8.4. Thermodynamic limit

In order to study formation and stability of exciton populations under ideal best case conditions, we assume that spontaneous emission can be suppressed such that a quasi-equilibrium between the electron–hole plasma and the excitons may be reached [4,125]. We want to study the stability of a certain exciton population at a given lattice temperature and carrier density. Therefore, we perform calculations where we take an initial exciton population and monitor its dynamic evolution in the presence of interacting electrons, holes, and phonons. Since we are only interested in the quasi-equilibrium state of the

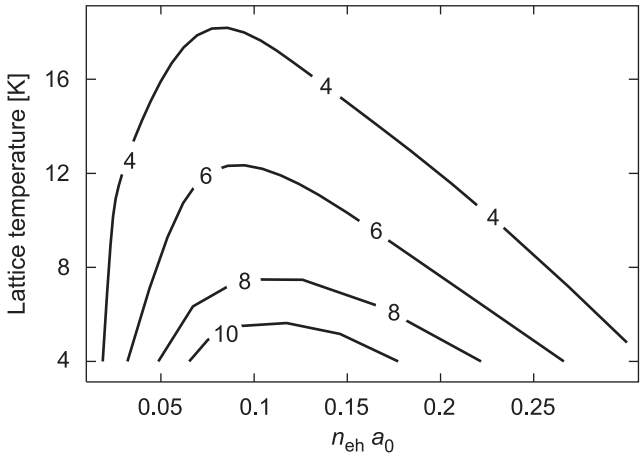

Fig. 34. Contour plot of exciton-formation rate $(\partial/\partial t)_A\langle N_{1s}\rangle/N_e$ for an initial carrier temperature of 60 K and varying lattice temperatures and carrier densities. Values are given in %/ns, i.e. they show the percentage of carriers bound to 1*s* excitons per nanosecond. The exciton-formation rates are taken after 1.2 ns of evolution. According to Ref. [29].

system, we start the calculations with several different initial conditions for the two-particle correlations. When the full dynamical evolution of the exciton correlation dynamics, including phonon scattering (286), is solved toward a steady state, the quasi-equilibrium configuration can be determined. In all cases studied here, we assume that the initial carrier densities are Fermi–Dirac distributions at the lattice temperature. Furthermore, we assume initially vanishing two-particle correlations $c^{q,k',k}_{c,c;c,c}$ and $c^{q,k',k}_{v,v;v,v}$ but we seed the system with excitonic correlations $c^{q,k',k}_{X}$ corresponding to different 1*s*-exciton fractions. This initial state can be expressed via

$$c_X^{\mathbf{q}_\parallel,\mathbf{k}'_\parallel-\mathbf{q}_e,\mathbf{k}_\parallel+\mathbf{q}_e}(t=0) \equiv \phi_{1s}(\mathbf{k}'_\parallel)\phi_{1s}(\mathbf{k}_\parallel)\Delta N_{1s}(\mathbf{q}_\parallel), \tag{288}$$

where $\Delta N_{1s}(\mathbf{q}_\parallel)$ is a Bose–Einstein distribution of 1s-excitons. In order to construct a physically consistent initial configuration with full excitonic correlations, we first evolve our coupled equations by artificially holding the exciton fraction constant for 120 ps before entering into the full calculations.

The temporal evolution of the 1*s*-exciton fraction for an initial carrier density $n_{eh}a_0 = 0.05$ and a lattice temperature $T = 20$ K is shown in Fig. 35. In order to find the quasi-equilibrium exciton fraction, the full exciton-formation dynamics is evaluated for different initial 1*s*-populations varying from $\Delta n_{1s} = 0$ to $\Delta n_{1s} = 0.3\,n_{eh}$. All of these runs are seen to converge to the same final level with a well defined quasi-equilibrium exciton fraction of $x_{1s} = 15.4\%$ showing the desired insensitivity of the final result to the choice of the initial conditions.

By repeating the analysis for many different densities and temperatures, we can construct the phase diagram presented in Fig. 36. We see that large exciton fractions are obtained only in the low temperature and density regime while x_{1s} is dramatically reduced for elevated temperatures and densities. The temperature dependence can be intuitively explained by thermodynamical arguments since for higher temperatures excitons should

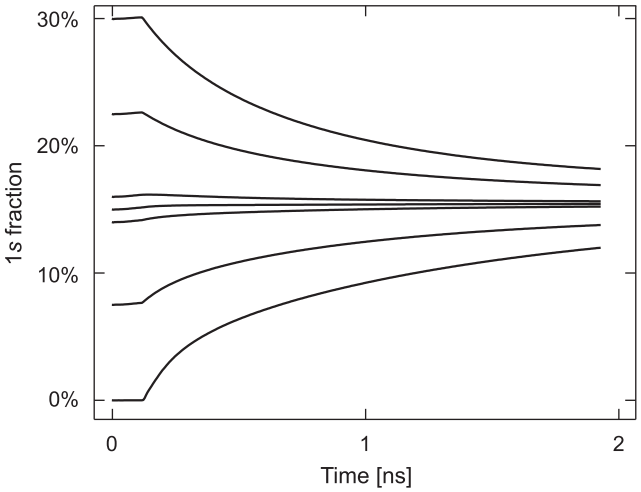

Fig. 35. Fraction of excitons, x_{1s}, with respect to density as function of time t. Initial values of x_{1s} are 0, 0.075, 0.14, 0.15, 0.16, 0.225 and 0.3 (from bottom to top) and computations have carrier density $n_{\mathrm{eh}}a_0 = 0.05$ and lattice temperature $T = 20\,\mathrm{K}$. According to Ref. [55].

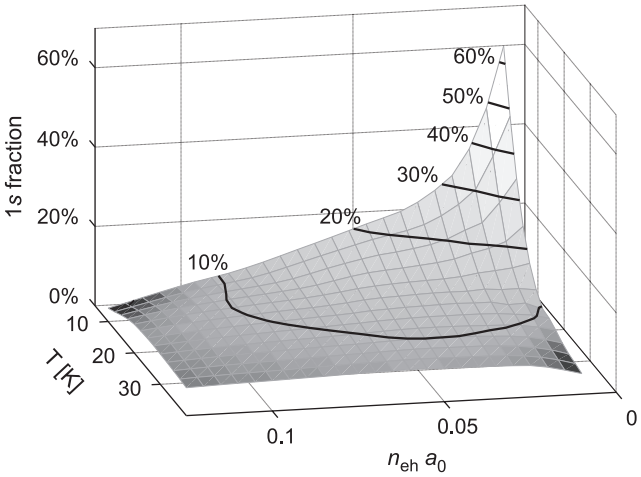

Fig. 36. Steady-state fraction of 1s excitons for various temperatures and carrier-densities. From Ref. [55].

become more ionized. The density dependence of x_{1s} follows from several effects: (i) the Coulomb potential becomes screened, which eventually ionizes the 1s state [56,106], (ii) the Fermionic substructure of the composite particles becomes important [88], and (iii) nonlinear scattering processes increase with increasing density.

It is interesting to compare the density dependence of the full steady-state computations to a dynamical exciton-formation investigation. In the dynamical study, we start the full exciton-formation calculation with vanishing exciton correlations and extract the number of bound electron–hole pairs after 0.5 ns of evolution. Fig. 37 shows for a $T = 10\,\mathrm{K}$ lattice temperature the comparison of steady-state (solid line) and fully dynamic (shaded area) computations.

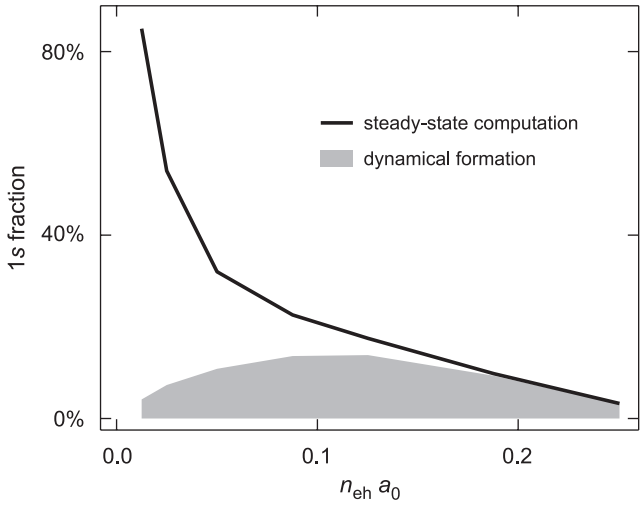

Fig. 37. A comparison of exciton fraction x_{1s} as function of density at a lattice temperature $T = 10\,\mathrm{K}$ obtained by steady-state computations (solid line), and dynamic formation (shaded area). According to Ref. [55].

For high densities, the results of the steady-state calculation is close to the dynamical one. However, the dynamical calculation yields rather slow formation rates for low to intermediate densities. The formation process exhibits a characteristic density dependency, being most efficient at intermediate densities of $n_{e,h}a_0 \approx 0.1$ and decreasing significantly for both lower and higher densities. The time required for significant exciton formation at low densities clearly exceeds 10 ns, which shows that under most conditions where radiative recombination events happen on a nanosecond time scale, no quasi-thermodynamical steady-state is ever reached for the exciton populations in direct-gap semiconductors.

9. Quantum-optical semiconductor excitations

In this section, we apply the complete microscopic theory presented in Section 4, to treat quantum-optical effects such as PL, squeezing, and entanglement [15,24–26,28,32]. The same theory can also be applied to describe quantum-optical effects in THz emission [35,69,70,126]. In general, the quantum aspects of light become particularly important when the light and carrier systems enter the incoherent regime. For these situations, the energy of the light field is completely stored in its quantum fluctuations such that all light–matter coupling effects are determined by quantum-optical aspects. Thus, both the light field and the related quasi-particle excitations must be treated fully quantum mechanically. As examples, we analyze luminescence and quantum-optical spectroscopy focusing on the differences in the semiconductor quasi-particle states resulting from quantum-optical instead of classical excitation.

9.1. Semiconductor luminescence equations

As a first step, we discuss how the light quantization effects the carrier system. Since we assume the completely incoherent regime, all coherent quantities (see discussion in Section 5.8

and Appendix E.2) vanish. Consequently, the carrier densities are the only relevant single-particle variables.

The generic Eq. (71) already contains the additional coupling to the quantum-optical correlations. Putting $\lambda = \lambda' = c$, we find

$$\left.\frac{\partial}{\partial t} f^{\mathrm{e}}_{\mathbf{k}_\parallel}\right|_{\mathrm{QED}} = \frac{\mathrm{i}}{\hbar}\sum_{\mathbf{q}_\parallel}\left[\Delta\langle E^{v}_{\mathbf{q}_\parallel} a^{\dagger}_{c,\mathbf{k}_\parallel} a_{v,\mathbf{k}_\parallel-\mathbf{q}_\parallel}\rangle - \Delta\langle (E^{v}_{\mathbf{q}_\parallel})^{\dagger} a^{\dagger}_{v,\mathbf{k}_\parallel-\mathbf{q}_\parallel} a_{c,\mathbf{k}_\parallel}\rangle\right]$$

$$= -2\,\mathrm{Re}\left[\sum_{\mathbf{q}_\parallel,q_\perp} \mathsf{F}^{v,\star}_{\mathbf{q}_\parallel,q_\perp}\,\Delta\langle B^{\dagger}_{\mathbf{q}_\parallel,q_\perp} a^{\dagger}_{v,\mathbf{k}_\parallel-\mathbf{q}_\parallel} a_{c,\mathbf{k}_\parallel}\rangle\right] \tag{289}$$

which follows by applying the definitions (27) and (63) and by putting the coherent correlations $\Delta\langle B a^{\dagger}_{v} a_{c}\rangle$ and $\Delta\langle B^{\dagger} a^{\dagger}_{c} a_{v}\rangle$ to zero. With very similar steps, we find the dynamic equation for the hole distributions,

$$\left.\frac{\partial}{\partial t} f^{\mathrm{h}}_{\mathbf{k}_\parallel}\right|_{\mathrm{QED}} = -2\,\mathrm{Re}\left[\sum_{\mathbf{q}_\parallel,q_\perp} \mathsf{F}^{v,\star}_{\mathbf{q}_\parallel,q_\perp}\,\Delta\langle B^{\dagger}_{\mathbf{q}_\parallel,q_\perp} a^{\dagger}_{v,\mathbf{k}_\parallel} a_{c,\mathbf{k}_\parallel-\mathbf{q}_\parallel}\rangle\right]. \tag{290}$$

From these equations we notice that the electron and hole densities couple to correlated processes, $\Delta\langle B^{\dagger} a^{\dagger}_{v} a_{c}\rangle$, where a photon is created by annihilating an electron–hole pair. The term $\Delta\langle B^{\dagger} a^{\dagger}_{v} a_{c}\rangle$ describes the correlated *photon-assisted electron–hole recombination*. In this process, the center-of-mass momentum $\mathbf{q}_\parallel$ of the electron–hole pair is conserved since the photon receives the same in-plane momentum. However, there is no momentum conservation in the $q_\perp$ direction for planar structures. We have already discussed in Section 5.7 how this feature leads to the radiative decay of excitations.

The expression $\Delta\langle B^{\dagger} a^{\dagger}_{v} a_{c}\rangle$ can also be interpreted as *photon-assisted polarization* because it contains the coupling of the photon to the polarization-type operator $a^{\dagger}_{v} a_{c}$. In the incoherent regime, this is the only relevant photon-carrier correlation such that we use the general form (81) to define the abbreviation

$$\Pi_{\mathbf{k}_\parallel;\mathbf{q}_\parallel,q_\perp} \equiv \Pi^{v,c}_{\mathbf{k}_\parallel;\mathbf{q}_\parallel,q_\perp} = \Delta\langle B^{\dagger}_{\mathbf{q}_\parallel,q_\perp} a^{\dagger}_{v,\mathbf{k}_\parallel-\mathbf{q}_\parallel} a_{c,\mathbf{k}_\parallel}\rangle. \tag{291}$$

Because Eqs. (289)–(290) contain Π in a summed form, it is also convenient to identify the collective quantity

$$\Pi_{\mathbf{k}_\parallel;\mathbf{q}_\parallel,\Sigma} \equiv \sum_{q_\perp} \mathsf{F}^{v,\star}_{\mathbf{q}_\parallel,q_\perp}\,\Pi_{\mathbf{k}_\parallel;\mathbf{q}_\parallel,q_\perp} \tag{292}$$

that contains all Π terms having the same in-plane momentum, in analogy to Eq. (27).

The photon-assisted polarization terms appear also in the dynamics of the incoherent two-particle carrier correlations $c_{c,v;c,v}$, $c_{c,c;c,c}$, and $c_{v,v;v,v}$. Usually, the coupling of photons to exciton correlations, $c_X \equiv c_{c,v;c,v}$ introduces the largest effects. Therefore, we present here only the quantum-optical contributions to c_X according to the generic Eq. (96). By implementing there $\lambda = c$, $\nu = v$, $\nu' = c$, and $\lambda' = v$, the quantum-optical coupling D_{QED} produces

$$\left.\frac{\partial}{\partial t} c^{\mathbf{q}_\parallel,\mathbf{k}'_\parallel,\mathbf{k}_\parallel}_{\mathrm{X}}\right|_{\mathrm{QED}} = -(1-f^{\mathrm{e}}_{\mathbf{k}_\parallel}-f^{\mathrm{h}}_{\mathbf{k}_\parallel+\mathbf{q}_\parallel})\Pi_{\mathbf{k}'_\parallel+\mathbf{q}_\parallel;\mathbf{q}_\parallel,\Sigma}$$

$$-(1-f^{\mathrm{e}}_{\mathbf{k}'_\parallel-\mathbf{q}_\parallel}-f^{\mathrm{h}}_{\mathbf{k}'_\parallel})\Pi^{\star}_{\mathbf{k}_\parallel-\mathbf{q}_\parallel;\mathbf{q}_\parallel,\Sigma}, \tag{293}$$

where all coherent contributions have been omitted. Alternatively, Eq. (293) can also be obtained from Eq. (F.12).

Our investigation in Section 6.5 shows that $\mathbf{q}_\parallel$ plays the role of the exciton center-of-mass momentum in c_X, see Eq. (233). At the same time, $\mathbf{q}_\parallel$ appears in Eq. (293) as the in-plane photon momentum for the Π terms. Thus, the in-plane photon and exciton momenta have to match whenever photon-assisted processes either create or destroy photons or electron–hole pairs. Since the photon momentum is very small, the exciton correlations couple to the incoherent light field only when their center-of-mass momentum $\mathbf{q}_\parallel$ is nearly vanishing. This momentum selective coupling is important only for excitons and not for the carrier densities since their quantum dynamics follows from

$$\frac{\partial}{\partial t} f^{\mathrm{e,QED}}_{\mathbf{k}_\parallel} = -2\sum_{\mathbf{q}_\parallel} \mathrm{Re}\,[\Pi_{\mathbf{k}_\parallel;\mathbf{q}_\parallel,\Sigma}], \quad \frac{\partial}{\partial t} f^{\mathrm{h,QED}}_{\mathbf{k}_\parallel} = -2\sum_{\mathbf{q}_\parallel} \mathrm{Re}[\Pi_{\mathbf{k}_\parallel+\mathbf{q}_\parallel;\mathbf{q}_\parallel,\Sigma}], \tag{294}$$

where the identification (292) has been applied. This general form shows that the carrier momentum $\mathbf{k}_\parallel$ can have any value and is not limited by the photon momentum.

In order to determine how the quantum-optical Π correlation influences the carrier dynamics, we apply the generic Eq. (83) for the band-index combination $\lambda' = v$ and $\lambda = c$. The straightforward substitution yields

$$\begin{aligned}
\mathrm{i}\hbar \frac{\partial}{\partial t} \Pi_{\mathbf{k}_\parallel,\mathbf{q}_\parallel,q_\perp} &= (\tilde{\varepsilon}^c_{\mathbf{k}_\parallel} - \tilde{\varepsilon}^v_{\mathbf{k}_\parallel-\mathbf{q}_\parallel} - \hbar\omega_{\mathbf{k}_\parallel,\mathbf{q}_\parallel,q_\perp})\Pi_{\mathbf{k}_\parallel,\mathbf{q}_\parallel,q_\perp} \\
&\quad - [1 - f^{\mathrm{e}}_{\mathbf{k}_\parallel} - f^{\mathrm{h}}_{\mathbf{k}_\parallel-\mathbf{q}_\parallel}] \sum_{\mathbf{l}_\parallel} V_{\mathbf{k}_\parallel-\mathbf{l}_\parallel} \Pi_{\mathbf{l}_\parallel;\mathbf{q}_\parallel,q_\perp} \\
&\quad + \mathrm{i}\hbar \mathsf{F}^v_{\mathbf{q}_\parallel,q_\perp} \left[f^{\mathrm{e}}_{\mathbf{k}_\parallel} f^{\mathrm{h}}_{\mathbf{k}_\parallel-\mathbf{q}_\parallel} + \sum_{\mathbf{l}_\parallel} c_X^{\mathbf{q}_\parallel,\mathbf{k}_\parallel-\mathbf{q}_\parallel,\mathbf{l}_\parallel} \right] \\
&\quad - \mathrm{i}\hbar [1 - f^{\mathrm{e}}_{\mathbf{k}_\parallel} - f^{\mathrm{h}}_{\mathbf{k}_\parallel-\mathbf{q}_\parallel}] \Delta\langle B^\dagger_{\mathbf{q}_\parallel,q_\perp} B_{\mathbf{q}_\parallel,\Sigma}\rangle + T^{\Pi}_{\mathbf{k}_\parallel;\mathbf{q}_\parallel,q_\perp},
\end{aligned} \tag{295}$$

in the incoherent limit. Here, we also identified the effective photon operator, $B_{\mathbf{q}_\Sigma} \equiv \sum_{q_\perp} \mathsf{F}^v_{\mathbf{q}_\parallel,q_\perp} B_{\mathbf{q}_\parallel,q_\perp}$, according to Eq. (27). The triplet-scattering term is obtained from Eq. (84) by setting $\lambda' = v$ and $\lambda = c$, yielding

$$\begin{aligned}
T^{\Pi}_{\mathbf{k}_\parallel;\mathbf{q}_\parallel,q_\perp} &\equiv V[\Pi^{v,c}_{\mathbf{k}_\parallel;\mathbf{q}_\parallel,q_\perp}]_{\mathrm{T}} \\
&= \sum_{v,\mathbf{k}'_\parallel,\mathbf{l}_\parallel} (V_{\mathbf{l}_\parallel} \Delta\langle B^\dagger_{\mathbf{q}_\parallel,q_\perp} a^\dagger_{v,\mathbf{k}_\parallel-\mathbf{q}_\parallel} a^\dagger_{v,\mathbf{k}'_\parallel+\mathbf{q}_\parallel} a_{v,\mathbf{k}'_\parallel+\mathbf{l}_\parallel} a_{c,\mathbf{k}_\parallel-\mathbf{l}_\parallel}\rangle \\
&\quad - V_{\mathbf{l}_\parallel-\mathbf{q}_\parallel} \Delta\langle B^\dagger_{\mathbf{q}_\parallel,q_\perp} a^\dagger_{v,\mathbf{k}_\parallel-\mathbf{l}_\parallel} a^\dagger_{v,\mathbf{k}'_\parallel+\mathbf{l}_\parallel} a_{v,\mathbf{k}'_\parallel} a_{c,\mathbf{k}_\parallel}\rangle) \\
&\quad - \mathrm{i}\hbar \sum_{\mathbf{l}_\parallel} (\Delta\langle B^\dagger_{\mathbf{q}_\parallel,q_\perp} B_{\mathbf{l}_\parallel,\Sigma} a^\dagger_{v,\mathbf{k}_\parallel-\mathbf{q}_\parallel} a_{v,\mathbf{k}_\parallel-\mathbf{l}_\parallel}\rangle - \Delta\langle B^\dagger_{\mathbf{q}_\parallel,q_\perp} B_{\mathbf{q}_\parallel-\mathbf{l}_\parallel,\Sigma} a^\dagger_{c,\mathbf{k}_\parallel-\mathbf{l}_\parallel} a_{c,\mathbf{k}_\parallel}\rangle) \\
&\quad + \sum_{\mathbf{l}_\parallel} (\Delta\langle B^\dagger_{\mathbf{q}_\parallel,q_\perp} Q^c_{\mathbf{l}_\parallel} a^\dagger_{v,\mathbf{k}_\parallel-\mathbf{q}_\parallel} a_{c,\mathbf{k}_\parallel-\mathbf{l}_\parallel}\rangle - \Delta\langle B^\dagger_{\mathbf{q}_\parallel,q_\perp} Q^v_{\mathbf{q}_\parallel-\mathbf{l}_\parallel} a^\dagger_{v,\mathbf{k}_\parallel-\mathbf{l}_\parallel} a_{c,\mathbf{k}_\parallel}\rangle).
\end{aligned} \tag{296}$$

Here, the terms given by the first sum on the RHS describe the influence of the Coulomb-induced scattering on the dynamics of Π, while the second and the third sums provide higher-order correlations due to the coupling to photons and phonons. The treatment of the Coulomb-induced triplets is presented explicitly in Refs. [24,101] at the scattering level (see also the discussion in Appendix D.2).

In general, Eq. (295) shows that Π is spontaneously driven by the term $(f^{e}f^{h}+\sum c_X)$ in the third line even when all correlations initially vanish. Thus, this contribution acts as a *spontaneous emission source* which has a natural cluster-expansion based division into its correlated c_X part and the $f^{e}f^{h}$ part related to the uncorrelated electron–hole plasma. Already the THz analysis in Sections 6.5–6.6 gives us a feeling for the physical relevance of this separation. In the context of spontaneous emission, we now see that only c_X can describe the effects of true exciton populations whereas the plasma contribution, $f^{e}_{\mathbf{k}_\parallel}f^{h}_{\mathbf{k}_\parallel-\mathbf{q}_\parallel}$, is an emission source due to the spontaneous recombination of uncorrelated electron–hole pairs. Clearly, this recombination process occurs as long as an electron and a hole are found simultaneously with momenta $\mathbf{k}_\parallel$ and $\mathbf{k}_\parallel-\mathbf{q}_\parallel$, respectively. The corresponding center-of-mass momentum $\mathbf{q}_\parallel$ is then transferred to the photon. The correlated c_X source includes both the contributions resulting from the presence of genuine exciton populations and/or a correlated electron–hole plasma (see also Section 6.5). Since neither the uncorrelated plasma nor the correlated sources depend on the photon frequency in any way, they both can initiate photon emission—that is observed as PL—in all relevant frequency ranges.

The spectral distribution of spontaneously emitted photons is strongly altered by the resonance structure related to the homogeneous part of the Π dynamics, i.e. the terms in the first and second line of Eq. (295). We see that the different $\mathbf{k}_\parallel$ components of the spontaneously generation Π are coupled via the Coulomb sum in the second line of Eq. (295). It is interesting to notice that this part of Eq. (295) shows strong analogies to the homogeneous part of the SBEs. Hence, we see that it is the Coulomb coupling that produces the excitonic resonances in the resulting PL in the same way as these resonances appear in the absorption spectra. This important fact implies that the specific form of the quasi-particle state of carriers in the spontaneous emission source does not determine whether or not PL shows excitonic resonances. Thus, *the detection of an excitonic resonance in a luminescence spectrum cannot be a unique signature for the presence of exciton populations*, in contrast to resonances in the THz response. Instead, "excitonic luminescence" may also result from quasi-particle states containing only a pure electron–hole plasma. This intriguing phenomenon was first predicted in Ref. [15] and later verified experimentally [31,34,127]. In general, the detailed signatures of plasma and exciton population contributions to the excitonic luminescence can be identified via a quantitative analysis [31,101,34].

The last line of Eq. (295) contains photon-number-like correlations that are particularly large when the semiconductor material either is inside an optical cavity or if it is optically pumped with incoherent light fields. Thus, this contribution provides either stimulated coupling or direct excitation effects due to external incoherent fields. To solve the corresponding dynamics, we apply Eq. (75) resulting in

$$\mathrm{i}\hbar\frac{\partial}{\partial t}\Delta\langle B^{\dagger}_{\mathbf{q}_\parallel,q_\perp}B_{\mathbf{q}_\parallel,q'_\perp}\rangle=\hbar(\omega_{\mathbf{q}'}-\omega_{\mathbf{q}})\Delta\langle B^{\dagger}_{\mathbf{q}_\parallel,q_\perp}B_{\mathbf{q}_\parallel,q'_\perp}\rangle+\mathrm{i}\hbar\sum_{\mathbf{k}_\parallel}[\mathsf{F}^{v}_{\mathbf{q}_\parallel,q_\perp}\Pi^{\star}_{\mathbf{k}_\parallel;\mathbf{q}_\parallel,q'_\perp}+\mathsf{F}^{v,\star}_{\mathbf{q}_\parallel,q'_\perp}\Pi_{\mathbf{k}_\parallel;\mathbf{q}_\parallel,q_\perp}],\tag{297}$$

where we again only included the incoherent correlations. If the carrier system is close to a quasi-equilibrium situation, the carrier quantities entering Eq. (295) are nearly constant. In this regime, Eqs. (295)–(297) are closed. They fully determine the photon flux for the

emitted light providing the steady-state luminescence spectrum according to

$$I_{\mathrm{PL}}(\omega_{\mathbf{q}}) = \frac{\partial}{\partial t}\, \Delta\langle B^{\dagger}_{\mathbf{q},q_\perp} B_{\mathbf{q},q_\perp}\rangle = 2\,\mathrm{Re}\left[\sum_{\mathbf{k}_\parallel} \mathsf{F}^{\star}_{\mathbf{q}_\parallel,q_\perp} \Pi^{\star}_{\mathbf{k}_\parallel;\mathbf{q}_\parallel,q_\perp}\right]. \tag{298}$$

In general, Eqs. (295)–(297) define the SLE [15,23] since they have an obvious structural similarity to the SBE discussed in Section 5.1. The SLE can be applied to systematically explain quantitative features of PL ranging from the low-density conditions [26,27] up to the gain regime [108,128,129]. The SLE can also be generalized for excitations containing coherences. For these situations, also quantum-optical correlations of the type $\Delta\langle BB\rangle$, $\Delta\langle Ba^{\dagger}_{v}a_{c}\rangle$, and $\Delta\langle Ba^{\dagger}_{\lambda}a_{\lambda}\rangle$ become relevant. These contributions lead to new quantum-optical effects such as squeezing in the resonance fluorescence [24], entanglement-generated quantum oscillations [25] and resonances in the probe transmission [28]. For a review of the generalization of the theory toward the coherent regime, see Ref. [26].

9.2. Radiative recombination of carriers and exciton populations

To analyze the effect of spontaneous emission on the exciton and carrier distributions, Fig. 38 shows them at different time moments after the coherent resonant 1*s*-excitation. These results have been obtained by solving the full singlet–doublet equations for the same planar arrangement of QWIs as in the previous chapters. In particular, we assumed here a 1 ps excitation pulse with a sufficiently weak intensity such that the conditions are analogous to those in Fig. 14. The snapshot times in Fig. 38 are chosen such that the polarization-to-population conversion is already complete. For these times, we see that both the carrier and the 1*s*-exciton distributions have a wide momentum spread due to the lack of a momentum sensitivity in the generation processes.

After the population generation, the excitons in the very low-momentum states, i.e. roughly those with $|\mathbf{q}_\parallel|a_0 < 0.1$, show a fast decay due to their PL related recombination. In other words, these are the optically active "*bright excitons*" that give rise to luminescence. Due to its momentum selectivity this recombination can lead to a significant hole burning in the exciton distributions [18]. This hole burning is supported by the fact that the exciton scattering times are relatively slow in comparison to the relatively fast ≈ 15 ps

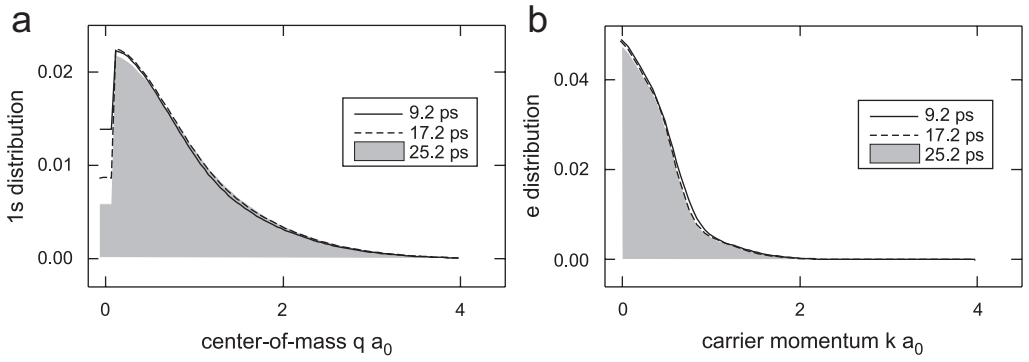

Fig. 38. (a) Computed 1*s*-exciton and (b) carrier distributions for a time sequence after the resonant 1*s* excitation with classical light (after Ref. [46]).

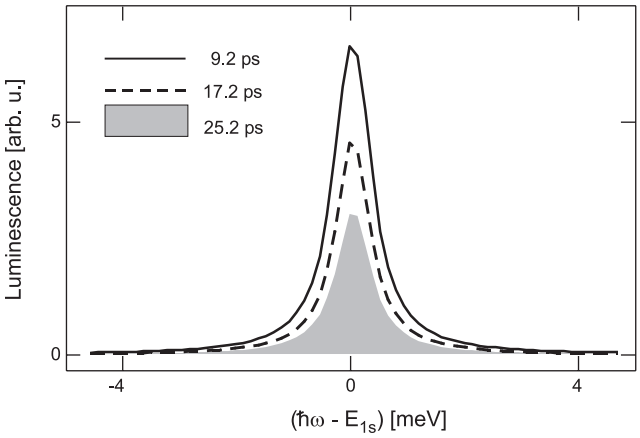

Fig. 39. Photoluminescence spectra computed for different times after the 1*s* excitation with classical field of Fig. 38 (after Ref. [46]).

recombination time, which is the same as that of the coherent polarization (see the discussion in Section 5.7). Hence, the bright excitons are strongly coupled to the light field, which rapidly depletes their population leaving the majority of the excitons in optically inactive "*dark states*".

Since an electron with an arbitrary momentum $\mathbf{k}_{\parallel}$ can recombine with a hole in the matching momentum state, $\mathbf{k}_{\parallel} - \mathbf{q}_{\parallel}$, all electron and hole states contribute to the emission, i.e. electron and hole distributions do not show a momentum selectivity. Consequently, the radiative recombination only leads to slow changes of their total electron–hole population on a nanosecond time scale [see Eq. (294)]. This important difference between exciton and carrier distributions is the reason for the fact, that excitons display highly non-thermal distributions, even if the carriers are basically in a thermal quasi-equilibrium state. As a result, *spontaneous emission is never a weak perturbation for exciton distributions in the usual direct-gap semiconductors* even though the total carrier recombination rate is slow.

The discussed fundamental differences between the optical coupling of exciton and electron–hole populations lead to strong non-equilibrium features in the exciton PL [31,34,101,130–132]. As an example, we show in Fig. 39 computed luminescence spectra, I_{PL}, for the different times used in Fig. 38. We observe that the luminescence decreases with increasing time, following the depletion of the bright exciton states. However, rather strong excitonic PL remains, even after the most of the optically active excitons are have decayed. This *excitonic PL without exciton populations* underlines the fact that also the uncorrelated electron–hole plasma produces an excitonic resonance in the luminescence [15,31,127].

9.3. Concept of quantum-optical spectroscopy

Parallel to atomic Bose–Einstein condensation studies [133–136], semiconductor researchers are on a persistent quest [137–145] to achieve Bosonic condensation of excitons. Due to the strong hole-burning signature in the exciton center-of-mass momentum distributions, it is obviously difficult to accumulate a macroscopic population of low-momentum excitons after excitation with classical light. As a result, a simple

thermodynamic Bose–Einstein condensation is difficult to realize in such direct-gap semiconductor systems even for very low temperatures. As a consequence, most of the exciton-condensation experiments concentrate either on the material Cu_2O [140,141] where the energetically lowest exciton state is dipole forbidden, or on indirect semiconductor systems [142–145] with strongly suppressed radiative coupling.

One may now ask if one can change the negative influence of incoherent quantum fields on the exciton condensation into a virtue by using truly incoherent quantum excitations to pump—not to drain—direct band-gap systems. Indeed the SLE show that it should be possible to use an incoherent quantum field, defined entirely by its $\Delta\langle B^\dagger B\rangle$ fluctuations, to induce strong photon-assisted polarization correlations. Once Π is generated, Eqs. (293)–(294) predict that it leads to the photon-assisted creation of correlated electron–hole pairs in low-momentum states matching the in-plane momentum of the exciting light. This spontaneous-absorption mechanism is the inverse process of the spontaneous emission. In contrast to a classical excitation, such a quantum excitation scheme should directly excite excitons into their zero-momentum state; i.e. one should be able to generate a quantum-degenerate exciton state with a macroscopic population of the lowest exciton state. These ideas outline the concept of *quantum-optical semiconductor spectroscopy* where the quantum statistics of the light is used both to control the excited state and to follow specific processes in the subsequent quasi-particle dynamics. This concept was proposed recently in Refs. [36,37] and we follow this discussion to summarize the most important aspects.

9.4. Quantum description of exciting light fields

To understand how excitation by coherent (i.e. classical) and incoherent (i.e. quantum) light differ from each other, we first have to identify the precise quantum mechanical states of the corresponding light sources. In general, light is a Bosonic field whose classical and quantum-optical aspects follow from its quantum statistics. The quantum statistics can be represented in several equivalent ways, e.g. by using the density matrix, the wavefunction, or all possible $(J+K)$-particle expectation values $\langle[B^\dagger]^J B^K\rangle$. Since we have adopted the cluster expansion approach that deals with expectation values, it is natural for us to analyze $\langle[B^\dagger]^J B^K\rangle$.

The properties of classical fields follow from the singlet factorization producing

$$\langle[B^\dagger]^J B^K\rangle|_{\text{classical}} = \langle B^\dagger\rangle^J \langle B\rangle^K \tag{299}$$

for any given mode. It is interesting to note that a coherent state [48,49],

$$|\beta\rangle \equiv D(\beta)|0\rangle, \quad D(\beta) \equiv \mathrm{e}^{\beta^\star B - \beta B^\dagger}, \tag{300}$$

corresponds to a classical field since $\langle[B^\dagger]^J B^K\rangle = \langle\beta|[B^\dagger]^J B^K|\beta\rangle = [\beta^\star]^J \beta^K$ produces the classical factorization in Eq. (299) after we identify $\beta = \langle B\rangle$. From a quantum-optical point of view, a coherent state—i.e. classical field—is obtained when the coherent displacement operator $D(\beta)$ acts on the vacuum state $|0\rangle$.

The conceptually simplest quantum source has a vanishing classical part, i.e. all singlets are zero such that the field is incoherent. If the field has only two-particle correlations $\Delta\langle B^\dagger B\rangle$, the cluster-expansion (43) produces the quantum statistics according to

$$\langle[B^\dagger]^J B^K\rangle|_{\text{quantum}} = \delta_{J,K} J!\Delta\langle B^\dagger B\rangle^J. \tag{301}$$

Such a *thermal light* field is described by its photon-number-like correlations. We can also find the corresponding density-matrix form via

$$\hat{\rho}_{\rm th} = \sum_{j=0}^{\infty} |j\rangle \frac{n_{\rm th}^{j}}{(1+n_{\rm th})^{j}} \langle j|, \tag{302}$$

where $|j\rangle$ is the usual Fock-number state [48,49]. Since this field has $\langle [B^{\dagger}]^{J} B^{K}\rangle = {\rm Tr}[[B^{\dagger}]^{J} B^{K} \hat{\rho}_{\rm th}] = \delta_{J,K} J! [n_{\rm th}]^{J}$, the quantum light in Eq. (301) is equivalent to $\hat{\rho}_{\rm th}$ after we identify $n_{\rm th} = \Delta\langle B^{\dagger} B\rangle$. There are in fact infinitely many other forms of $\langle [B^{\dagger}]^{J} B^{K}\rangle$ which could be used for the quantum excitation. However, the thermal light is the simplest quantum field and probably also the most easily accessible source in experiments.

9.5. Matching classical and quantum light sources

The position-dependent intensity of the initial pump light, which may be quantum or classical, follows from

$$\begin{aligned}&\langle E(\mathbf{r}_{\parallel}, r_{\perp}) E(\mathbf{r}_{\parallel}, r_{\perp})\rangle_{N} \\ &\quad = \frac{2}{\mathsf{V}} \sum_{\mathbf{q}_{\parallel}, \mathbf{q}'_{\parallel}} \sum_{q_{\perp}, q'_{\perp}} \mathsf{E}_{q} \mathsf{E}_{q'} \langle B^{\dagger}_{\mathbf{q}_{\parallel}, q_{\perp}} B_{\mathbf{q}'_{\parallel}, q'_{\perp}}\rangle \, {\rm e}^{{\rm i}(\mathbf{q}'_{\parallel} - \mathbf{q}_{\parallel})\cdot \mathbf{r}} \, {\rm e}^{{\rm i}(q'_{\perp} - q_{\perp}) r_{\perp}},\end{aligned} \tag{303}$$

where the subscript N indicates normal ordering of the operators related to the free-space eigenmodes of light. Terms $\langle BB\rangle$ and $\langle B^{\dagger} B^{\dagger}\rangle$ have been omitted here since they lead to strongly oscillating contributions like ${\rm e}^{{\rm i}(q'_{\perp} + q_{\perp}) r_{\perp}}$ which average to zero as the overall intensity is analyzed. Since the pump is initially propagating freely far away from the planar structure, we use a plane-wave presentation of the modes with a quantization volume $\mathsf{V} = \mathsf{LS}$ which can be divided into the quantization area S and length L.

For simplicity, we assume homogeneous excitation such that the intensity varies only in the direction perpendicular to the planar structure. Such a dependency is found only if the in-plane momenta of the photon operators match according to $\langle B^{\dagger}_{\mathbf{q}_{\parallel}, q_{\perp}} B_{\mathbf{q}'_{\parallel}, q'_{\perp}}\rangle = \delta_{\mathbf{q}_{\parallel}, \mathbf{q}'_{\parallel}} \langle B^{\dagger}_{\mathbf{q}_{\parallel}, q_{\perp}} B_{\mathbf{q}_{\parallel}, q'_{\perp}}\rangle$. This condition implies a generalized intensity

$$\begin{aligned}\langle E(\mathbf{r}, r_{\perp}) E(\mathbf{r}, r'_{\perp})\rangle_{N} &= \langle E(r_{\perp}) E(r'_{\perp})\rangle_{N} \\ &= \frac{2}{\mathsf{V}} \sum_{\mathbf{q}_{\parallel}, q_{\perp}, q'_{\perp}} \mathsf{E}_{q} \mathsf{E}_{q'} \langle B^{\dagger}_{\mathbf{q}_{\parallel}, q_{\perp}} B_{\mathbf{q}_{\parallel}, q'_{\perp}}\rangle \, {\rm e}^{{\rm i}(q'_{\perp} r'_{\perp} - q_{\perp} r_{\perp})}\end{aligned} \tag{304}$$

which depends only on the $r_{\perp}$ coordinate. By applying now the cluster expansion, we find a separation into singlets and doublets

$$\begin{aligned}\langle E(r_{\perp}) E(r'_{\perp})\rangle_{N} &= 2\langle E_{0}^{\dagger}(r_{\perp})\rangle \langle E_{0}(r_{\perp})\rangle \\ &\quad + \frac{2}{\mathsf{S}} \sum_{\mathbf{q}_{\parallel}} \left[\frac{1}{\mathsf{L}} \sum_{q_{\perp}, q'_{\perp}} \mathsf{E}_{q} \mathsf{E}_{q'} \Delta \langle B^{\dagger}_{\mathbf{q}_{\parallel}, q_{\perp}} B_{\mathbf{q}_{\parallel}, q'_{\perp}}\rangle {\rm e}^{{\rm i}(q'_{\perp} r'_{\perp} - q_{\perp} r_{\perp})} \right].\end{aligned} \tag{305}$$

Here, we made the identification $\langle E_{0}(r_{\perp})\rangle \equiv (1/\sqrt{\mathsf{SL}}) \sum_{q_{\perp}} {\rm i}\mathsf{E}_{q} \langle B_{0, q_{\perp}}\rangle {\rm e}^{{\rm i} q_{\perp} r_{\perp}}$ since only the component $\mathbf{q}_{\parallel} = 0$ contributes to the classical field propagating perpendicular to the planar structure.

With the help of Eq. (305), we obtain the separation,

$$\langle E(r_\perp)E(r'_\perp)\rangle_N \equiv \langle E(r_\perp)E(r'_\perp)\rangle_{\text{class}} + \langle E(r_\perp)E(r'_\perp)\rangle_{\text{quant}}, \tag{306}$$

$$\langle E(r_\perp)E(r'_\perp)\rangle_{\text{class}} = 2\langle E_0^\dagger(r_\perp)\rangle\langle E_0(r'_\perp)\rangle, \tag{307}$$

$$\langle E(r_\perp)E(r'_\perp)\rangle_{\text{quant}} = \frac{2}{\mathsf{LS}}\sum_{\mathbf{q}_\parallel,q_\perp,q'_\perp} \mathsf{E}_q\mathsf{E}_{q'}\Delta\langle B^\dagger_{\mathbf{q}_\parallel,q_\perp}B_{\mathbf{q}_\parallel,q'_\perp}\rangle \mathrm{e}^{\mathrm{i}(q'_\perp r'_\perp - q_\perp r_\perp)}, \tag{308}$$

between the classical and quantum intensity, respectively. For a purely classical case, $\langle E\,E\rangle_{\text{quant}}$ vanishes whereas $\langle E\,E\rangle_{\text{class}}$ is zero for pure quantum case.

Since we analyze how the quantum statistical aspects of light influence the quasi-particle excitations, we want to make sure that the configurations of the pure quantum and classical excitations are as close to each other as possible with respect to their intensity and their temporal, and spectral features. The general form of the intensity Eq. (306) suggests that—besides their drastically different quantum statistics—we can make the pure quantum and classical excitations nearly identical by demanding that the initial quantum pulse has the same spatial dependence as its classical counter part,

$$\langle E(r_\perp)E(r'_\perp)\rangle_{\text{quant}} = [2\langle E_0^\star(r_\perp)\rangle\langle E_0(r'_\perp)\rangle]_{\text{class}}. \tag{309}$$

By taking a Fourier transformation of Eq. (309) and inserting Eqs. (307)–(308), we find the condition

$$\begin{aligned}
&\frac{\mathsf{L}}{\mathsf{S}}\sum_{\mathbf{q}_\parallel} \mathsf{E}_q\mathsf{E}_{q'}\Delta\langle B^\dagger_{\mathbf{q}_\parallel,q_\perp}B_{\mathbf{q}_\parallel,q'_\perp}\rangle = \langle E_0^\dagger(q_\perp)\rangle\langle E_0(q'_\perp)\rangle,\\
&\langle E_0(q_\perp)\rangle \equiv \int \mathrm{d}r_\perp \langle E_0(r_\perp)\rangle\, \mathrm{e}^{-\mathrm{i}q_\perp r_\perp}.
\end{aligned} \tag{310}$$

Since this equation can be fulfilled by quantum fields that have different distributions of in-plane momenta, we specify the initial condition

$$\begin{aligned}
&\mathsf{E}_q\mathsf{E}_{q'}\Delta\langle B^\dagger_{\mathbf{q}_\parallel,q_\perp}B_{\mathbf{q}_\parallel,q'_\perp}\rangle = \frac{1}{\mathsf{L}}F(\mathbf{q}_\parallel)\langle E_0^\dagger(q_\perp)\rangle\langle E_0(q'_\perp)\rangle,\\
&\frac{1}{\mathsf{S}}\sum_{\mathbf{q}_\parallel} F(\mathbf{q}_\parallel) = 1,
\end{aligned} \tag{311}$$

where $F(\mathbf{q}_\parallel)$ defines the angular spread of the pure quantum field.

We are interested only in situations where all carrier-related quantities vanish before the quantum excitation reaches the unexcited semiconductor structure. Under such conditions, Eq. (297) can be solved analytically giving

$$\Delta\langle B^\dagger_{\mathbf{q}_\parallel,q_\perp}B_{\mathbf{q}_\parallel,q'_\perp}\rangle = \Delta\langle B^\dagger_{\mathbf{q}_\parallel,q_\perp}B_{\mathbf{q}_\parallel,q'_\perp}\rangle_0\, \mathrm{e}^{\mathrm{i}(\omega_q-\omega_{q'})t}. \tag{312}$$

If we assume a narrow angular spread for the quantum excitation, i.e. $F(\mathbf{q}_\parallel) = \mathsf{S}\delta_{\mathbf{q}_\parallel,0}$, this together with Eq. (308) produces

$$\langle E(r_\perp,t)E(r'_\perp,t)\rangle = \langle E(r_\perp - ct)E(r'_\perp - ct)\rangle_{\text{quant}}. \tag{313}$$

Hence, the quantum excitation propagates in the same way as the classical one. This observation also shows that the choice (310) provides the same temporal and spectral features for the quantum and classical excitations since the spatial features of the initial excitation are matched.

For our numerical examples, we use a quantum excitation into an angular window determined by $|\mathbf{q}_\parallel| < \Delta q$ where $\Delta q = (\omega_0/c)\sin\Delta\theta$ is defined by the central energy of the light $\hbar\omega_0 = 1.485\,\mathrm{eV}$ and the angular resolution $\Delta\theta$ of the excitation. For this configuration, $F(\mathbf{q}_\parallel) = (4\pi/\Delta q^2)\theta(\Delta q - |\mathbf{q}_\parallel|)$. As the material parameters are inserted, we find that the full 90° optical window corresponds to the maximum in-plane photon momentum $q_0 a_0 = 0.094$. In the computations, we use either $\Delta\theta = 45°$ or 90°. The spectral and temporal properties of the excitation are chosen to be a pulsed Gaussian excitation with

$$\langle E_0(q)\rangle_{\mathrm{pulsed}} = E_0\, \mathrm{e}^{(q-q_0)^2/\Delta Q^2}\, \mathrm{e}^{-\mathrm{i}qr_{\perp,0}}. \tag{314}$$

The spectral width and the temporal duration of the excitation is defined by ΔQ, its central frequency is given by $\omega_0 = cq_0$, and the intensity is controlled by $|E_0|^2$. The pulse is launched at $r_{\perp,0}$ which is far away from the planar semiconductor structure.

In the following, we present examples where we solve the full singlet–doublet dynamics, including the SLE, for the same QWI system used in the previous sections. These self-consistent computations allow us to determine what kind of quasi-particle states are generated via quantum vs. classical excitation pulses. Before the exciting light enters the semiconductor, it is assumed to be completely uncorrelated with the electronic system. Such situations are realized with all excitation sources that are external to and independent of the excited system. Similarly, the phonon system is assumed to be initially uncorrelated with both photons and carriers. As a result, the total density matrix $\hat{\rho}_{\mathrm{tot}}$ separates into light, phonon, and electronic parts i.e. $\hat{\rho}_{\mathrm{tot}} = \hat{\rho}_{\mathrm{light}} \otimes \hat{\rho}_{\mathrm{phonons}} \otimes \hat{\rho}_{\mathrm{electrons}}$ before the interactions take place. The specific form of $\hat{\rho}_{\mathrm{light}}$ follows from Eq. (300) or (302) and the phonon system is chosen to act as a thermal bath where the phonon occupations follow a Bose–Einstein distribution. The many-body features of the electronic system can be investigated in its purest form when we assume that the semiconductor before the excitation is in its ground state $|G\rangle$. Thus, we choose $\hat{\rho}_{\mathrm{electrons}} = |G\rangle\langle G|$ in our analysis. As the light interacts with the semiconductor, non-trivial electron–photon–phonon correlations build up.

9.6. Classical vs. quantum excitation

We now investigate the differences in the generated system of semiconductor quasi-particle excitations after classical or quantum excitations. In particular, we are interested to determine to which degree a quantum-degenerate 1*s*-exciton state can be generated via quantum excitation. We concentrate here on resonant 1*s*-excitation conditions since our studies in Section 6 indicate that for not too high intensities the corresponding classical pumping can produce an appreciable 1*s*-exciton fraction.

The numerical results for the classical excitation dynamics are presented in Fig. 40a where the optical pulse (dashed line, scaled), the induced optical polarization $|P|^2$ (shaded area, scaled), and the resulting density of bright 1*s* excitons (solid line) are shown. As in our earlier analysis in Section 6, the coherent excitation creates a polarization that eventually decays exponentially. Mostly via acoustical phonon interaction, a part of the polarization is converted into a 1*s*-exciton population. However, the density of optically active excitons, with $|\mathbf{q}_\parallel a_0| < 0.094$, remains rather low which suggest that a large fraction

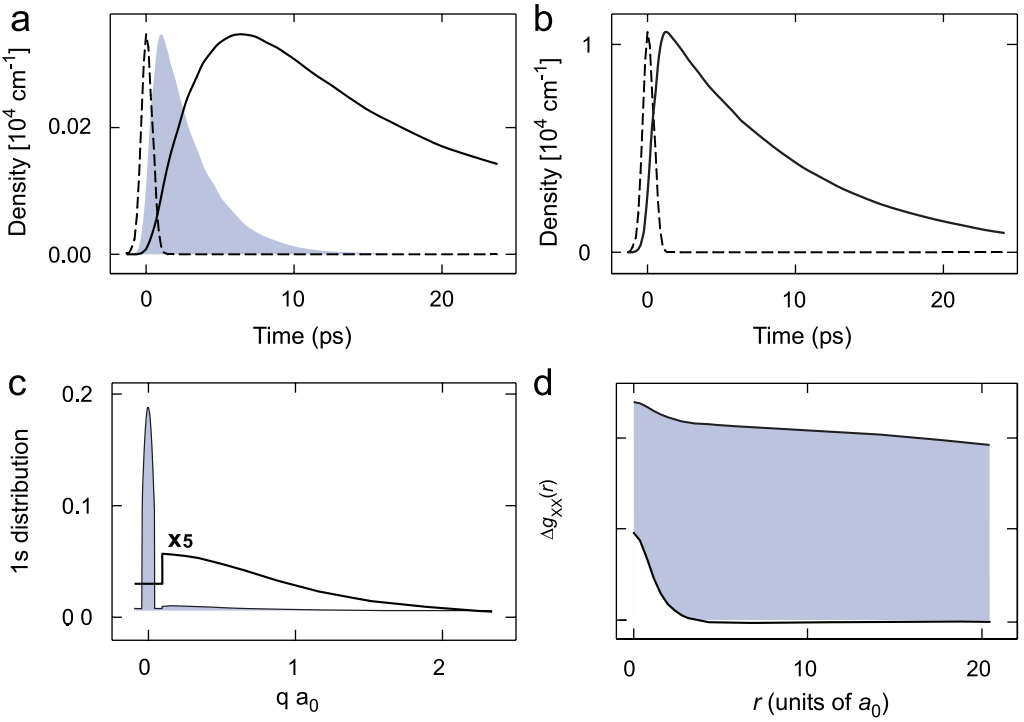

Fig. 40. Comparison of the excitation dynamics resulting from excitation with pulsed quantum and classical pump light. (a) Classical excitation; the optical excitation pulse (dashed line, scaled) is shown together with the optical polarization $|P|^2$ (shaded area, scaled), and the optically active 1*s*-exciton population (solid line). (b) Quantum excitation; the incoherent excitation pulse (dashed line, scaled) is presented together with the generates density of optically active 1*s* excitons (solid line). (c) The generated $\Delta N_{1s}(q_\parallel)$ resulting from quantum (shaded area) and classical excitation (solid line, multiplied by 5) 11 ps after pulse maximum. (d) The exciton–exciton pair-correlation function is shown as function of electron–hole-pair distance r (after Ref. [36]).

of the excitons is in dark states. Indeed, the final 1*s* distribution, presented as solid line in Fig. 40c, indicates a wide spread in momentum states and a pronounced depletion for small momentum states, in full agreement with Fig. 38.

An example for a quantum excitation is shown in Fig. 40b where we assumed an excitation pulse (dashed line, scaled) with thermal quantum statistics but otherwise the same properties as the classical pulse in Fig. 40a. The generated density of optically active 1*s* excitons is plotted as solid line. Its dynamics reveals a striking new phenomenon; *the quantum excitation by-passes the polarization-to-population conversion completely by directly generating an exciton population*. We also notice that the density of optically active excitons is significantly larger than that obtained after coherent excitation suggesting that the generated excitons predominantly occupy the states with nearly vanishing momentum. To verify this, $\Delta N_{1s}(\mathbf{q}_\parallel)$, corresponding to the quantum excitation, is presented in Fig. 40b as shaded area. Compared with the classical result, $\Delta N_{1s}(\mathbf{q}_\parallel)$ is now almost singular showing that a macroscopic occupation of the lowest momentum states is reached.

To resolve whether the generated quasi-particle state possesses long-range order, we investigate the pair-correlation function

$$\Delta g_{\mathrm{XX}}(\mathbf{r}_\parallel) \equiv \mathcal{A}\langle P^\dagger(\mathbf{r}_\parallel)P(0)\rangle, \quad P(\mathbf{r}) \equiv \frac{1}{S}\sum_{\mathbf{k}_\parallel,\mathbf{k}'_\parallel} a^\dagger_{v,\mathbf{k}_\parallel} a^\dagger_{c,\mathbf{k}'_\parallel} e^{i(\mathbf{k}'_\parallel-\mathbf{k}_\parallel)\cdot\mathbf{r}_\parallel}, \tag{315}$$

where $P(\mathbf{r}_\parallel)$ annihilates an electron–hole pair at the position $\mathbf{r}_\parallel$. The function $\Delta g_{\mathrm{XX}}(\mathbf{r}_\parallel)$ is fully determined by the two-particle correlations which tell how an electron–hole pair at position $\mathbf{r}_\parallel$ is correlated with another pair at $\mathbf{r}'_\parallel = 0$. Thus, a spatial extension of $\Delta g_{\mathrm{XX}}(\mathbf{r}_\parallel)$ to large distances implies that electron–hole-pair correlations exhibit long-range order. From a practical point of view, $\Delta g_{\mathrm{XX}}(\mathbf{r}_\parallel)$ is a two-particle quantity that can be evaluated exactly from the doublet correlations by using

$$\Delta g_{\mathrm{XX}}(\mathbf{r}_\parallel) = \frac{1}{S^2}\sum_{\mathbf{k}_\parallel,\mathbf{k}'_\parallel,\mathbf{q}_\parallel} c_X^{\mathbf{q}_\parallel,\mathbf{k}'_\parallel,\mathbf{k}_\parallel} e^{-i\mathbf{q}_\parallel\cdot\mathbf{r}_\parallel}. \tag{316}$$

Fig. 40d shows the numerical result for $\Delta g_{\mathrm{XX}}(\mathbf{r}_\parallel)$. We see that the quantum excitation (shaded area) leads to long-range order which is not the case for classical excitation (solid line). Hence, we conclude that the *thermal quantum excitation generates a quantum-degenerate exciton state, i.e. an exciton condensate.*

The condensate in Fig. 40 is directly coupled to the light field such that the entire population recombines radiatively. This radiative decay of the exciton condensate is depicted in Fig. 41a (b) on a linear (semilog) scale for the quantum excitation used in Fig. 40. We observe that the generated distribution remains ultra narrow during its entire lifetime and only a small tail develops toward high-momentum states. Thus, the exciton state remains degenerate throughout its radiative decay indicating that the exciton condensate experiences an anomalous reduction of Coulomb and phonon scattering. In addition, the semi-logarithmic presentation of the distributions nicely identifies that excitons, having momentum below $|qa_0| = 0.047$, belong to the condensate generated by the quantum excitation with the 45° angular resolution. The remaining bright excitons are found within $0.047 \leqslant |qa_0| \leqslant 0.094$ corresponding to the angles 45°–90° in the optical cone.

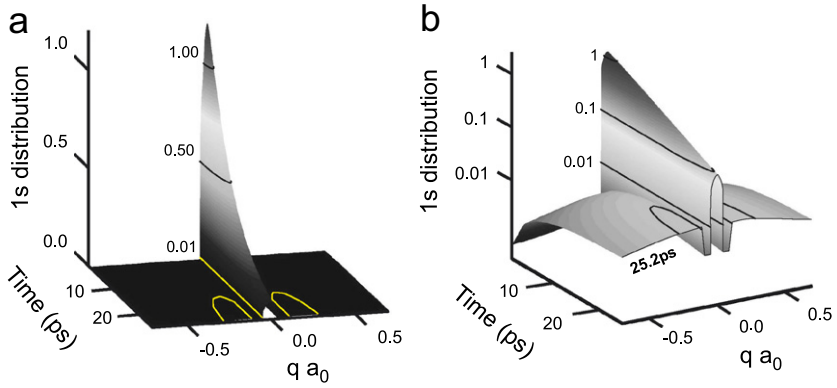

Fig. 41. Computed dynamics of the exciton condensate after pulsed quantum excitation used in Fig. 40. (a) The evolution of the 1*s*-exciton distribution $\Delta N_{1s}(\mathbf{q}_\parallel)$ is shown as function of time. (b) Same data presented on a semilogarithmic scale (after Ref. [36]).

Both, the condensate and the other bright excitons decay radiatively while the rest of the excitons with higher momenta are optically dark. Furthermore, $\Delta N_{1s}(\mathbf{q}_{\parallel})$ approaches more and more a delta function as the angular spread of the quantum excitation approaches 0°. For example, a two-orders of magnitude higher and narrower ΔN_{1s} is reached by simply using an 0.45° angular resolution instead of the 45° angular resolution as in Figs. 40 and 41.

9.7. Emission from the condensate

The macroscopic exciton population not only exhibits an anomalous reduction of scattering but it also displays unusual quantum emission. As an illustration, we present in Fig. 42a the computed luminescence, I_{PL}, into the direction allowed for the condensate emission (solid line) and into the remaining bright directions (hatched area). Here, we assumed the same pulsed quantum excitation as in Figs. 40 and 41. For comparison, the dashed line indicates the PL after the coherent excitation used in Fig. 40. Under these coherent excitation conditions, the PL is essentially the same in all directions such that we need only one direction to characterize its magnitude. To quantify the level of degeneracy after the quantum excitation, Fig. 42b also presents the time evolution of occupations for the exciton condensate (solid line), the bright excitons (hatched area), and the dark excitons (dark area) resulting from the quantum excitation.

We observe from Fig. 42a that the quantum excitation produces condensate emission which is more than two orders of magnitude larger than the emission in any other direction. The same ratio is found for the populations in Fig. 42b. Thus, we can correlate the strongly directional quantum emission directly with the highly singular exciton distributions. We also notice that the exciton distribution remains singular during its whole decay dynamics after the quantum excitation. Since the classical excitation does not produce a strongly peaked exciton population (see Fig. 40c), the used coherent excitation yields only a weak and mostly non-directional PL. Hence, *strong focusing of PL into one singular direction is a clear indication of the presence of exciton condensate*.

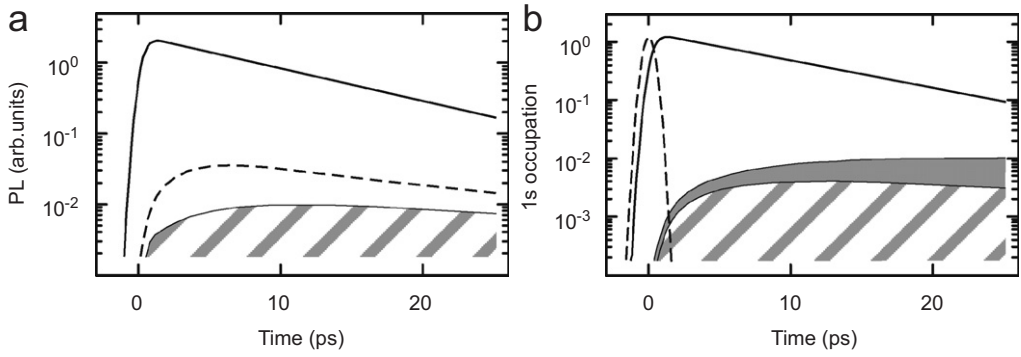

Fig. 42. (a) Quantum emission after pulsed quantum excitation. The evolution of the total luminescence $I_{\mathrm{PL}}(q)$ is presented for the emission direction allowed for the condensate (solid line) and the remaining bright excitons (hatched area). For comparison, we also plot the total luminescence resulting from the classical excitation in Fig. 40 as dashed line. (b) The corresponding occupations are plotted for the exciton condensate with $\Delta N_{1s}(0)$ (solid line), the remaining bright excitons with $\Delta N_{1s}(0.08)$ (hatched area), and the dark excitons (dark area) with $\Delta N_{1s}(0.2)$. The temporal dynamics of the quantum pump is displayed as the dashed line (after Ref. [36]).

In addition, we observe that the quantum excitation leads to orders of magnitude stronger PL in comparison with the classical excitation. As a consequence of this enhanced quantum emission, it is clear that PL from the seeded exciton condensate can be detected for much lower excitation levels than those needed for classical or non-resonant excitation schemes. It is interesting to notice that the enhanced coupling of the exciton condensate to the light field also implies a radiative decay of the quasi-particle excitations which is faster than that observed after classical or non-resonant excitations. After quantum excitation, the entire excitation decays with the radiative decay constant of the condensate studied in Fig. 40. Consequently, the excitation vanishes in some tens of picoseconds. In comparison with this, classical light generates quasi-particle excitations that remain in the system typically for nanoseconds due to the strongly reduced radiative coupling of the overall quasi-particle population.

We test the stability of the seeded exciton condensate by evaluating the 1*s*-exciton distribution, $\Delta N_{1s}(\mathbf{q}_\parallel)$, as function of the excitation intensity $\Delta I \equiv \Delta\langle B^\dagger B\rangle$ at 4 K. To have a clearer analysis, we use the full optical cone (0°–90°) in the excitation and assume $\frac{1}{10}$ reduction of the radiative coupling compared with Fig. 40. The result is presented in Fig. 43a showing that the degenerate state is remarkably stable against the increased scattering usually occurring at higher excitation levels. For similar excitation levels, classical excitation leads to configurations that suffer appreciable excitation-induced dephasing. Thus, we can conclude that *quantum excitation produces an anomalous reduction in the scattering even at high levels of excitation*.

Fig. 43a also shows that the population of the 1*s* state continuously increases up to the intensity level $\Delta I = 10$ which corresponds to a generated carrier density with $na_0 = 0.1$. For even higher excitation levels, the 1*s*-exciton population starts to decrease because the underlying Fermionic character of the electron–hole pairs gradually prevents the further exciton accumulation. The quantum-degenerate state ceases to exist above $\Delta I = 31$ with $na_0 = 0.3$. In other words, the macroscopic population is reduced even though the intensity of the excitation is increased. This phenomenon can be attributed predominantly to the

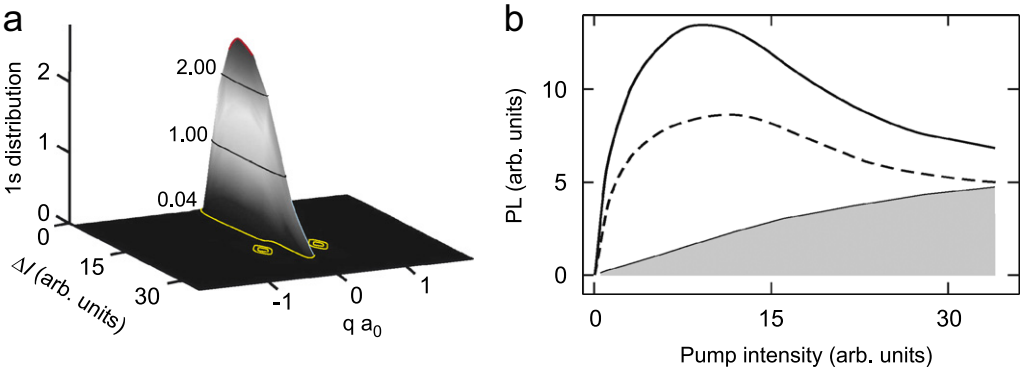

Fig. 43. (a) Stability of the exciton condensate after quantum excitation. The distribution $\Delta N_{1s}(q)$ is shown as function of the intensity of the quantum excitation. (b) The computed total photoluminescence $I_{\mathrm{PL}}(0)$ in the direction allowed for the condensate resulting from a mixture of pulsed classical and quantum excitations. The excitations have the same temporal dynamics as in Fig. 40 and the luminescence is determined 16 ps after the pulse maximum. The results of a full quantum excitation (solid line) are compared with 40% coherent (dashed line) and 100% coherent, i.e. fully classical, (shaded area) excitations (after Ref. [36]).

Fermionic blocking effects. We also notice that the 1*s*-exciton distribution remains remarkably narrow up to the largest densities. This again indicates that the quantum-source generated condensates experience an anomalous reduction of scattering even when the carrier density becomes appreciably high.

9.8. Exciton condensate under non-ideal conditions

Since our theory can also be applied for the cases where one mixes quantum and classical excitation schemes, we now investigate to which degree the predicted quantum effects are stable against the level of classical components in the pump source. As an example, we show in Fig. 43b the total luminescence as function of the pump intensity for pure quantum excitation (solid line), mixed excitation with 40% coherent part (dashed line), and fully classical excitation with 100% coherent part (shaded area). To have a one-to-one comparison, we use temporally and spectrally the same pump pulses as in Fig. 40. We see that for the relatively low levels of excitation studied here, the total luminescence for the 100% coherent—i.e. classical excitation—case exhibits the expected practically linear dependence on the excitation strength. However, when we include an incoherent quantum component to the excitation process, I_{PL} behaves nonmonotonously. Even more so, for weak to moderate intensities, the quantum excitation scheme leads to light emission that is enhanced by orders of magnitude in comparison with that of classical excitation.

If we now return to the quantitative analysis, we observe that the luminescence is maximized at the intensity level $\Delta I = 10$ corresponding to the maximum singularity of exciton distributions in Fig. 43a for 100% incoherent quantum excitation. Since the population of the zero momentum state decreases for elevated intensities, the luminescence decreases also until it reaches the same level as that for coherent excitation. This predicted distinctly non-monotonic behavior of I_{PL} should be directly observable in experiments, serving as a clear signature for the formation of the quantum-degenerate exciton state. We note in Fig. 43b, that I_{PL} has a maximum even in the presence of 40% coherent excitation, indicating that an appreciable population in the quantum-degenerate state is generated even in this imperfect case.

In the remainder of this section, we now discuss how the exciton condensate behaves if we assume different non-ideal conditions that are likely to be encountered in real experiments. We first investigate the stability of the exciton condensate as the lattice temperature is increased. Fig. 44a shows the computed 1*s*-exciton distribution, $\Delta N_{1s}(\mathbf{q})$, for four different lattice temperatures. Otherwise, this analysis is performed for the same initial conditions as those used in Fig. 43 in the low-excitation regime with $\Delta I = 0.5$. We observe that the degenerate state remains pronounced for all the lattice temperatures even though the degree of degeneracy is reduced for higher temperatures. To quantify the level of degeneracy, Fig. 44b presents the corresponding ratio of condensate- and dark-exciton occupations. We see that the condensate gradually diminishes for elevated temperatures due to increasing scattering with phonons while phonon scattering becomes orders of magnitude weaker as the temperature approaches zero. Hence, we conclude that the condensate is clearly observed for temperatures roughly below 10 K.

In fact, we do not observe an abrupt transition into or out of the condensate as function of lattice temperature or excitation density. Hence, the seeded condensate does not follow the typical thermodynamic Bose–Einstein condensation arguments. Instead, the light prepares the quasi-particle excitations into a quantum-degenerate state, which is clearly

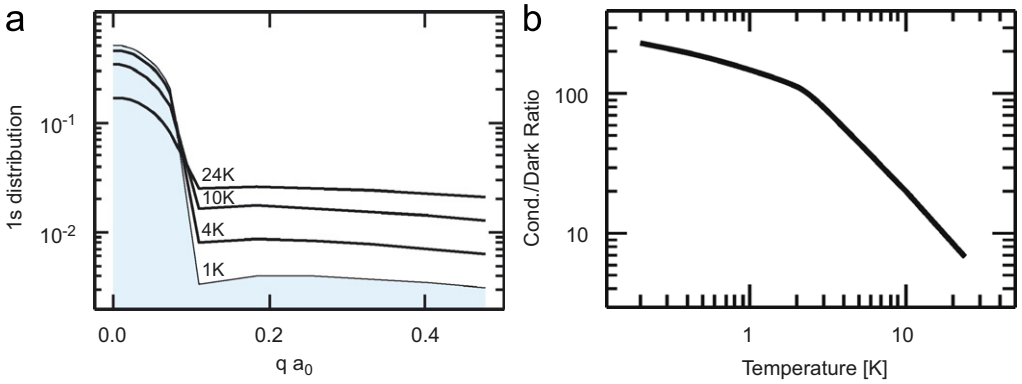

Fig. 44. Stability of the exciton condensate with respect to lattice temperature. (a) The computed $\Delta N_{1s}(q)$ is plotted 11 ps after the pulse maximum (see Fig. 40); the lattice temperature changes from 1 to 24 K (bottom to top). (b) The ratio of condensate and dark exciton occupation, $\Delta N_{1s}(0)/\Delta N_{1s}(0.2)$, is presented as function of lattice temperature (after Ref. [36]).

not a thermodynamic process. Fig. 44 shows that the survival of this seeded condensate depends on its scattering with the environment such that it can be gradually altered via the lattice temperature and/or the excitation level. At the same time, the scattering dynamics of the condensate is strongly altered by its quantum statistics which is controlled by the quantum statistics of the excitation. As a most vivid example, Fig. 43 demonstrates no appreciable increase in scattering as the intensity of the quantum excitation is elevated. Under otherwise identical conditions, a classical excitation yields an appreciable increase in dephasing due to the process of excitation-induced dephasing (see analysis of Section 5.10). We may consequently anticipate that the direct connection of quantum statistics and scattering opens up several possibilities to detect and control the condensate even with non-ideal conditions.

Clearly, one of the most important additional dephasing mechanisms results from the presence of disorder in the semiconductor system [76,146–155]. In a worst-case scenario, the disorder-related scattering may be independent of the quantum statistics of the condensate. However, even this does not prevent us from controlling and observing the effects related to the condensate and its quantum statistics because the overall scattering is a combination of disorder-, phonon-, and excitation-induced dephasing. The crystal quality of excellent present-day semiconductor samples is so high that one should easily be able to reach a regime where the excitation-induced dephasing effects dominate over all disorder-related effects, see e.g. Ref. [22]. For such samples, the optical response should display clear and characteristic signatures resulting from the quantum-statistics induced changes in the quasi-particle excitations. The key to such investigations is to use non-linear excitations where the classical pump creates a quasi-particle configuration that suffers from appreciable excitation-induced dephasing. In this intensity regime, one should be able to control the overall dephasing via the quantum statistics of the light since, e.g. a thermal quantum source produces an exciton condensate with the anomalous reduction in the excitation-induced dephasing. Thus, the *overall dephasing and the corresponding optical response depend strongly on the quantum statistics even for non-ideal conditions.*

In direct-gap semiconductors, the photon-momentum is directly transferred to the created electron–hole pairs. Since this momentum is small, the created state is automatically nearly degenerate. This momentum selectivity can be further enhanced in dimensionally confined semiconductor nanostructures where only the in-plane momentum transfer is conserved in the light–matter interaction. By using excitation with normal incidence in QWI and QW structures, the generated state is strongly confined to the zero momentum state, which provides the most ideal generation configuration for the condensate state. The numerical examples in this section concentrate on QWI systems. Nevertheless, the generation of an exciton condensate works analogously for QW systems [36,156]. In contrast to this, the condensate is always created into a small—but non-vanishing—momentum state in bulk systems. In addition, the bulk displays the well-known polariton propagation problem [157–159]. Hence, the seeded condensate investigations are simplest in QWI and QW systems.

In principle, the polariton problem does not exits for quantum-dot systems either. However, the quantum-dot states are discrete by definition such that it is not meaningful to discuss about condensates in this context. Nevertheless, quantum-optical excitations are interesting also for the dots. For example, one can expect to see new quantum-statistic dependent resonances in quantum-dot microcavity systems [38] according to the so-called rungs in the Jaynes-Cummings Ladder structure [160,161]. Also interesting single-photon emission, strong-coupling, and entanglement effects has already been measured [162–167]. First steps toward a cluster-expansion based quantum theory for dots is discussed e.g. in Ref. [168].

For the experimental realization of quantum-optical spectroscopy, one needs well-characterized sources of thermal light which can be reached e.g. by using the spectrally narrow spontaneous emission of other systems. There is also the theoretical prediction [121] that one can generate incoherent pulses by coherently controlling the spontaneous emission. Since it may be experimentally challenging to obtain temporally short incoherent light pulses, one can think of using excitations with a long incoherent, i.e. a quasi cw source with thermal statistics. Such excitation conditions can be directly implemented into our analysis by using the initial condition

$$\langle E_0(q)\rangle_{\mathrm{cw}} = \frac{E_0 \mathrm{e}^{-\mathrm{i}qr_{\perp,0}}}{\sinh[(q-q_0)/\Delta Q + \mathrm{i}\gamma_{\mathrm{cw}}]}, \tag{317}$$

where γ_{cw} defines the switch-on time of the field. In Ref. [36], we have shown that such quasi-cw pumping schemes can produce essentially the same exciton-condensate characteristics as the pulsed excitations.

Clearly, for experimental observations the detailed spectral, temporal, and directional diagnostics of the incoherent sources and the quantum emission are important. As a first step, one needs to verify that the quantum source has, e.g. a thermal statistics. From the point of view of the condensate, only that temporal mode that energetically matches with the 1*s* resonance is relevant. Thus, one only needs to verify that this single spectral mode is incoherent and displays thermal statistics. Since a spectral mode can also be understood as a temporal mode, the source must be thermal on a time scale corresponding to the excitonic dephasing time τ, which for typical GaAs samples, is in the range of 1–10 ps.

9.9. General principle of quantum-optical spectroscopy

For low enough carrier densities, the Fermionic substructure of the excitons is of reduced importance and one can assume predominantly Bosonic characteristics. In such situations, one may often omit higher-order scattering processes. Under these restrictions, one can show [36] that a given coherent or thermal source generates a quasi-particle state where the excitons have essentially the same quantum statistics as the exciting light field. For example, the analysis in Section 5.3 indicates that the coherent excitation produces a coherent exciton state, $|\Psi_{\rm coh}(t)\rangle = D[c]|G\rangle$, in the coherent limit according to Eqs. (145)–(146). Similarly, for the limit without scattering, Ref. [36] shows that thermal light generates an exciton condensate with the statistics of a thermal state. These observations lead to a more *general principle of quantum-optical spectroscopy* for direct-gap semiconductors:

(i) light seeds a quantum-degenerate quasi-particle state with nearly identical quantum statistics as that of the light,
(ii) the quantum statistics of the degenerate state determines how it interacts with other quasi-particles and states,
(iii) the properties of the state and its subsequent evolution show up in the quantum emission.

In atomic systems, quantum-degenerate states have been successfully realized via Bose–Einstein condensation [133–136]. Several impressive features like interference effects, long-range order, and entanglement have been observed [169,170]. As an even more intriguing feature, the degenerate state is internally an infinite-dimensional quantum object spanned by the number states of the harmonic oscillator. As our investigations show, exactly this quantum-statistical extension controls the character of interactions between the degenerate state and other states or systems. In atomic condensates, the connection of interactions and quantum statistics of number, squeezed, and coherent states has already been established experimentally [171]. The dependency of interactions on the quantum statistics is actually a general feature since, e.g. analogous quantum-state dependent quantum-Rabi oscillations have been predicted [160] and observed [161] between cavity photons and an atom. Since semiconductors inherently are strongly interacting systems, one would ultimately like to use a variety of degenerate states to explore and control the many-body interaction effects in solids via the different forms of the quantum states into which they can be excited.

10. Summary and outlook

In this review, we discuss many aspects related to the theoretical analysis of coherent and incoherent semiconductor spectroscopy and the optically generated and detected excitations states. Generally, it is by now widely accepted that optical spectroscopy is a very important and versatile tool for identifying and characterizing excitations and elementary interaction processes in a large variety of inorganic [1,27,98,172,173], organic [174,175], and biological [176–178] systems. Here, we focus on direct band-gap semiconductor systems where the light emission or absorption involves electron–hole-pair excitations. In particular, we show how a fully microscopic theory can be formulated

and applied to analyze the quasi-particle excitations for many experimentally relevant conditions.

After the presentation of the general theoretical framework, we devote Sections 5–8 to a detailed discussion of the phenomena that can be studied using spectroscopy with classical light, both in the optical and THz regime of the electromagnetic spectrum. These concepts are then generalized in Section 9 to the novel scheme of quantum-optical semiconductor spectroscopy where quantum-optical aspects of the excitation and the emission allow for an additional level of control and information. By solving the full many-body and quantum-optical correlations self-consistently, we apply these concepts to a variety of fascinating semiconductor problems, ranging from the formation and generation of excitons and exciton condensates to their interaction and scattering mechanisms.

In our comprehensive analysis of classical excitation configurations, we especially focus on the precise characterization of the particular quasi-particle states that are generated by light pulses with different frequencies and intensities. One emphasis here is on determining which role bound electron–hole pairs, i.e. true excitons, play under different conditions. We find that the coherent optical excitation induces a coherent interband polarization which may lead to the generation of populations via Coulomb and phonon scattering processes. This polarization-to-population conversion is shown to be very sensitive to the excitation frequency and the generated carrier density.

By performing the many-body analysis for a wide range of excitation parameters, we are able to map the phase space of the generated quasi-particle states. In particular, we find that resonant excitation at the 1*s*-absorption peak is efficiently converted into 1*s*-exciton populations. For 2*s* excitations, an interesting mix of 2*s* and 2*p* excitons is reached, and for non-resonant excitation no bound states are created; instead, we find a correlated electron–hole plasma. In this context, we show that the subsequent exciton formation is basically the same as that starting from an entirely uncorrelated electron–hole plasma population. On this basis, we perform an extensive study of exciton formation out of an incoherent plasma. Altogether, these investigations provide a detailed description of the quasi-particle excitation states reached after different optical excitations.

We also address how different the many-body states can be observed in actual measurements. Especially, we show that these states can be uniquely identified via their THz response. For a 1*s*-exciton population a distinct 1*s*-to-2*p* transition resonance is detected, whereas THz inversion and gain is observed for 2*s* excitation at low to moderate excitation intensities. For non-resonant excitation, a Drude-like response of an electron–hole plasma is obtained. Thus, it seems that a combination of optical excitations and response measurements combined with THz measurements should be a very efficient experimental tool to obtain detailed informations about the semiconductor system.

In Section 9, we explore the full potential of optical spectroscopy by utilizing the quantum-optical properties of light to expand the possibilities for generating desired quasi-particle states. Following up on this notion, we develop the concept of quantum-optical spectroscopy. With this method it should be possible to map the quantum statistical properties of the exciting light directly onto the generated state of the many-body excitations. Our calculations show that it should be possible to use experimentally accessible quantum-light sources to seed an exciton condensate which has a nearly singular momentum distribution leading to anomalously reduced Coulomb and phonon scattering. The quantum emission from this state is strongly enhanced, highly directional, and shows an unusual nonmonotonic intensity dependence.

Based on these ideas and concepts, it should be possible in the future to achieve a very high level of control and diagnostic capabilities by combining a sequence of classical, quantum-optical, and THz excitations to steer and monitor the many-body dynamics in solids. In this context, we expect that one should discover a new generation of spectroscopic, interferometric, and wave-mixing setups. Even though, we have so far investigated mostly GaAs-like material systems, it seems very interesting and promising to extend these studies also to other materials, such as wide-gap semiconductors, quantum dots, microcavities, photonic crystals, and many more. These kind of investigations should be directly possible based on the theoretical concepts discussed in this review.

Acknowledgements

This work was supported by the Deutsche Forschungsgemeinschaft through the Quantum Optics in Semiconductors Research Group and by the Optodynamics Center of the Philipps-Universität Marburg.

Appendix A. System Hamiltonian

In this Appendix, we summarize the details of the system Hamiltonian (18)–(21) for multiband QW and QWI systems. For this purpose, we generalize the notation such that the carrier index λ now also contains the subband index l. To emphasize the role of the confinement levels, we indicate the corresponding quantum number l explicitly. Using the general wavefunction Eq. (4) in the expansion of the field operator, Eq. (1), the Hamiltonian, Eqs. (18)–(21), can be written in the form

$$H_0 = \sum_{\lambda,l,\mathbf{k}_\parallel} \varepsilon^{\lambda,l}_{\mathbf{k}_\parallel} a^\dagger_{\lambda,\mathbf{k}_\parallel} a_{\lambda,\mathbf{k}_\parallel} + \sum_{\mathbf{q}_\parallel,q_\perp} \hbar\omega_{\mathbf{q}} \left[B^\dagger_{\mathbf{q}_\parallel,q_\perp} B_{\mathbf{q}_\parallel,q_\perp} + \frac{1}{2} \right] + \sum_{\mathbf{p}_\parallel,p_\perp} \hbar\Omega_{\mathbf{p}} \left[D^\dagger_{\mathbf{p}_\parallel,p_\perp} D_{\mathbf{p}_\parallel,p_\perp} + \frac{1}{2} \right], \tag{A.1}$$

$$H_{\mathrm{C}} = \frac{1}{2} \sum_{\substack{\lambda,\lambda',l \\ l',l'',l'''}} \sum_{\substack{\mathbf{k}_\parallel,\mathbf{k}'_\parallel \\ \mathbf{q}_\parallel \neq 0}} V^{\lambda,l,\lambda',l'}_{l'',l'''}|_{\mathbf{q}_\parallel} a^\dagger_{\lambda,l,\mathbf{k}_\parallel+\mathbf{q}_\parallel} a^\dagger_{\lambda',l',\mathbf{k}'_\parallel-\mathbf{q}_\parallel} a_{\lambda',l'',\mathbf{k}'_\parallel} a_{\lambda,l''',\mathbf{k}_\parallel}, \tag{A.2}$$

$$H_{\mathrm{D}} = -\mathrm{i}\hbar \sum_{\lambda,l,l'} \sum_{\mathbf{k}_\parallel,\mathbf{q}_\parallel} [B^{\lambda;l,l'}_{\mathbf{q}_\parallel,\Sigma} - (B^{\bar{\lambda}';l',l}_{-\mathbf{q}_\parallel,\Sigma})^\dagger] a^\dagger_{\lambda,l,\mathbf{k}_\parallel} a_{\bar{\lambda},l',\mathbf{k}_\parallel-\mathbf{q}_\parallel}, \tag{A.3}$$

$$H_{\mathrm{P}} = \hbar \sum_{\lambda,l,l'} \sum_{\mathbf{k}_\parallel,\mathbf{p}_\parallel} [D^{\lambda,l,l'}_{\mathbf{p}_\parallel,\Sigma} + (D^{\lambda,l',l}_{-\mathbf{p}_\parallel,\Sigma})^\dagger] a^\dagger_{\lambda,l,\mathbf{k}_\parallel} a_{\lambda,l',\mathbf{k}_\parallel-\mathbf{p}_\parallel}. \tag{A.4}$$

Here, the spin index is included implicitly in λ and λ'.

With the help of the confinement wavefunctions $\xi_{\lambda,l}(r_\perp)$, we can write the generalized QW Coulomb-matrix element as

$$V^{\lambda,l,\lambda',l'}_{l'',l'''}\Big|_{\mathbf{q}_\parallel} = \frac{e^2}{4\pi\varepsilon_0\varepsilon} \frac{1}{\mathsf{S}} \int \mathrm{d}r_\perp \, \mathrm{d}r'_\perp \, \mathrm{d}^2 r_\parallel \, \mathrm{e}^{-\mathrm{i}\mathbf{q}_\parallel \cdot \mathbf{r}_\parallel}$$

$$\times \frac{\xi^{\star}_{\lambda,l}(r_\perp)\xi^{\star}_{\lambda',l'}(r'_\perp)\xi_{\lambda',l''}(r'_\perp)\xi_{\lambda,l'''}(r_\perp)}{\sqrt{\mathbf{r}_\parallel^2+(r_\perp-r'_\perp)^2}}, \tag{A.5}$$

where S is the normalization area. Similarly, the light–matter interaction depends on the confinement index according to

$$B^{\lambda;l,l'}_{\mathbf{q}_\parallel,\Sigma} \equiv \sum_{q_\perp} \mathsf{F}^{\lambda;l,l'}_{\mathbf{q}_\parallel,q_\perp} B_{\mathbf{q}_\parallel,q_\perp}, \tag{A.6}$$

$$\mathsf{F}^{\lambda;l,l'}_{\mathbf{q}_\parallel,q_\perp} \equiv \frac{1}{\hbar}\, d^{\lambda,\bar{\lambda}}_{\mathbf{q}_\parallel,q_\perp} \mathsf{E}_{\mathbf{q}} \tilde{u}^{\lambda;l,l'}_{\mathbf{q}_\parallel,q_\perp}, \tag{A.7}$$

$$\tilde{u}^{\lambda;l,l'}_{\mathbf{q}_\parallel,q_\perp} = \frac{1}{\mathsf{S}} \int \mathrm{d}^2 r_\parallel\, \mathrm{d}r_\perp \xi^{\star}_{\lambda,l}(r_\perp)\xi_{\bar{\lambda},l'}(r_\perp) u_{\mathbf{q}_\parallel,q_\perp}(r_\perp)\, \mathrm{e}^{-\mathrm{i}\mathbf{q}_\parallel\cdot\mathbf{r}_\parallel}. \tag{A.8}$$

For the multi-band situation, the acoustic phonon interaction terms (30)–(31), are generalized as

$$\mathsf{G}^{\lambda,l,l'}_{\mathbf{p}} = \frac{F^{\lambda}}{\hbar} \sqrt{\frac{\hbar|\mathbf{p}|}{2c_{\mathrm{LA}}\rho \mathsf{L}^3}} \int \mathrm{d}r_\perp \xi^{\star}_{\lambda,l}(r_\perp)\xi_{\lambda,l'}(r_\perp)\, \mathrm{e}^{-\mathrm{i}\mathbf{q}_\perp\cdot r_\perp}, \tag{A.9}$$

$$D^{\lambda,l,l'}_{\mathbf{p}_\parallel,\Sigma} \equiv \sum_{p_\perp} \mathsf{G}^{\lambda,l,l'}_{\mathbf{p}_\parallel,p_\perp} D_{\mathbf{p}_\parallel,p_\perp}. \tag{A.10}$$

It is easy to see that Eqs. (A.1)–(A.10) reduce to Eqs. (18)–(31) in the limit of strong confinement. Furthermore, we notice that Eqs. (A.1)–(A.10) and Eqs. (18)–(31) are structurally similar such that all the derivations made for the two-band QW can be extended directly to multi-band systems by implementing the confinement index in the final steps of the derivations.

The QWI system can be treated analogously to the QW case by simply replacing the vectorial carrier momentum $\mathbf{k}_\parallel$ by the scalar $k_\parallel$ along the wire. In particular, the properties of the electrons in the lth QWI are determined by the Fermionic operators $a_{\lambda,l,k_\parallel}$ related to a Bloch electron propagating along the wire with momentum $k_\parallel$ in the band λ. The corresponding Bloch function is then

$$\phi_{\lambda,l,k_\parallel}(\mathbf{r}) = \xi_{\lambda,l}(\mathbf{r}_\perp)\, \frac{1}{\sqrt{\mathsf{L}}}\, \mathrm{e}^{\mathrm{i}k_\parallel r_\parallel} w_{\lambda,l,k_\perp}(\mathbf{r}), \tag{A.11}$$

where $\xi_{\lambda,l}(\mathbf{r}_\perp)$ is the confinement wavefunction of the wire l. Note that the in-plane direction is now scalar while the perpendicular direction is a vector due to the two-dimensional confinement. As a result, the wavefunction component related to the crystal-momentum is normalized with respect to the quantization length L.

If we now formally connect the wire index l with the confinement level index, Eqs. (A.1)–(A.4) produce directly the Hamiltonian for the QWI system

$$H_0 = \sum_{\lambda,l,k_\parallel} \varepsilon^{\lambda}_{k_\parallel} a^{\dagger}_{\lambda,l,k_\parallel} a_{\lambda,l,k_\parallel} + \sum_{\mathbf{q}_\parallel,q_\perp} \hbar\omega_{\mathbf{q}} \left[B^{\dagger}_{\mathbf{q}_\parallel,q_\perp} B_{\mathbf{q}_\parallel,q_\perp} + \frac{1}{2} \right]$$
$$+ \sum_{\mathbf{p}_\parallel,p_\perp} \hbar\Omega_{\mathbf{p}} \left[D^{\dagger}_{\mathbf{p}_\parallel,p_\perp} D_{\mathbf{p}_\parallel,p_\perp} + \frac{1}{2} \right], \tag{A.12}$$

$$H_{\mathrm{C}} = \frac{1}{2}\sum_{\lambda,\lambda',l}\sum_{k_\parallel,k'_\parallel,q_\parallel\neq 0} V_{q_\parallel} a^{\dagger}_{\lambda,l,k_\parallel+q_\parallel} a^{\dagger}_{\lambda',l,k'_\parallel-q_\parallel} a_{\lambda',l,k'_\parallel} a_{\lambda,l,k_\parallel}, \tag{A.13}$$

$$H_{\mathrm{D}} = -\mathrm{i}\hbar \sum_{\lambda,l,k_\parallel,q_\parallel} [B^{\lambda,l}_{q_\parallel,\Sigma} - (B^{\bar{\lambda},l}_{-q_\parallel,\Sigma})^{\dagger}] a^{\dagger}_{\lambda,k_\parallel} a_{\bar{\lambda},k_\parallel-q_\parallel}, \tag{A.14}$$

$$H_{\mathrm{P}} = \hbar \sum_{\lambda,l,k_\parallel,p_\parallel} [D^{\lambda,l}_{p_\parallel,\Sigma} + (D^{\lambda,l}_{-p_\parallel,\Sigma})^{\dagger}] a^{\dagger}_{\lambda,k_\parallel} a_{\lambda,k_\parallel-p_\parallel}. \tag{A.15}$$

Here we have assumed that all QWIs are identical except for their position. In the Coulomb interaction, we have applied the property that the confined wire states are electronically decoupled, i.e. we need to include only those Coulomb terms involving electrons within the same wire. As a result, the Coulomb-matrix element becomes

$$V_{q_\parallel} = \int \mathrm{d}^2 r_\perp \, \mathrm{d}^2 r'_\perp \, \mathrm{d}r_\parallel \, \frac{\mathrm{e}^2 |\xi(\mathbf{r}_\perp)|^2 |\xi(\mathbf{r}'_\perp)|^2}{4\pi\varepsilon_0\varepsilon \mathsf{S}\sqrt{r_\parallel^2 + (\mathbf{r}_\perp - \mathbf{r}'_\perp)^2}} \, \mathrm{e}^{-\mathrm{i}q_\parallel r_\parallel} \tag{A.16}$$

in the limit of strong confinement used here.

In analog to the QW expressions (A.6)–(A.8), the light–matter interaction can be presented compactly by introducing the collective photon-operator

$$B^{\lambda,l}_{q_\parallel,\Sigma} \equiv \sum_{\mathbf{q}_\perp} \mathsf{F}^{\lambda,l}_{q_\parallel,\mathbf{q}_\perp} B_{q_\parallel,\mathbf{q}_\perp}, \tag{A.17}$$

$$\mathsf{F}^{\lambda,l}_{q_\parallel,\mathbf{q}_\perp} \equiv \frac{1}{\hbar}\, \mathrm{d}^{\lambda}_{q_\parallel,\mathbf{q}_\perp} \mathsf{E}_{\mathbf{q}} \tilde{u}_{l,\mathbf{q}}, \tag{A.18}$$

$$\tilde{u}_{l,\mathbf{q}} = \frac{1}{\mathsf{L}} \int \mathrm{d}r_\parallel \, \mathrm{d}^2 r_\perp |\xi_l(\mathbf{r}_\perp)|^2 u_{q_\parallel,q_\perp}(r_\parallel, \mathbf{r}_\perp) \, \mathrm{e}^{-\mathrm{i}q_\parallel r_\parallel} \to u_{q_\parallel,q_\perp}(r_l, 0), \tag{A.19}$$

where r_l is the in-plane position and $\xi_l(\mathbf{r}_\perp)$ is the confinement wavefunction of the lth wire. The effective $\tilde{u}_{l,\mathbf{q}}$ approaches the mode function at the position r_l when the confinement is strong enough.

The interaction with the longitudinal acoustical phonons is described by the collective phonon operator,

$$D^{\lambda,l}_{p_\parallel,\Sigma} \equiv \sum_{\mathbf{p}_\perp} \mathsf{G}^{\lambda}_{p_\parallel,\mathbf{p}_\perp} D_{p_\parallel,\mathbf{p}_\perp}, \tag{A.20}$$

$$\mathsf{G}^{\lambda,l}_{\mathbf{p}} = \frac{F^{\lambda}}{\hbar} \sqrt{\frac{\hbar|\mathbf{p}|}{2c_{\mathrm{LA}}\rho \mathsf{L}^3}} \int \mathrm{d}^r_\perp |\xi_l(\mathbf{r}_\perp)|^2 \, \mathrm{e}^{-\mathrm{i}\mathbf{p}_\perp\cdot\mathbf{r}_\perp}. \tag{A.21}$$

We notice now the benefits of the implicit notation where we combine the wire number l implicitly with the band index, i.e. $(\lambda, l) \to \lambda$. This way, the QWI Hamiltonian becomes directly equivalent to that of the two-band QW. Thus, any further derivation performed explicitly for the QW structure can be easily generalized for the set of QWIs.

Appendix B. Implicit-notation formalism

When we perform the explicit factorizations according to Eq. (43) into clusters in Eq. (51), we end up with lengthy expressions for which an optimized notation scheme is desirable. For this purpose, we introduce an *implicit-notation formalism* that reduces the

amount of necessary labels for the band, sub-band, spin, and momentum indices into one generic symbol via the identification

$$\mathbf{k}_j \equiv a_{\lambda_j,\mathbf{k}_\parallel^{(j)}} = a_{\lambda_j,l_j,\sigma_j,\mathbf{k}_\parallel^{(j)}}, \quad \mathbf{k}_j^\dagger \equiv a^\dagger_{\lambda_j,\mathbf{k}_\parallel^{(j)}} = a^\dagger_{\lambda_j,l_j,\sigma_j,\mathbf{k}_\parallel^{(j)}},$$
$$\bar{\mathbf{k}}_j \equiv a_{\bar{\lambda}_j,\mathbf{k}_\parallel^{(j)}} = a_{\bar{\lambda}_j,l_j,\sigma_j,\mathbf{k}_\parallel^{(j)}}, \quad \bar{\mathbf{k}}_j^\dagger = a^\dagger_{\bar{\lambda}_j,\mathbf{k}_\parallel^{(j)}} = a^\dagger_{\bar{\lambda}_j,l_j,\sigma_j,\mathbf{k}_\parallel^{(j)}}. \tag{B.1}$$

This mapping allows us to uniquely identify the connection between the implicit label "j" and the full explicit index forms. The mapping is arranged such that the second form gives the separation into carrier type and its momentum while the last form expresses all indices explicitly. In addition, the "bar" in $\bar{\lambda}$ alters only the band index according to

$$\bar{c} = v, \quad \bar{v} = c, \tag{B.2}$$

as given earlier in Eq. (26). In our derivations, we label different values of j according to the notation rules

$$\lambda \equiv (\lambda_1, l_1, \sigma_1), \quad \lambda' \equiv (\lambda_{1'}, l_{1'}, \sigma_{1'}), \quad \mathbf{k}_\parallel \equiv \mathbf{k}_\parallel^{(1)} = \mathbf{k}_\parallel^{(1')},$$
$$v \equiv (\lambda_2, l_2, \sigma_2), \quad v' \equiv (\lambda_{2'}, l_{2'}, \sigma_{2'}), \quad \mathbf{k}'_\parallel \equiv \mathbf{k}_\parallel^{(2)} = \mathbf{k}_\parallel^{(2')},$$
$$\xi \equiv (\lambda_3, l_3, \sigma_3), \quad \xi' \equiv (\lambda_{3'}, l_{3'}, \sigma_{3'}), \quad \mathbf{k}''_\parallel \equiv \mathbf{k}_\parallel^{(3)} = \mathbf{k}_\parallel^{(3')}, \tag{B.3}$$

where we notice that the "prime" in $j = 1', 2', 3'$ changes the band index while the momentum index is unchanged.

Besides the different combinations of $\mathbf{k}_j^\dagger$ and $\mathbf{k}_j$, also sums of different momenta appear in the general singlet–doublet dynamics. For these situations, we introduce the convention that the labels j (or j') always define the band indices. Thus, we introduce the following compact notation rules for annihilation operators

$$\mathbf{k}_{1\mathbf{q}} \equiv a_{\lambda,\mathbf{k}_\parallel-\mathbf{q}_\parallel}, \quad \mathbf{k}_{1\mathbf{l}} \equiv a_{\lambda,\mathbf{k}_\parallel-\mathbf{l}_\parallel}, \quad \mathbf{k}_{1\mathbf{p}} \equiv a_{\lambda,\mathbf{k}_\parallel-\mathbf{p}_\parallel},$$
$$\mathbf{k}_{1(\mathbf{q}\pm\mathbf{l})} \equiv a_{\lambda,\mathbf{k}_\parallel-(\mathbf{q}_\parallel\pm\mathbf{l}_\parallel)}, \quad \mathbf{k}_{1'\mathbf{q}} \equiv a_{\lambda',\mathbf{k}_\parallel-\mathbf{q}_\parallel}, \quad \mathbf{k}_{1'\mathbf{l}} \equiv a_{\lambda',\mathbf{k}_\parallel-\mathbf{l}_\parallel},$$
$$\mathbf{k}_{1'\mathbf{p}} \equiv a_{\lambda',\mathbf{k}_\parallel-\mathbf{p}_\parallel}, \quad \mathbf{k}_{1'(\mathbf{q}\pm\mathbf{l})} \equiv a_{\lambda',\mathbf{k}_\parallel-(\mathbf{q}_\parallel\pm\mathbf{l}_\parallel)}, \quad \mathbf{k}_{2\mathbf{q}} \equiv a_{v,\mathbf{k}'_\parallel+\mathbf{q}_\parallel},$$
$$\mathbf{k}_{2\mathbf{l}} \equiv a_{v,\mathbf{k}'_\parallel+\mathbf{l}_\parallel}, \quad \mathbf{k}_{2\mathbf{p}} \equiv a_{v,\mathbf{k}'_\parallel+\mathbf{p}_\parallel}, \quad \mathbf{k}_{2(\mathbf{q}\pm\mathbf{l})} \equiv a_{v,\mathbf{k}'_\parallel+(\mathbf{q}_\parallel\pm\mathbf{l}_\parallel)},$$
$$\mathbf{k}_{3\mathbf{q}} \equiv a_{\xi,\mathbf{k}''_\parallel-\mathbf{q}_\parallel}, \quad \mathbf{k}_{3\mathbf{l}} \equiv a_{\xi,\mathbf{k}''_\parallel-\mathbf{l}_\parallel}. \tag{B.4}$$

The compact notation for the creation operators has an equivalent form where the added vectors $\mathbf{q}_\parallel$, $\mathbf{l}_\parallel$, $\mathbf{p}_\parallel$, and $(\mathbf{q}_\parallel \pm \mathbf{l}_\parallel)$ are presented in the subindex. These special forms are chosen because we need in our derivations only these momentum combinations.

In Eq. (90) we identified

$$\mathbf{j}_\parallel \equiv \mathbf{k}'_\parallel + \mathbf{q}_\parallel - \mathbf{k}_\parallel \tag{B.5}$$

as an important momentum combination. This appears occasionally together with $\mathbf{k}_1$ or $\mathbf{k}_2$ in a sum form

$$\mathbf{k}_{1\mathbf{j}} \equiv a_{\lambda,\mathbf{k}_\parallel+\mathbf{j}_\parallel} = a_{\lambda,\mathbf{k}'_\parallel+\mathbf{q}_\parallel} = \mathbf{k}_{2\mathbf{q},\lambda}, \quad \mathbf{k}_{1'\mathbf{j}} = \mathbf{k}_{2\mathbf{q},\lambda'},$$
$$\mathbf{k}_{2\mathbf{j}} \equiv a_{v,\mathbf{k}'_\parallel-\mathbf{j}_\parallel} = a_{v,\mathbf{k}_\parallel-\mathbf{q}_\parallel} = \mathbf{k}_{1\mathbf{q},v}, \quad \mathbf{k}_{2'\mathbf{j}} = \mathbf{k}_{1\mathbf{q},v'}, \tag{B.6}$$

which introduces the last rule in our implicit-notation scheme: whenever the band index is expressed explicitly, it overrides any other notation definition. In general, the relations (B.6) allow us to connect different $\mathbf{q}_\parallel$ and $\mathbf{j}_\parallel$ dependent terms.

The usefulness of the implicit-notation formalism becomes more transparent when we present the system Hamiltonian (18)–(21) with the help of the relations (B.1)–(B.4),

$$H_{\rm sys} = \sum_{\lambda,\mathbf{k}_\parallel} \varepsilon^\lambda_{\mathbf{k}_\parallel} \mathbf{k}^\dagger_1 \mathbf{k}_1 + \sum_{\mathbf{q}} \hbar\omega_{\mathbf{q}} \left[B^\dagger_{\mathbf{q}} B_{\mathbf{q}} + \frac{1}{2} \right] + \sum_{\mathbf{p}} \hbar\Omega_{\mathbf{p}} \left[D^\dagger_{\mathbf{p}} D_{\mathbf{p}} + \frac{1}{2} \right] + \frac{1}{2} \sum_{\mathbf{k}_1,\mathbf{k}_2,\mathbf{q}_\parallel \neq 0} V_{\mathbf{q}_\parallel} \mathbf{k}^\dagger_1 \mathbf{k}^\dagger_2 \mathbf{k}_{2\mathbf{q}} \mathbf{k}_{1\mathbf{q}} - \sum_{\mathbf{k}_1,\mathbf{q}_\parallel} E^\lambda_{\mathbf{q}_\parallel} \mathbf{k}^\dagger_1 \bar{\mathbf{k}}_{1\mathbf{q}} + \sum_{\mathbf{k}_1,\mathbf{p}_\parallel} Q^\lambda_{\mathbf{p}_\parallel} \mathbf{k}^\dagger_1 \mathbf{k}_{1\mathbf{p}}. \tag{B.7}$$

Here,

$$E^\lambda_{\mathbf{q}_\parallel} \equiv \mathrm{i}\hbar[B^\lambda_{\mathbf{q}_\parallel,\Sigma} - (B^{\bar{\lambda}}_{-\mathbf{q}_\parallel,\Sigma})^\dagger], \quad Q^\lambda_{\mathbf{p}_\parallel} \equiv \hbar[D^\lambda_{\mathbf{p}_\parallel,\Sigma} + (D^\lambda_{-\mathbf{p}_\parallel,\Sigma})^\dagger], \tag{B.8}$$

are identified according to Eqs. (63)–(64). One may use Eqs. (A.6) and (A.9) to write $E^\lambda_{\mathbf{q}_\parallel}$ and $Q^\lambda_{\mathbf{p}_\parallel}$ completely explicitly.

In the form of Eq. (B.7), the Hamiltonian is significantly more compact than the original $H_{\rm sys}$. Thus, we may anticipate that the implicit-notation formalism considerably simplifies the expressions in the operator dynamics, Eqs. (33)–(35) and (40)–(41). Indeed, they reduce into

$$\mathrm{i}\hbar \frac{\partial}{\partial t} B_{\mathbf{q}} = \hbar\omega_q B_{\mathbf{q}} + \mathrm{i}\hbar \sum_{\mathbf{k}_1} [\mathsf{F}^\lambda_{\mathbf{q}}]^\star \mathbf{k}^\dagger_{1\mathbf{q}} \bar{\mathbf{k}}_1, \tag{B.9}$$

$$\mathrm{i}\hbar \frac{\partial}{\partial t} B^\dagger_{\mathbf{q}} = -\hbar\omega_q B^\dagger_{\mathbf{q}} + \mathrm{i}\hbar \sum_{\mathbf{k}_1} \mathsf{F}^\lambda_{\mathbf{q}} \bar{\mathbf{k}}^\dagger_1 \mathbf{k}_{1\mathbf{q}}, \tag{B.10}$$

$$\mathrm{i}\hbar \frac{\partial}{\partial t} D_{\mathbf{p}} = \hbar\Omega_{\mathbf{p}} D_{\mathbf{p}} + \hbar \sum_{\mathbf{k}_1} G^\lambda_{\mathbf{p}} \mathbf{k}^\dagger_{1\mathbf{p}} \mathbf{k}_1, \tag{B.11}$$

$$\mathrm{i}\hbar \frac{\partial}{\partial t} D^\dagger_{\mathbf{p}} = -\hbar\Omega_{\mathbf{p}} D^\dagger_{\mathbf{p}} - \hbar \sum_{\mathbf{k}_1} G^\lambda_{\mathbf{p}} \mathbf{k}^\dagger_1 \mathbf{k}_{1\mathbf{p}}. \tag{B.12}$$

$$\mathrm{i}\hbar \frac{\partial}{\partial t} \mathbf{k}_1 = \varepsilon^\lambda_{\mathbf{k}_\parallel} \mathbf{k}_1 + \sum_{\mathbf{k}_2,\mathbf{l}_\parallel} V_{\mathbf{l}_\parallel} \mathbf{k}^\dagger_2 \mathbf{k}_{2\mathbf{l}} \mathbf{k}_{1\mathbf{l}} - \sum_{\mathbf{q}_\parallel} E^\lambda_{\mathbf{q}_\parallel} \bar{\mathbf{k}}_{1\mathbf{q}} + \sum_{\mathbf{p}_\parallel} Q^\lambda_{\mathbf{p}_\parallel} \mathbf{k}_{1\mathbf{p}}, \tag{B.13}$$

$$\mathrm{i}\hbar \frac{\partial}{\partial t} \mathbf{k}^\dagger_1 = -\varepsilon^\lambda_{\mathbf{k}_\parallel} \mathbf{k}^\dagger_1 - \sum_{\mathbf{k}_2,\mathbf{l}_\parallel} V_{\mathbf{l}_\parallel} \mathbf{k}^\dagger_{1\mathbf{l}} \mathbf{k}^\dagger_{2\mathbf{l}} \mathbf{k}_2 + \sum_{\mathbf{q}_\parallel} E^{\bar{\lambda}}_{-\mathbf{q}_\parallel} \bar{\mathbf{k}}^\dagger_{1\mathbf{q}} - \sum_{\mathbf{p}_\parallel} Q^\lambda_{-\mathbf{p}_\parallel} \mathbf{k}^\dagger_{1\mathbf{p}}. \tag{B.14}$$

We notice that each of these equations has now a compact presentation. Generally, the compact notation considerably helps us to simplify the book-keeping in any actual derivation.

Appendix C. Relevant singlet–doublet factorizations

In this Appendix, we present the factorization rules needed to derive the explicit forms for the generic singlet–doublet dynamics (51). The starting point is the consistent cluster-expansion factorization (43). In order to present the resulting equations in an efficient form, we apply the implicit-notation formalism introduced in Appendix B.

Before we explicitly discuss the factorizations, we present a simple scheme to deduce photon- or phonon-operator factorizations from pure carrier-operator terms. This can be done by using the formal analogy (37)–(38) between a generic Boson (either a photon or phonon) operator b and a pair of Fermion operators. In other words, we introduce a formal Boson-to-Fermion mapping

$$b \equiv \mathbf{k}_\alpha^\dagger \mathbf{k}_\beta, \quad b^\dagger \equiv \mathbf{k}_\beta^\dagger \mathbf{k}_\alpha, \tag{C.1}$$

where $\mathbf{k}_\alpha^\dagger \mathbf{k}_\beta$ indicates which Fermion operators are connected with the Boson operator according to Eqs. (37)–(38). At this point, Eq. (C.1) is a purely notational identification which should not be used in actual calculations to replace the true Boson operators. However, this notation becomes useful when we explicitly write the general factorization of N-particle expectation values into different clusters.

C.1. Two-particle factorizations

The singlet dynamics of Eq. (51) involves the factorization of the two-particle terms. With the help of the Hartree–Fock factorization, Eq. (44), we find the single-particle factorization

$$\langle \mathbf{k}_1^\dagger \mathbf{k}_\alpha^\dagger \mathbf{k}_\beta \mathbf{k}_4 \rangle_S = \langle \mathbf{k}_1^\dagger \mathbf{k}_4 \rangle \langle \mathbf{k}_\alpha^\dagger \mathbf{k}_\beta \rangle - \langle \mathbf{k}_1^\dagger \mathbf{k}_\beta \rangle \langle \mathbf{k}_\alpha^\dagger \mathbf{k}_4 \rangle \tag{C.2}$$

for pure carrier operators. This can be used directly to identify the singlet contributions of the expectation values with one or two Boson operators. If $\mathbf{k}_\alpha^\dagger \mathbf{k}_\beta \equiv O$ is a Boson operator (photon or phonon), it is natural to demand that $\mathbf{k}_\alpha^\dagger \mathbf{k}_\beta$ cannot be separated since a given Boson operator cannot be decomposed into lower-level operator elements. If this constraint is applied, Eq. (C.2) produces the correct classical factorization

$$\langle \mathbf{k}_1^\dagger O \mathbf{k}_4 \rangle_S = \langle \mathbf{k}_1^\dagger \mathbf{k}_\alpha^\dagger \mathbf{k}_\beta \mathbf{k}_4 \rangle_S = \langle \mathbf{k}_1^\dagger \mathbf{k}_4 \rangle \langle \mathbf{k}_\alpha^\dagger \mathbf{k}_\beta \rangle = \langle \mathbf{k}_1^\dagger \mathbf{k}_4 \rangle \langle O \rangle. \tag{C.3}$$

For two Bosons, $\mathbf{k}_\alpha^\dagger \mathbf{k}_\beta \equiv O_1$ and $\mathbf{k}_1^\dagger \mathbf{k}_4 \equiv O_2$, we similarly find

$$\langle O_1 O_2 \rangle_S = \langle O_1 \rangle \langle O_2 \rangle, \tag{C.4}$$

as long as $O_1 O_2$ is always a normally ordered combination of Boson operators.

These two examples introduce two constraints which have to be implemented together with the Boson-to-Fermion mapping, Eq. (C.1), in order to apply the pure Fermion factorization also to the mixed Fermion–Boson terms. Naturally, the results of the Boson-to-Fermion mapping can always be checked by applying the general factorization scheme, Eq. (43). After this is performed, one realizes that Eq. (C.1) can indeed be used to express factorizations compactly as long as: (i) boson operators are first normally ordered and (ii) the formal Fermion operators $\beta_1^\dagger$ and β_2 belonging to a given Boson operator are not separated in the factorization. Consequently, the identification (C.1) is both possible and useful.

The generic two-particle correlations follow now directly from Eqs. (C.2) to (C.4) yielding

$$\Delta \langle \mathbf{k}_1^\dagger \mathbf{k}_\alpha^\dagger \mathbf{k}_\beta \mathbf{k}_4 \rangle = \langle \mathbf{k}_1^\dagger \mathbf{k}_\alpha^\dagger \mathbf{k}_\beta \mathbf{k}_4 \rangle - \langle \mathbf{k}_1^\dagger \mathbf{k}_\alpha^\dagger \mathbf{k}_\beta \mathbf{k}_4 \rangle_S. \tag{C.5}$$

Such terms include correlations between carriers, photons, and phonons. For carriers alone, $\Delta \langle \mathbf{k}_1^\dagger \mathbf{k}_\alpha^\dagger \mathbf{k}_\beta \mathbf{k}_4 \rangle$ is responsible for Coulombic correlations such as exciton populations.

When photons are involved, $\Delta\langle \mathbf{k}_1^\dagger \mathbf{k}_\alpha^\dagger \mathbf{k}_\beta \mathbf{k}_4\rangle$ leads to quantum-optical correlation effects which may influence or even completely determine the PL, squeezing, and entanglement.

C.2. Three-particle factorizations

To solve the singlet–doublet dynamics of Eqs. (48)–(49), we have to determine the explicit form of the singlet–doublet factorization of three-particle quantities, i.e. $\langle \mathbf{k}_1^\dagger \mathbf{k}_2^\dagger \mathbf{k}_\alpha^\dagger \mathbf{k}_\beta \mathbf{k}_5 \mathbf{k}_6\rangle_{\mathrm{SD}}$. The singlet part for pure carriers can be obtained by using once again the Hartree–Fock factorization (44),

$$\begin{aligned}\langle \mathbf{k}_1^\dagger \mathbf{k}_2^\dagger \mathbf{k}_\alpha^\dagger \mathbf{k}_\beta \mathbf{k}_5 \mathbf{k}_6\rangle_{\mathrm{S}} = {} & \langle \mathbf{k}_1^\dagger \mathbf{k}_6\rangle\langle \mathbf{k}_2^\dagger \mathbf{k}_5\rangle\langle \mathbf{k}_\alpha^\dagger \mathbf{k}_\beta\rangle - \langle \mathbf{k}_1^\dagger \mathbf{k}_6\rangle\langle \mathbf{k}_2^\dagger \mathbf{k}_\beta\rangle\langle \mathbf{k}_\alpha^\dagger \mathbf{k}_5\rangle \\ & - \langle \mathbf{k}_1^\dagger \mathbf{k}_5\rangle\langle \mathbf{k}_2^\dagger \mathbf{k}_6\rangle\langle \mathbf{k}_\alpha^\dagger \mathbf{k}_\beta\rangle + \langle \mathbf{k}_1^\dagger \mathbf{k}_5\rangle\langle \mathbf{k}_2^\dagger \mathbf{k}_\beta\rangle\langle \mathbf{k}_\alpha^\dagger \mathbf{k}_6\rangle \\ & + \langle \mathbf{k}_1^\dagger \mathbf{k}_\beta\rangle\langle \mathbf{k}_2^\dagger \mathbf{k}_6\rangle\langle \mathbf{k}_\alpha^\dagger \mathbf{k}_5\rangle - \langle \mathbf{k}_1^\dagger \mathbf{k}_\beta\rangle\langle \mathbf{k}_2^\dagger \mathbf{k}_5\rangle\langle \mathbf{k}_\alpha^\dagger \mathbf{k}_6\rangle. \end{aligned} \tag{C.6}$$

With the help of the Boson-to-Fermion mapping, we find the singlet contributions produced by one, two, or three Bosons as

$$\langle \mathbf{k}_1^\dagger \mathbf{k}_2^\dagger O_1 \mathbf{k}_5 \mathbf{k}_6\rangle_{\mathrm{S}} = \langle \mathbf{k}_1^\dagger \mathbf{k}_6\rangle\langle \mathbf{k}_2^\dagger \mathbf{k}_5\rangle\langle O_1\rangle - \langle \mathbf{k}_1^\dagger \mathbf{k}_5\rangle\langle \mathbf{k}_2^\dagger \mathbf{k}_6\rangle\langle O_1\rangle, \tag{C.7}$$

$$\langle \mathbf{k}_1^\dagger O_1 O_2 \mathbf{k}_6\rangle_{\mathrm{S}} = \langle \mathbf{k}_1^\dagger \mathbf{k}_6\rangle\langle O_2\rangle\langle O_1\rangle, \tag{C.8}$$

$$\langle O_1 O_2 O_3\rangle_{\mathrm{S}} = \langle O_1\rangle\langle O_2\rangle\langle O_3\rangle, \tag{C.9}$$

respectively, where the Bosonic operators O_j are normally ordered. Finally, the singlet–doublet factorization of the three-particle expectation values follows from Eqs. (43) and (47) yielding

$$\begin{aligned}\langle \mathbf{k}_1^\dagger \mathbf{k}_2^\dagger \mathbf{k}_\alpha^\dagger \mathbf{k}_\beta \mathbf{k}_5 \mathbf{k}_6\rangle_{\mathrm{SD}} = {} & \langle \mathbf{k}_1^\dagger \mathbf{k}_2^\dagger \mathbf{k}_\alpha^\dagger \mathbf{k}_\beta \mathbf{k}_5 \mathbf{k}_6\rangle_{\mathrm{S}} \\ & + \langle \mathbf{k}_1^\dagger \mathbf{k}_6\rangle\Delta\langle \mathbf{k}_2^\dagger \mathbf{k}_\alpha^\dagger \mathbf{k}_\beta \mathbf{k}_5\rangle - \langle \mathbf{k}_1^\dagger \mathbf{k}_5\rangle\Delta\langle \mathbf{k}_2^\dagger \mathbf{k}_\alpha^\dagger \mathbf{k}_\beta \mathbf{k}_6\rangle \\ & + \langle \mathbf{k}_1^\dagger \mathbf{k}_\beta\rangle\Delta\langle \mathbf{k}_2^\dagger \mathbf{k}_\alpha^\dagger \mathbf{k}_5 \mathbf{k}_6\rangle - \langle \mathbf{k}_2^\dagger \mathbf{k}_6\rangle\Delta\langle \mathbf{k}_1^\dagger \mathbf{k}_\alpha^\dagger \mathbf{k}_\beta \mathbf{k}_5\rangle \\ & + \langle \mathbf{k}_2^\dagger \mathbf{k}_5\rangle\Delta\langle \mathbf{k}_1^\dagger \mathbf{k}_\alpha^\dagger \mathbf{k}_\beta \mathbf{k}_6\rangle - \langle \mathbf{k}_2^\dagger \mathbf{k}_\beta\rangle\Delta\langle \mathbf{k}_1^\dagger \mathbf{k}_\alpha^\dagger \mathbf{k}_5 \mathbf{k}_6\rangle \\ & + \langle \mathbf{k}_\alpha^\dagger \mathbf{k}_6\rangle\Delta\langle \mathbf{k}_1^\dagger \mathbf{k}_2^\dagger \mathbf{k}_\beta \mathbf{k}_5\rangle - \langle \mathbf{k}_\alpha^\dagger \mathbf{k}_5\rangle\Delta\langle \mathbf{k}_1^\dagger \mathbf{k}_2^\dagger \mathbf{k}_\beta \mathbf{k}_6\rangle \\ & + \langle \mathbf{k}_\alpha^\dagger \mathbf{k}_\beta\rangle\Delta\langle \mathbf{k}_1^\dagger \mathbf{k}_2^\dagger \mathbf{k}_5 \mathbf{k}_6\rangle, \end{aligned} \tag{C.10}$$

$$\begin{aligned}\langle \mathbf{k}_1^\dagger \mathbf{k}_2^\dagger O_1 \mathbf{k}_5 \mathbf{k}_6\rangle_{\mathrm{SD}} = {} & \langle \mathbf{k}_1^\dagger \mathbf{k}_2^\dagger O_1 \mathbf{k}_5 \mathbf{k}_6\rangle_{\mathrm{S}} \\ & + \langle \mathbf{k}_1^\dagger \mathbf{k}_6\rangle\Delta\langle \mathbf{k}_2^\dagger O_1 \mathbf{k}_5\rangle - \langle \mathbf{k}_1^\dagger \mathbf{k}_5\rangle\Delta\langle \mathbf{k}_2^\dagger O_1 \mathbf{k}_6\rangle \\ & - \langle \mathbf{k}_2^\dagger \mathbf{k}_6\rangle\Delta\langle \mathbf{k}_1^\dagger O_1 \mathbf{k}_5\rangle + \langle \mathbf{k}_2^\dagger \mathbf{k}_5\rangle\Delta\langle \mathbf{k}_1^\dagger O_1 \mathbf{k}_6\rangle \\ & + \langle O_1\rangle\Delta\langle \mathbf{k}_1^\dagger \mathbf{k}_2^\dagger \mathbf{k}_5 \mathbf{k}_6\rangle, \end{aligned} \tag{C.11}$$

$$\begin{aligned}\langle \mathbf{k}_1^\dagger O_1 O_2 \mathbf{k}_6\rangle_{\mathrm{SD}} = {} & \langle \mathbf{k}_1^\dagger O_1 O_2 \mathbf{k}_6\rangle_{\mathrm{S}} + \langle \mathbf{k}_1^\dagger \mathbf{k}_6\rangle\Delta\langle O_1 O_2\rangle + \langle O_2\rangle\Delta\langle \mathbf{k}_1^\dagger O_1 \mathbf{k}_6\rangle \\ & + \langle O_1\rangle\Delta\langle \mathbf{k}_1^\dagger O_2 \mathbf{k}_6\rangle, \end{aligned} \tag{C.12}$$

$$\begin{aligned}\langle O_1 O_2 O_3\rangle_{\mathrm{SD}} = {} & \langle O_1 O_2 O_3\rangle_{\mathrm{S}} \\ & + \langle O_3\rangle\Delta\langle O_1 O_2\rangle + \langle O_2\rangle\Delta\langle O_1 O_3\rangle + \langle O_1\rangle\Delta\langle O_2 O_3\rangle. \end{aligned} \tag{C.13}$$

The expectation values containing one, two, or three normally ordered Boson operators are once again obtained directly from the pure carrier factorizations by applying the Boson-to-Fermion mapping under the constraints of normal ordering and non-separability of the formal Fermion operators.

C.3. Constraints in homogeneously excited systems

As discussed earlier in Section 4.1, the condition of homogeneity introduces certain constraints to the allowed index combinations. As a result, only some of the factorization terms contribute to the singlet–doublet dynamics. Since we always assume homogeneous excitation configurations in this review, we collect here the most important forms and definitions resulting from such conditions.

For the singlet terms, the previously derived Eqs. (53)–(55) can be expressed via the implicit-notation formalism

$$\langle \mathbf{k}_1^\dagger \mathbf{k}_2 \rangle = \delta_{\mathbf{k}_\parallel^{(1)},\mathbf{k}_\parallel^{(2)}} \langle \mathbf{k}_1^\dagger \mathbf{k}_2 \rangle \equiv \delta_{\mathbf{k}_\parallel,\mathbf{k}'_\parallel} P_{\mathbf{k}_\parallel}^{\lambda,\lambda'}, \tag{C.14}$$

$$\langle B_{\mathbf{q}_\parallel,q_\perp} \rangle = \delta_{\mathbf{q}_\parallel,\mathbf{0}} \langle B_{\mathbf{0},q_\perp} \rangle, \quad \langle D_{\mathbf{p}_\parallel,p_\perp} \rangle = 0, \tag{C.15}$$

where the phonon amplitudes are set to zero since we do not allow for coherent phonon effects in the different examples discussed in this review. We also have used the generic identifications (B.3) and (55).

The homogeneous conditions limit also the possible two-particle correlation terms according to Section 4.1. Using the implicit notation formalism, Eq. (56) casts into the form

$$\begin{aligned} \Delta\langle \mathbf{k}_1^\dagger \mathbf{k}_2^\dagger \mathbf{k}_3 \mathbf{k}_4 \rangle &= \delta_{\mathbf{k}''_\parallel,\mathbf{k}'_\parallel+\mathbf{q}_\parallel} \delta_{\mathbf{k}'''_\parallel,\mathbf{k}_\parallel-\mathbf{q}_\parallel} \ \Delta\langle \mathbf{k}_1^\dagger \mathbf{k}_2^\dagger \mathbf{k}_{2'\mathbf{q}} \mathbf{k}_{1'\mathbf{q}} \rangle \\ &\equiv \delta_{\mathbf{k}''_\parallel,\mathbf{k}'_\parallel+\mathbf{q}_\parallel} \delta_{\mathbf{k}'''_\parallel,\mathbf{k}_\parallel-\mathbf{q}_\parallel} \ c_{\lambda,v;v',\lambda'}^{\mathbf{q}_\parallel,\mathbf{k}'_\parallel,\mathbf{k}_\parallel}. \end{aligned} \tag{C.16}$$

Here, we applied the rules (B.4)–(B.6) and identified the two-particle correlation via Eq. (57). The mixed operators and the pure Boson operators follow from Eqs. (58) to (59)

$$\begin{aligned} \Delta\langle 2 \rangle_{\mathrm{mix}} = \{ &\Delta\langle B_{\mathbf{q}_\parallel,q_\perp}^\dagger \mathbf{k}_{1\mathbf{q}}^\dagger \mathbf{k}_{1'} \rangle, \ \Delta\langle D_{\mathbf{p}_\parallel,q_\perp}^\dagger \mathbf{k}_{1\mathbf{q}}^\dagger \mathbf{k}_{1'} \rangle, \\ &\Delta\langle B_{\mathbf{q}_\parallel,q_\perp}^\dagger D_{\mathbf{q}_\parallel,p_\perp} \rangle, \ \Delta\langle B_{\mathbf{q}_\parallel,q_\perp} D_{-\mathbf{q}_\parallel,p_\perp} \rangle \}, \end{aligned} \tag{C.17}$$

$$\begin{aligned} \Delta\langle 2 \rangle_{\mathrm{bos}} = \{ &\Delta\langle B_{\mathbf{q}_\parallel,q_\perp}^\dagger B_{\mathbf{q}_\parallel,q'_\perp} \rangle, \ \Delta\langle B_{\mathbf{q}_\parallel,q_\perp} B_{-\mathbf{q}_\parallel,q'_\perp} \rangle, \\ &\Delta\langle D_{\mathbf{p}_\parallel,p_\perp}^\dagger D_{\mathbf{p}_\parallel,p'_\perp} \rangle, \ \Delta\langle D_{\mathbf{p}_\parallel,p_\perp} D_{-\mathbf{p}_\parallel,p_\perp} \rangle \}. \end{aligned} \tag{C.18}$$

In practical derivations, the generic singlet–doublet factorizations are applied first, while the conditions (C.14)–(C.18) are implemented in the last step to produce the final expressions.

Appendix D. Singlet–doublet dynamics for carriers

We derive in this Appendix the generic expressions entering the pure carrier dynamics. In particular, we concentrate on the detailed derivations of the two-particle correlation terms. For the sake of completeness, we first repeat the final form of the singlet

dynamics (71),

$$\begin{aligned}
\mathrm{i}\hbar\frac{\partial}{\partial t}P^{\lambda,\lambda'}_{\mathbf{k}_\parallel} &= (\tilde{\varepsilon}^{\lambda'}_{\mathbf{k}_\parallel}-\tilde{\varepsilon}^{\lambda}_{\mathbf{k}_\parallel})P^{\lambda,\lambda'}_{\mathbf{k}_\parallel}+\Omega^{\lambda}_{\mathbf{k}_\parallel}P^{\bar{\lambda},\lambda'}_{\mathbf{k}_\parallel}-P^{\lambda,\bar{\lambda}'}_{\mathbf{k}_\parallel}\Omega^{\bar{\lambda}'}_{\mathbf{k}_\parallel}\\
&\quad+\sum_{v,\mathbf{k}'_\parallel,\mathbf{q}_\parallel\neq\mathbf{0}}V_{\mathbf{q}_\parallel}[c^{\mathbf{q}_\parallel,\mathbf{k}'_\parallel,\mathbf{k}_\parallel}_{\lambda,v;v,\lambda'}-(c^{\mathbf{q}_\parallel,\mathbf{k}'_\parallel,\mathbf{k}_\parallel}_{\lambda',v;v,\lambda})^\star]\\
&\quad-\sum_{\mathbf{q}_\parallel}[\Delta\langle E^{\lambda'}_{\mathbf{q}_\parallel}a^\dagger_{\lambda,\mathbf{k}_\parallel}a_{\bar{\lambda}',\mathbf{k}_\parallel-\mathbf{q}_\parallel}\rangle-\Delta\langle(E^{\lambda}_{\mathbf{q}_\parallel})^\dagger a^\dagger_{\bar{\lambda},\mathbf{k}_\parallel-\mathbf{q}_\parallel}a_{\lambda',\mathbf{k}_\parallel}\rangle]\\
&\quad+\sum_{\mathbf{q}_\parallel}[\Delta\langle Q^{\lambda'}_{\mathbf{q}_\parallel}a^\dagger_{\lambda,\mathbf{k}_\parallel}a_{\lambda',\mathbf{k}_\parallel-\mathbf{q}_\parallel}\rangle-\Delta\langle(Q^{\lambda}_{\mathbf{q}_\parallel})^\dagger a^\dagger_{\lambda,\mathbf{k}_\parallel-\mathbf{q}_\parallel}a_{\lambda',\mathbf{k}_\parallel}\rangle].
\end{aligned}\tag{D.1}$$

For later reference, we also identify the renormalized kinetic energy and the renormalized Rabi frequency

$$\tilde{\varepsilon}^{\lambda}_{\mathbf{k}_\parallel}\equiv\varepsilon^{\lambda}_{\mathbf{k}_\parallel}-\sum_{\mathbf{k}'_\parallel}V_{\mathbf{k}'_\parallel-\mathbf{k}_\parallel}n^{\lambda}_{\mathbf{k}'_\parallel},\tag{D.2}$$

$$\Omega^{\lambda}_{\mathbf{k}_\parallel}\equiv\langle E^{\lambda}_{\mathbf{0}}\rangle+\sum_{\mathbf{k}'_\parallel}V_{\mathbf{k}'_\parallel-\mathbf{k}_\parallel}P^{\lambda,\bar{\lambda}}_{\mathbf{k}'_\parallel},\tag{D.3}$$

respectively.

D.1. Dynamics of two-particle correlations

The derivation of the dynamics for $c_{\lambda,v,v',\lambda'}$ follows from the procedure discussed in Section 4.3. First, we derive the dynamics of the pure two-particle quantities

$$\mathrm{i}\hbar\frac{\partial}{\partial t}\langle 2\rangle=\mathrm{i}\hbar\frac{\partial}{\partial t}\langle\mathbf{k}^\dagger_1\mathbf{k}^\dagger_2\mathbf{k}_{2'\mathbf{q}}\mathbf{k}_{1'\mathbf{q}}\rangle.\tag{D.4}$$

The dynamics of $c_{\lambda,v,v',\lambda'}$ is then obtained via a simple subtraction by applying Eq. (74) where the singlet part follows from Eq. (D.1).

The dynamics of $\langle 2\rangle$ can be derived compactly by applying Eqs. (B.13)–(B.14) several times. After we bring all expressions into normal order, we find

$$\begin{aligned}
\mathrm{i}\hbar\frac{\partial}{\partial t}\langle\mathbf{k}^\dagger_1\mathbf{k}^\dagger_2\mathbf{k}_{2'\mathbf{q}}\mathbf{k}_{1'\mathbf{q}}\rangle &= (\varepsilon^{\lambda'}_{\mathbf{k}_\parallel-\mathbf{q}_\parallel}+\varepsilon^{\nu'}_{\mathbf{k}'_\parallel+\mathbf{q}_\parallel}-\varepsilon^{\nu}_{\mathbf{k}'_\parallel}-\varepsilon^{\lambda}_{\mathbf{k}_\parallel})\langle\mathbf{k}^\dagger_1\mathbf{k}^\dagger_2\mathbf{k}_{2'\mathbf{q}}\mathbf{k}_{1'\mathbf{q}}\rangle\\
&\quad+\sum_{\mathbf{l}}V_{\mathbf{l}}[\langle\mathbf{k}^\dagger_1\mathbf{k}^\dagger_2\mathbf{k}_{2'(\mathbf{q}-\mathbf{l})}\mathbf{k}_{1'(\mathbf{q}+\mathbf{l})}\rangle-\langle\mathbf{k}^\dagger_{1\mathbf{l}}\mathbf{k}^\dagger_{2\mathbf{l}}\mathbf{k}_{2'\mathbf{q}}\mathbf{k}_{1'\mathbf{q}}\rangle]\\
&\quad+\sum_{\mathbf{k}_3,\mathbf{l}}V_{\mathbf{l}}[\langle\mathbf{k}^\dagger_1\mathbf{k}^\dagger_2\mathbf{k}^\dagger_{3\mathbf{l}}\mathbf{k}_3\mathbf{k}_{2'\mathbf{q}}\mathbf{k}_{1'(\mathbf{q}-\mathbf{l})}\rangle+\langle\mathbf{k}^\dagger_1\mathbf{k}^\dagger_2\mathbf{k}^\dagger_{3\mathbf{l}}\mathbf{k}_3\mathbf{k}_{2'(\mathbf{q}+\mathbf{l})}\mathbf{k}_{1'\mathbf{q}}\rangle]\\
&\quad-\sum_{\mathbf{k}_3,\mathbf{l}}V_{\mathbf{l}}[\langle\mathbf{k}^\dagger_1\mathbf{k}^\dagger_{2\mathbf{l}}\mathbf{k}^\dagger_3\mathbf{k}_{3\mathbf{l}}\mathbf{k}_{2'\mathbf{q}}\mathbf{k}_{1'\mathbf{q}}\rangle+\langle\mathbf{k}^\dagger_{1\mathbf{l}}\mathbf{k}^\dagger_2\mathbf{k}^\dagger_{3\mathbf{l}}\mathbf{k}_3\mathbf{k}_{2'\mathbf{q}}\mathbf{k}_{1'\mathbf{q}}\rangle].\\
&\quad-\sum_{\mathbf{l}}[\langle E^{\bar{\nu}'}_{\mathbf{l}_\parallel}\mathbf{k}^\dagger_1\mathbf{k}^\dagger_2\mathbf{k}_{2'\mathbf{q}}\bar{\mathbf{k}}_{1'(\mathbf{q}+\mathbf{l})}\rangle+\langle E^{\bar{\nu}'}_{-\mathbf{l}_\parallel}\mathbf{k}^\dagger_1\mathbf{k}^\dagger_2\bar{\mathbf{k}}_{2'(\mathbf{q}+\mathbf{l})}\mathbf{k}_{1'\mathbf{q}}\rangle]\\
&\quad+\sum_{\mathbf{l}}[\langle E^{\nu}_{\mathbf{l}_\parallel}\mathbf{k}^\dagger_1\bar{\mathbf{k}}^\dagger_{2\mathbf{l}}\mathbf{k}_{2'\mathbf{q}}\mathbf{k}_{1'\mathbf{q}}\rangle+\langle E^{\lambda}_{-\mathbf{l}_\parallel}\bar{\mathbf{k}}^\dagger_{1\mathbf{l}}\mathbf{k}^\dagger_2\mathbf{k}_{2'(\mathbf{q}}\mathbf{k}_{1'\mathbf{q}}\rangle]
\end{aligned}$$

$$+\sum_{\mathbf{l}}[\langle Q^{\lambda'}_{\mathbf{l}_\parallel}\mathbf{k}_1^\dagger\mathbf{k}_2^\dagger\mathbf{k}_{2'\mathbf{q}}\mathbf{k}_{1'(\mathbf{q}+\mathbf{l})}\rangle+\langle Q^{\nu'}_{-\mathbf{l}_\parallel}\mathbf{k}_1^\dagger\mathbf{k}_2^\dagger\mathbf{k}_{2'(\mathbf{q}+\mathbf{l})}\mathbf{k}_{1'\mathbf{q}}\rangle]$$
$$-\sum_{\mathbf{l}}[\langle Q^{\nu}_{\mathbf{l}_\parallel}\mathbf{k}_1^\dagger\mathbf{k}_{2\mathbf{l}}^\dagger\mathbf{k}_{2'\mathbf{q}}\mathbf{k}_{1'\mathbf{q}}\rangle+\langle Q^{\lambda}_{-\mathbf{l}_\parallel}\mathbf{k}_{1\mathbf{l}}^\dagger\mathbf{k}_2^\dagger\mathbf{k}_{2'(\mathbf{q}}\mathbf{k}_{1'\mathbf{q}}\rangle]. \tag{D.5}$$

The third and fourth lines of Eq. (D.5) contain the three-particle quantities induced by the Coulomb interaction. These four terms, T_j ($j=1,2,3,4$), lead to the most complicated factorizations. However, these terms have special symmetries

$$T_1\equiv\sum_{\mathbf{k}_3,\mathbf{l}}V_{\mathbf{l}}\langle\mathbf{k}_1^\dagger\mathbf{k}_2^\dagger\mathbf{k}_{3\mathbf{l}}^\dagger\mathbf{k}_3\mathbf{k}_{2'\mathbf{q}}\mathbf{k}_{1'(\mathbf{q}-\mathbf{l})}\rangle,$$
$$T_2\equiv\sum_{\mathbf{k}_3,\mathbf{l}}V_{\mathbf{l}}\langle\mathbf{k}_1^\dagger\mathbf{k}_2^\dagger\mathbf{k}_{3\mathbf{l}}^\dagger\mathbf{k}_3\mathbf{k}_{2'(\mathbf{q}+\mathbf{l})}\mathbf{k}_{1'\mathbf{q}}\rangle=T_1\Big|^{\mathbf{k}_1\leftrightarrow\mathbf{k}_2\ \mathbf{k}_{1'}\leftrightarrow\mathbf{k}_{2'}}_{\mathbf{q}\leftrightarrow[-\mathbf{q}]},$$
$$T_3\equiv\sum_{\mathbf{k}_3,\mathbf{l}}V_{\mathbf{l}}\langle\mathbf{k}_1^\dagger\mathbf{k}_{2\mathbf{l}}^\dagger\mathbf{k}_3^\dagger\mathbf{k}_{3\mathbf{l}}\mathbf{k}_{2'\mathbf{q}}\mathbf{k}_{1'\mathbf{q}}\rangle=\Big[T_1\Big|^{\mathbf{k}_1\leftrightarrow\mathbf{k}_{2'\mathbf{q}}}_{\mathbf{k}_2\leftrightarrow\mathbf{k}_{1'\mathbf{q}}}\Big]^\star,$$
$$T_4\equiv\sum_{\mathbf{k}_3,\mathbf{l}}V_{\mathbf{l}}\langle\mathbf{k}_{1\mathbf{l}}^\dagger\mathbf{k}_2^\dagger\mathbf{k}_{3\mathbf{l}}^\dagger\mathbf{k}_3\mathbf{k}_{2'\mathbf{q}}\mathbf{k}_{1'\mathbf{q}}\rangle=\Big[T_1\Big|^{\mathbf{k}_1\leftrightarrow\mathbf{k}_{1'\mathbf{q}}}_{\mathbf{k}_2\leftrightarrow\mathbf{k}_{2'\mathbf{q}}}\Big]^\star, \tag{D.6}$$

which are connected via simple substitutions indicated in the last equalities in the equations above. Since T_2, T_3, and T_4 follow directly from T_1, we only have to explicitly evaluate the three-particle factorizations for T_1 using Eq. (C.10). The mixed operator terms leads to a much simpler structure of terms as we apply Eq. (C.11).

Once all factorizations are performed, we may isolate the single-, two-, and three-particle correlation contributions in Eq. (D.5). At this stage, we implement the constraints, Eqs. (C.14)–(C.17), that are generally valid for homogeneous excitations. The result of this lengthy but straightforward derivation can be collected into the generic form

$$\begin{aligned}\mathrm{i}\hbar\frac{\partial}{\partial t}c^{\mathbf{q}_\parallel,\mathbf{k}'_\parallel,\mathbf{k}_\parallel}_{\lambda,\nu;\nu',\lambda'}&=(\tilde{\varepsilon}^{\lambda'}_{\mathbf{k}_\parallel-\mathbf{q}_\parallel}+\tilde{\varepsilon}^{\nu'}_{\mathbf{k}'_\parallel+\mathbf{q}_\parallel}-\tilde{\varepsilon}^{\nu}_{\mathbf{k}'_\parallel}-\tilde{\varepsilon}^{\lambda}_{\mathbf{k}_\parallel})c^{\mathbf{q}_\parallel,\mathbf{k}'_\parallel,\mathbf{k}_\parallel}_{\lambda,\nu;\nu',\lambda'}\\&+\Omega^{\lambda,\bar{\lambda}}_{\mathbf{k}_\parallel}c^{\mathbf{q}_\parallel,\mathbf{k}'_\parallel,\mathbf{k}_\parallel}_{\bar{\lambda},\nu;\nu',\lambda'}+\Omega^{\nu,\bar{\nu}}_{\mathbf{k}'_\parallel}c^{\mathbf{q}_\parallel,\mathbf{k}'_\parallel,\mathbf{k}_\parallel}_{\lambda,\bar{\nu};\nu',\lambda'}-\Omega^{\bar{\nu}',\nu'}_{\mathbf{k}'_\parallel+\mathbf{q}_\parallel}c^{\mathbf{q}_\parallel,\mathbf{k}'_\parallel,\mathbf{k}_\parallel}_{\lambda,\nu;\bar{\nu}',\lambda'}-\Omega^{\bar{\lambda}',\lambda'}_{\mathbf{k}_\parallel-\mathbf{q}_\parallel}c^{\mathbf{q}_\parallel,\mathbf{k}'_\parallel,\mathbf{k}_\parallel}_{\lambda,\nu;\nu',\bar{\lambda}'}\\&+\mathrm{S}^{\mathbf{q}_\parallel,\mathbf{k}'_\parallel,\mathbf{k}_\parallel}_{\lambda,\nu;\nu',\lambda'}+\mathrm{D}^{\mathbf{q}_\parallel,\mathbf{k}'_\parallel,\mathbf{k}_\parallel}_{\lambda,\nu;\nu',\lambda'}\\&+[G_{\mathrm{phon}}]^{\mathbf{q}_\parallel,\mathbf{k}'_\parallel,\mathbf{k}_\parallel}_{\lambda,\nu;\nu',\lambda'}+[G_{\mathrm{QED}}]^{\mathbf{q}_\parallel,\mathbf{k}'_\parallel,\mathbf{k}_\parallel}_{\lambda,\nu;\nu',\lambda'}+\mathrm{T}^{\mathbf{q}_\parallel,\mathbf{k}'_\parallel,\mathbf{k}_\parallel}_{\lambda,\nu;\nu',\lambda'},\end{aligned} \tag{D.7}$$

where the simplest contributions due to the energy-renormalization diagram (see Section 4.3.3 and Fig. 2) and the classical light-field factorizations are presented explicitly. The other contributions are collected together into remaining symbols.

The singlet factorization of the Coulomb induced two- and three-particle expectation values produces the singlet source

$$\begin{aligned}\mathrm{S}^{\mathbf{q}_\parallel,\mathbf{k}'_\parallel,\mathbf{k}_\parallel}_{\lambda,\nu;\nu',\lambda'}\equiv&\sum_{\beta}V_{\mathbf{j}_\parallel}[P^{\lambda,\beta}_{\mathbf{k}_\parallel}(P^{\beta,\nu'}_{\mathbf{k}'_\parallel+\mathbf{q}_\parallel}-\delta_{\beta,\nu'})(P^{\nu,\lambda'}_{\mathbf{k}'_\parallel}-P^{\nu,\lambda'}_{\mathbf{k}'_\parallel-\mathbf{j}_\parallel})\\&-P^{\beta,\lambda'}_{\mathbf{k}_\parallel-\mathbf{q}_\parallel}(P^{\nu,\beta}_{\mathbf{k}'_\parallel}-\delta_{\beta,\nu})(P^{\lambda,\nu'}_{\mathbf{k}_\parallel+\mathbf{j}_\parallel}-P^{\lambda,\nu'}_{\mathbf{k}_\parallel})]\\&+\sum_{\beta}V_{\mathbf{q}_\parallel}[P^{\lambda,\beta}_{\mathbf{k}_\parallel}(P^{\beta,\lambda'}_{\mathbf{k}_\parallel-\mathbf{q}_\parallel}-\delta_{\beta,\lambda'})(P^{\nu,\nu'}_{\mathbf{k}'_\parallel+\mathbf{q}_\parallel}-P^{\nu,\nu'}_{\mathbf{k}'_\parallel})\end{aligned}$$

$$- P^{\beta,\nu'}_{\mathbf{k}'_\parallel+\mathbf{q}_\parallel}(P^{\nu,\beta}_{\mathbf{k}'_\parallel} - \delta_{\beta,\nu})(P^{\lambda,\lambda'}_{\mathbf{k}_\parallel} - P^{\lambda,\lambda'}_{\mathbf{k}_\parallel-\mathbf{q}_\parallel})], \tag{D.8}$$

where the vector identification $\mathbf{j}_\parallel = \mathbf{k}'_\parallel + \mathbf{q}_\parallel - \mathbf{k}_\parallel$ is used according to Eq. (B.5). In general, $S_{\lambda,\nu;\nu',\lambda'}$ acts as a source that generates correlated carrier doublets out of carrier singlets. These terms are identified by the simplest diagram in Fig. 2.

The Coulomb-interaction induced three-particle contributions and their factorizations containing doublets are collected together into

$$\begin{aligned}
&D^{\mathbf{q}_\parallel,\mathbf{k}'_\parallel,\mathbf{k}_\parallel}_{\lambda,\nu;\nu',\lambda'}\\
&\quad\equiv V_{\mathbf{q}_\parallel}[(P^{\lambda,\lambda'}_{\mathbf{k}_\parallel} - P^{\lambda,\lambda'}_{\mathbf{k}_\parallel-\mathbf{q}_\parallel})\sum_{\beta,\mathbf{l}_\parallel} c^{\mathbf{q}_\parallel,\mathbf{k}'_\parallel,\mathbf{l}_\parallel}_{\beta,\nu;\nu',\beta} - (P^{\nu,\nu'}_{\mathbf{k}'_\parallel+\mathbf{q}_\parallel} - P^{\nu,\nu'}_{\mathbf{k}'_\parallel})\sum_{\beta,\mathbf{l}_\parallel} c^{\mathbf{q}_\parallel,\mathbf{l}_\parallel,\mathbf{k}_\parallel}_{\lambda,\beta;\beta,\lambda'}]\\
&\qquad + V_{\mathbf{j}_\parallel}[(P^{\lambda,\nu'}_{\mathbf{k}_\parallel+\mathbf{j}_\parallel} - P^{\lambda,\nu'}_{\mathbf{k}_\parallel})\sum_{\beta,\mathbf{l}_\parallel} c^{-\mathbf{j}_\parallel,\mathbf{k}'_\parallel,\mathbf{l}_\parallel}_{\beta,\nu;\lambda',\beta} - (P^{\nu,\lambda'}_{\mathbf{k}'_\parallel} - P^{\nu,\lambda'}_{\mathbf{k}'_\parallel-\mathbf{j}_\parallel})\sum_{\beta,\mathbf{l}_\parallel} c^{-\mathbf{j}_\parallel,\mathbf{l}_\parallel,\mathbf{k}_\parallel}_{\lambda,\beta;\beta,\nu'}]\\
&\qquad + \sum_{\beta,\mathbf{l}_\parallel} V_{\mathbf{l}_\parallel+\mathbf{q}_\parallel}[P^{\beta,\lambda}_{\mathbf{k}_\parallel} c^{\mathbf{l}_\parallel,\mathbf{k}'_\parallel+\mathbf{q}_\parallel,\mathbf{k}_\parallel-\mathbf{q}_\parallel}_{\lambda',\nu';\nu,\beta} + (P^{\beta,\nu}_{\mathbf{k}'_\parallel} - \delta_{\nu,\beta})c^{\mathbf{l}_\parallel,\mathbf{k}'_\parallel+\mathbf{q}_\parallel,\mathbf{k}_\parallel-\mathbf{q}_\parallel}_{\lambda',\nu';\beta,\lambda}]^\star\\
&\qquad - \sum_{\beta,\mathbf{l}_\parallel} V_{\mathbf{l}_\parallel-\mathbf{q}_\parallel}[P^{\beta,\lambda'}_{\mathbf{k}_\parallel-\mathbf{q}_\parallel} c^{\mathbf{l}_\parallel,\mathbf{k}'_\parallel,\mathbf{k}_\parallel}_{\lambda,\nu;\nu',\beta} + (P^{\beta,\nu'}_{\mathbf{k}'_\parallel+\mathbf{q}_\parallel} - \delta_{\beta,\nu'})c^{\mathbf{l}_\parallel,\mathbf{k}'_\parallel,\mathbf{k}_\parallel}_{\lambda,\nu;\beta,\lambda'}]\\
&\qquad - \sum_{\beta,\mathbf{l}_\parallel} P^{\lambda,\beta}_{\mathbf{k}_\parallel} V_{\mathbf{l}-\mathbf{k}_\parallel}[c^{\mathbf{q}_\parallel,\mathbf{k}'_\parallel,\mathbf{l}_\parallel}_{\beta,\nu;\nu',\lambda'} - c^{-\mathbf{j}_\parallel,\mathbf{k}'_\parallel,\mathbf{l}_\parallel}_{\beta,\nu;\lambda',\nu'}]\\
&\qquad - \sum_{\beta,\mathbf{l}_\parallel} P^{\nu,\beta}_{\mathbf{k}'_\parallel} V_{\mathbf{l}_\parallel-\mathbf{k}'_\parallel}[c^{\mathbf{q}_\parallel,\mathbf{l}_\parallel,\mathbf{k}_\parallel}_{\lambda,\beta;\nu',\lambda'} - c^{-\mathbf{j}_\parallel,\mathbf{l}_\parallel,\mathbf{k}_\parallel}_{\lambda,\beta;\lambda',\nu'}]\\
&\qquad + \sum_{\beta,\mathbf{l}_\parallel} P^{\beta,\lambda'}_{\mathbf{k}_\parallel-\mathbf{q}_\parallel}[V_{\mathbf{l}_\parallel-\mathbf{k}_\parallel} c^{\mathbf{q}_\parallel,\mathbf{k}'_\parallel,\mathbf{l}_\parallel}_{\lambda,\nu;\nu',\beta} - V_{\mathbf{l}_\parallel-\mathbf{k}'_\parallel} c^{\mathbf{j}_\parallel,\mathbf{k}_\parallel,\mathbf{l}_\parallel}_{\nu,\lambda;\nu',\beta}]\\
&\qquad + \sum_{\beta,\mathbf{l}_\parallel} P^{\beta,\nu'}_{\mathbf{k}'_\parallel+\mathbf{q}_\parallel}[V_{\mathbf{l}_\parallel-\mathbf{k}'_\parallel} c^{\mathbf{q}_\parallel,\mathbf{l}_\parallel,\mathbf{k}_\parallel}_{\lambda,\nu;\beta,\lambda'} - V_{\mathbf{l}_\parallel-\mathbf{k}_\parallel} c^{-\mathbf{j}_\parallel,\mathbf{k}'_\parallel,\mathbf{l}_\parallel}_{\lambda,\nu;\lambda',\beta}].
\end{aligned} \tag{D.9}$$

In this expression, one can identify the different diagram classes presented in Fig. 2 by following the index β, in particular by noting how this index is distributed among the creation and annihilation operators in the singlets and correlated doublets. From this analysis, one sees that the first two lines produce the screening diagrams [Eq. (101)] while the remaining terms constitute the most complicated class allowing for the formation of new quasi-particle states [Eqs. (105)–(106)].

The correlated carrier doublets couple also to phonon-assisted correlations which are collected into

$$\begin{aligned}
&[G_{\text{phon}}]^{\mathbf{q}_\parallel,\mathbf{k}'_\parallel,\mathbf{k}_\parallel}_{\lambda,\nu;\nu',\lambda'}\\
&\quad\equiv -P^{\lambda,\lambda'}_{\mathbf{k}_\parallel-\mathbf{q}_\parallel}\Delta\langle[Q^\lambda_{\mathbf{q}_\parallel}]^\dagger a^\dagger_{\nu,\mathbf{k}'_\parallel}a_{\nu',\mathbf{k}'_\parallel+\mathbf{q}_\parallel}\rangle + P^{\lambda,\nu'}_{\mathbf{k}'_\parallel+\mathbf{q}_\parallel}\Delta\langle Q^\lambda_{\mathbf{j}_\parallel}a^\dagger_{\nu,\mathbf{k}'_\parallel}a_{\lambda',\mathbf{k}'_\parallel-\mathbf{j}_\parallel}\rangle\\
&\qquad - P^{\nu,\nu'}_{\mathbf{k}'_\parallel+\mathbf{q}_\parallel}\Delta\langle Q^\nu_{\mathbf{q}_\parallel}a^\dagger_{\lambda,\mathbf{k}_\parallel}a_{\lambda',\mathbf{k}_\parallel-\mathbf{q}_\parallel}\rangle + P^{\nu,\lambda'}_{\mathbf{k}_\parallel-\mathbf{q}_\parallel}\Delta\langle[Q^\nu_{\mathbf{j}_\parallel}]^\dagger a^\dagger_{\lambda,\mathbf{k}_\parallel}a_{\nu',\mathbf{k}_\parallel+\mathbf{j}_\parallel}\rangle\\
&\qquad + P^{\nu,\nu'}_{\mathbf{k}'_\parallel}\Delta\langle Q^{\nu'}_{\mathbf{q}_\parallel}a^\dagger_{\lambda,\mathbf{k}_\parallel}a_{\lambda',\mathbf{k}_\parallel-\mathbf{q}_\parallel}\rangle - P^{\lambda,\nu'}_{\mathbf{k}_\parallel}\Delta\langle Q^{\nu'}_{\mathbf{j}_\parallel}a^\dagger_{\nu,\mathbf{k}'_\parallel}a_{\lambda',\mathbf{k}'_\parallel-\mathbf{j}_\parallel}\rangle\\
&\qquad + P^{\lambda,\lambda'}_{\mathbf{k}_\parallel}\Delta\langle[Q^{\lambda'}_{\mathbf{q}_\parallel}]^\dagger a^\dagger_{\nu,\mathbf{k}'_\parallel}a_{\nu',\mathbf{k}'_\parallel+\mathbf{q}_\parallel}\rangle - P^{\nu,\lambda'}_{\mathbf{k}'_\parallel}\Delta\langle[Q^{\lambda'}_{\mathbf{j}_\parallel}]^\dagger a^\dagger_{\lambda,\mathbf{k}'_\parallel}a_{\nu',\mathbf{k}_\parallel+\mathbf{j}_\parallel}\rangle.
\end{aligned} \tag{D.10}$$

Similarly, the quantum-optical correlations are obtained as

$$
\begin{aligned}
&[G_{\mathrm{QED}}]^{\mathbf{q}_\parallel,\mathbf{k}'_\parallel,\mathbf{k}_\parallel}_{\lambda,\nu;\nu',\lambda'} \\
&\quad\equiv +P^{\bar{\lambda},\lambda'}_{\mathbf{k}_\parallel-\mathbf{q}_\parallel}\Delta\langle[E^{\lambda}_{\mathbf{q}_\parallel}]^\dagger a^\dagger_{\nu,\mathbf{k}'_\parallel}a_{\nu',\mathbf{k}'_\parallel+\mathbf{q}_\parallel}\rangle - P^{\bar{\lambda},\nu'}_{\mathbf{k}'_\parallel+\mathbf{q}_\parallel}\Delta\langle E^{\bar{\lambda}}_{\mathbf{j}_\parallel}a^\dagger_{\nu,\mathbf{k}'_\parallel}a_{\lambda',\mathbf{k}'_\parallel-\mathbf{j}_\parallel}\rangle \\
&\qquad + P^{\bar{\nu},\nu'}_{\mathbf{k}'_\parallel+\mathbf{q}_\parallel}\Delta\langle E^{\bar{\nu}}_{\mathbf{q}_\parallel}a^\dagger_{\lambda,\mathbf{k}_\parallel}a_{\lambda',\mathbf{k}_\parallel-\mathbf{q}_\parallel}\rangle - P^{\bar{\nu},\lambda'}_{\mathbf{k}_\parallel-\mathbf{q}_\parallel}\Delta\langle[E^{\nu}_{\mathbf{j}_\parallel}]^\dagger a^\dagger_{\lambda,\mathbf{k}_\parallel}a_{\nu',\mathbf{k}_\parallel+\mathbf{j}_\parallel}\rangle \\
&\qquad - P^{\nu,\bar{\nu}'}_{\mathbf{k}'_\parallel}\Delta\langle E^{\nu'}_{\mathbf{q}_\parallel}a^\dagger_{\lambda,\mathbf{k}_\parallel}a_{\lambda',\mathbf{k}_\parallel-\mathbf{q}_\parallel}\rangle + P^{\lambda,\bar{\nu}'}_{\mathbf{k}_\parallel}\Delta\langle E^{\nu'}_{\mathbf{j}_\parallel}a^\dagger_{\nu,\mathbf{k}'_\parallel}a_{\lambda',\mathbf{k}'_\parallel-\mathbf{j}_\parallel}\rangle \\
&\qquad - P^{\lambda,\bar{\lambda}'}_{\mathbf{k}_\parallel}\Delta\langle[E^{\bar{\lambda}'}_{\mathbf{q}_\parallel}]^\dagger a^\dagger_{\nu,\mathbf{k}'_\parallel}a_{\nu',\mathbf{k}'_\parallel+\mathbf{q}_\parallel}\rangle + P^{\nu,\bar{\lambda}'}_{\mathbf{k}'_\parallel}\Delta\langle[E^{\bar{\lambda}'}_{\mathbf{j}_\parallel}]^\dagger a^\dagger_{\lambda,\mathbf{k}_\parallel}a_{\nu',\mathbf{k}_\parallel+\mathbf{j}_\parallel}\rangle. \qquad \text{(D.11)}
\end{aligned}
$$

The remaining expression $T_{\lambda,\nu;\nu',\lambda'}$ contains the correlated triplets due to Coulomb, phonon, and light–matter interaction. It follows directly from the correlated part of the three-particle terms in Eq. (D.5). We obtain

$$
\begin{aligned}
T^{\mathbf{q}_\parallel,\mathbf{k}'_\parallel,\mathbf{k}_\parallel}_{\lambda,\nu;\nu',\lambda'} \equiv{}& \sum_{\mathbf{k}_3,\mathbf{l}} V_{\mathbf{l}}\left[\Delta\langle\mathbf{k}^\dagger_1\mathbf{k}^\dagger_2\mathbf{k}^\dagger_{3\mathbf{l}}\mathbf{k}_3\mathbf{k}_{2'\mathbf{q}}\mathbf{k}_{1'(\mathbf{q}-\mathbf{l})}\rangle + \Delta\langle\mathbf{k}^\dagger_1\mathbf{k}^\dagger_2\mathbf{k}^\dagger_{3\mathbf{l}}\mathbf{k}_3\mathbf{k}_{2'(\mathbf{q}+\mathbf{l})}\mathbf{k}_{1'\mathbf{q}}\rangle\right] \\
&- \sum_{\mathbf{k}_3,\mathbf{l}} V_{\mathbf{l}}[\Delta\langle\mathbf{k}^\dagger_1\mathbf{k}^\dagger_{2\mathbf{l}}\mathbf{k}^\dagger_3\mathbf{k}_{3\mathbf{l}}\mathbf{k}_{2'\mathbf{q}}\mathbf{k}_{1'\mathbf{q}}\rangle + \Delta\langle\mathbf{k}^\dagger_{1\mathbf{l}}\mathbf{k}^\dagger_2\mathbf{k}^\dagger_{3\mathbf{l}}\mathbf{k}_3\mathbf{k}_{2'\mathbf{q}}\mathbf{k}_{1'\mathbf{q}}\rangle] \\
&- \sum_{\mathbf{l}}[\Delta\langle E^{\bar{\lambda}'}_{\mathbf{l}_\parallel}\mathbf{k}^\dagger_1\mathbf{k}^\dagger_2\mathbf{k}_{2'\mathbf{q}}\bar{\mathbf{k}}_{1'(\mathbf{q}+\mathbf{l})}\rangle + \Delta\langle E^{\bar{\nu}'}_{-\mathbf{l}_\parallel}\mathbf{k}^\dagger_1\mathbf{k}^\dagger_2\bar{\mathbf{k}}_{2'(\mathbf{q}+\mathbf{l})}\mathbf{k}_{1'\mathbf{q}}\rangle] \\
&+ \sum_{\mathbf{l}}[\Delta\langle E^{\nu}_{\mathbf{l}_\parallel}\mathbf{k}^\dagger_1\bar{\mathbf{k}}^\dagger_{2\mathbf{l}}\mathbf{k}_{2'\mathbf{q}}\mathbf{k}_{1'\mathbf{q}}\rangle + \Delta\langle E^{\lambda}_{-\mathbf{l}_\parallel}\bar{\mathbf{k}}^\dagger_{1\mathbf{l}}\mathbf{k}^\dagger_2\mathbf{k}_{2'(\mathbf{q}}\mathbf{k}_{1'\mathbf{q}}\rangle] \\
&+ \sum_{\mathbf{l}}[\Delta\langle Q^{\lambda'}_{\mathbf{l}_\parallel}\mathbf{k}^\dagger_1\mathbf{k}^\dagger_2\mathbf{k}_{2'\mathbf{q}}\mathbf{k}_{1'(\mathbf{q}+\mathbf{l})}\rangle + \Delta\langle Q^{\nu'}_{-\mathbf{l}_\parallel}\mathbf{k}^\dagger_1\mathbf{k}^\dagger_2\mathbf{k}_{2'(\mathbf{q}+\mathbf{l})}\mathbf{k}_{1'\mathbf{q}}\rangle] \\
&- \sum_{\mathbf{l}}[\Delta\langle Q^{\nu}_{\mathbf{l}_\parallel}\mathbf{k}^\dagger_1\mathbf{k}^\dagger_{2\mathbf{l}}\mathbf{k}_{2'\mathbf{q}}\mathbf{k}_{1'\mathbf{q}}\rangle + \Delta\langle Q^{\lambda}_{-\mathbf{l}_\parallel}\mathbf{k}^\dagger_{1\mathbf{l}}\mathbf{k}^\dagger_2\mathbf{k}_{2'(\mathbf{q}}\mathbf{k}_{1'\mathbf{q}}\rangle]. \qquad \text{(D.12)}
\end{aligned}
$$

These terms lead to microscopic scattering contributions in the two-particle correlations.

D.2. Formal aspects of the three-particle scattering term

We now outline the generic scheme how three-particle correlation terms in Eq. (D.12) can be treated on the scattering level. For this purpose, we start from Eq. (42) and include only terms up to three-particle correlations. This leads to the general equation structure

$$
\mathrm{i}\hbar\frac{\partial}{\partial t}\langle 1\rangle = T_1[\langle 1\rangle] + V_{1a}[\langle 2\rangle_{\mathrm{S}}] + V_{1b}[\Delta\langle 2\rangle], \qquad \text{(D.13)}
$$

$$
\mathrm{i}\hbar\frac{\partial}{\partial t}\Delta\langle 2\rangle = T_2[\Delta\langle 2\rangle] + V_{2a}[\langle 3\rangle_{\mathrm{SD}}] + V_{2b}[\Delta\langle 3\rangle], \qquad \text{(D.14)}
$$

$$
\mathrm{i}\hbar\frac{\partial}{\partial t}\Delta\langle 3\rangle = T_3[\Delta\langle 3\rangle] + V_3[\langle 4\rangle_{\mathrm{SDT}}], \qquad \text{(D.15)}
$$

where $T_{1(2,3)}$ and $V_{1(2,3)}$ are known functionals defined by the specific form of the respective Heisenberg equations of motion.

The numerical evaluation of the full singlet–doublet–triplet equations (D.13)–(D.15) is still beyond the current capabilities if one wants to study QW or QWI systems. However, one can find a clear physical way to simplify the triplet dynamics (D.15) since it contains two distinct classes of effects: (i) the simpler microscopic processes describe the scattering

of two-particle correlations from single-particle quantities while (ii) the more complicated terms are responsible for the formation of genuine three-particle correlations like trions. For example, the first class implies that an exciton can scatter with an electron, hole, or phonon, which leads to screening of the Coulomb interaction, dephasing of coherences, and formation or equilibration of excitons [18,55,29]. Since we are not interested here in the formation of trions and related effects, we omit the genuine three-particle correlations from the analysis.

The structure of the numerically solved triplet equations follows from

$$i\hbar\frac{\partial}{\partial t}\Delta\langle 3\rangle = T_3[\Delta\langle 3\rangle] + V_3[\langle 4\rangle_{SD}], \tag{D.16}$$

where the four-particle terms are factorized up to the level of two-particle terms. The simpler functional T_3 can be written in the form $T_3[\Delta\langle 3\rangle] = (\Delta E - i\gamma)\Delta\langle 3\rangle$ where ΔE is the energy difference of the in- and out-scattering for single-particle terms and two-particle correlations. As a consequence of our omission of genuine three-particle correlations, $V_3[\langle 4\rangle_{SD}]$ does not contain triplets in contrast to the full Eq. (D.15). Thus, $\Delta\langle 3\rangle$ can be solved analytically,

$$\Delta\langle 3\rangle = \frac{1}{i\hbar}\int_{-\infty}^{t} V_3[\langle 4\rangle_{SD}](u)\, e^{i[\Delta E - i\gamma](u-t)/\hbar}\, du. \tag{D.17}$$

As a general feature, the microscopic scattering effects in semiconductors display non-Markovian characteristics that are relevant mostly at femtosecond time scales. Since we are mostly interested in two to three orders of magnitude longer time scales, Eq. (D.17) can be solved using the Markov approximation leading to

$$\Delta\langle 3\rangle = -\frac{V_3[\langle 4\rangle_{SD}](t)}{\Delta E - i\gamma}. \tag{D.18}$$

Inserting this solution into Eq. (D.14), we find

$$i\hbar\frac{\partial}{\partial t}\langle 1\rangle = T_1[\langle 1\rangle] + V_{1a}[\langle 2\rangle_S] + V_{1b}[\Delta\langle 2\rangle], \tag{D.19}$$

$$i\hbar\frac{\partial}{\partial t}\Delta\langle 2\rangle = T_2[\Delta\langle 2\rangle] + V_{2a}[\langle 3\rangle_{SD}] + G[\langle 1\rangle, \Delta\langle 2\rangle], \tag{D.20}$$

where the functional $G[\langle 1\rangle, \Delta\langle 2\rangle]$ indicates that three-particle correlations are included at the scattering level. This fundamental form is the starting point of most of our current investigations of semiconductors. The explicit form of G for the phonon-induced scattering contributions is presented in Ref. [29].

Appendix E. Classification of correlations

Even though Eq. (D.7) establishes the generic dynamics of any given carrier correlation we still need the explicit form of the equations of motion for our actual computations. The different relevant contributions can be found by considering all possible combinations of the band index λ_j and spin index σ_j in $\Delta\langle \mathbf{k}^{\dagger}_{1,\lambda_1}\mathbf{k}^{\dagger}_{2,\lambda_2}\mathbf{k}_{2\mathbf{q},\lambda_3}\mathbf{k}_{1\mathbf{q},\lambda_4}\rangle$ with $\lambda_j = (\lambda_j, \sigma_j)$. However, we do not need to analyze all these possible combinations since several different forms of correlations may belong to the same class. In order to take advantage of the resulting

simplifications, we next determine which of the band- and spin-index combinations are relevant for the two-particle correlations.

If A and B denote the number of possible band and spin indices one carrier operator $a_{\mathbf{k}_j,\lambda_j}$ can have, the two-particle correlations have A^4B^4 different index combinations. This means that if we omit the spin and have either conduction- or valence-band electrons, we have 16 different combinations. With the inclusion of the spin we get already 256 combinations. In general, the correlations can be conveniently classified using an A- and B-based number representation

$$\begin{aligned}
&\mathbf{n} = (n_\lambda, n_\sigma),\\
&n_\lambda = \lambda_1 A^3 + \lambda_2 A^2 + \lambda_3 A^1 + \lambda_4 A^0,\\
&n_\sigma = \sigma_1 B^3 + \sigma_2 B^2 + \sigma_3 B^1 + \sigma_4 B^0.
\end{aligned} \tag{E.1}$$

Clearly, the combination (n_λ, n_σ) and the specific index combination in the correlations have a one-to-one correspondence. The different λ_j (σ_j) are chosen according to c(spin down) $\to 0$, v(spin up) $\to 1$. Even though we have A^4B^4 different correlations, we can reduce the number of relevant correlations by considering their general symmetries

$$\begin{aligned}
c^{\mathbf{q}_\parallel,\mathbf{k}'_\parallel,\mathbf{k}_\parallel}_{\lambda,\nu;\nu',\lambda'} &= \Delta\langle \mathbf{k}^\dagger_1 \mathbf{k}^\dagger_2 \mathbf{k}_{2'\mathbf{q}} \mathbf{k}_{1'\mathbf{q}}\rangle = \Delta\langle \mathbf{k}^\dagger_2 \mathbf{k}^\dagger_1 \mathbf{k}_{1'\mathbf{q}} \mathbf{k}_{2'\mathbf{q}}\rangle = c^{-\mathbf{q}_\parallel,\mathbf{k}_\parallel,\mathbf{k}'_\parallel}_{\nu,\lambda;\lambda',\nu'}\\
&= -\Delta\langle \mathbf{k}^\dagger_1 \mathbf{k}^\dagger_2 \mathbf{k}_{2\lambda'\mathbf{j}} \mathbf{k}_{1\nu'\mathbf{j}}\rangle = -c^{-\mathbf{j}_\parallel,\mathbf{k}'_\parallel,\mathbf{k}_\parallel}_{\lambda,\nu;\lambda',\nu'}\\
&= \Delta\langle \mathbf{k}^\dagger_2 \mathbf{k}^\dagger_1 \mathbf{k}_{2\lambda'\mathbf{j}} \mathbf{k}_{1\nu'\mathbf{j}}\rangle = -c^{\mathbf{j}_\parallel,\mathbf{k}_\parallel,\mathbf{k}'_\parallel}_{\nu,\lambda;\lambda',\nu'}\\
&= [\Delta\langle \mathbf{k}^\dagger_{1'\mathbf{q}} \mathbf{k}^\dagger_{2'\mathbf{q}} \mathbf{k}_2 \mathbf{k}_1\rangle]^\star = [c^{-\mathbf{q}_\parallel,\mathbf{k}'_\parallel+\mathbf{q}_\parallel,\mathbf{k}_\parallel-\mathbf{q}_\parallel}_{\lambda',\nu';\nu,\lambda}]^\star
\end{aligned} \tag{E.2}$$

which follow from the Fermionic commutation relations of $a_{\mathbf{k}_j,\lambda_j}$, complex conjugation, and sums of carrier momenta.

By omitting the spin, i.e. $n_\sigma = 0$, we can introduce the following groups:

$$\begin{aligned}
&\{0\} = \{c_{c,c;c,c}|_0\},\\
&\{1\} = \{c_{c,c;c,v}|_1,\ c_{c,c;v,c}|_2,\ c_{c,v;c,c}|_4,\ c_{v,c;c,c}|_8\},\\
&\{2\} = \{c_{c,c;v,v}|_3,\ c_{v,v;c,c}|_{12}\},\\
&\{3\} = \{c_{c,v;c,v}|_5,\ c_{c,v;v,c}|_6,\ c_{v,c;c,v}|_9,\ c_{v,c;v,c}|_{10}\},\\
&\{4\} = \{c_{c,v;v,v}|_7,\ c_{v,c;v,v}|_{11},\ c_{v,v;c,v}|_{13},\ c_{v,v;v,c}|_{14}\},\\
&\{5\} = \{c_{v,v;v,v}|_{15}\},
\end{aligned} \tag{E.3}$$

where the subindex determines the n_λ-number according to Eq. (E.1). Within each group, the elements can be transformed from one to another using Eq. (E.2). The groups {1} and {4} as well as {0} and {5} are obtained from each other via an exchange of the c and v indices. As a result, instead of the original 16 one finds only four different equation structures. An analogous analysis can be made if one includes the spin index by fixing n_λ. The resulting groups have a full analogy to (E.3) such that only four relevant spin combinations remain. Thus, the total problem reduces to 16 terms with different spin and band indices compared to the initial 256 terms.

E.1. Spin-related symmetries

The effect of the spin index can most simply be classified by analyzing how it enters the singlet source $S_{\lambda,v;v',\lambda'}$ that drives the correlations. In particular, we can identify the correlations that have a non-vanishing $S_{\lambda,v;v',\lambda'}$. For optical excitations, one finds the simple spin-selection rule

$$\langle a^{\dagger}_{\lambda',\sigma',\mathbf{k}_{\parallel}} a_{\lambda,\sigma,\mathbf{k}_{\parallel}}\rangle = \delta_{\sigma,\sigma'}\langle a^{\dagger}_{\lambda',\sigma,\mathbf{k}_{\parallel}} a_{\lambda,\sigma,\mathbf{k}_{\parallel}}\rangle = \delta_{\sigma,\sigma'} P^{\lambda',\sigma;\lambda,\sigma}_{\mathbf{k}_{\parallel}} \tag{E.4}$$

which states that only the same spin indices appear within the singlet contributions. This constraint influences $S_{\lambda,v;v',\lambda'}$ and thus $c_{\lambda,v;v',\lambda'}$ such that always two spin indices have to be pairwise equal. Due to the Fermionic exchange symmetries, all relevant spin combinations can be presented in the form

$$c_{\lambda,v;v',\lambda'} \equiv c_{(\lambda,\sigma),(v,\sigma');(v',\sigma'),(\lambda',\sigma)} \tag{E.5}$$

which reduces the total number of relevant spin contributions.

E.2. Coherent vs. incoherent contributions

The single-particle quantities can generally be divided into coherent and incoherent quantities,

$$\{[\langle 1\rangle]_{\mathrm{coh}}\} = \{P^{\lambda,v\neq\lambda},\ \langle B\rangle,\ \langle B^{\dagger}\rangle,\ \langle D\rangle,\ \langle D^{\dagger}\rangle\}, \tag{E.6}$$

$$\{[\langle 1\rangle]_{\mathrm{inc}}\} = \{P^{\lambda,\lambda}\}. \tag{E.7}$$

Since the two-particle correlations are generated via the single-particle source, $S_{\lambda,v;v',\lambda'}$, also the two-particle quantities can be classified according to the property if coherent singlets are required for their generation. Among the pure carrier quantities, the groups {1}, {2} and {4} in Eq. (E.3) are coherent, i.e.

$$\begin{aligned}\{[\Delta\langle 2\rangle]_{\mathrm{coh}}\} = \{&c_{c,c;c,v},\ c_{c,c;v,c},\ c_{c,v;c,c},\ c_{v,c;c,c},\ c_{c,c;v,v},\\ &c_{v,v;v,c},\ c_{v,v;c,v},\ c_{v,c;v,v},\ c_{c,v;v,v},\ c_{v,v;c,c}\}.\end{aligned} \tag{E.8}$$

The remaining groups {0}, {3} and {5} in Eq. (E.3) are incoherent

$$\{[\Delta\langle 2\rangle]_{\mathrm{inc}}\} = \{c_{c,c;c,c},\ c_{c,v;c,v},\ c_{c,v;v,c},\ c_{v,c;c,v},\ c_{v,c;v,c},\ c_{v,v;v,v}\}. \tag{E.9}$$

If we use only one representative element of each group (E.3), we find the coherent–incoherent separation of Eqs. (180)–(181), discussed in Section 5.8. A similar division into coherent vs. incoherent quantities can be made for terms containing photon and phonon operators.

In general, Eq. (D.7) mixes the dynamics of coherent and incoherent contributions. To see how this happens, we sort the terms into coherent and incoherent ones according to

$$\begin{aligned}i\hbar\frac{\partial}{\partial t} c^{\mathbf{q}_{\parallel},\mathbf{k}'_{\parallel},\mathbf{k}_{\parallel}}_{\lambda,v;v',\lambda'} = {}&(\tilde{\varepsilon}^{\lambda'}_{\mathbf{k}_{\parallel}-\mathbf{q}_{\parallel}} + \tilde{\varepsilon}^{v'}_{\mathbf{k}'_{\parallel}+\mathbf{q}_{\parallel}} - \tilde{\varepsilon}^{v}_{\mathbf{k}'_{\parallel}} - \tilde{\varepsilon}^{\lambda}_{\mathbf{k}_{\parallel}}) c^{\mathbf{q}_{\parallel},\mathbf{k}'_{\parallel},\mathbf{k}_{\parallel}}_{\lambda,v;v',\lambda'}\\ &+ [[D_{\mathrm{clas}}]^{\mathbf{q}_{\parallel},\mathbf{k}'_{\parallel},\mathbf{k}_{\parallel}}_{\lambda,v;v',\lambda'} + S^{\mathbf{q}_{\parallel},\mathbf{k}'_{\parallel},\mathbf{k}_{\parallel}}_{\lambda,v;v',\lambda'} + D^{\mathbf{q}_{\parallel},\mathbf{k}'_{\parallel},\mathbf{k}_{\parallel}}_{\lambda,v;v',\lambda'}]_{\mathrm{coh}}\\ &+ [[D_{\mathrm{clas}}]^{\mathbf{q}_{\parallel},\mathbf{k}'_{\parallel},\mathbf{k}_{\parallel}}_{\lambda,v;v',\lambda'} + S^{\mathbf{q}_{\parallel},\mathbf{k}'_{\parallel},\mathbf{k}_{\parallel}}_{\lambda,v;v',\lambda'} + D^{\mathbf{q}_{\parallel},\mathbf{k}'_{\parallel},\mathbf{k}_{\parallel}}_{\lambda,v;v',\lambda'}]_{\mathrm{inc}}\end{aligned}$$

$$+[[G_{\text{phon}}]^{\mathbf{q}_\parallel,\mathbf{k}'_\parallel,\mathbf{k}_\parallel}_{\lambda,v;v',\lambda'}+[G_{\text{QED}}]^{\mathbf{q}_\parallel,\mathbf{k}'_\parallel,\mathbf{k}_\parallel}_{\lambda,v;v',\lambda'}+T^{\mathbf{q}_\parallel,\mathbf{k}'_\parallel,\mathbf{k}_\parallel}_{\lambda,v;v',\lambda'}]_{\text{coh}}$$
$$+[[G_{\text{phon}}]^{\mathbf{q}_\parallel,\mathbf{k}'_\parallel,\mathbf{k}_\parallel}_{\lambda,v;v',\lambda'}+[G_{\text{QED}}]^{\mathbf{q}_\parallel,\mathbf{k}'_\parallel,\mathbf{k}_\parallel}_{\lambda,v;v',\lambda'}+T^{\mathbf{q}_\parallel,\mathbf{k}'_\parallel,\mathbf{k}_\parallel}_{\lambda,v;v',\lambda'}]_{\text{inc}}. \tag{E.10}$$

This sorting procedure is performed after all the terms have been expressed explicitly (see e.g. Appendix F). More precisely, $[..]_{\text{coh}}$ contains only coherent correlations and the remaining terms, $[..]_{\text{inc}}$, are incoherent.

E.3. Fermionic exchange symmetry

As discussed in Section 4.3.3, the carrier correlations obey the symmetries (87)–(89) resulting from the Fermionic symmetry of the carrier operators. It is straightforward to show that the explicit singlet–doublet factorization result, Eq. (D.7), fulfills exactly the same symmetries. More precisely, we find the connections

$$\begin{aligned}
&S^{\mathbf{q}_\parallel,\mathbf{k}'_\parallel,\mathbf{k}_\parallel}_{\lambda,v;v',\lambda'}\equiv \text{Sym}_{\text{F}}([\tfrac{1}{2}S^{(1)}-S^{(2)}]^{\mathbf{q}_\parallel,\mathbf{k}'_\parallel,\mathbf{k}_\parallel}_{\lambda,v;v',\lambda'}),\\
&[D_{\text{clas}}]^{\mathbf{q}_\parallel,\mathbf{k}'_\parallel,\mathbf{k}_\parallel}_{\lambda,v;v',\lambda'}\equiv \text{Sym}_{\text{F}}([\tfrac{1}{2}D_{\text{clas}}]\mathbf{q}_\parallel,\mathbf{k}'_\parallel,\mathbf{k}_{\parallel\,\lambda,v;v',\lambda'}),\\
&D^{\mathbf{q}_\parallel,\mathbf{k}'_\parallel,\mathbf{k}_\parallel}_{\lambda,v;v',\lambda'}\equiv \text{Sym}_{\text{F}}([D_{\text{Scr}}]^{\mathbf{q}_\parallel,\mathbf{k}'_\parallel,\mathbf{k}_\parallel}_{\lambda,v;v',\lambda'}+[\tfrac{1}{4}D^{(0)}_{\text{Coul}}-\tfrac{1}{2}D^{(1)}_{\text{Coul}}+D^{(2)}_{\text{Coul}}]^{\mathbf{q}_\parallel,\mathbf{k}'_\parallel,\mathbf{k}_\parallel}_{\lambda,v;v',\lambda'}),\\
&[G_{\text{phon}}]^{\mathbf{q}_\parallel,\mathbf{k}'_\parallel,\mathbf{k}_\parallel}_{\lambda,v;v',\lambda'}\equiv \text{Sym}_{\text{F}}([D_{\text{phon}}]^{\mathbf{q}_\parallel,\mathbf{k}'_\parallel,\mathbf{k}_\parallel}_{\lambda,v;v',\lambda'}),\\
&[G_{\text{QED}}]^{\mathbf{q}_\parallel,\mathbf{k}'_\parallel,\mathbf{k}_\parallel}_{\lambda,v;v',\lambda'}\equiv \text{Sym}_{\text{F}}([D_{\text{QED}}]^{\mathbf{q}_\parallel,\mathbf{k}'_\parallel,\mathbf{k}_\parallel}_{\lambda,v;v',\lambda'}),
\end{aligned} \tag{E.11}$$

where $\text{Sym}_{\text{F}}(..)$ performs the Fermion-symmetry operation according to Eq. (91). The explicit form of the right-hand side in Eq. (E.11) is obtained from Eqs. (97)–(98), (100)–(101), (105)–(106), and (107)–(108).

Appendix F. Exciton-correlation dynamics

The full singlet–doublet dynamics is derived in Appendix D and the result for a generic correlation is given in Eq. (D.7). For the solution of a specific problem we need to unravel these expressions explicitly. For this purpose, we present in this Appendix the explicit form for the exciton correlations,

$$c^{\mathbf{q}_\parallel,\mathbf{k}'_\parallel,\mathbf{k}_\parallel}_X\equiv c^{\mathbf{q}_\parallel,\mathbf{k}'_\parallel,\mathbf{k}_\parallel}_{c,v;c,v}. \tag{F.1}$$

First of all, we insert the band-index combinations ($\lambda=c,v=v;v'=c,\lambda'=v$) into Eqs. (D.7)–(D.11) to obtain

$$\begin{aligned}
\text{i}\hbar\frac{\partial}{\partial t}c^{\mathbf{q}_\parallel,\mathbf{k}'_\parallel,\mathbf{k}_\parallel}_{c,v;c,v}&=(\tilde{\varepsilon}^{\text{e}}_{\mathbf{k}'_\parallel+\mathbf{q}_\parallel}+\tilde{\varepsilon}^{\text{h}}_{\mathbf{k}'_\parallel}-\tilde{\varepsilon}^{\text{e}}_{\mathbf{k}_\parallel}-\tilde{\varepsilon}^{\text{h}}_{\mathbf{k}_\parallel-\mathbf{q}_\parallel})c^{\mathbf{q}_\parallel,\mathbf{k}'_\parallel,\mathbf{k}_\parallel}_{c,v;c,v}+\Omega^{c,v}_{\mathbf{k}_\parallel}c^{\mathbf{q}_\parallel,\mathbf{k}'_\parallel,\mathbf{k}_\parallel}_{v,v;c,v}\\
&\quad+\Omega^{v,c}_{\mathbf{k}'_\parallel}c^{\mathbf{q}_\parallel,\mathbf{k}'_\parallel,\mathbf{k}_\parallel}_{c,c;c,v}-\Omega^{v,c}_{\mathbf{k}'_\parallel+\mathbf{q}_\parallel}c^{\mathbf{q}_\parallel,\mathbf{k}'_\parallel,\mathbf{k}_\parallel}_{c,v;v,v}-\Omega^{c,v}_{\mathbf{k}_\parallel-\mathbf{q}_\parallel}c^{\mathbf{q}_\parallel,\mathbf{k}'_\parallel,\mathbf{k}_\parallel}_{c,v;c,c}\\
&\quad+\text{S}^{\mathbf{q}_\parallel,\mathbf{k}'_\parallel,\mathbf{k}_\parallel}_{c,v;c,v}+\text{D}^{\mathbf{q}_\parallel,\mathbf{k}'_\parallel,\mathbf{k}_\parallel}_{c,v;c,v}+[G_{\text{phon}}]^{\mathbf{q}_\parallel,\mathbf{k}'_\parallel,\mathbf{k}_\parallel}_{c,v;c,v}+[G_{\text{QED}}]^{\mathbf{q}_\parallel,\mathbf{k}'_\parallel,\mathbf{k}_\parallel}_{c,v;c,v}+\text{T}^{\mathbf{q}_\parallel,\mathbf{k}'_\parallel,\mathbf{k}_\parallel}_{c,v;c,v}.
\end{aligned} \tag{F.2}$$

The remaining implicit terms are evaluated separately in the following subsections.

F.1. Single-particle source

By choosing the spin combination according to Eq. (E.5), Eq. (D.8) produces the fully explicit singlet source

$$\begin{aligned}
S_{c,v;c,v}^{\mathbf{q}_\parallel,\mathbf{k}'_\parallel,\mathbf{k}_\parallel} \equiv{}& \delta_{\sigma,\sigma'} V_{\mathbf{j}_\parallel}[(f^{e}_{\mathbf{k}'_\parallel+\mathbf{q}_\parallel} f^{h}_{\mathbf{k}'_\parallel} \bar{f}^{e}_{\mathbf{k}_\parallel} \bar{f}^{h}_{\mathbf{k}_\parallel-\mathbf{q}_\parallel})_\Sigma \\
&+ P^{\star}_{\mathbf{k}_\parallel} P_{\mathbf{k}'_\parallel+\mathbf{q}_\parallel} (f^{h}_{\mathbf{k}_\parallel-\mathbf{q}_\parallel} - f^{h}_{\mathbf{k}'_\parallel}) + P^{\star}_{\mathbf{k}_\parallel-\mathbf{q}_\parallel} P_{\mathbf{k}'_\parallel} (f^{e}_{\mathbf{k}_\parallel} - f^{e}_{\mathbf{k}'_\parallel+\mathbf{q}_\parallel})] \\
&+ V_{\mathbf{q}_\parallel}[P^{\star}_{\mathbf{k}_\parallel} P_{\mathbf{k}'_\parallel} (f^{h}_{\mathbf{k}_\parallel-\mathbf{q}_\parallel} - f^{e}_{\mathbf{k}'_\parallel+\mathbf{q}_\parallel}) - P^{\star}_{\mathbf{k}_\parallel-\mathbf{q}_\parallel} P_{\mathbf{k}'_\parallel+\mathbf{q}_\parallel} (f^{h}_{\mathbf{k}'_\parallel} - f^{e}_{\mathbf{k}_\parallel}) \\
&- P^{\star}_{\mathbf{k}_\parallel-\mathbf{q}_\parallel} P_{\mathbf{k}'_\parallel} (f^{e}_{\mathbf{k}_\parallel} - f^{e}_{\mathbf{k}'_\parallel+\mathbf{q}_\parallel}) + P^{\star}_{\mathbf{k}_\parallel} P_{\mathbf{k}'_\parallel+\mathbf{q}_\parallel} (f^{h}_{\mathbf{k}'_\parallel} - f^{h}_{\mathbf{k}_\parallel-\mathbf{q}_\parallel})],
\end{aligned} \tag{F.3}$$

where the condition (E.4) has been applied. Additionally, we introduced the abbreviation

$$(f^{\lambda}_{\mathbf{k}_\parallel} f^{\lambda'}_{\mathbf{k}'_\parallel} \bar{f}^{\lambda''}_{\mathbf{k}''_\parallel} \bar{f}^{\lambda'''}_{\mathbf{k}'''_\parallel})_\Sigma \equiv f^{\lambda}_{\mathbf{k}_\parallel} f^{\lambda'}_{\mathbf{k}'_\parallel} (1 - f^{\lambda''}_{\mathbf{k}''_\parallel})(1 - f^{\lambda'''}_{\mathbf{k}'''_\parallel}) - (1 - f^{\lambda}_{\mathbf{k}_\parallel})(1 - f^{\lambda'}_{\mathbf{k}'_\parallel}) \bar{f}^{\lambda''}_{\mathbf{k}''_\parallel} \bar{f}^{\lambda'''}_{\mathbf{k}'''_\parallel} \tag{F.4}$$

which identifies the in- and out-scattering terms discussed earlier in connection with Eq. (99).

F.2. Two-particle correlations

The correlated Coulomb-induced doublets are obtained from (D.9). We may now separate the terms with incoherent from those containing coherent correlations, see Appendix E.2. As a result, we find

$$D_{c,v;c,v}^{\mathbf{q}_\parallel,\mathbf{k}'_\parallel,\mathbf{k}_\parallel} = [D_{c,v;c,v}^{\mathbf{q}_\parallel,\mathbf{k}'_\parallel,\mathbf{k}_\parallel}]_{\mathrm{inc}} + [D_{c,v;c,v}^{\mathbf{q}_\parallel,\mathbf{k}'_\parallel,\mathbf{k}_\parallel}]_{\mathrm{coh}}, \tag{F.5}$$

$$\begin{aligned}
&[D_{c,v;c,v}^{\mathbf{q}_\parallel,\mathbf{k}'_\parallel,\mathbf{k}_\parallel}]_{\mathrm{inc}} \\
&\quad\equiv (1 - f^{e}_{\mathbf{k}_\parallel} - f^{h}_{\mathbf{k}_\parallel-\mathbf{q}_\parallel}) \sum_{\mathbf{l}_\parallel} V_{\mathbf{l}-\mathbf{k}_\parallel} c_{c,v;c,v}^{\mathbf{q}_\parallel,\mathbf{k}'_\parallel,\mathbf{l}_\parallel} - (1 - f^{e}_{\mathbf{k}'_\parallel+\mathbf{q}_\parallel} - f^{h}_{\mathbf{k}'_\parallel}) \sum_{\mathbf{l}_\parallel} V_{\mathbf{l}_\parallel-\mathbf{k}'_\parallel} c_{c,v;c,v}^{\mathbf{q}_\parallel,\mathbf{l}_\parallel,\mathbf{k}_\parallel} \\
&\qquad+ (f^{e}_{\mathbf{k}_\parallel} - f^{h}_{\mathbf{k}'_\parallel}) \sum_{\mathbf{l}_\parallel} V_{\mathbf{l}_\parallel+\mathbf{q}_\parallel} [c_{v,c;v,c}^{\mathbf{l}_\parallel,\mathbf{k}'_\parallel+\mathbf{q}_\parallel,\mathbf{k}_\parallel-\mathbf{q}_\parallel}]^{\star} \\
&\qquad+ (f^{h}_{\mathbf{k}_\parallel-\mathbf{q}_\parallel} - f^{e}_{\mathbf{k}'_\parallel+\mathbf{q}_\parallel}) \sum_{\mathbf{l}_\parallel} V_{\mathbf{l}_\parallel-\mathbf{q}_\parallel} c_{c,v;c,v}^{\mathbf{l}_\parallel,\mathbf{k}'_\parallel,\mathbf{k}_\parallel} \\
&\qquad+ (f^{e}_{\mathbf{k}_\parallel} - f^{e}_{\mathbf{k}'_\parallel+\mathbf{q}_\parallel}) \sum_{\mathbf{l}_\parallel} V_{\mathbf{l}-\mathbf{k}_\parallel} c_{c,v;v,c}^{-\mathbf{j}_\parallel,\mathbf{k}'_\parallel,\mathbf{l}_\parallel} + (f^{h}_{\mathbf{k}'_\parallel} - f^{h}_{\mathbf{k}_\parallel-\mathbf{q}_\parallel}) \sum_{\mathbf{l}_\parallel} V_{\mathbf{l}_\parallel-\mathbf{k}'_\parallel} c_{c,v;v,c}^{-\mathbf{j}_\parallel,\mathbf{l}_\parallel,\mathbf{k}_\parallel} \\
&\qquad+ \delta_{\sigma,\sigma'} V_{\mathbf{j}_\parallel} (f^{e}_{\mathbf{k}_\parallel+\mathbf{j}_\parallel} - f^{e}_{\mathbf{k}_\parallel}) \sum_{\mathbf{l}_\parallel} (c_{c,v;v,c}^{-\mathbf{j}_\parallel,\mathbf{k}'_\parallel,\mathbf{l}_\parallel} + c_{v,v;v,v}^{-\mathbf{j}_\parallel,\mathbf{k}'_\parallel,\mathbf{l}_\parallel}) \\
&\qquad+ \delta_{\sigma,\sigma'} V_{\mathbf{j}_\parallel} (f^{h}_{\mathbf{k}'_\parallel} - f^{h}_{\mathbf{k}'_\parallel-\mathbf{j}_\parallel}) \sum_{\mathbf{l}_\parallel} (c_{c,c;c,c}^{-\mathbf{j}_\parallel,\mathbf{l}_\parallel,\mathbf{k}_\parallel} + c_{c,v;v,c}^{-\mathbf{j}_\parallel,\mathbf{l}_\parallel,\mathbf{k}_\parallel}),
\end{aligned} \tag{F.6}$$

which contains the dominant *main-sum approximation* terms in the second line. The spin-index dependence follows from the choice (E.5) and the condition (E.4). The coherent part

of the doublets results from

$$
\begin{aligned}
&[D^{\mathbf{q}_\parallel,\mathbf{k}'_\parallel,\mathbf{k}_\parallel}_{c,v;c,v}]_{\mathrm{coh}} \\
&\quad = +V_{\mathbf{q}_\parallel}(P^{\star}_{\mathbf{k}_\parallel} - P^{\star}_{\mathbf{k}_\parallel-\mathbf{q}_\parallel}) \sum_{\mathbf{l}_\parallel} (c^{\mathbf{q}_\parallel,\mathbf{k}'_\parallel,\mathbf{l}_\parallel}_{c,v;c,c} + c^{\mathbf{q}_\parallel,\mathbf{k}'_\parallel,\mathbf{l}_\parallel}_{v,v;c,v}) \\
&\qquad - V_{\mathbf{q}_\parallel}(P_{\mathbf{k}'_\parallel+\mathbf{q}_\parallel} - P_{\mathbf{k}'_\parallel}) \sum_{\mathbf{l}_\parallel} (c^{\mathbf{q}_\parallel,\mathbf{l}_\parallel,\mathbf{k}_\parallel}_{c,c;c,v} + c^{\mathbf{q}_\parallel,\mathbf{l}_\parallel,\mathbf{k}_\parallel}_{c,v;v,v}) \\
&\qquad + \sum_{\mathbf{l}_\parallel} V_{\mathbf{l}_\parallel-\mathbf{k}_\parallel}(P^{\star}_{\mathbf{k}_\parallel}[c^{-\mathbf{j}_\parallel,\mathbf{k}'_\parallel,\mathbf{l}_\parallel}_{v,v;v,c} - c^{\mathbf{q}_\parallel,\mathbf{k}'_\parallel,\mathbf{l}_\parallel}_{v,v;c,v}] + P^{\star}_{\mathbf{k}_\parallel-\mathbf{q}_\parallel} c^{\mathbf{q}_\parallel,\mathbf{k}'_\parallel,\mathbf{l}_\parallel}_{c,v;c,c} - P_{\mathbf{k}'_\parallel+\mathbf{q}_\parallel} c^{-\mathbf{j}_\parallel,\mathbf{k}'_\parallel,\mathbf{l}_\parallel}_{c,v;v,v}) \\
&\qquad + \sum_{\mathbf{l}_\parallel} V_{\mathbf{l}_\parallel-\mathbf{k}'_\parallel}(P_{\mathbf{k}'_\parallel}[c^{-\mathbf{j}_\parallel,\mathbf{l}_\parallel,\mathbf{k}_\parallel}_{c,c;v,c} - c^{\mathbf{q}_\parallel,\mathbf{l}_\parallel,\mathbf{k}_\parallel}_{c,c;c,v}] - P^{\star}_{\mathbf{k}_\parallel-\mathbf{q}_\parallel} c^{\mathbf{j}_\parallel,\mathbf{k}_\parallel,\mathbf{l}_\parallel}_{v,c;c,c} + P_{\mathbf{k}'_\parallel+\mathbf{q}_\parallel} c^{\mathbf{q}_\parallel,\mathbf{l}_\parallel,\mathbf{k}_\parallel}_{c,v;v,v}) \\
&\qquad + \sum_{\mathbf{l}_\parallel} V_{\mathbf{l}_\parallel+\mathbf{q}_\parallel}[P^{\star}_{\mathbf{k}'_\parallel} c^{\mathbf{l}_\parallel,\mathbf{k}'_\parallel+\mathbf{q}_\parallel,\mathbf{k}_\parallel-\mathbf{q}_\parallel}_{v,c;c,c} + P_{\mathbf{k}_\parallel} c^{\mathbf{l}_\parallel,\mathbf{k}'_\parallel+\mathbf{q}_\parallel,\mathbf{k}_\parallel-\mathbf{q}_\parallel}_{v,c;v,v}]^{\star} \\
&\qquad - \sum_{\mathbf{l}_\parallel} V_{\mathbf{l}_\parallel-\mathbf{q}_\parallel}[P^{\star}_{\mathbf{k}_\parallel-\mathbf{q}_\parallel} c^{\mathbf{l}_\parallel,\mathbf{k}'_\parallel,\mathbf{k}_\parallel}_{c,v;c,c} + P_{\mathbf{k}'_\parallel+\mathbf{q}_\parallel} c^{\mathbf{l}_\parallel,\mathbf{k}'_\parallel,\mathbf{k}_\parallel}_{c,v;v,v}]. \qquad \text{(F.7)}
\end{aligned}
$$

One can also subdivide the phonon-correlation contributions into incoherent and coherent ones, i.e.

$$
[G_{\mathrm{phon}}]^{\mathbf{q}_\parallel,\mathbf{k}'_\parallel,\mathbf{k}_\parallel}_{c,v;c,v} \equiv [G^{\mathrm{inc}}_{\mathrm{phon}}]^{\mathbf{q}_\parallel,\mathbf{k}'_\parallel,\mathbf{k}_\parallel}_{c,v;c,v} + [G^{\mathrm{coh}}_{\mathrm{phon}}]^{\mathbf{q}_\parallel,\mathbf{k}'_\parallel,\mathbf{k}_\parallel}_{c,v;c,v}, \qquad \text{(F.8)}
$$

$$
\begin{aligned}
[G^{\mathrm{inc}}_{\mathrm{phon}}]^{\mathbf{q}_\parallel,\mathbf{k}'_\parallel,\mathbf{k}_\parallel}_{c,v;c,v} &= (f^{\mathrm{e}}_{\mathbf{k}'_\parallel+\mathbf{q}_\parallel} - f^{\mathrm{e}}_{\mathbf{k}_\parallel}) \Delta \langle Q^{c}_{\mathbf{j}_\parallel} a^{\dagger}_{v,\mathbf{k}'_\parallel} a_{v,\mathbf{k}'_\parallel-\mathbf{j}_\parallel} \rangle \\
&\quad + (f^{\mathrm{h}}_{\mathbf{k}'_\parallel} - f^{\mathrm{h}}_{\mathbf{k}_\parallel-\mathbf{q}_\parallel}) \Delta \langle [Q^{v}_{\mathbf{j}_\parallel}]^{\dagger} a^{\dagger}_{c,\mathbf{k}_\parallel} a_{c,\mathbf{k}_\parallel+\mathbf{j}_\parallel} \rangle, \qquad \text{(F.9)}
\end{aligned}
$$

$$
\begin{aligned}
[G^{\mathrm{coh}}_{\mathrm{phon}}]^{\mathbf{q}_\parallel,\mathbf{k}'_\parallel,\mathbf{k}_\parallel}_{c,v;c,v} &= P^{\star}_{\mathbf{k}_\parallel} \Delta \langle [Q^{v}_{\mathbf{q}_\parallel}]^{\dagger} a^{\dagger}_{v,\mathbf{k}'_\parallel} a_{c,\mathbf{k}'_\parallel+\mathbf{q}_\parallel} \rangle - P^{\star}_{\mathbf{k}_\parallel-\mathbf{q}_\parallel} \Delta \langle [Q^{c}_{\mathbf{q}_\parallel}]^{\dagger} a^{\dagger}_{v,\mathbf{k}'_\parallel} a_{c,\mathbf{k}'_\parallel+\mathbf{q}_\parallel} \rangle \\
&\quad + P_{\mathbf{k}'_\parallel} \Delta \langle Q^{c}_{\mathbf{q}_\parallel} a^{\dagger}_{c,\mathbf{k}_\parallel} a_{v,\mathbf{k}_\parallel-\mathbf{q}_\parallel} \rangle - P_{\mathbf{k}'_\parallel+\mathbf{q}_\parallel} \Delta \langle Q^{v}_{\mathbf{q}_\parallel} a^{\dagger}_{c,\mathbf{k}_\parallel} a_{v,\mathbf{k}_\parallel-\mathbf{q}_\parallel} \rangle. \qquad \text{(F.10)}
\end{aligned}
$$

Also the quantum-optical correlations may change the doublet correlations. As for all the other contributions, we make a distinction between coherent and incoherent correlation contributions,

$$
[G_{\mathrm{QED}}]^{\mathbf{q}_\parallel,\mathbf{k}'_\parallel,\mathbf{k}_\parallel}_{c,v;c,v} \equiv [G^{\mathrm{inc}}_{\mathrm{QED}}]^{\mathbf{q}_\parallel,\mathbf{k}'_\parallel,\mathbf{k}_\parallel}_{c,v;c,v} + [G^{\mathrm{coh}}_{\mathrm{QED}}]^{\mathbf{q}_\parallel,\mathbf{k}'_\parallel,\mathbf{k}_\parallel}_{c,v;c,v}, \qquad \text{(F.11)}
$$

$$
\begin{aligned}
[G^{\mathrm{inc}}_{\mathrm{QED}}]^{\mathbf{q}_\parallel,\mathbf{k}'_\parallel,\mathbf{k}_\parallel}_{c,v;c,v} &= +(1 - f^{\mathrm{e}}_{\mathbf{k}_\parallel} - f^{\mathrm{h}}_{\mathbf{k}_\parallel-\mathbf{q}_\parallel}) \Delta \langle [E^{c}_{\mathbf{q}_\parallel}]^{\dagger} a^{\dagger}_{v,\mathbf{k}'_\parallel} a_{c,\mathbf{k}'_\parallel+\mathbf{q}_\parallel} \rangle \\
&\quad - (1 - f^{\mathrm{e}}_{\mathbf{k}'_\parallel+\mathbf{q}_\parallel} - f^{\mathrm{h}}_{\mathbf{k}'_\parallel}) \Delta \langle E^{c}_{\mathbf{q}_\parallel} a^{\dagger}_{c,\mathbf{k}_\parallel} a_{v,\mathbf{k}_\parallel-\mathbf{q}_\parallel} \rangle, \qquad \text{(F.12)}
\end{aligned}
$$

$$
\begin{aligned}
[G^{\mathrm{coh}}_{\mathrm{QED}}]^{\mathbf{q}_\parallel,\mathbf{k}'_\parallel,\mathbf{k}_\parallel}_{c,v;c,v} &= P_{\mathbf{k}'_\parallel} \Delta \langle [E^{c}_{\mathbf{j}_\parallel}]^{\dagger} a^{\dagger}_{c,\mathbf{k}_\parallel} a_{c,\mathbf{k}_\parallel+\mathbf{j}_\parallel} \rangle - P_{\mathbf{k}'_\parallel+\mathbf{q}_\parallel} \Delta \langle E^{v}_{\mathbf{j}_\parallel} a^{\dagger}_{v,\mathbf{k}'_\parallel} a_{v,\mathbf{k}'_\parallel-\mathbf{j}_\parallel} \rangle \\
&\quad + P^{\star}_{\mathbf{k}_\parallel} \Delta \langle E^{c}_{\mathbf{j}_\parallel} a^{\dagger}_{v,\mathbf{k}'_\parallel} a_{v,\mathbf{k}'_\parallel-\mathbf{j}_\parallel} \rangle - P^{\star}_{\mathbf{k}_\parallel-\mathbf{q}_\parallel} \Delta \langle [E^{v}_{\mathbf{j}_\parallel}]^{\dagger} a^{\dagger}_{c,\mathbf{k}_\parallel} a_{c,\mathbf{k}_\parallel+\mathbf{j}_\parallel} \rangle. \qquad \text{(F.13)}
\end{aligned}
$$

These terms introduce the coupling of the pure carrier correlations to phonon- and photon-induced correlations. The exciton-correlation dynamics contains also a three-particle correlations that can be unraveled with the help of Eq. (D.12).

F.3. Energy transfer

It is straightforward to see that the total average energy $\langle H_{\rm carr}\rangle$ of the carrier system contains only the single- and two-particle clusters according to Eqs. (199)–(202). One can also show, by applying the full singlet–doublet dynamics discussed in Section 4, that the consistent singlet–doublet approach always conserves the total energy of the system. This means that the energy of the singlets may be transferred to the doublets and vice versa, but there is not energy gain or loss. In the following, we investigate these energy transfer mechanism between the most important coherent and incoherent quantities in the carrier system.

According to Eq. (201), the coherent singlets contain the energy

$$[E^{\rm S}_{\rm carr}]_{\rm coh} = -\sum_{\mathbf{k}_\parallel,\mathbf{k}'_\parallel} V_{\mathbf{k}_\parallel-\mathbf{k}'_\parallel} P^{\star}_{\mathbf{k}_\parallel} P_{\mathbf{k}'_\parallel}. \tag{F.14}$$

Since the numerical analysis in Section 6 shows that the coherent polarization may be converted into incoherent exciton populations, we compare the changes in $[E^{\rm S}_{\rm carr}]_{\rm coh}$ to those in the excitonic-correlation energy,

$$[E^{\rm D}_{\rm carr}]_{\rm X} \equiv -\sum_{\mathbf{k}_\parallel,\mathbf{k}'_\parallel,\mathbf{q}_\parallel} V_{\mathbf{k}'_\parallel+\mathbf{q}_\parallel-\mathbf{k}_\parallel} c_X^{\mathbf{q}_\parallel,\mathbf{k}'_\parallel,\mathbf{k}_\parallel}, \tag{F.15}$$

which is the last term of Eq. (202).

The phonon- and Coulomb-scattering induced dephasing influence on $[E^{\rm S}_{\rm carr}]_{\rm coh}$ follows directly from Eq. (D.1) producing

$$i\hbar\frac{\partial}{\partial t}[E^{\rm S}_{\rm carr}]_{\rm coh} = i\hbar\frac{\partial}{\partial t}[E^{\rm S}_{\rm carr}]^{\rm Coul}_{\rm coh} + i\hbar\frac{\partial}{\partial t}[E^{\rm S}_{\rm carr}]^{\rm phon}_{\rm coh}, \tag{F.16}$$

$$\begin{aligned} i\hbar\frac{\partial}{\partial t}&[E^{\rm S}_{\rm carr}]^{\rm Coul}_{\rm coh} \\ &= +\sum_{\mathbf{q}_\parallel,\mathbf{k}'_\parallel,\mathbf{k}_\parallel,\mathbf{l}_\parallel} V_{\mathbf{k}'_\parallel+\mathbf{q}_\parallel-\mathbf{k}_\parallel} V_{\mathbf{q}_\parallel}(P^{\star}_{\mathbf{k}_\parallel} - P^{\star}_{\mathbf{k}_\parallel-\mathbf{q}_\parallel})(c^{\mathbf{q}_\parallel,\mathbf{k}'_\parallel,\mathbf{l}_\parallel}_{c,v;c,c} + c^{\mathbf{q}_\parallel,\mathbf{k}'_\parallel,\mathbf{l}_\parallel}_{v,v;c,v}) \\ &\quad -\sum_{\mathbf{q}_\parallel,\mathbf{k}'_\parallel,\mathbf{k}_\parallel,\mathbf{l}_\parallel} V_{\mathbf{k}'_\parallel+\mathbf{q}_\parallel-\mathbf{k}_\parallel} V_{\mathbf{q}_\parallel}(P_{\mathbf{k}'_\parallel+\mathbf{q}_\parallel} - P_{\mathbf{k}'_\parallel})(c^{\mathbf{q}_\parallel,\mathbf{l}_\parallel,\mathbf{k}_\parallel}_{c,c;c,v} + c^{\mathbf{q}_\parallel,\mathbf{l}_\parallel,\mathbf{k}_\parallel}_{c,v;v,v}), \end{aligned} \tag{F.17}$$

$$\begin{aligned} i\hbar\frac{\partial}{\partial t}&[E^{\rm S}_{\rm carr}]^{\rm phon}_{\rm coh} \\ &= -\sum_{\mathbf{q}_\parallel,\mathbf{k}'_\parallel,\mathbf{k}_\parallel} V_{\mathbf{k}'_\parallel-\mathbf{k}_\parallel}\{P^{\star}_{\mathbf{k}_\parallel}[\Delta\langle Q^{v}_{-\mathbf{q}_\parallel} a^{\dagger}_{v,\mathbf{k}'_\parallel-\mathbf{q}_\parallel} a_{c,\mathbf{k}'_\parallel}\rangle - \Delta\langle Q^{c}_{\mathbf{q}_\parallel} a^{\dagger}_{v,\mathbf{k}'_\parallel} a_{c,\mathbf{k}'_\parallel-\mathbf{q}_\parallel}\rangle] \\ &\quad + [\Delta\langle Q^{c}_{-\mathbf{q}_\parallel} a^{\dagger}_{c,\mathbf{k}_\parallel-\mathbf{q}_\parallel} a_{v,\mathbf{k}_\parallel}\rangle - \Delta\langle Q^{v}_{\mathbf{q}_\parallel} a^{\dagger}_{c,\mathbf{k}_\parallel} a_{v,\mathbf{k}_\parallel-\mathbf{q}_\parallel}\rangle]P_{\mathbf{k}'_\parallel}\}, \end{aligned} \tag{F.18}$$

which follow after suitable changes in summation indices and by applying the generic relation $[Q^{\lambda}_{\mathbf{q}_\parallel}]^{\dagger} = Q^{\lambda}_{-\mathbf{q}_\parallel}$. These coherent two-particle correlations are exactly the same as those that induce the dephasing of the polarization and the loss of coherent energy, as discussed in Section 6.2.

To track where this energy is transferred to, we analyze the dynamics of $[E^{\mathrm{D}}_{\mathrm{carr}}]_{\mathrm{X}}$ induced by the coherences. Substitution of Eq. (F.7) into Eq. (F.15) yields

$$\begin{aligned}
\mathrm{i}\hbar\frac{\partial}{\partial t}[E^{\mathrm{D}}_{\mathrm{carr}}]^{\mathrm{coh}}_{\mathrm{X,Coul}} &= -\sum_{\mathbf{q}_\parallel,\mathbf{k}'_\parallel,\mathbf{k}_\parallel} V_{\mathbf{k}'_\parallel+\mathbf{q}_\parallel-\mathbf{k}_\parallel}[D^{\mathbf{q}_\parallel,\mathbf{k}'_\parallel,\mathbf{k}_\parallel}_{c,v;c,v}]_{\mathrm{coh}} \\
&= -\sum_{\mathbf{q}_\parallel,\mathbf{k}'_\parallel,\mathbf{k}_\parallel,\mathbf{l}_\parallel} V_{\mathbf{k}'_\parallel+\mathbf{q}_\parallel-\mathbf{k}_\parallel} V_{\mathbf{q}_\parallel}(P^{\star}_{\mathbf{k}_\parallel}-P^{\star}_{\mathbf{k}_\parallel-\mathbf{q}_\parallel})(c^{\mathbf{q}_\parallel,\mathbf{k}'_\parallel,\mathbf{l}_\parallel}_{c,v;c,c}+c^{\mathbf{q}_\parallel,\mathbf{k}'_\parallel,\mathbf{l}_\parallel}_{v,v;c,v}) \\
&\quad+\sum_{\mathbf{q}_\parallel,\mathbf{k}'_\parallel,\mathbf{k}_\parallel,\mathbf{l}_\parallel} V_{\mathbf{k}'_\parallel+\mathbf{q}_\parallel-\mathbf{k}_\parallel} V_{\mathbf{q}_\parallel}(P_{\mathbf{k}'_\parallel+\mathbf{q}_\parallel}-P_{\mathbf{k}'_\parallel})(c^{\mathbf{q}_\parallel,\mathbf{l}_\parallel,\mathbf{k}_\parallel}_{c,c;c,v}+c^{\mathbf{q}_\parallel,\mathbf{l}_\parallel,\mathbf{k}_\parallel}_{c,v;v,v}).
\end{aligned} \tag{F.19}$$

A similar substitution of Eq. (F.10) into Eq. (F.15) produces

$$\begin{aligned}
\mathrm{i}\hbar\frac{\partial}{\partial t}[E^{\mathrm{D}}_{\mathrm{carr}}]^{\mathrm{coh}}_{\mathrm{X,phon}} &= -\sum_{\mathbf{q}_\parallel,\mathbf{k}'_\parallel,\mathbf{k}_\parallel} V_{\mathbf{k}'_\parallel+\mathbf{q}_\parallel-\mathbf{k}_\parallel}[G^{\mathrm{phon}}_{\mathrm{coh}}]^{\mathbf{q}_\parallel,\mathbf{k}'_\parallel,\mathbf{k}_\parallel}_{c,v;c,v} \\
&= \sum_{\mathbf{q}_\parallel,\mathbf{k}'_\parallel,\mathbf{k}_\parallel} V_{\mathbf{k}'_\parallel-\mathbf{k}_\parallel}\{P^{\star}_{\mathbf{k}_\parallel}[\Delta\langle Q^{v}_{-\mathbf{q}_\parallel}a^{\dagger}_{v,\mathbf{k}'_\parallel-\mathbf{q}_\parallel}a_{c,\mathbf{k}'_\parallel}\rangle-\Delta\langle Q^{c}_{\mathbf{q}_\parallel}a^{\dagger}_{v,\mathbf{k}'_\parallel}a_{c,\mathbf{k}'_\parallel-\mathbf{q}_\parallel}\rangle] \\
&\quad-[\Delta\langle Q^{c}_{-\mathbf{q}_\parallel}a^{\dagger}_{c,\mathbf{k}_\parallel-\mathbf{q}_\parallel}a_{v,\mathbf{k}_\parallel}\rangle-\Delta\langle Q^{v}_{\mathbf{q}_\parallel}a^{\dagger}_{c,\mathbf{k}_\parallel}a_{v,\mathbf{k}_\parallel-\mathbf{q}_\parallel}\rangle]P_{\mathbf{k}'_\parallel}\},
\end{aligned} \tag{F.20}$$

which is obtained after suitable changes in the summation indices.

By comparing Eq. (F.17) with (F.20) and Eq. (F.18) with (F.20), respectively, we notice that the energy lost from the coherent singlets is transferred into exciton correlations since

$$\begin{aligned}
\mathrm{i}\hbar\frac{\partial}{\partial t}([E^{\mathrm{S}}_{\mathrm{carr}}]^{\mathrm{Coul}}_{\mathrm{coh}}+[E^{\mathrm{D}}_{\mathrm{carr}}]^{\mathrm{coh}}_{\mathrm{X,Coul}}) &= 0, \\
\mathrm{i}\hbar\frac{\partial}{\partial t}([E^{\mathrm{S}}_{\mathrm{carr}}]^{\mathrm{phon}}_{\mathrm{coh}}+[E^{\mathrm{D}}_{\mathrm{carr}}]^{\mathrm{coh}}_{\mathrm{X,phon}}) &= 0.
\end{aligned} \tag{F.21}$$

This analysis shows how energy stored in the optical polarization can be converted into the energy of incoherent excitons via Coulomb- and phonon-induced scattering. This process results in the polarization-to-population conversion discussed in Section 6.

Appendix G. Excitation induced dephasing

The semiconductor Bloch equations contain pure carrier-correlation terms of the type $c_{\lambda,\lambda,\lambda,\bar{\lambda}}$ which lead to excitation-induced dephasing of the polarization as discussed in Section 6 and Appendix F.3. At the same time, these correlations also mediate the polarization-to-population conversion.

The dynamics of different $c_{\lambda,\lambda,\lambda,\bar{\lambda}}$ terms has an identical form, such that it is sufficient to derive only one equation explicitly. The rest follows as we make the substitution $c\leftrightarrow v$ and/or apply complex conjugation. We evaluate here the full explicit singlet–doublet dynamics for the combination $c_{v,v,v,c}$ such that the generic band-index sequence is given by $(\lambda=v,\nu=v;\nu'=v,\lambda'=c)$. The dynamics of $c_{v,v,v,c}$ can be obtained from the

generic result (D.7)–(D.11) yielding

$$\begin{aligned}
\mathrm{i}\hbar\frac{\partial}{\partial t}c^{\mathbf{q}_\parallel,\mathbf{k}'_\parallel,\mathbf{k}_\parallel}_{v,v;v,c} &= (\tilde{\varepsilon}^{\mathrm{e}}_{\mathbf{k}_\parallel-\mathbf{q}_\parallel}+\tilde{\varepsilon}^{\mathrm{h}}_{\mathbf{k}_\parallel}-\tilde{\varepsilon}^{\mathrm{h}}_{\mathbf{k}'_\parallel+\mathbf{q}_\parallel}+\tilde{\varepsilon}^{\mathrm{h}}_{\mathbf{k}'_\parallel})c^{\mathbf{q}_\parallel,\mathbf{k}'_\parallel,\mathbf{k}_\parallel}_{v,v;v,c}\\
&\quad+\Omega^{v,c}_{\mathbf{k}_\parallel}c^{\mathbf{q}_\parallel,\mathbf{k}'_\parallel,\mathbf{k}_\parallel}_{c,v;v,c}+\Omega^{v,c}_{\mathbf{k}'_\parallel}c^{\mathbf{q}_\parallel,\mathbf{k}'_\parallel,\mathbf{k}_\parallel}_{v,c;v,c}-\Omega^{c,v}_{\mathbf{k}'_\parallel+\mathbf{q}_\parallel}c^{\mathbf{q}_\parallel,\mathbf{k}'_\parallel,\mathbf{k}_\parallel}_{v,v;c,c}-\Omega^{v,c}_{\mathbf{k}_\parallel-\mathbf{q}_\parallel}c^{\mathbf{q}_\parallel,\mathbf{k}'_\parallel,\mathbf{k}_\parallel}_{v,v;v,v}\\
&\quad+\mathrm{S}^{\mathbf{q}_\parallel,\mathbf{k}'_\parallel,\mathbf{k}_\parallel}_{v,v;v,c}+\mathrm{D}^{\mathbf{q}_\parallel,\mathbf{k}'_\parallel,\mathbf{k}_\parallel}_{v,v;v,c}\\
&\quad+[G_{\mathrm{phon}}]^{\mathbf{q}_\parallel,\mathbf{k}'_\parallel,\mathbf{k}_\parallel}_{v,v;v,c}+[G_{\mathrm{QED}}]^{\mathbf{q}_\parallel,\mathbf{k}'_\parallel,\mathbf{k}_\parallel}_{v,v;v,c}+\mathrm{T}^{\mathbf{q}_\parallel,\mathbf{k}'_\parallel,\mathbf{k}_\parallel}_{v,v;v,c}.
\end{aligned}\tag{G.1}$$

The explicit single-particle scattering source follows from

$$\begin{aligned}
\mathrm{S}^{\mathbf{q}_\parallel,\mathbf{k}'_\parallel,\mathbf{k}_\parallel}_{v,v;v,c} &\equiv \delta_{\sigma,\sigma'}V_{\mathbf{j}_\parallel}[P_{\mathbf{k}_\parallel-\mathbf{q}_\parallel}(f^{\mathrm{h}}_{\mathbf{k}_\parallel}f^{\mathrm{h}}_{\mathbf{k}'_\parallel}\bar{f}^{\mathrm{h}}_{\mathbf{k}'_\parallel+\mathbf{q}_\parallel})_\Sigma-P_{\mathbf{k}'_\parallel}(f^{\mathrm{h}}_{\mathbf{k}_\parallel}f^{\mathrm{e}}_{\mathbf{k}_\parallel-\mathbf{q}_\parallel}\bar{f}^{\mathrm{h}}_{\mathbf{k}'_\parallel+\mathbf{q}_\parallel})_\Sigma\\
&\quad+P_{\mathbf{k}_\parallel}P^{\star}_{\mathbf{k}'_\parallel+\mathbf{q}_\parallel}(P_{\mathbf{k}'_\parallel}-P_{\mathbf{k}_\parallel-\mathbf{q}_\parallel})]\\
&\quad+V_{\mathbf{q}_\parallel}[P_{\mathbf{k}_\parallel}(f^{\mathrm{h}}_{\mathbf{k}'_\parallel}f^{\mathrm{e}}_{\mathbf{k}_\parallel-\mathbf{q}_\parallel}\bar{f}^{\mathrm{h}}_{\mathbf{k}'_\parallel+\mathbf{q}_\parallel})_\Sigma-P_{\mathbf{k}_\parallel-\mathbf{q}_\parallel}(f^{\mathrm{h}}_{\mathbf{k}_\parallel}f^{\mathrm{h}}_{\mathbf{k}'_\parallel}\bar{f}^{\mathrm{h}}_{\mathbf{k}'_\parallel+\mathbf{q}_\parallel})_\Sigma\\
&\quad+P_{\mathbf{k}'_\parallel}P^{\star}_{\mathbf{k}'_\parallel+\mathbf{q}_\parallel}(P_{\mathbf{k}_\parallel-\mathbf{q}_\parallel}-P_{\mathbf{k}_\parallel})],
\end{aligned}\tag{G.2}$$

where the spin-index dependence is expressed explicitly according to Eqs. (D.8)–(E.5). If the correlations are initially vanishing, the $\mathrm{S}_{v,v;v,c}$ source is the only driving term for $c_{v,v;v,c}$. We observe that all terms contain an optical polarization, which verifies that c_{vvvc} can be generated only in the coherent regime.

To express S_{vvvc} compactly, we introduced the abbreviation

$$(f^{\lambda}_{\mathbf{k}_\parallel}f^{\lambda'}_{\mathbf{k}'_\parallel}\bar{f}^{\lambda''}_{\mathbf{k}''_\parallel})_\Sigma\equiv f^{\lambda}_{\mathbf{k}_\parallel}f^{\lambda'}_{\mathbf{k}'_\parallel}(1-f^{\lambda''}_{\mathbf{k}''_\parallel})+(1-f^{\lambda}_{\mathbf{k}_\parallel})(1-f^{\lambda'}_{\mathbf{k}'_\parallel})\bar{f}^{\lambda''}_{\mathbf{k}''_\parallel}.\tag{G.3}$$

This form shows that S_{vvvc} contains terms describing the scattering of polarization from densities. The remaining terms are non-linear in P and define polarization–polarization scattering.

In analogy to the exciton correlations, the dynamics of c_{vvvc} contains Coulomb-induced doublets which can be divided into coherent and incoherent contributions according to

$$D^{\mathbf{q}_\parallel,\mathbf{k}'_\parallel,\mathbf{k}_\parallel}_{v,v;v,c}\equiv[D^{\mathbf{q}_\parallel,\mathbf{k}'_\parallel,\mathbf{k}_\parallel}_{v,v;v,c}]_{\mathrm{coh}}+[D^{\mathbf{q}_\parallel,\mathbf{k}'_\parallel,\mathbf{k}_\parallel}_{v,v;v,c}]_{\mathrm{inc}},\tag{G.4}$$

$$\begin{aligned}
[D^{\mathbf{q}_\parallel,\mathbf{k}'_\parallel,\mathbf{k}_\parallel}_{v,v;v,c}]_{\mathrm{inc}} &= V_{\mathbf{q}_\parallel}(P_{\mathbf{k}_\parallel}-P_{\mathbf{k}_\parallel-\mathbf{q}_\parallel})\sum_{\mathbf{l}_\parallel}(c^{\mathbf{q}_\parallel,\mathbf{k}'_\parallel,\mathbf{l}_\parallel}_{c,v;v,c}+c^{\mathbf{q}_\parallel,\mathbf{k}'_\parallel,\mathbf{l}_\parallel}_{v,v;v,v})\\
&\quad-V_{\mathbf{j}_\parallel}(P_{\mathbf{k}'_\parallel}-P_{\mathbf{k}'_\parallel-\mathbf{j}_\parallel})\sum_{\mathbf{l}_\parallel}(c^{-\mathbf{j}_\parallel,\mathbf{l}_\parallel,\mathbf{k}_\parallel}_{v,c;c,v}+c^{-\mathbf{j}_\parallel,\mathbf{l}_\parallel,\mathbf{k}_\parallel}_{v,v;v,v})\\
&\quad+\sum_{\mathbf{l}_\parallel}V_{\mathbf{l}-\mathbf{k}_\parallel}(P_{\mathbf{k}_\parallel-\mathbf{q}_\parallel}c^{\mathbf{q}_\parallel,\mathbf{k}'_\parallel,\mathbf{l}_\parallel}_{v,v;v,v}-P_{\mathbf{k}_\parallel}[c^{\mathbf{q}_\parallel,\mathbf{k}'_\parallel,\mathbf{l}_\parallel}_{c,v;v,c}-c^{-\mathbf{j}_\parallel,\mathbf{k}'_\parallel,\mathbf{l}_\parallel}_{c,v;c,v}])\\
&\quad-\sum_{\mathbf{l}_\parallel}V_{\mathbf{l}_\parallel-\mathbf{k}'_\parallel}(P_{\mathbf{k}'_\parallel}[c^{\mathbf{q}_\parallel,\mathbf{l}_\parallel,\mathbf{k}_\parallel}_{v,c;v,c}-c^{-\mathbf{j}_\parallel,\mathbf{l}_\parallel,\mathbf{k}_\parallel}_{v,c;c,v}]+P_{\mathbf{k}_\parallel-\mathbf{q}_\parallel}c^{\mathbf{j}_\parallel,\mathbf{k}_\parallel,\mathbf{l}_\parallel}_{v,v;v,v})\\
&\quad+\sum_{\mathbf{l}_\parallel}V_{\mathbf{l}_\parallel+\mathbf{q}_\parallel}[P^{\star}_{\mathbf{k}'_\parallel}c^{\mathbf{l}_\parallel,\mathbf{k}'_\parallel+\mathbf{q}_\parallel,\mathbf{k}_\parallel-\mathbf{q}_\parallel}_{c,v;v,c}+P^{\star}_{\mathbf{k}'_\parallel}c^{\mathbf{l}_\parallel,\mathbf{k}'_\parallel+\mathbf{q}_\parallel,\mathbf{k}_\parallel-\mathbf{q}_\parallel}_{c,v;c,v}]^{\star}\\
&\quad-\sum_{\mathbf{l}_\parallel}V_{\mathbf{l}_\parallel-\mathbf{q}_\parallel}P_{\mathbf{k}_\parallel-\mathbf{q}_\parallel}c^{\mathbf{l}_\parallel,\mathbf{k}'_\parallel,\mathbf{k}_\parallel}_{v,v;v,v},
\end{aligned}\tag{G.5}$$

$$
\begin{aligned}
[D^{\mathbf{q}_\parallel,\mathbf{k}'_\parallel,\mathbf{k}_\parallel}_{v,v;v,c}]_{\mathrm{coh}} = {} & V_{\mathbf{q}_\parallel}(f^{\mathrm{h}}_{\mathbf{k}'_\parallel+\mathbf{q}_\parallel} - f^{\mathrm{h}}_{\mathbf{k}'_\parallel}) \sum_{\mathbf{l}_\parallel} (c^{\mathbf{q}_\parallel,\mathbf{l}_\parallel,\mathbf{k}_\parallel}_{v,c;c,c} + c^{\mathbf{q}_\parallel,\mathbf{l}_\parallel,\mathbf{k}_\parallel}_{v,v;v,c}) \\
& + V_{\mathbf{j}_\parallel}(f^{\mathrm{h}}_{\mathbf{k}_\parallel} - f^{\mathrm{h}}_{\mathbf{k}_\parallel+\mathbf{j}_\parallel}) \sum_{\beta,\mathbf{l}_\parallel} (c^{-\mathbf{j}_\parallel,\mathbf{k}'_\parallel,\mathbf{l}_\parallel}_{c,v;c,c} + c^{-\mathbf{j}_\parallel,\mathbf{k}'_\parallel,\mathbf{l}_\parallel}_{v,v;c,v}) \\
& + (1 - f^{\mathrm{h}}_{\mathbf{k}_\parallel} - f^{\mathrm{h}}_{\mathbf{k}'_\parallel}) \sum_{\mathbf{l}_\parallel} V_{\mathbf{l}_\parallel+\mathbf{q}_\parallel} [c^{\mathbf{l}_\parallel,\mathbf{k}'_\parallel+\mathbf{q}_\parallel,\mathbf{k}_\parallel-\mathbf{q}_\parallel}_{c,v;v,v}]^\star \\
& - (1 - f^{\mathrm{e}}_{\mathbf{k}_\parallel-\mathbf{q}_\parallel} - f^{\mathrm{h}}_{\mathbf{k}_\parallel}) \sum_{\mathbf{l}_\parallel} V_{\mathbf{l}-\mathbf{k}_\parallel} c^{\mathbf{q}_\parallel,\mathbf{k}'_\parallel,\mathbf{l}_\parallel}_{v,v;v,c} \\
& + (1 - f^{\mathrm{e}}_{\mathbf{k}_\parallel-\mathbf{q}_\parallel} - f^{\mathrm{h}}_{\mathbf{k}'_\parallel}) \sum_{\mathbf{l}_\parallel} V_{\mathbf{l}-\mathbf{k}'_\parallel} c^{\mathbf{j}_\parallel,\mathbf{l}_\parallel,\mathbf{k}_\parallel}_{v,v;v,c} \\
& + (f^{\mathrm{h}}_{\mathbf{k}'_\parallel+\mathbf{q}_\parallel} - f^{\mathrm{h}}_{\mathbf{k}_\parallel}) \sum_{\mathbf{l}_\parallel} V_{\mathbf{l}-\mathbf{k}_\parallel} [c^{-\mathbf{j}_\parallel,\mathbf{k}'_\parallel,\mathbf{l}_\parallel}_{v,v;c,v}] \\
& + (f^{\mathrm{h}}_{\mathbf{k}'_\parallel} - f^{\mathrm{h}}_{\mathbf{k}'_\parallel+\mathbf{q}_\parallel}) \sum_{\mathbf{l}_\parallel} V_{\mathbf{l}_\parallel-\mathbf{k}'_\parallel} c^{\mathbf{q}_\parallel,\mathbf{l}_\parallel,\mathbf{k}_\parallel}_{v,v;v,c} \\
& - (f^{\mathrm{e}}_{\mathbf{k}_\parallel-\mathbf{q}_\parallel} - f^{\mathrm{h}}_{\mathbf{k}'_\parallel+\mathbf{q}_\parallel}) \sum_{\mathbf{l}_\parallel} V_{\mathbf{l}_\parallel-\mathbf{q}_\parallel} c^{\mathbf{l}_\parallel,\mathbf{k}'_\parallel,\mathbf{k}_\parallel}_{v,v;v,c} \\
& + P^\star_{\mathbf{k}'_\parallel+\mathbf{q}_\parallel} \sum_{\mathbf{l}_\parallel} [V_{\mathbf{l}_\parallel-\mathbf{k}'_\parallel} c^{\mathbf{q}_\parallel,\mathbf{l}_\parallel,\mathbf{k}_\parallel}_{v,v;c,c} - V_{\mathbf{l}_\parallel-\mathbf{k}_\parallel} c^{-\mathbf{j}_\parallel,\mathbf{k}'_\parallel,\mathbf{l}_\parallel}_{v,v;c,c} - V_{\mathbf{l}_\parallel-\mathbf{q}_\parallel} c^{\mathbf{l}_\parallel,\mathbf{k}'_\parallel,\mathbf{k}_\parallel}_{v,v;c,c}].
\end{aligned}
\tag{G.6}
$$

The coherent and incoherent phonon-correlation terms are given by

$$
\begin{aligned}
[G^{\mathrm{coh}}_{\mathrm{phon}}]^{\mathbf{q}_\parallel,\mathbf{k}'_\parallel,\mathbf{k}_\parallel}_{v,v;v,c} \equiv {} & + (f^{\mathrm{h}}_{\mathbf{k}_\parallel} - f^{\mathrm{h}}_{\mathbf{k}_\parallel+\mathbf{j}_\parallel}) \Delta \langle Q^v_{\mathbf{j}_\parallel} a^\dagger_{v,\mathbf{k}'_\parallel} a_{c,\mathbf{k}'_\parallel-\mathbf{j}_\parallel} \rangle \\
& - (f^{\mathrm{h}}_{\mathbf{k}'_\parallel} - f^{\mathrm{h}}_{\mathbf{k}'_\parallel+\mathbf{q}_\parallel}) \Delta \langle Q^v_{\mathbf{q}_\parallel} a^\dagger_{v,\mathbf{k}_\parallel} a_{c,\mathbf{k}_\parallel-\mathbf{q}_\parallel} \rangle,
\end{aligned}
\tag{G.7}
$$

$$
\begin{aligned}
[G^{\mathrm{inc}}_{\mathrm{phon}}]^{\mathbf{q}_\parallel,\mathbf{k}'_\parallel,\mathbf{k}_\parallel}_{v,v;v,c} \equiv {} & + P_{\mathbf{k}_\parallel} \Delta \langle [Q^c_{\mathbf{q}_\parallel}]^\dagger a^\dagger_{v,\mathbf{k}'_\parallel} a_{v,\mathbf{k}'_\parallel+\mathbf{q}_\parallel} \rangle - P_{\mathbf{k}_\parallel-\mathbf{q}_\parallel} \Delta \langle [Q^v_{\mathbf{q}_\parallel}]^\dagger a^\dagger_{v,\mathbf{k}'_\parallel} a_{v,\mathbf{k}'_\parallel+\mathbf{q}_\parallel} \rangle \\
& + P_{\mathbf{k}'_\parallel+\mathbf{j}_\parallel} \Delta \langle [Q^v_{\mathbf{j}_\parallel}]^\dagger a^\dagger_{v,\mathbf{k}_\parallel} a_{v,\mathbf{k}_\parallel+\mathbf{j}_\parallel} \rangle - P_{\mathbf{k}'_\parallel} \Delta \langle [Q^c_{\mathbf{j}_\parallel}]^\dagger a^\dagger_{v,\mathbf{k}'_\parallel} a_{v,\mathbf{k}_\parallel+\mathbf{j}_\parallel} \rangle,
\end{aligned}
\tag{G.8}
$$

respectively. The quantum-optical correlations are

$$
\begin{aligned}
[G^{\mathrm{coh}}_{\mathrm{QED}}]^{\mathbf{q}_\parallel,\mathbf{k}'_\parallel,\mathbf{k}_\parallel}_{v,v;v,c} \equiv {} & - (1 - f^{\mathrm{h}}_{\mathbf{k}_\parallel} - f^{\mathrm{e}}_{\mathbf{k}_\parallel-\mathbf{q}_\parallel}) \Delta \langle [E^v_{\mathbf{q}_\parallel}]^\dagger a^\dagger_{v,\mathbf{k}'_\parallel} a_{v,\mathbf{k}'_\parallel+\mathbf{q}_\parallel} \rangle \\
& + (1 - f^{\mathrm{h}}_{\mathbf{k}'_\parallel} - f^{\mathrm{e}}_{\mathbf{k}'_\parallel-\mathbf{j}_\parallel}) \Delta \langle [E^v_{\mathbf{j}_\parallel}]^\dagger a^\dagger_{v,\mathbf{k}_\parallel} a_{v,\mathbf{k}_\parallel+\mathbf{j}_\parallel} \rangle \\
& - P^\star_{\mathbf{k}'_\parallel+\mathbf{q}_\parallel} \Delta \langle E^c_{\mathbf{j}_\parallel} a^\dagger_{v,\mathbf{k}'_\parallel} a_{c,\mathbf{k}'_\parallel-\mathbf{j}_\parallel} \rangle + P^\star_{\mathbf{k}'_\parallel+\mathbf{q}_\parallel} \Delta \langle E^c_{\mathbf{q}_\parallel} a^\dagger_{v,\mathbf{k}_\parallel} a_{c,\mathbf{k}_\parallel-\mathbf{q}_\parallel} \rangle,
\end{aligned}
\tag{G.9}
$$

$$
[G^{\mathrm{inc}}_{\mathrm{QED}}]^{\mathbf{q}_\parallel,\mathbf{k}'_\parallel,\mathbf{k}_\parallel}_{v,v;v,c} \equiv + P_{\mathbf{k}_\parallel} \Delta \langle E^v_{\mathbf{j}_\parallel} a^\dagger_{v,\mathbf{k}'_\parallel} a_{c,\mathbf{k}'_\parallel-\mathbf{j}_\parallel} \rangle - P_{\mathbf{k}'_\parallel} \Delta \langle E^v_{\mathbf{q}_\parallel} a^\dagger_{v,\mathbf{k}_\parallel} a_{c,\mathbf{k}_\parallel-\mathbf{q}_\parallel} \rangle.
\tag{G.10}
$$

Additionally, $c_{v,v;v,c}$ is also coupled to three-particle correlations that can be unraveled with the help of Eq. (D.12).

References

[1] H. Haug, S.W. Koch, Quantum Theory of the Optical and Electronic Properties of Semiconductors, fourth ed., World Scientific Publishing, Singapore, 2004.
[2] C. Klingshirn, Semiconductor Optics, second ed., Springer, Berlin, 2005.
[3] W. Schäfer, M. Wegener, Semiconductor Optics and Transport Phenomena, first ed., Springer, Berlin, 2002.
[4] R. Zimmermann, Many-Particle Theory of Highly Excited Semiconductors, first ed., Teubner Verlagsgesellschaft, Leipzig, 1988.
[5] R. Elliott, Theory of excitons, in: C. Kuper, G. Whitefield (Eds.), Polarons and Excitons, Oliver and Boyd, Edinburgh, 1963, pp. 269–293.
[6] J. Frenkel, On the transformation of light into heat in solids II, Physical Review 37 (1931) 1276–1294.
[7] G.H. Wannier, The structure of electronic excitation levels in insulating crystals, Physical Review 52 (1937) 191–197.
[8] R.S. Knox, Theory of excitons, in: F. Seitz, D. Turnbull (Eds.), Solid State Physics, supplement 5, Academic Press, New York, 1963.
[9] D.I. Dexter, R.S. Knox, Excitons, Wiley, New York, 1981.
[10] V.G. Lysenko, V.I. Revenko, Exciton spectrum in case of high-density non-equilibrium carriers in CdS crystals, Fizika Tverdogo Tela 20 (1978) 2144–2147.
[11] H.M. Gibbs, A.C. Gossard, S.L. McCall, A. Passner, W. Wiegmann, T.N.C. Venkatesan, Saturation of the free exciton resonance in GaAs, Solid State Communications 30 (1979) 271–275.
[12] G.W. Fehrenbach, W. Schäfer, J. Treusch, R.G. Ulbrich, Transient optical spectra of a dense exciton gas in a direct-gap semiconductor, Physical Review Letters 57 (1982) 1281–1284.
[13] Y.H. Lee, A. Chavezpirson, S.W. Koch, H.M. Gibbs, S.H. Park, J. Morhange, A. Jeffery, N. Peyghambarian, L. Banyai, A.C. Gossard, W. Wiegmann, Room-temperature optical nonlinearities in GaAs, Physical Review Letters 57 (1986) 2446–2449.
[14] S. Schmitt-Rink, D.S. Chemla, D.A.B. Miller, Linear and nonlinear optical properties of semiconductor quantum wells, Advances in Physics 38 (1989) 89–188.
[15] M. Kira, F. Jahnke, S.W. Koch, Microscopic theory of excitonic signatures in semiconductor photoluminescence, Physical Review Letters 81 (1998) 3263–3266.
[16] R.M. Groeneveld, D. Grischkowsky, Picosecond time-resolved far-infrared experiments on carriers and excitons in GaAs-AlGaAs multiple-quantum wells, Journal of the Optical Society of America B 11 (1994) 2502–2507.
[17] J. Cerne, J. Kono, M.S. Sherwin, M. Sundaram, A.C. Gossard, G.E.W. Bauer, Terahertz dynamics of excitons in GaAs/AlGaAs quantum wells, Physical Review Letters 77 (1996) 1131–1134.
[18] M. Kira, W. Hoyer, T. Stroucken, S.W. Koch, Exciton formation in semiconductors and the influence of a photonic environment, Physical Review Letters 87 (2001) 176401.
[19] R.A. Kaindl, M.A. Carnahan, D. Hagele, R. Lovenich, D.S. Chemla, Ultrafast terahertz probes of transient conducting and insulating phases in an electron–hole gas, Nature 423 (2003) 734–738.
[20] M. Kubouchi, K. Yoshioka, R. Shimano, A. Mysyrowicz, M. Kuwata-Gonokami, Study of orthoexciton-to-paraexciton conversion in Cu_2O by excitonic Lyman spectroscopy, Physical Review Letters 94 (2005) 016403.
[21] M. Jörger, T. Fleck, C. Klingshirn, R. von Baltz, Midinfrared properties of cuprous oxide: high-order lattice vibrations and intraexcitonic transitions of the 1 s paraexciton, Physical Review B 71 (2005) 235219.
[22] F. Jahnke, M. Kira, S.W. Koch, G. Khitrova, E.K. Lindmark, T.R. Nelson Jr., D.V. Wick, J.D. Berger, O. Lyngnes, H.M. Gibbs, K. Tai, Excitonic nonlinearities of semiconductor microcavities in the nonperturbative regime, Physical Review Letters 77 (1996) 5257–5260.
[23] M. Kira, F. Jahnke, S.W. Koch, J.D. Berger, D.V. Wick, T.R. Nelson Jr., G. Khitrova, H.M. Gibbs, Quantum theory of nonlinear semiconductor microcavity luminescence explaining "Boser" experiments, Physical Review Letters 79 (1997) 5170–5173.
[24] M. Kira, F. Jahnke, S.W. Koch, Quantum theory of secondary emission in optically excited semiconductor quantum wells, Physical Review Letters 82 (1999) 3544–3547.
[25] Y.-S. Lee, T.B. Norris, M. Kira, F. Jahnke, S.W. Koch, G. Khitrova, H.M. Gibbs, Quantum correlations and intraband coherences in semiconductor cavity QED, Physical Review Letters 83 (1999) 5338–5341.
[26] M. Kira, F. Jahnke, W. Hoyer, S.W. Koch, Quantum theory of spontaneous emission and coherent effects in semiconductor microstructures, Progress in Quantum Electronics 23 (1999) 189–279.

[27] G. Khitrova, H.M. Gibbs, F. Jahnke, M. Kira, S.W. Koch, Nonlinear optics of normal-mode-coupling semiconductor microcavities, Reviews of Modern Physics 71 (1999) 1591–1639.
[28] C. Ell, P. Brick, M. Hübner, E.S. Lee, O. Lyngnes, J.P. Prineas, G. Khitrova, H.M. Gibbs, M. Kira, F. Jahnke, S.W. Koch, D.G. Deppe, D.L. Huffaker, Quantum correlations in the nonperturbative regime of semiconductor microcavities, Physical Review Letters 85 (2000) 5392–5395.
[29] W. Hoyer, M. Kira, S.W. Koch, Influence of Coulomb and phonon interaction on the exciton formation dynamics in semiconductor heterostructures, Physical Review B 67 (2003) 155113.
[30] M. Kira, S.W. Koch, Exciton-population inversion and terahertz gain in resonantly excited semiconductors, Physical Review Letters 93 (2004) 076402.
[31] S. Chatterjee, C. Ell, S. Mosor, G. Khitrova, H.M. Gibbs, W. Hoyer, M. Kira, S.W. Koch, J.P. Prineas, H. Stolz, Excitonic photoluminescence in semiconductor quantum wells: plasma versus excitons, Physical Review Letters 92 (2004) 067402.
[32] W. Hoyer, M. Kira, S.W. Koch, H. Stolz, S. Mosor, J. Sweet, C. Ell, G. Khitrova, H.M. Gibbs, Entanglement between a photon and a quantum well, Physical Review Letters 93 (2004) 067401.
[33] M. Kira, W. Hoyer, S.W. Koch, Terahertz signatures of the exciton formation dynamics in non-resonantly excited semiconductors, Solid State Communications 129 (2004) 733–736.
[34] W. Hoyer, C. Ell, M. Kira, S.W. Koch, S. Chatterjee, S. Mosor, G. Khitrova, H.M. Gibbs, H. Stolz, Many-body dynamics and exciton formation studied by time-resolved photoluminescence, Physical Review B 72 (2005) 075324.
[35] W. Hoyer, A. Knorr, J.V. Moloney, E.M. Wright, M. Kira, S.W. Koch, Photoluminescence and terahertz emission from femtosecond laser-induced plasma channels, Physical Review Letters 94 (2005) 115004.
[36] M. Kira, S.W. Koch, Quantum-optical spectroscopy of semiconductors, Physical Review A 73 (2006) 013813.
[37] S.W. Koch, M. Kira, G. Khitrova, H.M. Gibbs, Excitons in new light, Nature Materials 5 (2006) 523–531.
[38] G. Khitrova, H.M. Gibbs, M. Kira, S.W. Koch, A. Scherer, Vacuum rabi splitting in semiconductors, Nature Physics 2 (2006) 81–90.
[39] H.W. Wyld, B.D. Fried, Quantum mechanical kinetic equations, Annals of Physics 23 (1963) 374–389.
[40] J. Cízek, On correlation problem in atomic and molecular systems. Calculation of wavefunction components in ursell-type expansion using quantum-field theoretical methods, Journal of Chemical Physics 45 (1966) 4256.
[41] G.D. Purvis, R.J. Bartlett, A full coupled-cluster singles and doubles model: the inclusion of disconnected triples, Journal of Chemical Physics 76 (1982) 1910–1918.
[42] F.E. Harris, H.J. Monkhorst, D.L. Freeman, Algebraic and Diagrammatic Methods in Many-Fermion Theory, first ed., Oxford Press, New York, 1992.
[43] J. Fricke, Transport equations including many-particle correlations for an arbitrary quantum system: a general formalism, Annals of Physics 252 (2) (1996) 479–498.
[44] M. Kira, W. Hoyer, S.W. Koch, Excitons and luminescence in semiconductor heterostructures, Nonlinear Optics 29 (2002) 481–489.
[45] W. Hoyer, M. Kira, S.W. Koch, Cluster expansion in semiconductor quantum optics, in: K. Morawetz (Ed.), Nonequilibrium Physics at Short Time Scales, Springer, Berlin, 2004, pp. 309–335.
[46] M. Kira, S.W. Koch, Microscopic theory of optical excitations photoluminescence, and terahertz response in semiconductors, European Journal of Physics D 36 (2005) 143–157.
[47] M.L. Cohen, J.R. Chelikowsky, Electronic Structure and Optical Properties of Semiconductors, vol. 75, Springer, Berlin, 1988.
[48] C. Cohen-Tannoudji, J. Dupont-Roc, G. Grynberg, Photons & Atoms, third ed., Wiley, New York, 1989.
[49] D.F. Walls, G.J. Milburn, Quantum Optics, first ed., Springer, New York, 1994.
[50] E. Merzbacher, Quantum Mechanics, first ed., Wiley, New York, 1961.
[51] N.W. Ashcroft, N.D. Mermin, Solid State Physics, Saunders College (HRW), Philadelphia, 1976.
[52] F. Jahnke, M. Kira, S.W. Koch, Linear and nonlinear optical properties of quantum confined excitons in semiconductor microcavities, Zeitschrift fur Physik B 104 (1997) 559–572.
[53] M. Kira, W. Hoyer, S.W. Koch, P. Brick, C. Ell, M. Hübner, G. Khitrova, H.M. Gibbs, Quantum correlations in semiconductor microcavities, Semiconductor Science and Technology 18 (2003) S405–S410.
[54] S.W. Koch, M. Kira, Excitons in semiconductors, in: H. Kalt, M. Hetterich (Eds.), Optics of Semiconductors and their Nanostructures—Springer Series in Solid-State Sciences, vol. 146, Springer, Berlin, 2004, pp. 1–18.

[55] S. Siggelkow, W. Hoyer, M. Kira, S.W. Koch, Exciton formation and stability in semiconductor heterostructures, Physical Review B 69 (2004) 073104.
[56] S.W. Koch, M. Kira, W. Hoyer, V.S. Filinov, Exciton ionization in semiconductors, Physica Status Solidi (b) 238 (2003) 404–410.
[57] V.S. Filinov, W. Hoyer, M. Bonitz, M. Kira, V.E. Fortov, S.W. Koch, Spontaneous emission of semiconductors in the Wigner approach, Journal of Optics B 5 (2003) S299–S305.
[58] V.M. Axt, A. Stahl, Role of exchange interaction in coulomb quantum kinetics, Physical Review B 67 (2003) 115311.
[59] M. Hartmann, H. Stolz, R. Zimmermann, Kinetics of screening in optically-excited semiconductors, Physica Statuts Solidi B 159 (1990) 35–42.
[60] L. Banyai, Q.T. Vu, B. Mieck, H. Haug, Ultrafast quantum kinetics of time-dependent RPA-screened Coulomb scattering, Physical Review Letters 81 (1998) 882–885.
[61] G. Manzke, K. Henneberger, J. Heeg, K. El Sayed, S. Schuster, H. Haug, Dynamics of screening and field fluctuation on ulstrashort time scales, Physica Status Solidi B 188 (1995) 395–403.
[62] J. Shah, second ed., Ultrafast Spectroscopy of Semiconductors and Semiconductor Nanostructures—Springer Series in Solid State Sciences, vol. 115, Springer, New York, 1999.
[63] D.J. Jones, S.A. Diddams, J.K. Ranka, A. Stenz, R.S. Windeler, J.L. Hall, S.T. Cundiff, Carrier-envelope phase control of femtosecond mode-locked lasers and direct optical frequency synthesis, Science 288 (2000) 635–639.
[64] T. Udem, R. Holzwarth, T.W. Hänsch, Optical frequency metrology, Nature 416 (2002) 233–237.
[65] M. Hentschel, R. Kienberger, C. Spielmann, G.A. Reider, N. Milosevic, T. Brabec, P. Corkum, U. Heinzmann, M. Drescher, F. Krausz, Attosecond metrology, Nature 414 (2001) 509–513.
[66] R. Huber, F. Tauser, A. Brodschelm, M. Bichler, G. Abstreiter, A. Leitenstorfer, How many-particle interactions develop after ultrafast excitation of an electron–hole plasma, Nature 414 (2001) 286–289.
[67] R. Huber, C. Kubler, S. Tubel, A. Leitenstofer, Q.T. Vu, H. Haug, F. Kohler, M.C. Amann, Femtosecond formation of coupled phonon–plasmon modes in inp: Ultrabroadband THz experiment and quantum kinetic theory, Physical Review Letters 94 (2005) 027401.
[68] J. van Tilborg, C. Schroeder, C. Filip, C. Toth, C. Geddes, G. Fubiani, R. Huber, R. Kaindl, E. Esarey, W. Leemans, Temporal characterization of femtosecond laser-plasma-accelerated electron bunches using terahertz radiation, Physical Review Letters 96 (2006) 014801.
[69] S. Hoffmann, M. Hofmann, E. Bründermann, M. Havenith, M. Matus, J.V. Moloney, A.S. Moskalenko, M. Kira, S.W. Koch, S. Saito, K. Sakai, Four-wave mixing and direct terahertz emission with two-color semiconductor lasers, Applied Physics Letters 84 (2004) 3585–3587.
[70] S. Hoffmann, M. Hofmann, M. Kira, S.W. Koch, Two-colour diode lasers for generation of THz radiation, Semiconductor Science and Technology 20 (2005) 205–210.
[71] C. Weisbuch, M. Nishioka, A. Ishikawa, Y. Arakawa, Observation of the coupled exciton-photon mode splitting in a semiconductor quantum microcavity, Physical Review Letters 69 (1992) 3314–3317.
[72] T.B. Norris, J.-K. Rhee, C.-Y. Sung, Y. Arakawa, M. Nishioka, C. Weisbuch, Time-resolved vacuum rabi oscillations in a semiconductor quantum microcavity, Physical Review B 50 (1994) 14663–14666.
[73] L. Schultheis, M.D. Sturge, J. Hegarty, Photon-echoes from two-dimensional excitons in GaAs-AlGaAs quantum wells, Applied Physics Letters 47 (1985) 995–997.
[74] L. Schultheis, J. Kuhl, A. Honold, C.W. Tu, Ultrafast phase relaxation of excitons via exciton–exciton and exciton–electron collisions, Physical Review Letters 57 (1986) 1635–1638.
[75] T. Rappen, G. Mohs, M. Wegener, Polariton dynamics in quantum wells studied by femtosecond four-wave mixing, Physical Review B 47 (1993) 9658–9662.
[76] H. Stolz, Time Resolved Light Scattering from Excitons, Springer, Berlin, 1994.
[77] J. Kuhl, Optical dephasing of excitons in iii–v semiconductors, in: R. Phillips (Ed.), Coherent Optical Interactions in Semiconductors, Plenum Press, New York, 1994, pp. 1–31.
[78] W. Schäfer, D.S. Kim, J. Shah, T.C. Damen, J.E. Cunningham, L.N.P.K.W. Goossen, K. Köhler, Femtosecond coherent fields induced by many-particle correlations in transient four-wave-mixing, Physical Review B 53 (1996) 16429–16443.
[79] S. Cundiff, M. Koch, W.H. Knox, J. Shah, W. Stolz, Optical coherence in semiconductors: strong emission mediated by nondegenerate interactions, Physical Review Letters 77 (1996) 1107–1110.
[80] P. Kner, W. Schäfer, R. Lövenich, D.S. Chemla, Coherence of four-particle correlations in semiconductors, Physical Review Letters 81 (1998) 5386–5389.

[81] W. Schäfer, R. Lövenich, N.A. Fromer, D.S. Chemla, From coherently excited highly correlated states to incoherent relaxation processes in semiconductors, Physical Review Letters 86 (2001) 344–347.
[82] D. Chemla, J. Shah, Many-body and correlation effects in semiconductors, Nature 411 (2001) 549–557.
[83] A.L. Smirl, The vectorial dynamics of coherent emission from excitons, in: K.-T. Tsen (Ed.), Ultrafast Phenomena in Semiconductors, Springer, New York, 2001, pp. 443–507.
[84] M. Lindberg, S.W. Koch, Effective Bloch equations for semiconductors, Physical Review B 38 (1988) 3342–3350.
[85] L.V. Keldysh, Y.V. Kopaev, Possible instability of the semimetal state toward coulomb interaction, Soviet Physics Solid State 6 (1965) 2219–2224.
[86] H. Haug, S. Schmitt-Rink, Electron theory of the optical properties of laser excited semiconductors, Progress in Quantum Electronics 9 (1984) 3–100.
[87] C. Klingshirn, H. Haug, Optical properties of highly excited direct gap semiconductors, Physics Reports 70 (1981) 315–410.
[88] T. Usui, Excitations in a high density electron gas, Progress in Theoretical Physics 23 (1960) 787–798.
[89] C.I. Ivanov, H. Barentzen, M.D. Girardeau, On the theory of dense exciton systems, Physica A 140 (1987) 612–628.
[90] M. Combescot, O. Betbeder-Matibet, Scattering rates and lifetime of exact and boson excitons, Physical Review Letters 93 (2004) 016403.
[91] M. Kira, F. Jahnke, S.W. Koch, Ultrashort pulse propagation effects in semiconductor microcavities, Solid State Communications 102 (1997) 703–707.
[92] F. Jahnke, M. Ruopp, M. Kira, S.W. Koch, Ultrashort pulse propagation and excitonic nonlinearities in semiconductor microcavities, Festkörperprobleme/Advances in Solid State Physics 37 (1997) 191–206.
[93] L.C. Andreani, F. Tassone, F. Bassani, Radiative lifetime of free excitons in quantum wells, Solid State Communications 77 (1991) 641–645.
[94] E.L. Ivchenko, Exciton polaritons in periodic quantum-well structures, Fizika Tverdogo Tela 33 (1991) 2388–2393.
[95] S. Jorda, Spontaneous emission of quantum-well excitons in planar dielectric multilayer cavities, Solid State Communications 93 (1995) 45–48.
[96] T. Stroucken, A. Knorr, P. Thomas, S.W. Koch, Coherent dynamics of radiatively coupled quantum-well excitons, Physical Review B 53 (1996) 2026–2033.
[97] V.M. Agranovich, O.A. Dubowskii, Effect of retarded interaction of exciton spectrum in 1-dimensional and 2-dimensional crystals, JETP Letters 3 (1966) 223.
[98] J.J. Hopfield, Theory of the contribution of excitons to the complex dielectric constant of crystals, Physical Review 112 (1958) 1555–1567.
[99] K. Cho, Excitons—Topics in Current Physics, vol. 14, Springer, Berlin, 1979.
[100] A. Stahl, I. Balslev, Electrodynamics of the Semiconductor Band Edge—Springer Tracts in Modern Physics 110, first ed., Springer, Berlin, 1987.
[101] W. Hoyer, M. Kira, S.W. Koch, Influence of bound and unbound electron–hole-pair populations and interaction effects on the excitonic luminescence in semiconductor quantum wells, cond-mat (2006) 0604349.
[102] S.W. Koch, N. Peyghambarian, M. Lindberg, Transient and steady-state optical nonlinearities in semiconductors, Journal of Physics C: Solid State Physics 21 (1988) 5229–5249.
[103] T. Rappen, U.G. Peter, M. Wegener, W. Schäfer, Polarization dependence of dephasing processes—a probe for many-body effects, Physical Review B 49 (1994) 10774–10777.
[104] B. Mieck, H. Haug, W.A. Hügel, M.F. Heinrich, M. Wegener, Quantum-kinetic dephasing in resonantly excited semiconductor quantum wells, Physical Review B 62 (2000) 2686–2695.
[105] W.W. Chow, S.W. Koch, Semiconductor Laser Fundamentals, first ed., Springer, New York, 1999.
[106] N.F. Mott, The transition to the metallic state, Philosophical Magazine 6 (1961) 287–309.
[107] J. Hader, J.V. Moloney, S.W. Koch, W.W. Chow, Microscopic modelling of gain and luminescence in semiconductors, Journal of Selected Topics in Quantum Electronics 9 (2003) 688–697.
[108] J. Hader, S.W. Koch, J.V. Moloney, Microscopic theory of gain and spontaneous emission in GaInNAs laser material, Solid State Electronics 47 (2003) 513–521.
[109] W.W. Chow, S.W. Koch, M. Sargent III, Semiconductor-Laser Physics, corrected second printing 1997 ed., Springer, Berlin, 1994.
[110] W.W. Chow, A.F. Wright, A. Girndt, F. Jahnke, S.W. Koch, Microscopic theory of gain in an inhomogeneously broadened ingan/algan quantum-well laser, Applied Physics Letters 71 (1997) 2608–2610.

[111] L. Bányai, D.B.T. Thoai, E. Reitsamer, H. Haug, D. Steinbach, M.U. Wehner, M. Wegener, T. Marschner, W. Stolz, Exciton-LO-phonon quantum kinetics—evidence of memory effects in bulk GaAs, Physical Review Letters 75 (1995) 2188–2191.
[112] L. Bányai, E. Reitsamer, D.B.T. Thoai, H. Haug, Quantum kinetics of femtosecond four-wave mixing in semiconductors, Journal of Optical Society of America B 13 (1996) 1278–1283.
[113] O. Lyngnes, J.D. Berger, J.P. Prineas, S. Park, G. Khitrova, H.M. Gibbs, F. Jahnke, M. Kira, S.W. Koch, Nonlinear emission dynamics from semiconductor microcavities in the nonperturbative regime, Solid State Communications 104 (1997) 297–300.
[114] Q.T. Vu, H. Haug, L.V. Keldysh, Dynamics of the electron–hole correlation in femtosecond pulse excited semiconductors, Solid State Communications 115 (2000) 63–65.
[115] M. Lindberg, Y.Z. Hu, R. Binder, S.W. Koch, $\chi^{(3)}$ formalism in optically excited semiconductors and its applications in four-wave-mixing spectroscopy, Physical Review B 50 (1994) 18060–18072.
[116] V.M. Axt, A. Stahl, A dynamics-controlled truncation scheme for the hierarchy of density matrices in semiconductor optics, Zeitshrift fur Physik B 93 (1994) 195–204.
[117] A. Thränhardt, S. Kuckenburg, A. Knorr, T. Meier, S.W. Koch, Quantum theory of phonon-assisted exciton formation and luminescence in semiconductor quantum wells, Physical Review B 62 (4) (2000) 2706–2720.
[118] E.M. Gershenzon, G.N. Goltsman, M.G. Ptitsina, Investigation of free excitons in Ge and their condensation at submillimeter waves, Zhurnal Eksperimentalnoi I Teoreticheskoi Fiziki 70 (1976) 224–234.
[119] T. Timusk, R. Navarro, N.O. Lipari, M. Altarelli, Far-infrared absorption by excitons in silicon, Solid State Communications 25 (1978) 217–219.
[120] M. Kira, W. Hoyer, S.W. Koch, Microscopic theory of the semiconductor terahertz response, Physica Status Solidi (b) 238 (2003) 443–450.
[121] M. Kira, W. Hoyer, S. Koch, Y.-S. Lee, T.B. Norris, G. Khitrova, H.M. Gibbs, Incoherent pulse generation in semiconductor microcavities, Physica Status Solidi (c) 0 (2003) 1397–1400.
[122] R. Huber, B. Schmid, Y. Shen, D. Chemla, R. Kaindl, Stimulated terahertz emission from intraexcitonic transitions in Cu_2O, Physical Review Letters 96 (2006) 017402.
[123] V. Savona, F. Tassone, C. Piermarocchi, A. Quattropani, P. Schwendimann, Theory of polariton photoluminescence in arbitrary semiconductor microcavity structures, Physical Review B 53 (1996) 13051–13062.
[124] P.E. Selbmann, M. Gulia, F. Rossi, E. Molinari, P.H. Lugli, Coupled free-carrier and exciton relaxation in optically excited semiconductors, Physical Review B 54 (1996) 4660–4673.
[125] M.E. Portnoi, I. Galbraith, Ionization degree of the electron–hole plasma in semiconductor quantum wells, Physical Review B 60 (1999) 5570–5581.
[126] M. Richter, M. Schaarschmidt, A. Knorr, W. Hoyer, J.V. Moloney, E.M. Wright, M. Kira, S.W. Koch, Quantum theory of incoherent THz-emission of an interacting electron–ion plasma, Physical Review A 71 (2005) 053819.
[127] I. Galbraith, R. Chari, S. Pellegrini, P.J. Phillips, C.J. Dent, A.F.G. van der Meer, D.G. Clarke, A.K. Kar, G.S. Buller, C.R. Pidgeon, B.N. Murdin, J. Allam, G. Strasser, Excitonic signatures in the photoluminescence and terahertz absorption of a $GaAs/Al_xGa_{1-x}As$ multiple quantum well, Physical Review B 71 (2005) 073302.
[128] W. Chow, M. Kira, S.W. Koch, Microscopic theory of optical nonlinearities and spontaneous emission lifetime in group iii nitride quantum wells, Physical Review B 60 (1999) 1947–1952.
[129] K. Hantke, J.D. Heber, C. Schlichenmaier, A. Thränhardt, T. Meier, B. Kunert, K. Volz, W. Stolz, S.W. Koch, W.W. Rühle, Time-resolved photoluminescence of type-i and type-ii (GaIn)As/Ga(NAs) heterostructures, Physical Review B 71 (2005) 165320.
[130] R.F. Schnabel, R. Zimmermann, D. Bimberg, H. Nickel, R. Lösch, W. Schlapp, Influence of exciton localization on recombination line shapes: $In_xGa_{1-x}As/GaAs$ quantum wells as a model, Physical Review B 46 (1992) 9873–9876.
[131] J. Szczytko, L. Kappei, J. Berney, F. Morier-Genoud, M.T. Portella-Oberli, B. Deveaud, Determination of the exciton formation in quantum wells from time-resolved interband luminescence, Physical Review Letters 93 (2004) 137401.
[132] J. Szczytko, L. Kappei, J. Berney, F. Morier-Genoud, M.T. Portella-Oberli, B. Deveaud, Origin of excitonic luminescence in quantum wells: direct comparison of the exciton population and coulomb correlated plasma models, Physical Review B 71 (2005) 195313.

[133] M.H. Anderson, J.R. Ensher, M.R. Matthews, C.E. Weiman, E.A. Cornell, Observation of Bose–Einstein condensation in a dilute atomic vapor, Science 269 (1995) 198–201.
[134] K.B. Davis, M.-O. Mewes, M.R. Andrews, N.J. van Druten, D.S. Durfee, D.M. Kurn, W. Ketterle, Bose–Einstein condensation in a gas of sodium atoms, Physical Review Letters 75 (1995) 3969–3973.
[135] E.A. Cornell, C.E. Wieman, Nobel lecture: Bose–Einstein condensation in a dilute gas the first 70 years and some recent experiments, Reviews of Modern Physics 74 (2002) 875–893.
[136] W. Ketterle, Nobel lecture: when atoms behave as waves: Bose–Einstein condensation and the atom laser, Reviews of Modern Physics 74 (2002) 1131–1151.
[137] M. Girardeau, R. Arnowitt, Theory of many-bosons systems-pair theory, Physical Review 113 (1959) 755–761.
[138] E. Hanamura, H. Haug, Condensation effects of excitons, Physics Letters 33 (1977) 209–284.
[139] L. Chase, N. Peyghambarian, G. Grynberg, A. Mysyrowicz, Evidence for Bose–Einstein condensation of biexcitons in CuCl, Physical Review Letters 42 (1979) 1231–1234.
[140] D. Snoke, J.P. Wolfe, A. Mysyrowicz, Quantum saturation of a Bose gas: excitons in Cu_2O, Physical Review Letters 59 (1987) 827–830.
[141] J.L. Lin, J.P. Wolfe, Bose–Einstein condensation of paraexcitons in stressed Cu_2O, Physical Review Letters 71 (1993) 1222–1225.
[142] L. Butov, A. Zrenner, G. Abstreiter, G. Bohm, G. Weimann, Condensation of indirect excitons in coupled AlAs/GaAs quantum-wells, Physical Review Letters 73 (1994) 304–307.
[143] L. Butov, A. Gossard, D. Chemla, Macroscopically ordered state in an exciton system, Nature 418 (2002) 751–754.
[144] D. Snoke, S. Denev, Y. Liu, L. Pfeiffer, K. West, Long-range transport in excitonic dark states in coupled quantum wells, Nature 418 (2002) 754–757.
[145] R. Rapaport, G. Chen, D. Snoke, S.H. Simon, L. Pfeiffer, K. West, Y. Liu, S. Denev, Charge separation of dense two-dimensional electron–hole gases: mechanism for exciton ring pattern formation, Physical Review Letters 92 (2004) 117405.
[146] H. Stolz, D. Schwarze, W. von der Osten, G. Weimann, Transient resonant Rayleigh scattering from electronic states in disordered systems: excitons in $GaAs/Al_xGa_{1-x}As$ multiple-quantum-well structures, Physical Review B 47 (1993) 9669–9675.
[147] R. Zimmermann, Theory of resonant Rayleigh scattering of excitons in semiconductor quantum wells, Nuovo Cimento D 17 (1995) 1801–1805.
[148] D. Citrin, Time-domain theory of resonant Rayleigh scattering by quantum wells: early-time evolution, Physical Review B 54 (1996) 14572–14579.
[149] S. Haacke, R.A. Taylor, R. Zimmermann, I. Bar-Joseph, B. Devaud, Resonant femtosecond emission from quantum well excitons: the role of Rayleigh scattering and luminescence, Physical Review Letters 78 (1997) 2228–2231.
[150] D. Birkedal, J. Shah, Femtosecond spectral interferometry of resonant secondary emission from quantum wells: resonance Rayleigh scattering in the nonergodic regime, Physical Review Letters 81 (1998) 2372–2375.
[151] W. Langbein, J.M. Hvam, R. Zimmermann, Time resolved speckle analysis: a new approach of coherence and dephasing of optical excitations in solids, Physical Review Letters 82 (1999) 1040–1043.
[152] V. Savona, R. Zimmermann, Time-resolved Rayleigh scattering of excitons: evidence for level repulsion in a disordered system, Physical Review B 60 (1999) 4928–4936.
[153] A. Thränhardt, C. Ell, S. Mosor, G. Rupper, G. Khitrova, H.M. Gibbs, S.W. Koch, Interplay of phonon and disorder scattering in semiconductor quantum wells, Physical Review B 68 (2003) 035316.
[154] P. Bozsoki, M. Kira, W. Hoyer, T. Meier, I. Varga, P. Thomas, S. Koch, Microscopic modeling of photoluminescence of strongly disordered semiconductors, Journal of Luminescence, accepted for publication.
[155] P. Bozsoki, P. Thomas, M. Kira, W. Hoyer, T. Meier, S. Koch, K. Maschke, I. Varga, H. Stolz, Characterization of disorder in semiconductors via single-photon interferometry, Physical Review Letters 97 (2006) 227402.
[156] M. Schäfer, M. Wercher, W. Hoyer, M. Kira, S. Koch, Quantum theory of luminescence in multiple-quantum-well Bragg structures, Physical Review B 74 (2006) 155135.
[157] J.J. Hopfield, D.J. Thomas, Polariton absorption lines, Physical Review Letters 15 (1965) 22.
[158] J. Tignon, T. Hasche, D. Chemla, H. Schneider, F. Jahnke, S. Koch, Unified picture of polariton propagation in bulk gas semiconductors, Physical Review Letters 84 (2000) 3382.

[159] H.C. Schneider, F. Jahnke, S.W. Koch, J. Tignon, T. Hasche, D.S. Chemla, Polariton propagation in high-quality semiconductors—microscopic theory and experiment versus additional boundary conditions, Physical Review B 63 (2001) 045202.
[160] E.T. Jaynes, F.W. Cummings, Comparison of quantum and semiclassical radiation theories with application to beam maser, Proceedings of IEEE 51 (1963) 89–109.
[161] M. Brune, F. Schmidt-Kaler, A. Maali, J. Dreyer, E. Hagley, J.M. Raimond, S. Haroche, Quantum Rabi oscillation: a direct test of field quantization in a cavity, Physical Review Letters 76 (1996) 1800–1803.
[162] P. Michler, A. Kiraz, C. Becher, W.V. Schoenfeld, P.M. Petroff, L.D. Zhang, E. Hu, A. Imamoglu, A quantum dot single-photon turnstile device, Science 290 (2000) 2282–2285.
[163] E. Moreau, I. Robert, J.M. Gerard, I. Abram, L. Manin, V. Thierry-Mieg, Single-mode solid-state single photon source based on isolated quantum dots in pillar microcavities, Applied Physics Letters 79 (2001) 2865–2867.
[164] M. Pelton, C. Santori, J. Vuckovic, B.Y. Zhang, G. Solomon, J. Plant, Y. Yamamoto, Efficient source of single photons: a single quantum dot in a micropost microcavity, Physical Review Letters 89 (2002) 233602.
[165] O. Benson, C. Santori, M. Pelton, Y. Yamamoto, Regulated and entangled photons from a single quantum dot, Physical Review Letters 84 (2000) 2513–2516.
[166] J.P. Reithmaier, G. Sek, A. Loffler, C. Hofmann, S. Kuhn, S. Reitzenstein, L.V. Keldysh, V.D. Kulakovskii, T.L. Reinecke, A. Forchel, Strong coupling in a single quantum dot-semiconductor microcavity system, Nature 432 (2004) 197–200.
[167] T. Yoshie, A. Scherer, J. Hendrickson, G. Khitrova, H.M. Gibbs, G. Rupper, C. Ell, O.B. Shchekin, D.G. Deppe, Vacuum Rabi splitting with a single quantum dot in a photonic crystal nanocavity, Nature 432 (2004) 200–203.
[168] T. Feldtmann, L. Schneebeli, M. Kira, S.W. Koch, Quantum theory of light emission from a semiconductor quantum dot, Physical Review B 73 (2006) 155319.
[169] M.R. Andrews, C.G. Townsend, H.-J. Miesner, D.S. Durfee, D.M. Kurn, W. Ketterle, Observation of interference between two Bose condensates, Science 275 (1997) 637–641.
[170] M.A. Kasevich, Coherence with atoms, Science 298 (2002) 1363–1368.
[171] C. Orzel, A.K. Tuchman, M.L. Fenselau, M. Yasuda, M.A. Kasevich, Squeezed states in a Bose–Einstein condensate, Science 291 (2001) 2386–2389.
[172] A.H. Zewail, Femtochemistry—Ultrafast Dynamics of the Chemical Bond, vols. I & II, World Scientific Publishing, Singapore, 1994.
[173] U. Hofer, I.L. Shumay, C. Reuss, U. Thomann, W. Wallauer, T. Fauster, Time-resolved coherent photoelectron spectroscopy of quantized electronic states on metal surfaces, Science 277 (1997) 1480–1482.
[174] D.G. Lidzey, D. Bradley, M.S. Skolnick, T. Virgili, S. Walker, D.M. Whittaker, Strong exciton-photon coupling in an organic semiconductor microcavity, Nature 395 (1998) 53–55.
[175] F. Wang, G. Dukovic, L.E. Brus, T.F. Heinz, The optical resonances in carbon nanotubes arise from excitons, Science 308 (2005) 838–841.
[176] A. van Oijen, M. Ketelaars, J. Kohler, T.J. Aartsma, J. Schmidt, Unraveling the electronic structure of individual photosynthetic pigment-protein complexes, Science 285 (1999) 400–402.
[177] N.E. Holt, D. Zigmantas, L. Valkunas, X.P. Li, K.K. Niyogi, G.R. Fleming, Carotenoid cation formation and the regulation of photosynthetic light harvesting, Science 307 (2005) 433–436.
[178] S. Bellafiore, F. Bameche, G. Peltier, J.D. Rochaix, State transitions and light adaptation require chloroplast thylakoid protein kinase STN7, Nature 433 (2005) 892–895.